

**HOLOCENE ENVIRONMENTS AND GEOMORPHIC  
EVOLUTION OF THE GREAT RANN OF KACHCHH,  
WESTERN INDIA**

A  
Thesis  
submitted to  
THE M. S. UNIVERSITY OF BARODA  
for the degree of  
DOCTOR OF PHILOSOPHY  
in Geology

By  
**NITESHKUMAR N. KHONDE**

**Department of Geology  
Faculty of Science  
The M. S. University of Baroda  
Vadodara-390 002  
2013**

## Acknowledgments

The present work was a wonderful journey which I began with lots of enthusiasm, energy, curiosity and confidence. Soon after few months I started realizing the difference between thinking and doing, identifying and solving scientific problems, technical, non-technical, ethical, unethical, moral and immoral, achievable and unreachable things in the system and my own abilities. There was a large mob that modified, upgraded me to adjust, understand, and survive to execute my work with proper guidance if I am doing so today. On completion of this rigorous training of scientific and non-scientific things, I look behind and find myself as one of the grown, nurtured, cultured, scientifically trained and predictable animal on earth. Therefore, for this fantastic achievement of mine I should not only feel proud but also I should express my sense of gratitude towards those persons who untiringly supported, helped me, understood me and encouraged me in all situations.

First of all I would like to express my deepest sense of gratitude towards my guide Dr. D. M. Maurya who believed in me as a potential researcher and accepted me under his guidance. He not only guided me for the doctoral work but he has always been there to develop me as a keen learner of science. I thank him for his constant encouragement, discussions and always orienting me towards work. His meticulous style of working, decision making ability and sincerity towards research shall always remain a constant motivating force for me.

I am extremely indebted to Prof. L. S. Chamyal, Head, Department of Geology, for his unconditional guidance, co-operation and encouragements since my post graduation days. I also thank him for providing me all the required facilities in the department and encouraging me always to work hard. I express my deepest thanks to him for all kinds of help throughout my work.

I gratefully acknowledge the financial support in the form of Junior Research Fellow (JRF) from a Department of Science and Technology (DST), New Delhi sponsored research project sanctioned to Dr. D. M. Maurya. The DST also provided generous funding in this project for carrying out core drilling in the Great Rann of Kachchh. I am also thankful to the CSIR for awarding me CSIR-Senior Research Fellowship.

I am grateful to Prof. Rajamani for his constant encouragement and support. It's my pleasure to express my respect and gratitude towards Prof. A. D. Singh, BHU, Banaras Hindu University, Varanasi for his affectionate help, guidance and training on foraminiferal studies. During my stay in BHU he has extended his guidance to learn about foraminifera and kindled my interest in micropalaentology. He has always been supportive during every stage of my work. I express my utmost respect for Prof. M. S. Srinivasan for his encouragement for studying foraminifera. I also thank Mr. Abhishek Mishra and Ms. Komal Verma for always helping me throughout various stages of my work. I also thank Prof. J.N. Goswami for allowing me to work at the Geosciences division, Physical Research Laboratory (PRL), Ahmedabad for my thesis work. I extend my special gratitude to Dr. Ravi Bhushan, PRL for his proactive help in carrying out geochemical studies. I am also grateful to Dr. Sunil Kumar Singh, PRL for his guidance, support and help for carrying out Sr-Nd isotopic studies. I am also thankful to Dr. Vinai K. Rai and Ms. Sowmya Kamath for their help during the ICP-MS measurements. I am also thankful to Sudhir sir for his help during the experimental work. The Lab Assistant Mr. Bhavsar also helped me a lot during the elemental geochemical studies. Furthermore, the excellent team of students in chemistry lab including Srinivas bhai, Satinder bhai, Veeneet bhai, Prashant bhai, Sneha, Balaji, Damodar, Upasna, Vyenkatesh, Chandana

were always helpful throughout my stay. Exciting discussions with Srinivas and Satindar bhai always improved my understanding of geochemical proxies and related aspects.

I would also like to thank Dr. Rajiv Nigam (Dy. Director, NIO) for discussions, kind help and support. I am also thankful to Dr. V. P. Rao for allowing me to do XRD-Clay mineralogical studies at NIO. Also Dr. Pratima Kessarkar, Shynu and Mr. Girish Prabhu are acknowledged for their help during the sample preparation and XRD measurements. I am also thankful to Prof. Kanchan Panday and Dr. Gorge Mathew of the Department of Earth Sciences, IIT, Mumbai for allowing to carrying out SEM (Scanning Electron Microscopy) photography of microfossils and XRD clay mineralogy of my samples. Mrs. Shilpa Nerukar and Mrs. Trupti Gurav are also acknowledged for their help at IITB.

I thankful to Dr. Satish Patel and Dr. Nilesh Bhatt for their help and encouragement. My close associates including Mr. Siddharth Prizomwala, Mr. Vikas Chowksey were always there when I needed them. Mr. Vishal Ukey, Ms. Jaquiline Joseph, Ms. Archana Das, Ms. Parul Joshi and Ms. Mamta Tiwari also helped during various stages of work. Prabhin Sukumaran, Shashi Bhushan Shukla and Atul Patidar as my senior colleagues always supported me and encouraged me in good and bad situations. Also Mr. Tathagata Ghosh (Geography Department, MSU) who was also my hostelmate since my post graduation remains a very good friend and source for inspiration.

I take this opportunity to thank my teachers Dr. M. V. Baride, Mrs. Arti Baride, Dr. J. B. Pawar and Dr. Amit Kumar Ray (Calcutta). Without their unconditional love, affection and motivation I would not have walked on this path.

I would like to thank my close friends for always being with me- Hemraj Patil, Rahul Nagrale, Bharat Sharma, Lotan Suryawanshi, Prashant Wagh, Sachin-Bhushan, Nilesh Desale, and Sunil Patil. I must thank my close friends Rajesh S. V., Hemand Mande, Harish Talele, Mohit, Rahul Dhande, Anoop Markande, Vrushab Mahesh, Jagat Rathod and Subramaniam, Narayan and Samudrabhai for joyful moments.

Last but not least, I would like to express my deepest sense of gratitude towards my father who passed away during the course of my present study, My mother and lovely sister (Nilakshi) courageously encouraged me to continue with my work. I also thank my uncle Deelip S. Khonde who always stood behind me and my family throughout life and have always been my inspiration. I express my love to my little cousin brothers and sisters Ghanasham, Deepu, Aayush, Gunjan and Rani. Finally I dedicate this thesis to my father who would have been the happiest person on this earth to see me get a doctorate.

Niteshkumar N. Khonde

# **CERTIFICATE**

This is to certify that the contents of this thesis comprise original research of the candidate and have at no time been submitted for any other degree.

**(Niteshkumar N. Khonde)**  
Candidate

**(D. M. Maurya)**  
Guide

**(L. S. Chamyal)**  
Head  
Department of Geology

# CONTENTS

<b>CHAPTER 1 INTRODUCTION</b>	<b>1-14</b>
RATIONALE	1
OBJECTIVES	3
METHODOLOGY	3
REGIONAL PERSPECTIVE OF THE KACHCHH BASIN	4
Mesozoic stratigraphy	5
Tertiary stratigraphy	9
SUMMARY OF AVAILABLE GEOLOGICAL DATA ON THE GREAT RANN	12
<b>CHAPTER 2 MATERIALS AND METHODS</b>	<b>15-29</b>
GEOMORPHOLOGICAL STUDIES	15
CORE DRILLING	16
LOGGING, X-RAY RADIOGRAPHY AND SAMPLING	18
LABORATORY ANALYSIS	20
TEXTURAL ATTRIBUTES	21
MICROFAUNAL STUDIES	21
Foraminifera separation	
CLAY MINERALOGICAL STUDIES	22
Subsurface Rann Sediments (Core Sediments)	
CaCO <sub>3</sub> , ORGANIC CARBON AND NITROGEN	23
MAJOR AND TRACE ELEMENTS	24
ISOTOPIC STUDIES	25
Sr and Nd isotopic measurements in silicate fraction	
<b>CHAPTER 3 TECTONO-GEOMORPHIC STUDIES IN THE GREAT RANN BASIN</b>	<b>29-52</b>
GEOMORPHOLOGY OF THE GREAT RANN	29
Geomorphic Divisions	30
TECTONO-GEOMORPHIC ANALYSIS	36
The Bet zone	37
Banni Plain	38
The Allahbund Fault scarp	41
The Island Belt Fault (IBF) scarp	44
GEOMORPHIC EVIDENCE OF UPLIFT OF THE ISLAND BELT	48
Raised Rann sediments along island margins	48
Marine Erosional Features	49
NEOTECTONIC UPLIFT	51
<b>CHAPTER 4 PRESENT DAY ENVIRONMENT OF THE BET ZONE</b>	<b>53-73</b>
SAMPLING AND LABORATORY METHODS-	53
Grain size analysis	53
Foraminiferal Studies	54
SEDIMENT CHARACTERISTICS	55
FORAMINIFERAL ASSEMBLAGE	59
PRESENT DAY ENVIRONMENTAL CONDITIONS	69
<b>CHAPTER 5 RAISED RANN SEDIMENTS ALONG ISLAND MARGINS: PALAEOENVIRONMENTAL IMPLICATIONS</b>	<b>73-86</b>
SEDIMENTARY CHARACTERISTICS	75
CHRONOLOGY	79
MICROPALAEONTOLOGICAL STUDIES	80
PALAEOENVIRONMENTAL IMPLICATIONS	83

<b>CHAPTER 6</b>	<b>TEXTURAL CLASSIFICATION AND LITHOSTRATIGRAPHY OF THE CORE SEDIMENTS</b>	<b>87-104</b>
	CORE DRILLING	87
	RADIOCARBON DATING	91
	Age Model	91
	STRATIGRAPHY OF THE CORES	93
	Dhordo core	93
	Berada core	99
<b>CHAPTER 7</b>	<b>FORAMINIFERAL STUDIES ON CORE SEDIMENTS</b>	<b>105-123</b>
	FORAMINIFERAL ASSEMBLAGE	105
	SYSTEMATIC TAXONOMY	106
	PALAEOENVIRONMENTAL CHANGES IN THE DHORDO CORE	114
	PALAEOENVIRONMENTAL CHANGES IN THE BERADA CORE	120
<b>CHAPTER 8</b>	<b>MAJOR AND TRACE ELEMENT STUDIES ON CORES</b>	<b>130-150</b>
	ELEMENTAL PROXIES	130
	RESULTS AND INTERPRETATION – DHORDO CORE	132
	Major Elements	132
	C/N Ratio (Land-Marine Interaction)	136
	Trace Elements	140
	RESULTS AND INTERPRETATION – BERADA CORE	143
	Major Elements	143
	C/N ratio (Land-Marine interaction)	145
	Trace Elements	148
<b>CHAPTER 9</b>	<b>CLAY MINERALOGICAL STUDIES</b>	<b>151-174</b>
	CLAY MINERALS AS A REGIONAL PALAEO- PROXY RESULTS	151
	Clay Mineralogy of Dhordo Core	154
	Clay Mineralogy of Berada Core	158
	IMPLICATION FOR PROVENANCE OF THE RANN SEDIMENTS	162
	PALAEOENVIRONMENTAL IMPLICATIONS	167
	Dhordo Core	167
	Berada Core	171
<b>CHAPTER 10</b>	<b>Sr-Nd ISOTOPIC STUDIES ON CORE SEDIMENTS</b>	<b>175-194</b>
	PROVENANCE STUDIES	175
	PROVENANCE TRACKING OF THE GREAT RANN SEDIMENTS	176
	TEMPORAL VARIATIONS IN DHORDO CORE	188
	TEMPORAL VARIATIONS IN BERADA CORE	191
<b>CHAPTER 11</b>	<b>CONCLUDING DISCUSSION</b>	<b>195-209</b>
<b>CHAPTER 12</b>	<b>CONCLUSIONS</b>	<b>210-213</b>
<b>REFERENCES</b>		<b>214-224</b>
<b>LIST OF PUBLICATIONS BY THE CANDIDATE</b>		

## LIST OF FIGURES

		<b>Page No.</b>
Figure 1.1	Map of Kachchh basin showing major geomorphic divisions. Note the vast area covered by the Great Rann and the Little Rann.	2
Figure 1.2	Structural map of the Kachchh basin (after Biswas and Deshpande, 1970)	5
Figure 1.3	Geological map of the Kachchh basin (after Biswas, 1993).	7
Figure 2.1	Field photographs showing drilling sites at both the core locations and core pipe measurements during operation. (a) Dhordo core site, (b) Berada core site. Please note the foreground at Dhordo drill core site showing the salt encrusted rann surface whereas at Berada drill core site denotes typical banni surface with polygonal cracks on surface. (c) Pipe recovery after drilling and (d) Core recovery measurements, on site logging and packing of individual core pipes. Note that each pipe is having details of core length, recovery and filed logging information. Also, top and bottom of each core pipe is denoted.	17
Figure 2.2	X-Ray radiographs of all core pipes from Dhordo core site. Note the core excellent recovery and fine scale laminations in the core pipes.	18
Figure 2.3	X-Ray radiographs of all core pipes from Berada core site. Note the excellent core recovery and fine scale laminations in the core pipes.	19
Figure 2.4	Schematic view of the multi-proxy studies carried out during the study.	20
Figure 2.5	Schematic view of digestion procedure followed for Major, Trace and REE's in sediment samples.	26
Figure 2.6	Schematic view of sample processing protocol for Sr-Nd isotopic studies.	27
Figure 3.1	Satellite image of Great Rann of Kachchh basin showing the variations in surface morphology. The image shows the completely dry rann surface as it appeared in the extreme arid season in May, 2003 (Source- <a href="http://www.earthobservatory.nasa.gov">www.earthobservatory.nasa.gov</a> ). The geomorphological divisions of the Great Rann (1-4) are also indicated. 1-Banni plain, 2-Supra tidal salt flat, 3-Inland saline flats and 4-Bet zone. (Pa-Pachham island, Kh-Khadir island, Be-Bela island, Ch-Chorar island).	30
Figure 3.2	N-S topographic profile across the Great Rann basin showing the geomorphic divisions. Vertical scale is highly exaggerated. The elevation data is based on the SOI topographical maps (survey years-1960-66).	31
Figure 3.3	a- Photograph showing the typical nature of the surface of the Banni plain. b- Photograph showing the typical extensive flat surface of the supra tidal salt flat. c- Close view of the large polygonal cracks in the salt crust. d- Photograph showing the thickness (~10 cm) of the salt crust.	33
Figure 3.4	a-View of the Inland saline flat to the north of Bela island. The scarp in the background marks the geomorphic expression of the Island Belt Fault (IBF). b- View of the typical salt crust free surface of the Bet zone. c- Northward view of the developing gullies in the northern most part of the Bet zone. d- Surface of the Bet zone covered with numerous bivalve shells which thrive during periods of submergence.	35
Figure 3.5	E-W trending topographic profile across the Bet zone.	37
Figure 3.6	Google image showing a prominent channel feature. Red lines depict the transect of cross profiles given in Fig. 3.7.	41
Figure 3.7	Cross profiles across the channel feature shown in Fig. 3.6.	42
Figure 3.8	Topographic profile drawn over the crest of the Allahbund scarp. The	42

	supra tidal salt flat surface is also shown to indicate the height of the scarp. Vertical scale is highly exaggerated. The elevation data is based on the Survey of India topographical maps (survey years-1960-66).	
Figure 3.9	a- View of the Allahbund scarp. Note the degraded nature of the scarp. b- View of the crest part of the Allahbund scarp. A short stream incising through the crest and merging with the supra tidal salt flat in the distant background can be seen. c- View of the gullied surface over the Allahbund scarp. Note the depth of incision in the gully. The surface here is free of aeolian sediments.	43
Figure 3.10	Topographic cross sections drawn across the E-W trending Allahbund scarp. The top profile is from the western extremity while the bottom one is from the eastern extremity of the scarp. The elevation data is based on the SOI topographical maps (survey years-1960-66).	44
Figure 3.11	a – Photomosaic of the northern escarpment of the Bela island. In the foreground is the rann surface. b- View of the Khadir scarp. Note the fresh nature of the escarpments.	45
Figure 3.12	E-W topographic profiles drawn over the crest of the northern escarpments of (a) Bela, (b) Khadir and (c) Bhanjada islands.	47
Figure 3.13	a- Distant view of the western margin of the Khadir island. b- Close view of the exposed section of the raised rann sediments. c- Flat terraced surface of raised intertidal sediments. d- View of the surface of raised intertidal sediments at the margin of the Bhanjada island.	49
Figure 3.14	a- View of a sea cave at the northern margin of Bela island (Loc. North of Kuda). b- Close view of the lower notch in Bela island (Loc. North of Kuda).	50
Figure 4.1	Geomorphic map of the Bet Zone of Great Rann of Kachchh with spatial distribution of sampling stations along two transects. Transect-1 is ESE-WNW oriented transect along the southern margin of Bet Zone. Transect-2 is roughly N-S oriented transect running across the eastern margin of the Bet Zone.	54
Figure 4.2	Topographic profiles along the two transects. a) Transect-1 and b) Transect-2. The profiles drawn are based on the elevation variations data from the Survey of India topographic maps. Note the elevation variations i.e. microgeomorphic variations of the respective sampling sites as shown in figure.	56
Figure 4.3	Grain Size distribution at the sampling stations along two transects a) Transect-1 and b) Transect-2. Note that the sand proportions increases at the stations directly in contact with the inundating waters whereas the silty to clayey sediments belongs to the sheltered areas (low lying areas, depressions).	58
Figure 4.4	SEM photographs of the recovered foraminiferal assemblage. 1. <i>Ammonia beccarii</i> (Linne, 1758): 1a.Spiral view; 1b. Umbilical view. 2. <i>Ammonia tepida</i> (Cushman); 2a.Spiral view; 2b. Umbilical view. 3. <i>Ammonia parkinsoniana</i> (d'Orbigny, 1839); 3a.Spiral view; 3b. Umbilical view. 4. <i>Elphidium excavatum</i> (Terquem) 4a.Spiral view; 4b. Umbilical view. 5. <i>Elphidium discoidale</i> (d'Orbigny) 5a.Spiral view; 5b. Umbilical view. 6. <i>Elphidium sp.</i> 7. <i>Globigerinella sp.</i> 8. <i>Glogigerina bulloides</i> (d'Orbigny). 9. <i>Globorotaloides sp.</i> 10. <i>Bolivina spathulata</i> (Williamson). 11. <i>Nonian asterizans</i> (Eichtel & Moll). 12a. <i>Bulimina marginata</i> (d'Orbigny 1826); 12b. A close view showing short blunt spines 13. <i>Cibicides refulgens</i> (de Montfort, 1808). 14. <i>Helenina anderseni</i> (Warren) 14a. Spiral view; 14b. Umbilical view. 15. <i>Gallitellia Sp.</i> 16a. <i>Brizalina striatula</i> (Cushman, 1992); 16b. A close view showing the longitudinal coaste.	64
Figure 4.5	Graph showing spatial distribution of <i>Ammonia</i> genus along the two	67

	transects.	
Figure 4.6	Graphs showing spatial distribution of foraminifera along the two transects.	68
Figure 5.1	<i>a</i> , Map of Kachchh basin showing the fault-controlled geomorphic set-up. Note the vast extent of the Great Rann forming the northern part of the basin. Unshaded areas are occupied by Mesozoic and Tertiary rocks. Boxed area shows the rocky islands of Pachcham and Khadir within the Great Rann. (Inset) Location map. <i>b</i> , Satellite image of the northwestern part of Khadir and Bhanjada islands showing the location of the sections studied (source: www.googleearth.com). <i>c</i> , Satellite image of the northwestern part of Pachcham and Kuar Bet island showing the location of the sections studied (source: www.googleearth.com).	74
Figure 5.2.	<i>a</i> , View of the northwestern margin of the Khadir island. The foreground is the salt-encrusted rann surface and vertical cliff section of the raised rann sediments at the base of the island. <i>b</i> , View of the southern cliff face of raised rann sediments rising above the rann surface at eastern fringe of the Bhanjada island. Part of the rocky island is visible to the left. <i>c</i> , View of the raised rann sediments at southern margin of the Kuar Bet island. Rann surface is seen in the background.	76
Figure 5.3	Lithologs of the raised rann sediments in Khadir, Bhanjada and Kuar Bet islands in the Great Rann. Note the dominantly fine-grained lithology and the similarity in gross lithology in all the three islands. OSL dates obtained are also shown.	78
Figure 5.4	<i>a</i> , Photomicrograph of the sediments showing discoidal and nodular gypsum crystals. <i>b</i> , Photomicrograph showing discoidal gypsum forming large agglumates in the sediments.	78
Figure 5.5	Graphs showing vertical distribution and abundance zones of foraminiferal tests throughout the cliff sections at Khadir, Bhanjada and Kuar Bet islands.	81
Figure 6.1	Geomorphic map of the Great Rann of Kachchh basin with major faults. Locations of the two drilled cores are shown as solid squares.	88
Figure 6.2	Topographic section along the line covering core locations in the Great Rann of Kachch basin. Vertical scale is highly exaggerated. Note the locations of the cores (DH and BRD) with respect to the basin and the distance between two.	88
Figure 6.3	Photographs of the split core pipes of Dhordo core raised from north of Pachcham Island, Great Rann of Kachchh basin. Note the excellent recovery of the sediments.	89
Figure 6.4	Photographs of the split core pipes of Berada core raised from Banni plain of Great Rann basin. Note the excellent recovery of the sediments.	90
Figure 6.5	Age Model for the Great Rann of Kachchh sedimentation during past ~17ka BP based on six <sup>14</sup> C dating horizons from both the cores (Dhordo and Berada cores).	92
Figure 6.6	The downcore grain size variations in Dhordo core is shown in the form of graphs with their textural classes following Flemming 2000.	94
Figure 6.7	The downcore grain size variations in Berada core is shown in the form of graphs with their textural classes following Flemming 2000.	100
Figure 7.1	Plate showing the foraminiferal assemblage recovered from Dhordo and Berada cores 1a, 1b. Globorotaloid sp. ; 2. <i>Ammonia parkinsoniana</i> 2a. Spiral view 2b. Umbilical view; 3. <i>Ammonia tepida</i> . 3a Spiral view 3b. Umbilical view; 4. <i>Ammonia beccarii</i> 4a Spiral view 4b. Umbilical view; 5. <i>Calcarina carcal</i> ; 6a. <i>Elphidium excavatum</i> , 6b. Close view showing the umbilicus and granules along the sutures. 7. <i>Elphidium clavatum</i> ; 8a. <i>Elphidium williamsoni</i> , 8b. Close view; <i>Criboelphidium ocenansis</i> ; 10a. <i>Haynesina depressula</i> , 10b. Close view showing the	112

	postules. 11a Nonian sp. 11b. Close view showing the smooth surface of the species; 12. Nonian <i>commune</i> ; 13. Nonionella sp.; 14. Nonionella <i>atlantica</i> ; 15. Nonionella <i>labradorica</i> ; 16. Nonionoides <i>grateleupi</i> ; 17. Globorotaloides sp.; 18. Bolivina <i>variabilis</i> ; 19a. Bolovina <i>psuedoplicata</i> , 19b Close view of showing the anostomosing pattern costae; 20. Brizalina <i>spathulata</i> ; 21. Lagena sp.; 22. Lagena <i>striata</i> ; 23. Lagena <i>levis</i> ; 24 Hopensinella <i>pacifica</i> ; 25. Gallitellia <i>vivans</i> ; 26a. Uvigerina sp. 26b. Close view showing the parallel striata or ribs.	
Figure 7.2	SEM images of the recovered foraminifera from the Dhordo and Berada Cores	113
	1. Triloculina <i>tricarinata</i> ; 2. Miliolina <i>australis</i> ; 3. Milonella <i>grata</i> ; 4. Quniquiloculina <i>seminula</i> ; 5. Quniquiloculina <i>levigata</i> ; 6. Quniquiloculina <i>oblonga</i> ; 7. Triloculina <i>levigata</i> ; 8. Cycloforina; 9. Quniquiloculina sp.; 10. Miliamina <i>fusca</i> ; 11, Triloculina <i>oblonga</i> ; 12 Fursenkonia sp.; 13. Triloculina sp.p; 14. Spiroculina sp.	
Figure 7.3	Graphs showing down core variations of foraminiferal species in Dhordo core	115
Figure 7.4	Graphs showing down core variations of foraminiferal species in Dhordo core	117
Figure 7.5	Graphs showing down core variations of foraminiferal species in Dhordo core	118
Figure 7.6	Graphs showing down core variations of foraminiferal species in Berada core	121
Figure 7.7	Graphs showing down core variations of foraminiferal species in Berada core.	122
Figure 8.1	Down core variations in Al and other ‘Al normalized’ major elements from Dhordo core.	134
Figure 8.2	Downcore variations in N, C, C/N ratio and CaCO <sub>3</sub> content in Dhordo core.	138
Figure 8.3	Trace element distribution (in ppm) in Dhordo core.	141
Figure 8.4	Down core variations in the major elements (Al normalized) in Bearada core.	145
Figure 8.5	Down core variations in the N, C, C/N ratio and CaCO <sub>3</sub> content in Berada core.	148
Figure 8.6	Down core variations in the trace elements (Al normalized) in Berada core.	149
Figure 9.1	a) Down core variations in major Clay minerals (Smectite, Illite, Kaolinite and Chlorite), Illite Crystallinity, Illite Chemistry and (Sm+Ka)/(Ill+Ch) ratio. b) Downcore variations in environmentally sensitive clay mineral ratio proxies in Dhordo Core. The divisible zones and the overall timeframe of deposition also indicated.	153
Figure 9.2	a) Down Vvariations in major Clay minerals (Smectite, Illite, Kaolinite and Chlorite), Illite Crystallinity, Illite Chemistry and (Sm+Ka)/(Ill+Ch) ratio. b) Downcore variations in environmentally sensitive clay mineral ratio proxies in Berada Core. The divisible zones and the overall timeframe of deposition is also indicated.	161
Figure 9.3.	Clay mineral characteristics of Indus river system from its flood plains, river mouth (delta) and shelf region compared with Great Rann basin, Kachchh. a) The Eastern Punjab (Pakistan) flood plains near Behwalpur region comprising Marot, Tilwalla cores and Fort Abbas and Derawar trenches in flood plains covering from ~49Ka to recent (Alizai <i>et.al.</i> 2012). b) The clay mineralogy of from the present day confluence of the eastern and western tributaries of Indus river that represents the older river sediments essentially of Himalayan origin but not necessarily of	164

	river Nara (Alizai <i>et.al.</i> 2012), Keti Bander core is from the Indus delta region near to the river mouth (Alizai <i>et.al.</i> 2012) and Indus-23, Indus-10 core records are from north of Indus canyon and off Karachi (Pakistan) respectively (Limmer <i>et.al.</i> 2012). C) Clay mineral data of rann sediments near Shakti bet (Tyagi <i>et.al.</i> 2012) western great rann and present study i.e. Central and Marginal Great Rann of Kachchh basin.	
Figure 9.4	Plots showing Illite crystallinity Vs Chemical weathering proxies for the individual time frames for Dhordo Core samples. (a) Smectite/(Illite+Chlorite) Vs Illite crystallinity, and (b) Kaolinite/(Illite+Chlorite) Vs Illite crystallinity. Note that the L. Pleistocene values are more sparsely arranged, L. Pleistocene to E. Holocene values shows lowered degree of Illite crystallinity with increased hydrolization processes; whereas; Mid-Late Holocene values are more or less indicating higher leaching and variable degree Illite crystallinity.	169
Figure 9.5	Plots showing Illite crystallinity Vs Chemical weathering proxies for the individual time frames for Dhordo Core samples. (a) Smectite/(Illite+Chlorite) Vs Illite crystallinity, and (b) Kaolinite/(Illite+Chlorite) Vs Illite crystallinity. Note that the E. Holocene values shows lowered degree of Illite crystallinity with increased hydrolization processes; Early-Mid Holocene values are more sparse and shows evidences of high-lower degree of hydrolization processes; whereas; Mid-Late Holocene values essentially shows higher order of leaching processes.	172
Figure 10.1	Map of Kachchh and adjoining regions showing multiple sediment sources.	181
Figure 10.2	Satellite image showing the course of palaeo Saraswati River. A, Delhi–Kalka Ridge; B, Delhi–Sargodha Ridge; C, Jaisalmer–Mari Arch. (after Mitra and Bhadu, 2012).	182
Figure 10.3	Scatter plot showing the distribution of $^{87}\text{Sr}/^{86}\text{Sr}$ , $\epsilon\text{Nd}$ isotopic composition of the Arabian Sea (Clift <i>et.al.</i> 2010; Kessarkar <i>et.al.</i> 2003), Indus-Tsangpo suture zone, Tibetan Sedimentary Series, High Himalayan Crystallines and Lesser Himalaya (Tripathi <i>et.al.</i> 2013 and references therein). Note that the Dhordo and Berada core samples show high radiogenic Sr values than the Arabian Sea and less radiogenic Nd.	183
Figure 10.4	Scatter plot showing the Sr-Nd isotopic composition of the Rann sediments from Dhordo and Berada cores with various potential end members. Note that the Thar Desert values are from 1.8-9.1ka B.P. old sediments; Ghaggar River 3.4ka B.P.; 0 to 28ka B.P. and Gularchy 3-11ka B.P.	185
Figure 10.5	Temporal scale variations in $\epsilon\text{Nd}$ values of Keti Bunder (Indus delta), Dhordo core (central rann basin) and Berada Core (marginal rann basin). Note that the Indus delta at its bottom to top varies with high to low radiogenic Nd (with stable values during most of the Holocene) whereas the rann samples as both locations shows opposite trend i.e. low radiogenic Nd at the bottom that changes into high radiogenic Nd upwards.	187
Figure 10.6	Temporal variations in $^{87}\text{Sr}/^{86}\text{Sr}$ and $\epsilon\text{ND}$ in Dhordo core.	189
Figure 10.7	Temporal variations in $^{87}\text{Sr}/^{86}\text{Sr}$ and $\epsilon\text{ND}$ in Berada core.	192

## LIST OF TABLES

		<b>Page No.</b>
Table 1.1	Lithostratigraphy of Mesozoic rocks of Kachchh Basin, (after Biswas, 1977)	6
Table 1.2	Stratigraphy of Tertiary sediments of Kachchh basin (after Biswas, 1992).	9
Table 2.1	Table showing NOVA Standard values with the measured values during the analysis.	24
Table 2.2	Reproducibility of elemental and isotopic composition of Sr for the sediment samples	28
Table 2.3	Reproducibility of elemental and isotopic composition of Nd for the sediment samples.	28
Table 4.1	Table showing the grain size variation in the surface sediment samples along two transects in the Bet Zone of Great Rann of Kachchh, Western India.	57
Table 4.2	Table showing the dataset of recovered foraminifera along two transects for sampling stations 1-17.	61
Table 5.1	Table showing single aliquot regeneration OSL ages and data for raised sediments from Khadir and Bhanjada bet islands.	80
Table 6.1	Table showing the samples from Dhordo and Berada Cores dated using <sup>14</sup> C dating by AMS method.	91
Table 6.2	Summary of textural characteristics of the various lithounits of the Dhordo core.	95
Table 6.3	Summary of textural characteristics of the various lithounits of the Berada core.	101
Table 7.1	Table showing the foraminiferal abundance (in percentage) in the Dhordo core.	124
Table 7.2	Table showing the foraminiferal abundance (in percentage) in Berada core.	127
Table 8.1	Downcore variations in Major and Trace elements (Al normalized) in Dhordo core.	133
Table 8.2	Downcore variations in CaCO <sub>3</sub> & N%, C% and C/N ratio in Dhordo core.	136
Table 8.3	Downcore variations in Major and Trace elements (Al normalized) in Berada core.	144
Table 8.4	Downcore variations in CaCO <sub>3</sub> & N%, C% and C/N ratio in Berada core.	145
Table 9.1	List of the clay mineral ratio proxies for paleoclimatic and environmental studies. These proxies are adopted from Biscay, 1989; Gingele, 1996; Colin <i>et.al.</i> 2012 and Alizai <i>et.al.</i> 2012 and references therein.	153
Table 9.2	Table showing clay mineral variations in Dhordo Core.	155
Table 9.3	Table showing clay mineral variations in Berada Core.	160
Table 9.4	Comparison of relative abundance of clay mineral in core sediments of Great Rann with surrounding regions.	163
Table 10.1	Downcore variations in the <sup>87</sup> Sr/ <sup>86</sup> Sr and Sr (ppm) isotopic concentration in the Dhordo and Berada Core in Great Rann basin of Kachchh, and rivers draining from the Aravallis.	177

Table 10.2	Downcore variations in the $^{143}\text{Nd}/^{144}\text{Nd}$ , $\epsilon\text{Nd}$ and Nd (ppm) isotopic concentration in the Dhordo and Berada Core in Great Rann basin of Kachchh, and rivers draining from the Aravallis.	179
Table 10.3	$^{87}\text{Sr}/^{86}\text{Sr}$ and $\epsilon\text{Nd}$ isotopic composition of the potential end members for the rann sediment provenance.	182

### INTRODUCTION

#### RATIONALE

The landscape of Kachchh basin includes a geomorphologically unique and intriguing Quaternary terrain of Western India comprising the saline wastelands of the Great Rann. The Great Rann of Kachchh forms almost half of the area of the Kachchh basin (Fig. 1.1), covering almost 45,000 sq. km. area and comprise a flat barren landscape that occurs about 2-6 m amsl (Merh 2005). Previous workers have described the terrain as 'intriguing' to 'without any counterpart in the world (Burnes 1835, Roy and Merh 1981). Based on its peculiar geomorphic characteristics, archaeological evidence and historical records, it is generally agreed that the Great Rann marks the site of an ancient gulf connected to the sea in the west. The Rann, therefore, marks a significant time period of continuous Quaternary marine sedimentation which is not yet properly understood. The Great Rann of Kachchh presents one of the best examples of Quaternary basins that provided sedimentation in fault controlled and tectonically active basins. However, no information as yet exists on the sediments comprising the Ranns of Kachchh and its Quaternary evolutionary history.

The Great Rann comprise unique example of Holocene sedimentation (Merh, 1995). The plain of Banni represents huge mudflats that are more or less flat, almost gradientless saline grassland covering an area about 3000 sq km raises 3 to 10m above the Rann surface. The Banni plains in all probability correspond to a raised mudflat (Kar 1995). Parts of the Banni are believed to be representing a mixed zone of interaction between the marine processes operating in the north and fluvial deposition by the rivers draining the Kachchh Mainland in the south. The presence of gullies and incised fluvial channels on the elevated eastern part of the Banni Plain are indicative of the latest phase of uplift (Biswas 1974). The Rann represent filled up gulfs of a Holocene sea, marking the sites of ancient river mouths. Historical accounts also suggest that there was a navigable sea belonging to archaeological sites of Harrappan civilization including port town of Dholavira. Till now there is no information that exists on the sediment comprising the Banni plain apart from the few geomorphological details.

Some of the intriguing questions yet to be answered in respect of the geological evolution of the Great Rann are (1) what was the paleoenvironmental conditions that

existed in the Great Rann of Kachchh? (2) As it is believed Rann was fully submerged by a sea, if there was a sea then since when it submerged when it dried out? (3) What were the various depositional environments that existed? And (4) from where sediments (i.e. source) were coming that filled up the Rann basins? It is therefore essential to generate data on the crucial area of the Ranns of Kachchh and delineate its tectono-geomorphic evolution, which perhaps holds the key to understanding the Quaternary evolutionary history of Kachchh. The present study carried out in Great Rann of Kachchh is an attempt at filling this huge gap in the Quaternary evolutionary history of Kachchh.

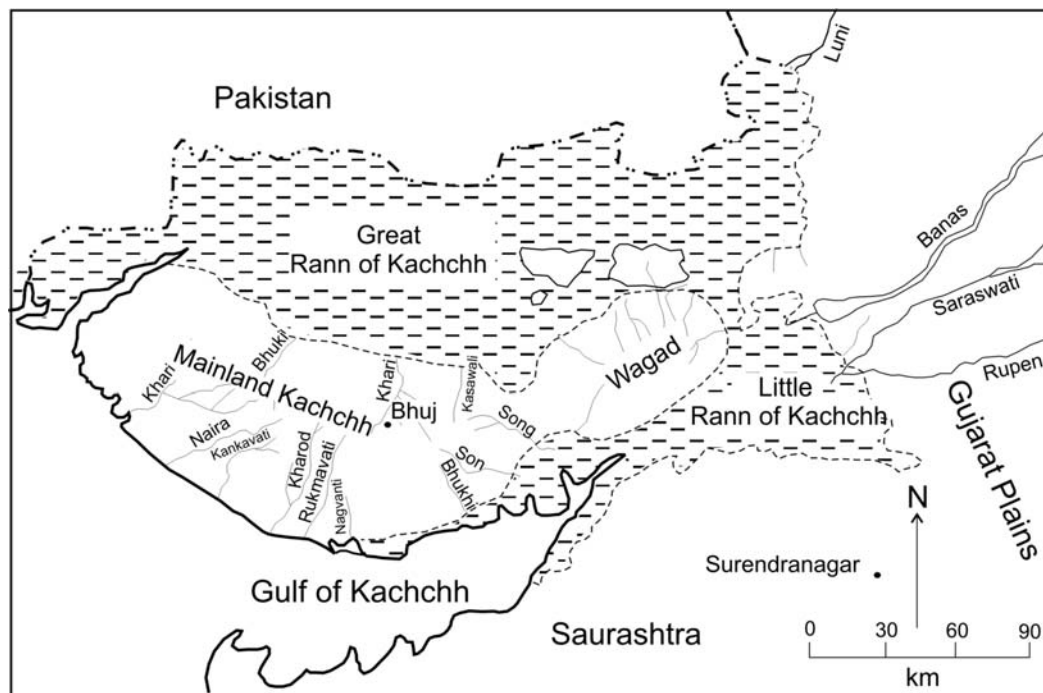


**Figure 1.1** Map of Kachchh basin showing major geomorphic divisions. Note the vast area covered by the Great Rann and the Little Rann.

The biggest handicap in studying the Quaternary deposits of the Ranns of Kachchh is the harsh, inhospitable flat and largely unnavigable terrain that is compounded by the lack of exposures. The only way, therefore, to investigate these deposits is by obtaining continuous cores along the length and breadth of the basin. An important component of the proposed study has therefore been to obtain continuous cores for multidisciplinary studies to delineate the geological evolution of the Ranns of Kachchh. Two continuous cores, one from the central part of the Great Rann basin (~60m depth) and the other from the marginal part of the basin in Banni plain (~50m) were raised. The salient features of the study carried out during the project duration include detailed understanding of the geomorphological characteristics, influence of

structural elements, study of surface and exposed (cliff) sections of rann sediments along island margins, stratigraphy of subsurface rann sediments, and the palaeoceanographic conditions that existed when the basin was occupied by a shallow sea.

## **OBJECTIVES**

The present study was undertaken to address the following objectives.

1. Reconstruct subsurface stratigraphy and palaeoenvironmental changes in the Great Rann of Kachchh.
2. Identify the sediment sources and reconstruct the Quaternary evolutionary history of the Great Rann of Kachchh

## **METHODOLOGY**

The broad methodology adopted for carrying out the present study was as follows.

1. Available geological and subsurface data on the Ranns of Kachchh was collected and critically evaluated to delineate the deep seated subsurface structural features and infer on the nature of basement configuration.
2. Satellite data combined with field checks were used for studies on geomorphology and inundation patterns of the Ranns.
3. Shallow pits and trenches were excavated at numerous sites to record lithology, stratigraphy, seismicity related minor structural features and collection of samples for understanding the nature of near-surface and surface sediments.
4. Rann sediments exposed in the form of vertical cliffs along the various island margins were also investigated in details for inferring depositional conditions and environments.
5. All samples collected were subjected to sedimentologic, micropalaeontological and chronostratigraphic studies to infer about the palaeoenvironmental conditions.
6. Core drilling carried out in Great Rann at two sites that were selected based on geomorphologic studies two continuous cores up to ~60m and ~50m depths.
7. The cores sliced into two equal halves with one half used for sampling while the other half is preserved in sub-zero temperatures. The sampling for both cores was done at 2cm interval.

8. Selected core samples were subjected to multidisciplinary studies like textural, geochemical, isotopic, clay mineralogical, stratigraphic and micropalaeontological studies for deducing palaeoenvironmental conditions in the Great Rann.
9. Few samples of the cores were sent for AMS dating to outside lab.
10. The data generated was synthesised and critically evaluated to reconstruct the Quaternary evolutionary history of the Ranns of Kachchh.

## **REGIONAL PERSPECTIVE OF THE KACHCHH BASIN**

The Kachchh basin is an E-W trending palaeorift graben that is located on the western continental margin of India. The basin originated in early Mesozoic and exposes a full sequence of rocks from middle Jurassic till present (Fig. 1.2). The Mesozoic sedimentation took place during the rift phase of the basin that ended in the late Cretaceous. The basin was inverted at the end of Cretaceous (Biswas and Khatri 2002). Since then, the basin suffered intermittent phases of uplift and flexuring along the various E-W trending faults (Biswas and Khatri 2002). The Cenozoic sediments (Tertiary and Quaternary) were laid down in the geomorphic lows that resulted from the differential uplift of the basin along faults (Biswas 1993). The present landscape framework of Kachchh is therefore largely the result of pre-Quaternary tectonic evolution of the basin (Biswas 1974). Continued tectonic instability of the basin and the active nature of various faults is evidenced by several large magnitude earthquakes in historic times including the 2001 earthquake that have occurred in the region (Biswas and Khatri 2002).

The evolution of Kachchh, Narmada and Cambay rift grabens is related to the breakup of Gondwanaland in the Late Triassic/Early Jurassic and the subsequent spreading history of the Eastern Indian Ocean (Biswas 1982, 1987). The Saurashtra block remained as a horst while the Kachchh, Cambay and Surat basins subsided around it for the deposition of Cenozoic sediments. The Kachchh rift was initiated in the Late Triassic along the Delhi trend as evidenced by continental Rhaetic sediments in the northern part of the basin (Kosal 1984). The Kachchh rift basin was formed by subsidence of a block between the Nagarparkar Hills and the southwest extension of the Aravalli Range (Biswas 1982, 1987). The Kachchh graben became a fully marine basin during the Middle Jurassic period (Biswas 1981). In the Late Cretaceous, uplift of the Jurassic sediments took place in the Kachchh Basin. The major structural

elements that have played a significant role in the post Mesozoic geological and geomorphological evolution of southern Mainland Kachchh are shown in Fig. 1.2.

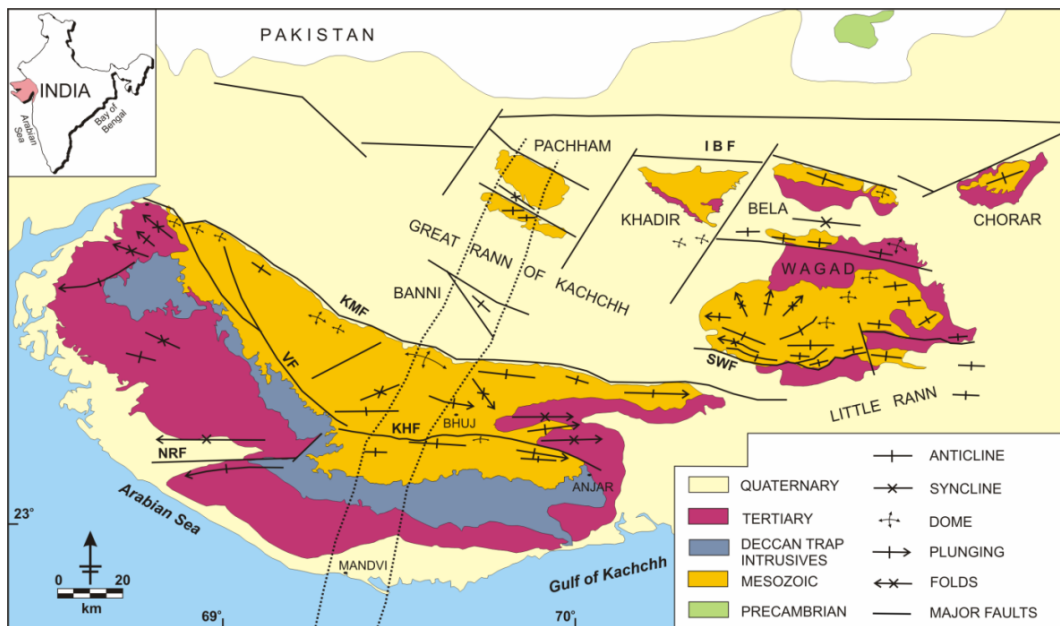


**Figure 1.2** Structural map of the Kachchh basin (after Biswas and Deshpande, 1970)

### Mesozoic stratigraphy

The Kachchh basin preserves about 2000 to 3000 m of Mesozoic and 1000 m of Cenozoic sediments (Biswas 1977, 1982). The Tertiary rocks are exposed along the coastal belt of southern and western Kachchh bordering the Mesozoic rocks. The pre-Quaternary evolutionary history of the Kachchh basin is dealt at length by Biswas (1982, 1987) which has implications for the seismic instability (Biswas and Khattri 2002).

Mesozoic rocks of Kachchh were first mapped by Wynne (1872) who classified the sequence into upper and lower Jurassic Groups. Waagen (1875) proposed the popular four-fold subdivisions, namely, Pachchham, Chari, Katrol and Umia Series. Rajnath (1942) restricted the term ‘Umia’ only to the lower Umia of the Waggen (1875); the upper Umia made up of non-marine beds with plant fossils was called by him as Bhuj Series of Middle Cretaceous or even slightly younger age. Biswas (1977) recognized three main lithologic provinces within the basin and rocks of each province were classified separately (Table 1.1) and named the units according to their stratotypes (Biswas 1977). The lithostratigraphic sequence of Mainland is divided into four formations named as the Jhurio (Jhura), Jumara, Jhuran and Bhuj Formations (Biswas 1977, 1981).

**Table 1.1** Lithostratigraphy of Mesozoic rocks of Kachchh Basin, (after Biswas 1977)

Mainland		Pachham Island		Eastern-Kutch (Khadir-Bela-Wagad)		
Formation	Member	Formation	Member	Formation	Member	
Bhuj	Upper			Wagad Sandstone	Gamdau	
	Ukra					
	Ghuneri					
Jhuran	Katesar				Kanthkot	
	Upper					
	Middle					
	Lower					
Jhumara	Dhosa Oolite				Washtawa	Bhambhanka shale
	Middle					
	Lower				Goradongar	Modar hill
Jhurio	Upper	Goradongar	Raimalro			
	Middle		Gadaputa			
		Lower	Kaladongar	Flagstone	Hadibhadang	
	Kaladongar Sandstone					
		Kuarbet	Khadir (Khadir Island)	Cheriya bet		
				Precambrian		

The major lithological characteristics of these formations worked out mainly by Biswas (1974, 1977, 1982, 1987) is briefly described below.

**Jhurio Formation** : A thick sequence of limestone and shales with bands of ‘golden oolites’ has been named as the Jhurio Formation after the type section in Jhurio hill, in

North-Central Mainland. The upper part of the formation is made up of thinly bedded white to cream coloured limestones (pelmicrite and biomicrite) with thin bands of 'golden oolite' (Balgopal 1973). The middle part is composed of thick beds of grey yellow weathered shales alternated with thick beds of golden oolitic limestones and the lower part comprises thin beds of yellow and grey limestones (Agarwal 1957, Balgopal 1973). The physical and biological aspects of the formation indicates littoral to infra-littoral environment. The formation ranges from Bathonian to lower Callovian.

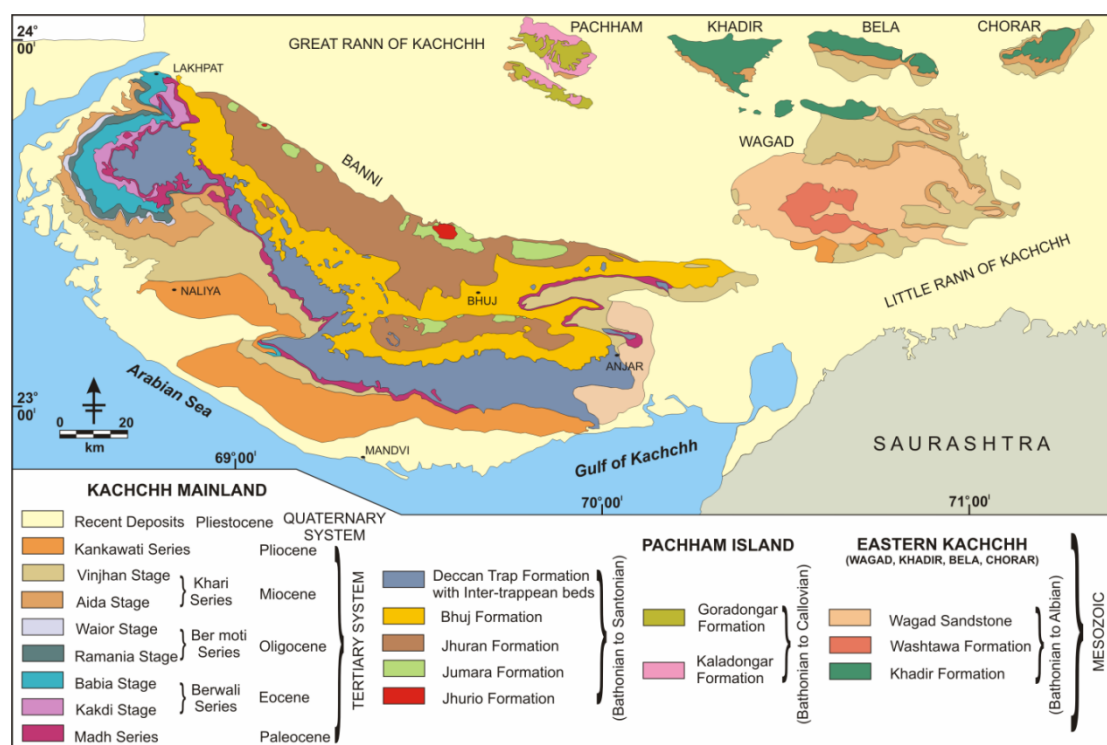


**Figure 1.3** Geological map of the Kachchh basin (after Biswas, 1993).

**Jumara Formation** : A thick argillaceous formation conformably overlying the Jhurio Formation has been named after its type section in Jumara hill near the Rann, north of Jumara village. The formation is characterised by monotonous olive-grey gypseous laminated shales with thin red ferruginous bands. The ~300m thickness of the formation is uniform throughout the area. Local disconformity is observed at places where the Jhuran shales are seen resting over the eroded Dhosa oolite member. The Jumara formation ranges between Callovian to Oxfordian.

**Jhuran Formation** : It comprises a thick sequence of alternating beds of sandstones and shales. The formation is divided into four members-lower, middle (Rudramata Shale), upper and Katesar member (Biswas 1977). The formation is extensively exposed along the southern flanks of the northern and central hill ranges in two wide

east-west strips. In the central and western parts of the Mainland, the lower, middle and the lower part of the upper members are exposed. The lower member consists of alternating red and yellow sandstone and shale. The middle member is mostly shaly comprising dark grey to black laminated gypseous shales. The upper member is predominantly arenaceous and composed of red and yellow massive current bedded sandstones with intercalations of shale, siltstone and calcareous sandstone. Kimmeridgian to Valanginian age is fixed for this formation.

***Bhuj Formation*** : Named after its type locality around Bhuj, this formation is characterised by a huge thickness of non-marine sandstones of uniform character. These rocks occupy about 3/4<sup>th</sup> of the total area of the Mesozoic outcrop in Mainland Kachchh. The lower member is characterised by cyclic repetition of ferruginous or lateritic bands, shales and sandstones. The upper member consists of wheatish to pale brown, massive, current bedded, coarse grained, well sorted sandstones. The formation is bounded by the plains of disconformity. In the south, Deccan trap flows rest on the eroded undulating surface of this formation. The sediments represent deltaic deposits with distal part (delta front) towards the west and the proximal part (fluvial) to the east in the direction of the land. Lower Cretaceous (Valanginian) to Santonian time range is fixed for this formation.

***Deccan Trap*** : The Deccan Traps form a more or less linear outcrop extending across the Mainland with a maximum width of about 10 km in the east near the town of Anjar and gradually tapering westward. Lava flows are dominantly tholeiitic basalts occupying the southern and southwestern slopes of the Central Highland. The trappean flows show gentle southerly dips and are believed to be of pahoe-hoe type (Biswas and Deshpande 1973). Six major flows have been reported at the eastern extremity (Dhola hills near Anjar) where they show alternations of columnar and amygdaloidal basalts, occasionally separated by inter-trappean beds. Associated with the trappean flows are a number of long narrow dykes that occur to the N, NW and NE of the lava flow occurrences. Most of the dykes occur along transverse faults extending N-S, NNE-SSW and NNW-SSE. An interesting aspect of the Deccan volcanism in Kachchh is the occurrence of alkaline basalt and its derivatives as plugs, laccoliths and sills within the domal structures in the Mesozoic rocks. The inter-trappeans were deposited in shallow basins and depressions over trappen surfaces, fed by simultaneously formed rivulets. An uppermost Cretaceous (Maastrichian age) is inferred for these inter-trappeans. The laterites form a narrow elongate Paleocene belt, a few hundred meters wide and several

hundred kilometers long sandwiched between the basalts of the Deccan Trap and the Tertiaries, and forms a terrain that is characterized by 10 to 15 m high elongated ridges separated by broad intermittent valleys.

### **Tertiary stratigraphy**

Wynne and Fedden (1872) studied these rocks for the first time. Biswas (1974) proposed a revised stratigraphy and established that the Tertiary sediments in Kachchh were deposited on the eroded surface of the Deccan Trap and the Mesozoic sedimentaries, and deposition started with a marine transgression during Lower Eocene that ended in Pliocene (Fig. 1.3). During Paleogene, deposition was restricted to the western part of the Kachchh Mainland, the thickest part being exposed in the southwestern coastal plains which was the deepest part of the basin.

**Table 1.2** Stratigraphy of Tertiary sediments of Kachchh basin (after Biswas, 1992).

<b>Age</b>	<b>Formation</b>	<b>Members</b>
Pliocene	Sandhan	
Lower Miocene (Burdigalian)	Chhasra	Siltstone
		Claystone
Lower Miocene (Late Aquitanian)	Khari Nadi	
Oligocene	Maniyara Fort	Bermoti
		Coral Limestone
		Lumpy clay Basal member
Late Middle Eocene	Fulra Limestone	
Middle Eocene	Harudi	
Late Paleocene	Naredi	Ferr. Claystone Assilina Limestone Gypseous Shale
Upper Paleocene	Matanomadh	
Cretaceous–Lower Palaeocene	Deccan Trap	

The following is a brief summary of the Tertiary formations as described by Biswas (1974, 1993).

***Madh Series*** : The type area of the rocks of this series is the well known village of Mata-No-Madh in western Kachchh. It consists of volcanoclastic sediments deposited in variable environments, ranging from fluviatile to littoral. The sediments were mainly derived from the Deccan Trap and the pyroclastics ejected during the waning

phase of the volcanism. The Madh series overlies the basalt but underlies the Kakadi Stage of Lower Eocene. On the basis of plant fossils, the rocks of Madh Series have been assigned a Paleocene to Lower Eocene age (Biswas 1974).

***Berwali Series*** : The type section of this series is exposed along the Berwali Nadi in southwestern Kachchh, between the villages Baranda and Ber-Nana. The series is divisible into two stages, the lower consisting of gypseous and ochreous clays and marl containing varieties of molluscs and foraminifers seen in Kakdi Nadi section (Kakdi Stage). The upper stage is well exposed in Babia hill in western Kachchh comprising a fossiliferous fragmental limestone with a basal calcareous clay bed (Babia Stage). The base of Kakdi Stage indicates an unconformity with the underlying volcanoclastic rocks of the Madh Series.

***Bermoti Series*** : This series forms a well exposed continuous belt south of Lakhpat in northwestern Kachchh. It is divisible into two stages, the lower Ramania Stage consists of greenish-grey marl and argillaceous limestone with a basal bouldary clayey marl bed deposited in an epineritic environment of a slowly regressive sea. Named after the village Waior, the constituent rocks of the upper stage are banded fossiliferous marl, the base comprising of rusty oolitic marl. Biswas (1974) has assigned an Oligocene age to the Ramania Stage. The Waior Stage has been considered as Aquitanian.

***Khari Series*** : This series overlies unconformably the Bermoti Series and is well exposed in the cliffy banks of the Khari river in southwestern Kachchh. The Khari Series is made up of two distinct stages i.e. the lower Aida Stage is composed of variegated siltstone, the lower 16 m of which is barren, but the upper part contains Lower Burdigalian fossil assemblage. The upper part of the series, the Vinjhan Stage consists of grey to khakhi-coloured gypseous clay with hard marl bands packed with fossils. This stage forms the main bulk of the Lower Miocene of Kachchh. The clays of this stage contain a rich assemblage of Upper Burdigalian fossils. As the Khari series is seen overlapping the Deccan Trap directly, it suggests that this marine transgression was the most powerful one in the history of the Tertiary sedimentation in Kachchh.

***Kankawati Series*** : Well exposed around Kankawati river between Sandhan and Vinjhan, this series consists of grey micaceous and calcareous sandstone, lenticular bands of conglomerate and Khakhi grey clay. The upper part is mainly pinkish hard calcareous grit and conglomerate containing abundant foraminifers. This series has

been tentatively assigned a Pliocene age and has been correlated with the Manchhar Series of Sindh-Baluchistan.

### **Geology of the Island Belt**

The Island Belt consists of four discontinuous landmasses called as the Pachham, Khadir, Bela and Chorar islands. The islands are surrounded by the ranns (local word meaning saline wasteland) that is characterized by the flat salt-encrusted surface and occurs at few meters above the mean sea level. The ranns are considered to be uplifted floor of the former gulf (Merh 2005, Maurya et al., 2008) which was navigable upto ~2ka as suggested by historical accounts (Oldham 1926). The Rann surface is inundated under a thin sheet of water during the annual monsoon rains and storm tides from the western end where it opens up into the Arabian sea (Roy & Merh 1981). The term 'island' is therefore used here in a descriptive sense and not in the true sense of the word.

The four islands though occurring as disjointed land masses show comparable geological, structural and geomorphic set up (Biswas 1977, 1987, 1992, 1993). The general stratigraphy of Island belt comprises of Mesozoic and Tertiary Rock (Fig. 1.3). Tertiary rocks are exposed only in the south eastern and south western fringe of Khadir Island while it covers two-thirds of the Bela island. The Cheriya Bet Conglomerate Member is the oldest rock of the Kachchh Basin that is exposed in the northern part of the Khadir island. This is overlain by Hadibadhang Shale Member followed by the Hadibadhang Sandstone Member. The Ghadada Member occupies most of the island which is capped by the Bhambhanka Member. In Bela island, a comparable succession of Mesozoic rocks is exposed, however, the basal Cheriya Bet Conglomerate Member is not exposed. The Bhanjada island is a stock like basic intrusive body related to magmatic activity during the end of Mesozoic (Biswas 1993).

The Mesozoic sequence is unconformably overlain by Tertiary rocks of Chhasra and Sandhan Formation. Chhasra Formation is comprises of a Lower Claystone Member and Upper Siltstone Member (Biswas 1992). The Lower Claystone Member consists of grey and khakhi coloured, laminated to splintery gypseous shale and clay stone with thin fossiliferous limestone. While Upper Siltstone Member comprises of micaceous siltstone and laminated khakhi colour silty shale. This Formation is exposed in Bela island only. This is overlain by Sandhan Formation mostly comprising sandstones with subordinate amount of conglomerate, claystone, laminated siltstone and fossiliferous limestone. This formation is exposed in both Bela and Khadir island.

In Bela and Khadir island, the Mesozoic rocks are folded into E-W trending flexures called as the Lodrani anticline and the Khadir anticline respectively (Biswas, 1993). The escarpment is formed in the southern limb of the anticlines while the northern limb is eroded away. The straight northern margins of the islands are attributed to the E-W trending Island Belt Fault (IBF) in the north that is presently buried below the marine sediments of the Rann. Overall, the geomorphic set up and landscape of the islands is strongly controlled by the inherited structural framework. Neotectonic tilting of the islands towards south occurred in response to tectonic activity along the E-W trending Island Belt Fault (IBF) has been documented (Chowksey et al. 2010).

#### **SUMMARY OF AVAILABLE GEOLOGICAL DATA ON THE GREAT RANN**

Previous works on the Ranns of Kachchh have been very few and far between. Earliest systematic descriptions of the rann surface comprise mainly the reports that documented the dramatic geomorphological changes brought about by the well known 1819 Allahbund earthquake (for example Burnes 1835, Oldham 1926). Most of these works deal with geomorphologic and seismotectonic aspects of the Great Rann. All workers have considered the ranns as a surface that has emerged out of the sea in geologically very recent times. The flat landscape of the Ranns is variously described as 'intriguing' to 'unique' to 'without any counterpart in the world' (Burnes 1835, Roy and Merh 1981). In local dialect, the term 'rann' means 'saline wasteland'. In general, the Great and Little Ranns are considered to be uplifted floor of the former gulfs (Merh 2005, Maurya et al. 2008). The Great Rann was an E-W trending gulf that joined up with the Arabian Sea in the west while the Little Rann is believed to mark the landward extension of the present day Gulf of Kachchh. Historical accounts suggest that a navigable sea existed at least upto ~2000 yr B.P (Oldham 1926). Preliminary studies on the surficial sediments of the ranns indicate that these are mostly clay rich which is in agreement with the marine origin of the terrain (Srivastava 1971, Glennie and Evans 1976). Glennie and Evans (1976) described the present conditions existing in the rann as coastal sabkha to supratidal environments. However, no further details on the subsurface stratigraphy or the nature of basin are available. Moreover, very little information exists on the sedimentologic, stratigraphic and neotectonic aspects of the Rann sediments. This may in part be attributed to the marshy nature of the surface, very shallow water table and the hostile and inhospitable

terrain. Moreover, the ranns get submerged annually under a thin sheet of water (Roy and Merh 1981). The Ranns are approachable only during the summer months when the Rann surface dries out with temperatures hovering above 45°C.

In recent times, one aspect of the ranns that has received considerable attention from the contemporary workers is the repeated liquefaction of the Rann sediments due to large magnitude earthquakes that have occurred along various E-W trending faults of the Kachchh basin. The Ranns of Kachchh is a crucial Quaternary terrain of western India, which has witnessed some of the rigours known earthquakes in the Indian subcontinent. Role of coseismic deformation is aptly demonstrated by the 1819 earthquake which about large scale geomorphic changes in the Great Rann. The 1819 earthquake is believed to have produced a ~90 km long scarp in the northern part of the Great Rann and widespread liquefaction in the Ranns (Oldham 1926, Bilham 1998, Rajendran and Rajendran 2001). Rajendran and Rajendran (2001) have interpreted the Allahbund scarp as a surface fold related to movement along a subsurface fault and suggested that the previous event of comparable magnitude occurred about 800-1000 ya ago in the Great Rann. Liquefaction features related to past earthquakes in historic times have been reported from the Great Rann of Kachchh (Sohoni and Malik 1998; Rajendran et al. 1998). The 1956 Anjar earthquake and the 2001 Bhuj earthquake also resulted in widespread liquefaction in the rann sediments whereby large amounts of saline water and sandy sediments were ejected from the subsurface (Chung and Gao 1995, Tuttle et al. 2002). A Ground Penetrating Radar (GPR) based subsurface study of large sand blow craters produced during the 2001 earthquake suggest that the liquefiable sand rich sediments occur at >6m (Maurya et al. 2006). This is inferred from the continuity of feeder vents up to that depth. It has been suggested that these craters can serve as modern analogues for investigating similar features formed during previous large magnitude earthquakes (Thakkar et al. 2012). In general, the geomorphic setting of the rann is attributed to the complex interplay of sea level and co-seismic tectonic activity during the Holocene (Merh 2005) which continues even today.

Overall, the available literature convincingly establishes that the rann basins were submerged under sea due to the rapid eustatic sea level rise during the Holocene (Fig. 2). However, it is clear from the above summary that practically all geological researches have been directed at the Great Rann while Little Rann has received negligible attention. Gupta (1975) based on study of subsurface sediments and

radiocarbon dating near Surajbari and Kharaghoda has suggested that the Holocene sequence is divisible into two distinct layers – the upper silty clay (4,200 to 1,500 yr BP and sandy clay (9,000 to 4,200 yr BP). Below -15 m these sediments show erosional contact with yellowish clay dated to 16,200 yr BP (late Pliocene). It is not clear whether the late Pliocene sediments are of marine or fluvial origin, however, they are shown to be devoid of marine megafossils. It has also been suggested that the Little Rann was under 4 m water depth up to ~2 ka B.P (Gupta 1975). However, as the data is based on study of sediments at Surajbari and Kharaghoda, at the extreme ends (margins) of the basin, it does not reflect the true thickness of the Holocene Rann sediments.

From the above summary, it can be seen that the geological evolution of the rann remains intriguing as there are very few studies document the nature of the rann sediments and the present and past depositional environments. Unfortunately, studies that adequately describe the Quaternary sediments Ranns of Kachchh in terms of lithostratigraphy, depositional processes and palaeoenvironments are non-existent.

### MATERIALS AND METHODS

Present work is a systematic attempt to understand the overall geological evolution of the Great Rann of Kachchh basin using comprehensive field studies and multiproxy studies on two deep cores obtained from the difficult terrain of the Great Rann for the first time. An integrated approach of field and various laboratory analyses applied to achieve objectives of this study by using several scientific methods. The field survey and geomorphic mapping are used as a primary component to study the present geomorphic set-up of the rann basin. The surface and exposed sediments were subjected to sedimentological, mineralogical and micropalaeontological studies to decipher the modern and past environmental conditions. However, to reconstruct the palaeoclimatic, palaeoenvironmental and provenance history of the basin a complete depositional record is required, therefore drilling and coring formed an important part of the present study. The cores were subjected then for sedimentological, clay mineralogical, micropalaeontological, geochemical and isotopic studies. The present chapter describes the approach and methodological aspects of the field as well as laboratory exercises included in the study.

#### GEOMORPHOLOGICAL STUDIES

The Great Rann has long been considered as a geologically enigmatic terrain that has primarily resulted from continuous shallow marine sedimentation in an embayed gulf and subsequent drying up (Maurya et al. 2013). On mega-geomorphic scale, the entire Great Rann is regarded as a vast, flat saline terrain. However, the most intriguing feature of the Great Rann is the spatially variable annual submergence during the monsoon season which imparts a general heterogeneity to the otherwise flat monotonous dry flat landscape in the hot and arid summer season. The spatial variability of the degree of submergence points to the subtle variations of the surface of the Great Rann on micro-scale. In the present study, efforts were made to characterise the subtle variations in the topography of the monotonous flat terrain. For this purpose, a detailed topographic analysis of the Great Rann was attempted. Several topographical cross sections were prepared to bring out the relief characteristics of the surface of the Great Rann. The topographic profiles were

prepared on the basis of the elevation data available on the Survey of India topographical maps on 1:50,000 scale. Several cross profiles were also constructed from the Googleearth data (source-www.googleearth.com). The results of the topographic analysis were interpreted in terms of the surface and subsurface structural features delineated by previous workers.

The detailed field studies were carried over the past four years in various pockets of the basin. The field approach applied during the present study led to the discovery of the raised rann sediments, marine erosional and depositional features along the island margins which have significant implications for understanding the palaeoenvironments and neotectonic activity. The raised rann sediment sequences were sampled at high resolution (5cm interval) by step trenching for dating and various laboratory analyses.

## **CORE DRILLING**

A few raised rann sediment sequences in the form of continuous cliffs are significant yet insufficient to provide insights into the overall evolution of the basin. Therefore, drill cores were raised from two different locations in the year of 2010. The selection of the sites for core drilling was done on the basis of detailed field studies and an overall understanding of the subsurface structural framework of the Great Rann basin.

The core drilling operation was performed using rotary drilling method in April 2010. Two continuous drill cores were raised from the central and marginal parts of the Great Rann of Kachchh basin. The tough quality PVC pipes of 63mm diameter with variable lengths were used to recover the complete, undisturbed sediment cores at both the locations. Logging while drilling (LWD) based on the bit core samples was also done simultaneously during the operation.

The first drilling site was on the salt encrusted rann surface in 2-3km north of Dhordo village located at the northern edge of the Banni plain. It lies in present day seasonal inundation zone of the rann basin. During the SW monsoon, tidal waters occupy this region for several months and dry out only in the month of March/April till June every year that leaves the thin salt encrusted rann surface (Fig. 2.1a). The Dhordo Core site (N 23°49' 37.9"; E 69° 39' 09.0") is located in the central part of the Great Rann basin and is

expected to represent the long depositional history of the rann basin as a whole. This core recovered a continuous sediment record for ~60.40 m below the rann surface.

The second drilling site is located to the north of Berada village in the Banni plain region which is close to the rocky mainland Kachchh hills further in the south. The Berada Core (N23° 28.9' 12"; E 69° 54' 36.34") runs up to ~51m below the typical Banni surface (Fig. 2.1b). The Banni plain represents the southern marginal part of the Great Rann basin.



**Figure 2.1** Field photographs showing drilling sites at both the core locations and core pipe measurements during operation. (a) Dhordo Core site, (b) Berada Core site. Please note the foreground at Dhordo drill core site showing the salt encrusted rann surface whereas at Berada drill core site denotes typical banni surface with polygonal cracks on surface. (c) Pipe recovery after drilling and (d) Core recovery measurements, on site logging and packing of individual core pipes.

## LOGGING, X-RAY RADIOGRAPHY AND SAMPLING

A Logging While Drilling (LWD) based on the bit core samples was done to build a filed litholog of the subsurface sediments (Fig. 2.1c and 2.1d). Each individual pipe was systematically numbered, classified and placed in a large container jeep to move the base at Bhuj. Each individual core pipe was then undergone to X-ray radiography in the nearest possible location at Bhuj to avoid the secondary disturbance in the sediment/sediment structures (Fig. 2.2 and Fig. 2.3). After X-Ray radiography all the core pipes were moved to the Micropalaentology/Core Lab at Department of Geology, Faculty of Science, The Maharaja Sayajirao University of Baroda, Vadodara.

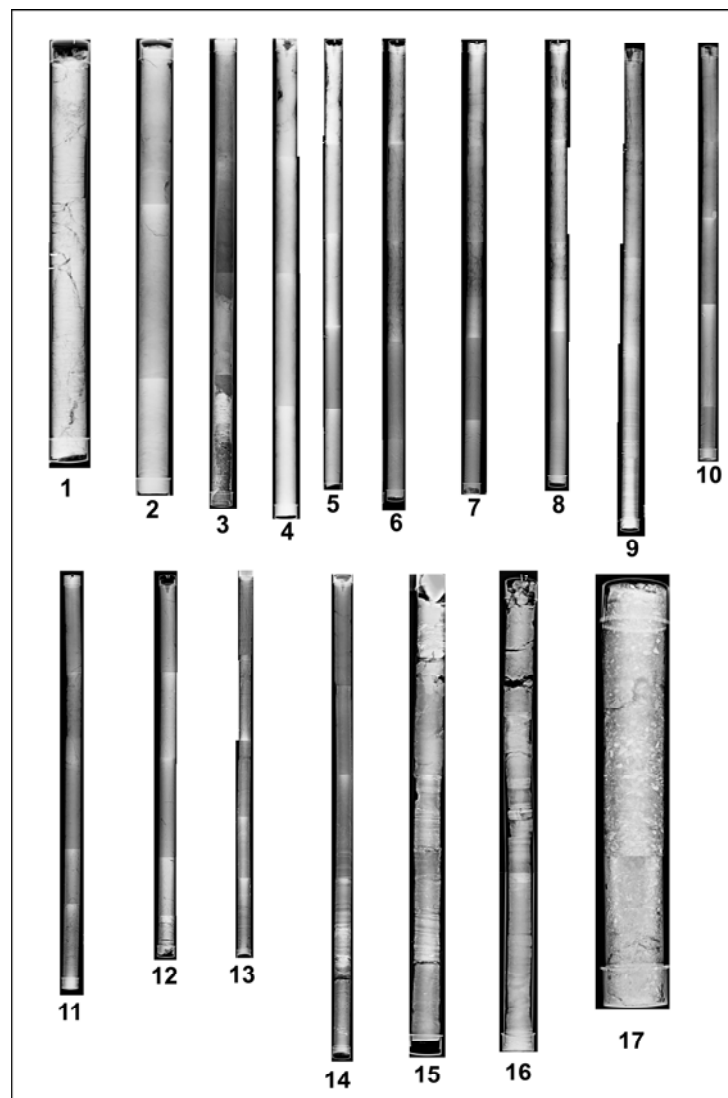


**Figure 2.2** X-Ray radiographs of all core pipes from Berada Core site. Note the excellent core recovery and fine scale laminations in the core pipes.

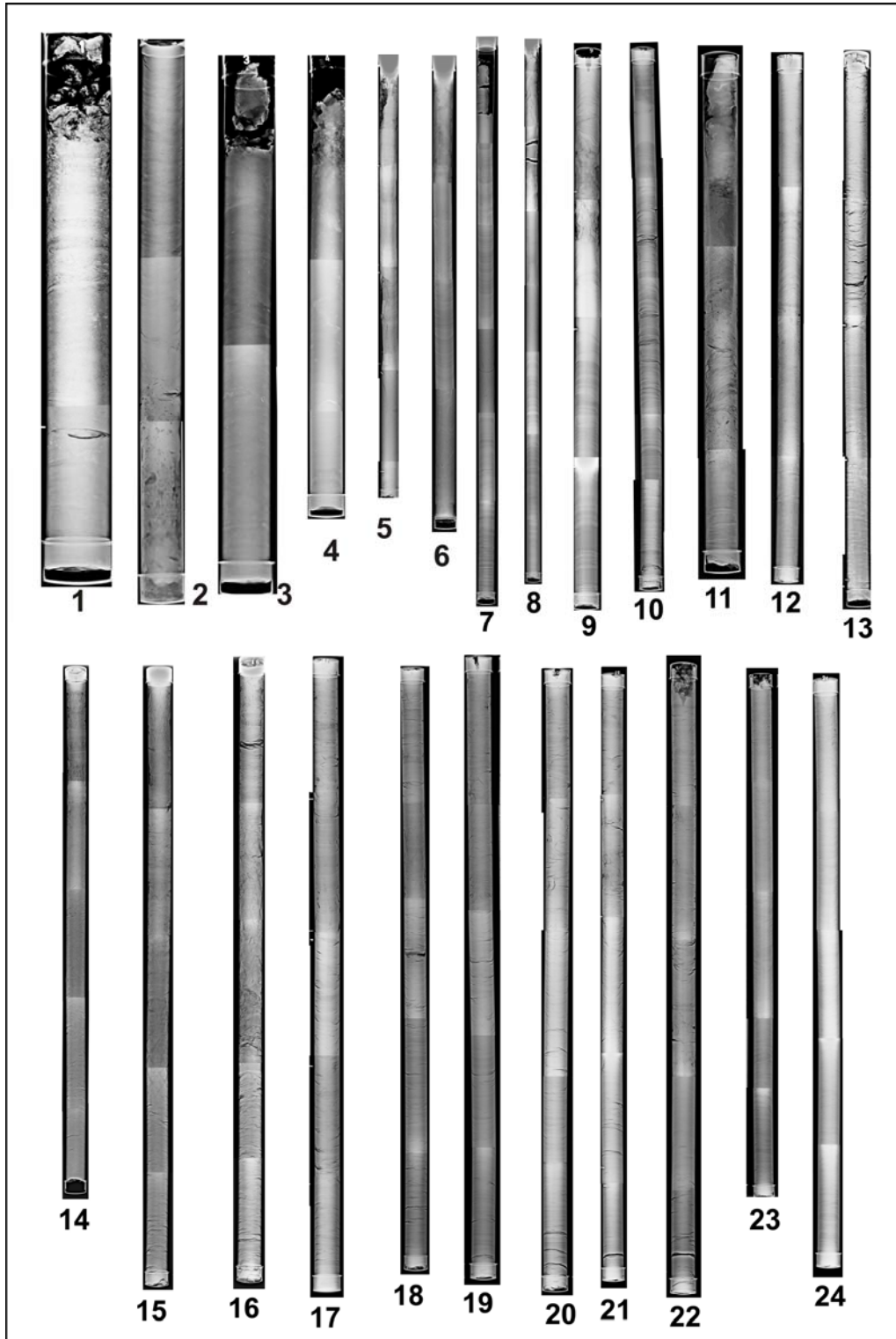


**Figure 2.3** X-Ray radiographs of all core pipes from Dhordo Core site. Note the core excellent recovery and fine scale laminations in the core pipes.

The Core cutting and splitting was done in the core lab using suitable apparatus. The detailed physical examination and photography of all the core sections was done after splitting. The entire colour, textural variations were noted for each individual core pipe and sub-sampled at ~2cm interval. All the labeled samples and one half core section is preserved in two separate deep freezers at subzero temperatures at Micropalaentology/Core Lab, Department of Geology, Faculty of Science, The Maharaja Sayajirao University of Baroda, Vadodara.

### LABORATORY ANALYSIS

The present study employed multiproxy laboratory based analysis to fulfill the objectives of the study. A schematic view of the adopted tools are given in Fig. 2.4.

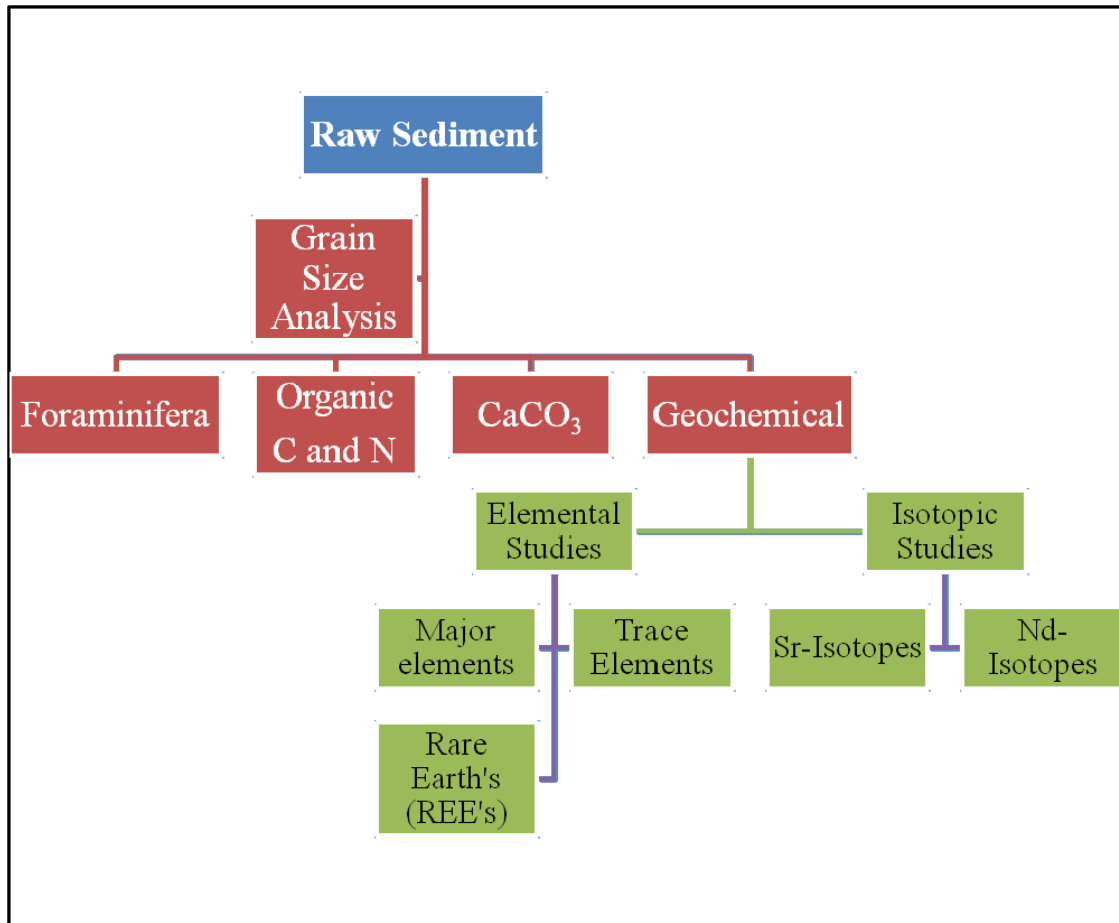


**Figure 2.4** Schematic view of the multi-proxy studies carried out during the study

## **TEXTURAL ATTRIBUTES**

Sediment samples collected from the modern rann surface in the northwestern rann i.e. Bet Zone, raised rann sediments from the cliff sections and core sediments were subjected to the grain size analysis using conventional pipette method as described by Folk (1974). All the sediment samples first dried at ~90° C for overnight and allowed to cool at room temperature. Organic content in the sediments was removed by treating with mild Hydrogen Peroxide solution (6%). The dried samples were then sieved through ASTM (American standards for testing materials) standard 63micron sieve to separate the sandy fraction in the sediments. Silt and clay fractions were then calculated by pipetting silt fraction. The grain size parameters were calculated for each sample and their textural classes have been assigned following Flemming (2000).

## **MICROFAUNAL STUDIES**

Microfaunal studies on the rann sediments (modern surface sediments, raised rann sediments and core sediments) was attempted to understand the modern and past environmental conditions. Foraminifera are wide spread, typical of the marine environments and sensitive to even small scale change in the environments therefore they can be useful in reconstructing the palaeoenvironmental history of the region (Murray 2006). Therefore, foraminifera is the major tool used for the present study, although, other microfossils such as algae, ostracods, bivalve and gastropods were also collected.

### **Foraminifera separation**

The sediment volume of about ~5-10g of each sample was homogenized and taken into 400ml beaker filled with distilled water. A 6% mild Hydrogen Peroxide (6%) was used to oxidize the organic matter. If necessary, a small amount Sodium Hexametaphosphate added as dispersing agent at 60-70° C. The sediment was then wet sieved through the ASTM standard 63 micron sieve. The collected sand fraction of these sediments was homogenized by coning and quartering after drying. Foraminiferal separation from these sediments was done by conventional hand picking method under stereoscopic stereozoom binocular microscope. The separated foraminiferal tests were then classified into various genera and species level using the standard literature for the recent environments (Loeblich and Tappan 1988, Murray 2006, Walton and Sloan 1990,

Carboni and Bella 1996, Hayward and Holis, 1994). The conformation of the identification was based on the comparison of the morphological features documented in the reliable literature and SEM (Scanning Electron Microscope) images. Identified assemblage is tabulated for the quantification and environmental interpretations.

## **CLAY MINERALOGICAL STUDIES**

The clay mineralogical studies using X-Ray Diffraction is now widely accepted proxy for the palaeoenvironmental, paleoclimatic and provenance studies (Biscay 1965, Gingele 1999, Singer 1984, Kolla et.al. 1982). In present work, the clay mineralogical study was done for deciphering the provenance of the rann sediments. The surface sediments from the northwestern rann and both core samples were studied for the clay mineral assemblage to know the present as well as the past source of the rann clays. Clay mineralogy is also useful indicator for the environmental and weathering history of the hinterland region (Alizai et.al. 2012) and is also used in present study. The sample details and methodology is described below-

### **Subsurface Rann Sediments (Core Sediments)**

To represent the overall distribution of clay minerals in both Dhordo and Berada core total 53 samples were selected for the X-Ray Diffraction studies from various litho-units identified in each core. Selected samples were treated for the desalinization by repeated wash with the distilled water. The organic content was removed with the help of Hydrogen Peroxide (6%) solution. Following the standard procedure as mentioned by Folk (1968) the clay mineral (>63mm size) slide samples were prepared by the settling velocity principle based on Stock's law. The processed sample was then placed on the glass slide by pipetting of concentrated clay aliquot and allowed to air dry in lab. The oriented slides were then exposed to Ethelene Glycol solution at 100<sup>0</sup> C for one hour to allow glycolation process. All the glycolated samples were then scanned from 2<sup>0</sup>-30<sup>0</sup> 2θ on RIGAKU X-Ray Diffractometer (Model-Ultima IV) using Nickel filtered CuKα radiations operated at 40 kV and 20 mA.

The generated data for each sample was then plotted in XY graph with the help of Origin 9.2 and baseline correction was done by assigning points manually. Identification of the major mineral groups of Smectite, Chlorite, Kaolinite and Illite was done. Semi-

quantification for each mineral was done as per Biscay (1965) formula. For calculating relative percentages of the major clay mineral groups present in the given samples factor of 1 to Smectite (17Å), 4 to Illite (10Å) and 2 to Kaolinite and Chlorite (7Å) together was multiplied. Kaolinite and Chlorite individual percentages were calculated with peak areas of (3.54 Å) and (3.58 Å) respectively. The Illite chemistry was deciphered by using peak area of 5 Å and 10 Å peak areas of illite (Esquevin 1969). The ratio below 0.5 represents Fe, Mg-rich illites (biotites, micas), which are characteristic for physically eroded, unweathered rocks whereas above 0.5 indicate Al rich illites which are formed by strong hydrolysis (Gingele 1996). Crystallinity index was measured by HHW (Half Height Width) of 10 Å peak of illite.

### **CACO<sub>3</sub>, ORGANIC CARBON AND NITROGEN**

Total carbon and nitrogen in the rann sediments was measured using the NC analyzer (FISONS model NA 1500) and Calcium carbonate (CaCO<sub>3</sub>) was determined using Coulometer (UIC Coulometer; 5012) at Physical Research Laboratory, Ahmedabad.

For total organic carbon and nitrogen analysis, the dried samples were treated with the 10% HCl at 70°C for 2-3 hours and washed and dried again. The dried residue about 10-20 mg sample packed in tin foil/cup, which later released into combustion chamber at 1050° C. The evolved CO<sub>2</sub> and nitrogen oxides are then passed through a reduction chamber controlled at 650° C that contains copper mettle. After further purification the gases are passed through a gas chromatograph (kept at 60° C) that releases them sequentially. The gases enter into a thermal conductivity detector, which generate electric signals proportional to the concentrations of the gases present. The calibration curve is prepared using LOSS (Low Organic Sediment Sample) containing 1.65% and 0.52%; Deer River Black Shale as a standard, having 2.53% C and 0.12% N as a reference material (Bhushan et.al. 2001).

For CaCO<sub>3</sub> measurement bulk sediment samples were used. CO<sub>2</sub> was evolved from samples through the extraction unit by treating nearly ~10-30 mg of sample with 5ml of 30% H<sub>3</sub>PO<sub>4</sub> at 70° C. CO<sub>2</sub> free air (stripped by passing it through a 50% KOH solution) was used as carrier gas for flushing CO<sub>2</sub> from the system. The CO<sub>2</sub> liberate was flushed by the carrier gas and dried by passing it though a column of activated silica gel

and anhydrous  $MgClO_4$ . The dried  $CO_2$  thus obtained was then passed through the coulometer titration cell (with Pt cathode and Ag anode) containing monoethanol amine solution and an indicator. Pure and dried  $Na_2CO_3$  was used as a standard for calibration. The precision of  $CaCO_3$  measurement by coulometric analysis is less than 1% (Bhushan et.al. 2001).

## MAJOR AND TRACE ELEMENTS

Approximately 0.2 gm of bulk, dried sediment sample was subjected to closed digestion (in Thermo Microwave digestion system) by treating with HCl, HF and  $HNO_3$  acids using standard protocol (PRL, Ahmadabad). The digested samples were again dried and underwent open digestion if the silica or organic particles remained. The dried precipitate after open digestion was diluted in 0.6N HCl in total volume of 25ml.

**Table 2.1** Table showing NOVA Standard values with the measured values during the analysis

Element	Measured	ICP-MS value
Fe (%)	5.59	5.82
Mg (%)	2.18	2.33
Al (%)	8.32	8.21
Cr (ppm)	85.49±0.11	84
Co (ppm)	106.96±1.57	101
Ni (ppm)	214.95±2.38	224
Cu (ppm)	386.59±2.34	403
Zn (ppm)	144.27±2.96	146
Sr (ppm)	170.72±1.93	182

A schematic view of the sample digestion procedure is given in Fig. 2.5. The measurement for the Major elements was done in ICP-AES (JOBIN-YVON, Model- 38S) and Trace was measured in Quadrapole-ICP-MS. An internal laboratory standard NOVA was prepared and standardized during the analyses of sediment samples. NOVA is a deep-sea clay sediment collected from the North Pacific (NOVA III-13; 3 55.6 N, 178 47.3 W) at water depth of 5351m (Amin et.al. 1972).

## ISOTOPIC STUDIES

### Sr and Nd isotopic measurements in silicate fraction

The sediment samples, ~1gm were dried at 90°C for 1-2 days; powdered with the help of agate mortar. This fine fraction was then sieved through a 100µm nylon mesh and homogenized. To remove the organic/inorganic carbonate content in the sediments the fine fraction is leached in 15ml centrifuge tubes with the help of 0.6N HCl at 60°C for ~30 minutes with ultrasonication. The leached fraction repeatedly centrifuged and treated with 0.6N HCl at 60°C with ultrasonication and finally washed with Milli-Q. This slurry was then ashed at 550°C to oxidize the organic matter in the sediments.

A known amount of ~100 mg of carbonate and organic matter free sample was taken into the taflon vials (Savillex®). The sediments were spiked with  $^{84}\text{Sr}$  and  $^{150}\text{Nd}$  and subjected to close digestion with the concentrated HF-HNO<sub>3</sub>-HCl acids at 90°C to bring the sediments into completely in liquid form. The digestion is repeatedly done if the particles remained in the dried residue. Pure Sr and Nd fractions were separated from the solution following standard ion exchange procedures (Rahman et.al. 2009, Singh et.al. 2008). A schematic view of the protocol is given in Figure 2.6. The collected pure Sr and Nd fractions was then dried and re-dissolved in 4ml of 0.4N HNO<sub>3</sub>. Both Sr and Nd measurements was done on MC-ICP-MS in static multicollection mode. In case of the strong electrical signals, samples are again suitably diluted with 0.4N HNO<sub>3</sub> acid.

After measurements the samples were corrected for the  $^{87}\text{Sr}/^{86}\text{Sr}$  and  $^{143}\text{Nd}/^{144}\text{Nd}$  for instrumental mass fractionation by normalizing measured  $^{86}\text{Sr}/^{87}\text{Sr}$  and  $^{146}\text{Nd}/^{144}\text{Nd}$  with respect to their natural values, viz. 0.1196 and 0.7219 respectively. The Sr and Nd concentration for these samples were obtained by isotope dilution method. A standard solution of 200 ppb of Neptune Sr-standard was measured several times on MC-ICP-MS, that yielded an average value of  $0.710303 \pm 0.000015$  (1  $\sigma$ , n= 10) for  $^{87}\text{Sr}/^{86}\text{Sr}$ . A few replicate samples were also measured for Sr and Nd concentration and isotopic composition to check the overall reproducibility of the Sr-Nd measurements (Table 2.2 and 2.3). Based on replicate measurements, the average variation between sets of repeats was determined to be 0.0002 and 0.2 for  $^{87}\text{Sr}/^{86}\text{Sr}$  and  $\epsilon\text{Nd}$  respectively.

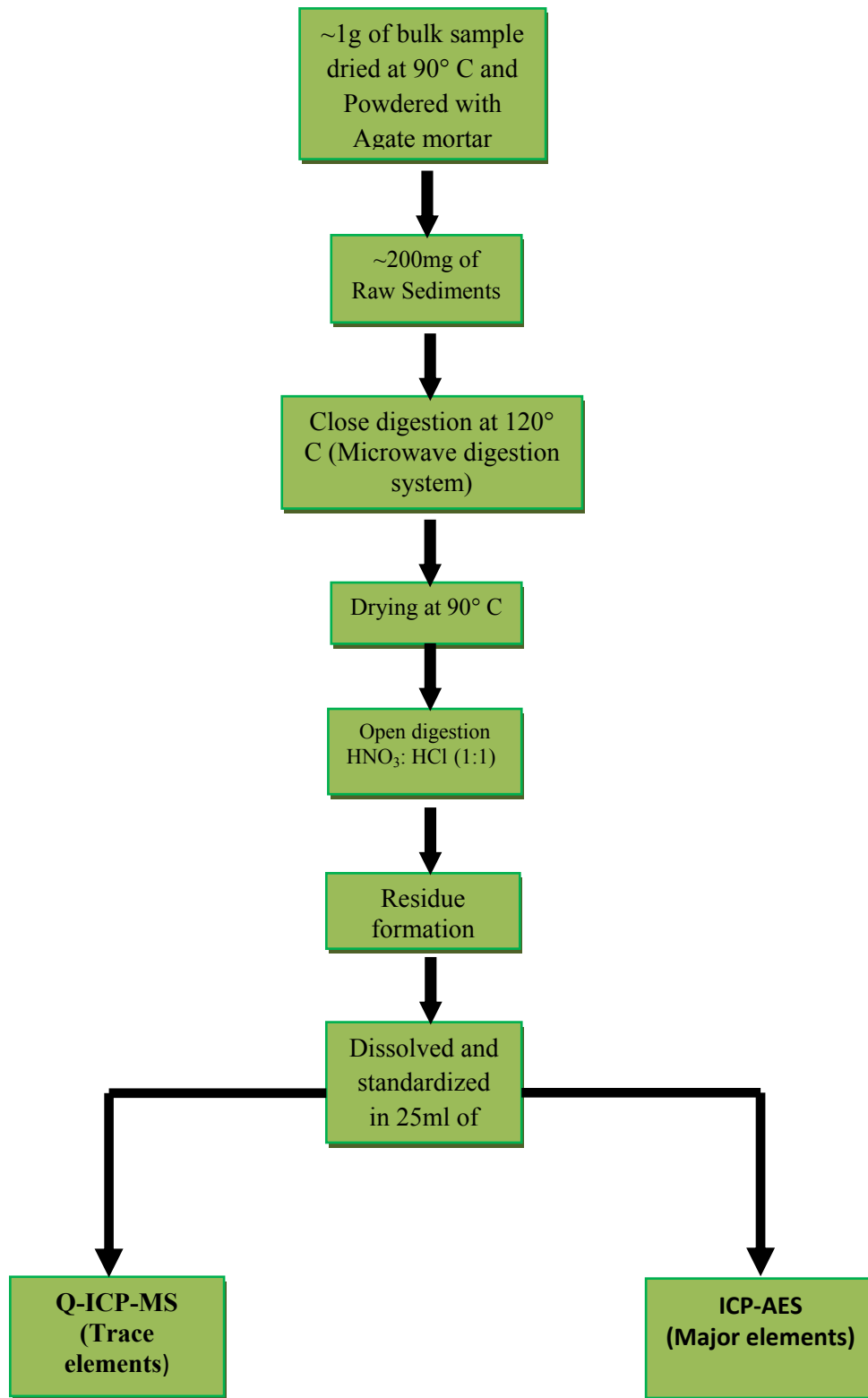


**Figure 2.5** Schematic view of digestion procedure followed for Major, Trace and REE's in sediment samples.

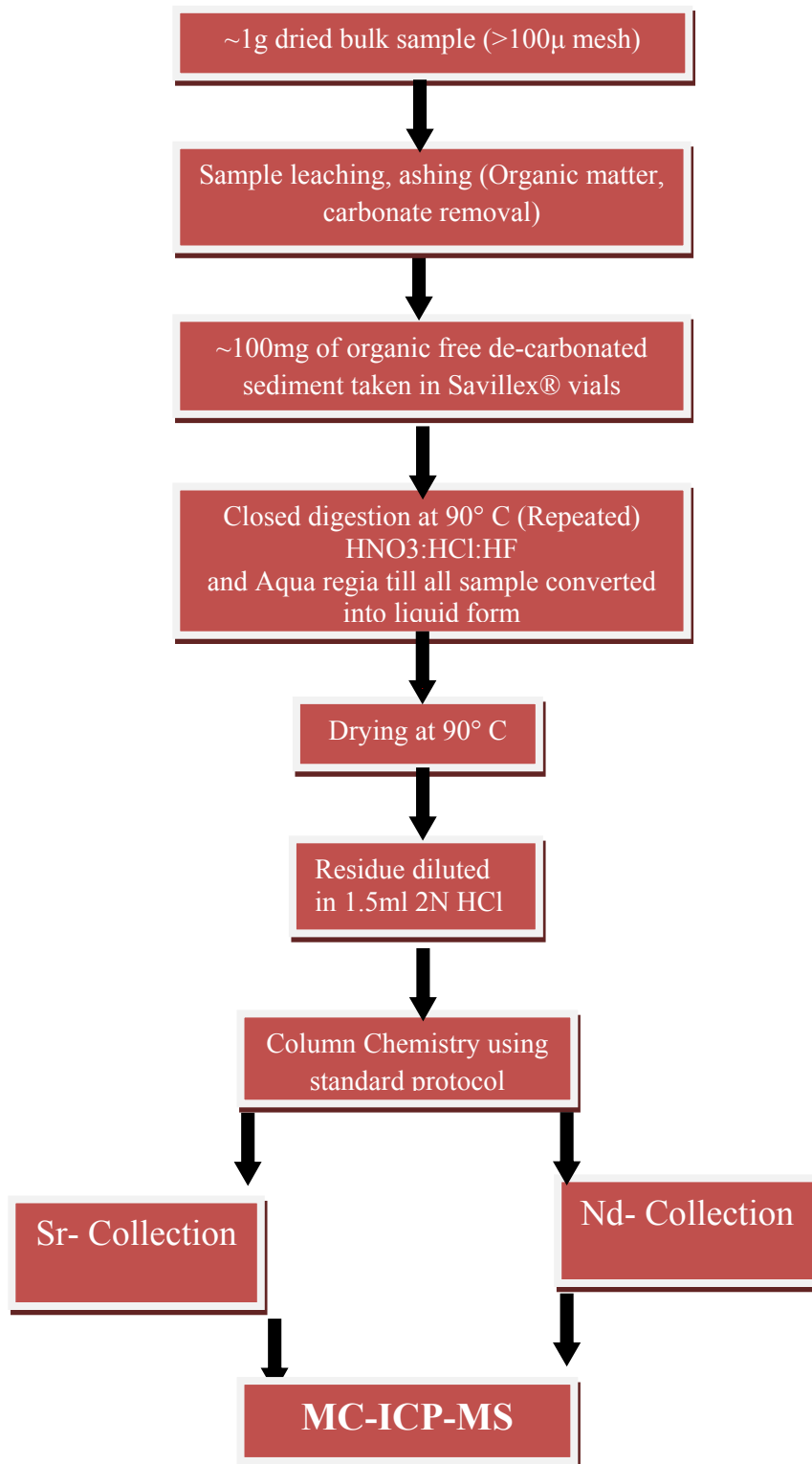


**Figure 2.6** Schematic view of sample processing protocol for Sr-Nd isotopic studies

**Table 2.2** Reproducibility of elemental and isotopic composition of Sr for the sediment samples

Sample ID	$^{87}\text{Sr}/^{86}\text{Sr}$	$^{87}\text{Sr}/^{86}\text{Sr}$ Std Error %	Sr ( $\mu\text{g/g}$ )	Sr ( $\mu\text{g/g}$ ) Std Error %
<b>DH-5-48</b>	0.72680	0.0016	121.2	0.0050
	0.72671	0.0011	120.9	0.0061
<b>DH-7-62</b>	0.72690	0.0021	117.5	0.0084
	0.72710	0.0009	117.7	0.0042
<b>DH-11-49</b>	0.73053	0.0011	148.4	0.0060
	0.73082	0.0012	147.9	0.0033
<b>DH-14-29</b>	0.72959	0.0033	107.2	0.0142
	0.72974	0.0025	107.3	0.0090
<b>BRD-4-19</b>	0.72826	0.0025	109.1	0.0110
	0.72798	0.0014	108.9	0.0053
<b>LUNI</b>	0.72992	0.0009	131.5	0.0029
	0.73010	0.0022	131.2	0.0066

**Table 2.3** Reproducibility of elemental and isotopic composition of Nd for the sediment samples

Sample ID	$^{143}\text{Nd}/^{144}\text{Nd}$	$^{143}\text{Nd}/^{144}\text{Nd}$ Std Error %	$\epsilon\text{Nd}$	$\epsilon\text{Nd}$ Std Error %	Nd ( $\mu\text{g/g}$ )	Nd ( $\mu\text{g/g}$ ) Std Error %
<b>BRD-1-19</b>	0.51195	0.0009	-13.4	0.7	16.3	0.0024
	0.51194	0.0010	-13.6	0.7	16.0	0.0024
<b>BRD-8-29</b>	0.51193	0.0009	-13.9	0.6	15.4	0.0029
	0.51194	0.0009	-13.7	0.7	15.1	0.0028
<b>DH-5-48</b>	0.51199	0.0019	-12.7	1.5	14.7	0.0044
	0.51198	0.0008	-12.9	0.6	14.8	0.0028
<b>DH-11-49</b>	0.51188	0.0007	-14.8	0.5	17.2	0.0018
	0.51190	0.0008	-14.5	0.5	14.6	0.0020
<b>DH-14-29</b>	0.51196	0.0012	-13.3	0.9	16.4	0.0027
	0.51193	0.0011	-13.7	0.8	16.4	0.0036
<b>RUPEN</b>	0.51188	0.0005	-14.8	0.3	17.7	0.0015
	0.51188	0.0005	-14.9	0.3	17.7	0.0015



**TECTONO-GEOMORPHIC STUDIES IN THE  
GREAT RANN BASIN**

The Great Rann is a tectonically formed basin that is bounded by the Kachchh Mainland Fault (KMF) in the south and the Nagar Parkar Fault (NPF) along the Indo-Pak border in the north (Biswas 1987). The eastern margin is marked by the West Cambay Basin Margin Fault (WCBMF). Towards the west the basin opens up to the Arabian Sea and the Indus delta region. The Kachchh Mainland Fault (KMF) forms the southern basin bounding fault of the Great Rann basin (Fig. 3.1). The fault has been known to be active during Quaternary and is responsible for the 1956 Anjar earthquake and the 2001 Bhuj earthquake (Biswas and Khattri 2002, Chouksey et al. 2011). The KMF is marked by E-W trending north facing line of scarps that separate the Northern Hill Range to the south and the Banni plain in the downthrown northern block. A 2-3m wide zone of deeply incised Quaternary colluvio-fluvial and fluvial deposits separate the Banni plain from the deformed Mesozoic rocks of the Northern Hill Range. Various rivers draining the mainland disappear into the Banni plain. Presumably, the Quaternary tectonic activity along the KMF and the NPF resulted in the subsidence of the Great Rann basin which facilitated the incursion of the sea and deposition of a huge thickness of marine sediments in the Great Rann basin. No details on the Quaternary tectonic activity along the northern basin bounding fault, the E-W trending Nagar Parkar Fault (NPF) is known. The basin formed a major sink for sediments that are believed to have come from variety of source regions viz. Aravalli rocks, Mesozoic and Tertiary rocks within the Kachchh basin and Himalayan rocks (Merh, 1995).

**GEOMORPHOLOGY OF THE GREAT RANN**

The major factor responsible for the unique present day geomorphic characteristics of the rann surface is its periodic submergence by sea water and monsoon precipitation. The flat rann surface and the negligible gradient allows extensive inundation by sea water from the Arabian sea in the west and by river waters from the north east and south during the monsoon season (Roy and Merh 1981). The inundation periods are separated by relative long periods of dry and hot saline wasteland conditions during the summer season. Overall, the alternate wet and dry

condition in the Great Rann of Kachchh has resulted in a unique and hostile terrain whose environmental condition fluctuates between extremes.

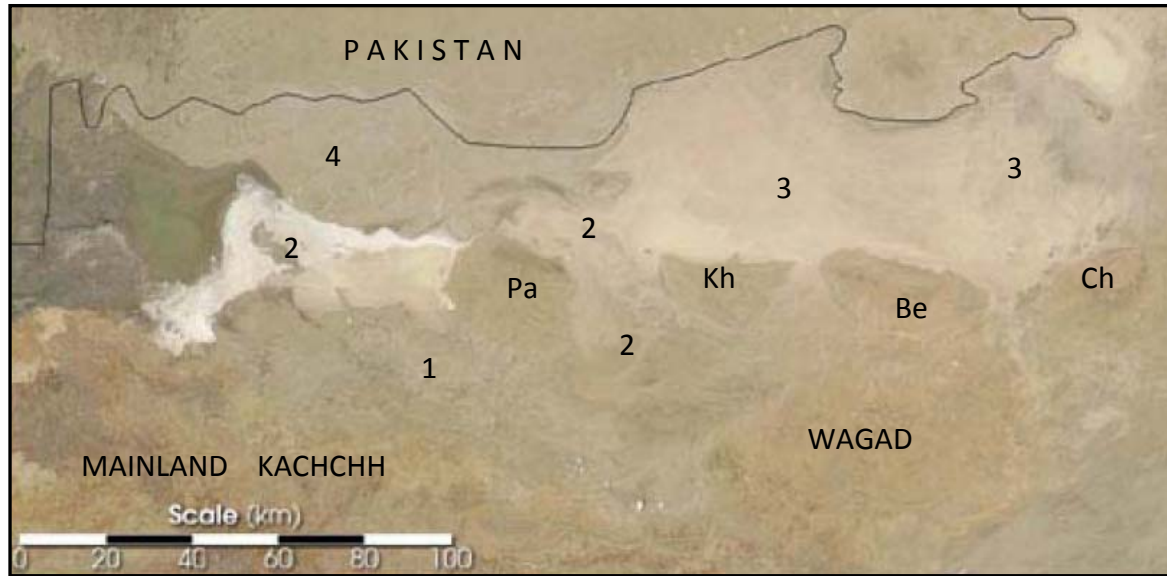


**Figure 3.1** Satellite image of Great Rann of Kachchh basin showing the variations in surface morphology. The image shows the completely dry rann surface as it appeared in the extreme arid season in May, 2003 (Source-[www.earthobservatory.nasa.gov](http://www.earthobservatory.nasa.gov)). The geomorphological divisions of the Great Rann (1-4) are also indicated. 1-Banni plain, 2-Supra tidal salt flat, 3-Inland saline flats and 4-Bet zone. (Pa-Pachham island, Kh-Khadir island, Be-Bela island, Ch-Chorar island)

### Geomorphic Divisions

The major geomorphic components of the Great Rann are the almost flat and gradientless surface, hereafter described as the rann surface, several islands (locally called ‘bet’) of different shapes and sizes and the roughly E-W trending Allahbund scarp (Fig. 2.1). Part of the extensive rann surface is salt encrusted while the remaining part is free of salt crust though the sediments are inherently saline. The most overbearing part of the rann is the flatness of the rann surface that lies 2-6m amsl (Fig. 3.2). The rann surface is dotted with several large to small islands that remain above the submergence level. These include the structurally controlled large rocky islands like Pachham, Khadir, Bela, Chorar and small rocky islands like the Bhanjada bet, Kuar bet, Mori bet and the Gainda bet (Fig. 3.1). All these islands show rocky hilly topography and expose Mesozoic and Tertiary rocks. In addition to these, there are several smaller islands rising up to 1-10m above the rann surface, especially in the northern part of the Great Rann and consist of sediments similar to the rann surface raised to a higher level. The top cover of these islands is usually made up of 0.5 - 2m thick aeolian sediment blown from the wind- swept surface of the rann.

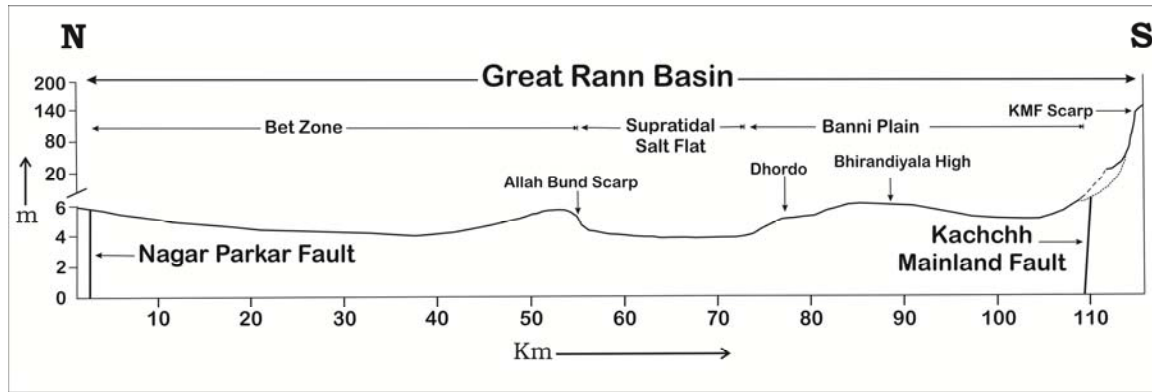


**Figure 3.2** N-S topographic profile across the Great Rann basin showing the geomorphic divisions. Vertical scale is highly exaggerated. The elevation data is based on the SOI topographical maps (survey years-1960-66).

Glennie and Evans (1976) described the present conditions existing in the rann as coastal sabkha to supra tidal environments. Based on the present day submergence pattern and surficial characteristics, the Great Rann of Kachchh has been geomorphologically divisible into four units (Roy and Merh 1981) - Bet Zone, Linear Trench Zone, Banni plain and the Great Barren Zone. However, many of the terms used so far for describing the rann surface do not take into the precise environmental characteristics and the causative processes. For example the terms ‘sabkha’ and ‘playa’ used by Glennie and Evans (1976) are commonly used in the geological literature to describe salt encrusted plains. The usage of these terms over a period time for describing closely related terrains have led to geological definitions that are at variance with their literal translations, and their usage is therefore subject to confusion (Goodall and Al-Belushi, 1997). Similarly, the term saline pan is also avoidable, because of conflicting definitions (Shaw & Thomas 1997). According to Goodall et al. (2000), use of the descriptive term salt flat is preferable for such terrains as it has a geomorphic as well as environmental connotation, instead of the Arabic word ‘sabkha’ or the Spanish word ‘playa’. However, the term salt flat cannot be used exclusively for describing the Great Rann as the entire area of the Great Rann is not a salt flat. In fact, there are large areas like the Banni plain, the northern part of the Bet zone and the eastern extremity of the basin which are free of salt crust. Moreover, the terms Linear Trench zone and the Great Barren zone used by Roy and Merh (1981) to describe the respective marine and monsoon precipitation influenced low level areas of the rann also do not clearly convey the environmental characteristics. As a result of the present geomorphic investigations of the Great Rann, a new set of terms is proposed to define the various parts of the Great Rann showing variable geomorphic characteristics. Owing to very

small variation in elevation and imperceptible gradient, the boundaries between the various divisions are gradational. The geomorphic divisions of the Great Rann (Fig. 3.1) as delineated in the present study are - the Banni plain, the Supra tidal salt flat, the Inland saline flat and the Bet zone

### ***The Banni plain***

The Banni plain is a vast flat terrain, highly vegetated with shrubs and grasses, and extending from the mainland Kachchh in the south and the Pachham island in the north (Fig. 3.1, 3.3a). It is a distinct geomorphic surface of the Great Rann that occurs at the highest elevation and is consequently completely free of marine influence (Fig. 3.2). The sediments are however, inherently saline in nature. It also forms the only part of the Great Rann that is inhabited. The surface morphology is shaped by the annual submergence by thin sheet monsoon rains and aeolian activity. The surface elevation varies from 4-10 amsl with the scattered villages occurring on isolated high grounds while the rest of the part suffers annual submergence by rain water. Small depressions remain filled with water for longer periods of time and on drying up are covered by thin layer of salt. The entire terrain of the Banni plain is regarded as a vast raised mudflat (Kar 1995) that coincides with the subsurface Median High. Based on variations in elevation, Kar (1995) has divided the Banni plain into three sub-units- high level mudflat, an undifferentiated and sloping low level mudflat and a residual depression. The southern part of the Banni plain is at a relatively lower level. The western half of the Banni plain slopes towards west. The highest elevations occur in N-S alignment passing through Bhirandiyala in the northern part of the Banni plain. This geomorphic high overlies a E-W subsurface structural high documented by Biswas (1987).

### ***Supra tidal salt flat***

The supra tidal salt flat is a vast but linear and narrow E-W trending low lying zone with several centimetres thick salt crust between the Banni plain in the south and the Bet zone to the north (Fig. 3.2). This zone occurs at the lowest elevation (~2m) in the west and gradually rises to ~4m towards east (Fig. 3.1). Being at the lowest elevation, this zone forms the main pathway through which the saline waters of the Arabian sea in the west enter and spread out submerging about two-thirds of the rann surface to varying degrees depending upon the volume/magnitude of the ingress resulting in a thick salt crust (Fig. 3.3b). The very low gradients in the supra tidal salt flat allow storm-driven marine flooding to reach inland, typically up to the region

around Khadir island which is ~70 km from the limit of normal high tide level in the west. This flooding gives rise to shallow sheet of sea water, which persists for at least few weeks until the water evaporates. Evaporation to dryness results in several centimetres thick, residual salt crusts, which characterize the surface of the supra tidal salt flats (Fig. 3.3b, c, d). The extensive salt crust is basically a precipitated crust form by the evaporation marine waters forming brine like conditions. Salts crystallize within the progressively concentrating brine, usually at the water-air interface, and then fall to the bottom of the ponded brine to form a layered crust. This process is similar to the saline pan model of Lowenstein & Hardie (1985), with the precipitated crusts forming beneath standing water.



**Figure 3.3** a- Photograph showing the typical nature of the surface of the Banni plain. Sand storms as seen in the picture are a common sight during the peak summers. b- Photograph showing the typical extensive flat surface of the supra tidal salt flat. The salt crust is the result of regular marine inundation of the surface. c- Close view of the large polygonal cracks in the salt crust. d- Photograph showing the thickness (~10 cm) of the salt crust.

The formation of these crusts begins when the salt flats are flooded by marine water flooding, or by monsoon precipitation or by both. Evaporation causes the standing water body to become supersaturated with salts, mainly halite. Halite usually

begins to crystallize on the surface of the brine pool as rafts of laterally linked tabular crystals or hoppers (Dellwig 1955). The crystal rafts may be blown to the edges of the pools or may become too heavy to float and sink to the bottom (Handford 1991). Those that sink form the nuclei for the growth of cubic halite crystals. As the brine continues to evaporate, the pools become shallower, and wind-induced waves may cause the crystals on the bottom to be worked into straight-crested, symmetrical ripples (Goodall et al. 2000). By the time the brines have completely evaporated, a loose aggregate of up to 3 cm of halite rafts may have accumulated on the floor of the pool. This crust is initially planar, and the individual crystals are clearly visible but, after a few weeks, the original cubic form of the surface crystals is lost through dissolution by desert dew and through abrasion by wind-blown sediment.

The salt crust, composed principally of halite, commonly displays a distinctive pattern of ridges that are polygonal in plan form (Fig. 3.3c). The diameter of the polygons usually ranges from 1m to 4m. The polygonal pattern is the result of fracturing as a result of volume reduction brought about by either thermal contraction or desiccation. By analogy with polygon formation in periglacial settings and basalt columns, thermal contraction is the preferred causative agent of some workers (e.g. Lachenbruch 1962, Tucker, 1981). Comparison with polygonal cracks in clay soils, which undoubtedly form as a result of water removal (producing collapse of the clay mineral crystal lattices) (Abuhejleh and Znidarcic 1995, Konrad and Ayad 1997), has stimulated others to attribute the occurrence of this phenomenon in salt crusts to a desiccation origin (e.g. Neal et al., 1968).

Small-scale, salt-encrusted ridges or furrows, referred to as salt-crust wrinkles, are formed as a result of the modification of the surface morphology of pre-existing surface features. Fine, powdery halite may crystallize in the top few millimetres (<5 mm) of the surface sediment, which has the effect of destroying the original subsurface structures. At the surface, however, the halite cements the sediment only lightly, and its effect on the surface morphology is subtle. The addition of the halite delicately wrinkles the surface morphology.

### ***Inland saline flat***

This zone comprises the easternmost part of the Great Rann that is not influenced by marine submergence, but is inundated by monsoon precipitation and by the rivers from the east and north. The elevation rises towards the margins of the zone, giving it a shallow bowl like morphology and comprise inherently saline rann

sediments (Roy and Merh 1981). The fringes of this zone are free of salt crust (Fig. 3.4a). However, the central deeper part of this zone may show very thin millimetre scale salt crust. This is formed by concentration of flooding waters in salt content due to evaporation. These river waters, meteoric waters, rain or dew, may become enriched in two ways. When water collects in ephemeral ponds, it fully or partially dissolves any pre-existing crusts and forms concentrated brine when it evaporates. Such brines have a composition that is highly modified because of the fractional dissolution of the older crusts (Kendall 1984).



**Figure 3.4** a-View of the Inland saline flat to the north of Bela island. The scarp in the background marks the geomorphic expression of the Island Belt Fault (IBF). b- View of the typical salt crust free surface of the Bet zone. Note the contrast with the supra tidal salt flat shown in Fig. 3.3b. c- Northward view of the developing gullies in the northern most part of the Bet zone. The northward upslope nature of the surface is also clearly visible. d- Surface of the Bet zone covered with numerous bivalve shells which thrive during periods of submergence.

In addition, salt may arrive as windblown dust (Wood and Sanford 1995). Such crusts are usually less than 1 cm thick and have a high proportion of included sediment and adhering aeolian dust, which makes them dark-coloured (brown or grey). Seasonal rain causes these crusts to dissolve partially, and the ensuing evaporation leads to the

precipitation of small patches of white salts in hollows on the crust surface (Fig. 3.4a). After a few months, the white salt is darkened again by adhering dust. The surfaces of the crusts are typically very irregular and variable in relief.

### ***The Bet zone***

The Bet zone comprises the flat rann surface in the northwestern part of the Great Rann shows several bets occurring few metres above the rann surface (Fig. 3.4b, c, d). The Bet zone is delimited by the Kuar and Bedia bets in the east and the supra tidal salt flat in the south (Fig. 3.1, 3.2). To the north lie the sand ridges of Sind (Pakistan). Towards the west, the Bet zone imperceptibly merges with the Indus delta. The southern boundary of the Bet zone is marked by the Allahbund fault scarp. This zone comprises several bets (islands) of varying sizes with the rann surface occupying the inter-bet depressions. The Kuar bet, Mori bet and Gainda bet located at the SE margin of the zone expose Mesozoic rocks and exhibit cliffy margins. The other bets consist of sediments similar to those comprising the rann surface and are overlain by 0.5-2m thick windblown rann sediments. Some these bets like the Sarbela bet, Shakti bet and few others show vertical cliffs along their margins which abruptly rise above the rann surface.

## **TECTONO-GEOMORPHIC ANALYSIS**

The basin bounding faults as well as the intrabasinal structural features within the Great Rann like the Island Belt Fault (IBF), the Allahbund Fault (ABF) and the subsurface Banni faults show remarkable correlation with the geomorphic divisions described above. A critical evaluation of the elevation differences of the various geomorphic divisions of the Great Rann shows a remarkable correlation with the above mentioned regional structural elements worked out by Biswas (1987, 1993). All structural features have prominent geomorphic expressions. The Banni plain astrides the subsurface Median High, while the supra tidal salt flat and the inner saline flats occupy a structural depression to the north of the subsurface Bhirandiyala high and the Island Belt Fault (IBF). The extension of the supra tidal flats into a depression to the south of the island belt bounded by the anticlinal/domal flexure zone of the islands in the north, the N-S trending Median high in the west, the Wagad highland to the east and the mainland in the south. The Bet zone occurs on the upthrown northern block of the roughly E-W trending Allahbund Fault.

## The Bet zone

In addition to the bets with well defined margins, several elevated parts within the rann surface also exist which gradually rise above the rann surface. Many of these are comparable to the bets in terms of their size. Their surfaces comprise aeolian sediments and generally support small vegetation like scrubs and grasses of various size. Morphologically, the shapes of all bets and almost all elevated tracts described above are elongated in N-S direction, which, on a map gives the misleading impression of wide N-S trending channels separated by bets. However, these are not 'channels' in any sense as they are basically flat rann surfaces several tens of kilometers wide comprising the inter-bet regions (Fig. 3.5). The inter-bet rann surfaces get inundated by the northward ingression of the sea water from the supra tidal flat zone especially under the influence of strong monsoon winds. Once submerged, the water remains for a long period of time until it gets evaporated. Downward infiltration is negligible owing to the clay rich and impervious nature of the rann sediments. The marine submergence is complimented by the rain water and rivers debouching from the northern side. The northward and southward submergence directions appear to be responsible for the carving of bets and similar elevated tracts into N-S elongated shapes which is fundamentally related to the overall uplift of the Bet zone. The bets do not get submerged during inundation of the rann surface. However, many of the elevated tracts are submerged especially during the extreme submergence events. The surface of the Bet zone shows a very gradual northward slope away from the Allahbund scarp which testifies to the uplift along the ABF (Fig. 3.2).

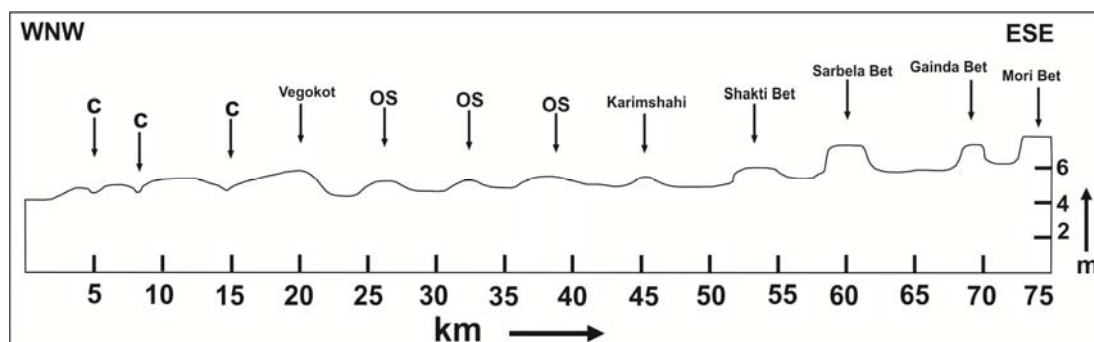


**Figure. 3.5** E-W trending topographic profile across the Bet zone. Vertical scale is highly exaggerated.

The western part of the Bet zone i.e. the area around Vigukot and further west shows submergence characteristics which is slightly different from the rest of the Bet zone and the Great Rann. This part of the Bet zone witnessed drastic geomorphological

changes after the 1819 Allahbund earthquake and subsequent flooding events of the now defunct distributary of Indus River that flowed into this region joined Kori creek in the south before the earthquake (Burnes 1835, Oldham 1926, Bilham 1998). Presently also, the region to the west and SW of Vigukot is prone to flooding frequently by river floods by few perennial rivers coming from the north and relatively less frequently by sea water influx from the south. In addition numerous small shallow (~0.5m deep) channels of uncertain affinity are also present. Overall, the role of rivers is evidently more pronounced in the western most part than the rest of the Bet zone. Contrary to the rest of the Great Rann, the Bet zone shows wide variation in elevation due to the presence of bets and is dotted by several seasonal short distance channels, pools i.e. local depressions and elevated surfaces (Fig. 3.5). The seasonal nature of the supra-tidal environment marks this region as special and of unique character to understand the biotic forms which are sensitive to the ecological changes that takes place during and after monsoon. This presumably results in the formation of several microenvironments in the overall strongly seasonal supra-tidal environment.

### **Banni Plain**

Most part of the Banni plain is submerged by a vast stretch of water during the monsoon and remains muddy and waterlogged for 2-4 months in years of normal rainfall. The settlements in Banni are therefore widely scattered and occur in areas which remain above submergence. Owing to the different submergence characteristics, the Banni plain displays geomorphological characteristics that are unique and distinctly different from the rest of the terrain of the Great Rann. A detailed topographic analysis of the Banni plain was attempted. For this purpose, several topographical cross sections were prepared to bring out the relief characteristics of the Banni plain. The topographic profiles were prepared on the basis of the elevation data available on the Survey of India topographical maps on 1:50,000 scale. Several cross profiles were also constructed from the Googleearth data (source-[www.googleearth.com](http://www.googleearth.com)). It is also found that the distribution of vegetation cover comprising the *prosopis juliflora* and grasses is also highly variable. The vegetation density varies from dense scrubland to a complete absence of vegetation.

The cross section shown in Fig. 3.2 reveal that the Banni plain occurs at a higher level than the salt encrusted rann surface which is regularly submerged by tidal waters. The profiles also show that the surface of the Banni plain is not flat in the literal sense, but shows marked variation in relief. A distinct geomorphic high termed

here as the Bhirandiyala High, is observed in the northern part of the Banni plain. This geomorphic high also correlates with the maximum vegetation density and location of several villages over it. The average elevation of this high is ~8m. The geomorphic high shows very gentle slopes towards the north and south. This geomorphic high correlates with an E-W trending structural high in the subsurface Mesozoic and Tertiary rocks. The formation of the geomorphic high is therefore attributed to neotectonic activity along the subsurface structures of the Banni plain.

Complementing the geomorphic high in the northern part is an E-W trending geomorphic low in the southern part of the Banni plain (Fig. 3.2). This geomorphic low occurs between the geomorphic high in the north and the rocky landmass of the mainland Kachchh in the south. The low comprises a surface that shows several water bodies and stretches of salt encrusted saline surfaces formed due to drying up of submerging waters in depressions. The low appears to be asymmetrical as the lowest elevations are not found exactly in the central part but towards the southern side. In other words, the gently southward sloping surface of the northern flank of the low is longer while the northward sloping surface forming the southern flank is short and relatively steeper. Also the gradient in this tract appears to be towards the west with a short but gentle eastward slope towards the rann surface in the eastern fringe.

The E-W trending asymmetric geomorphic low in the southern part of the Banni plain corresponds to a synclinal structure formed by the Mesozoic and Tertiary rocks in the subsurface. The subsurface synclinal structure is also asymmetric whose steeper southern limb is attributed to downfaulting along the Kachchh Mainland Fault (KMF). The northern limb of the syncline is gentler and rises towards the north and is exposed in the Pachcham island further north of the Banni plain. It has been indicated that the maximum thickness of the Quaternary sediments in the Banni plain occurs in the central part of this syncline.

Overall, the elevation variations of the surface of the Banni plain show a remarkable correspondence with the subsurface structural features. The elevation variation shows a one to one correspondence with the subsurface structural framework of the Banni plain delineated by Biswas (1987). The topography of the Banni plain is therefore attributed to neotectonic reactivation of the subsurface structures. The structurally controlled topography is responsible for the spatial variability in the submergence pattern which in turn influences the surface characteristics and vegetation distribution in the Banni plain.

### *Channel features*

Several channel features are also observed in different parts of the Banni plain. These are recognized based on their distinct tonal characteristics and linear morphology. The channels are, in general, broad, shallow and are occupied by vegetation. The channels are found to occur preferentially in three broad zones. The first zone occurs between the Pachcham island and the E-W trending geomorphic high passing through Bhirandiyala. All channels in this zone parallel to subparallel and are oriented in N-S direction. The northern part of these channels are a continuation of the south flowing streams of the Goradungar Range that extend over a prominently south sloping surface of the Banni plain. In contrast, the southern parts of these channels are located over the northward sloping northern flank of the geomorphic high. The parallel drainage pattern in this zone is consistent with the tectonically generated gentle slopes. The channels, however, appear to have been formed by the merging of channels developed on the converging north and south oriented tectonic slopes. The southern parts of the channels are shaped by the tendency of the rain water to flow northward along the northward flank of the geomorphic high. Few eastward and southward flowing channel features are also seen in the eastern fringe of the geomorphic high forming a radial drainage pattern in conformity with the radiating slopes around the topographic high.

The second zone lies all along the eastern part of the Banni plain where several parallel to subparallel channels are also mapped which flow eastwards into the rann surface. The most intriguing channel forms are seen in the central part to the south of the Bhirandiyala High. Two subparallel channels of different sizes, one being the main channel and the other being its side channel, are observed which trend in E-W direction. The channels are located in the E-W trending geomorphic low to the south of the Bhirandiyala High. The channels all along their length are characterized by intermediate to dense vegetation, which is in sharp contrast to almost vegetation free Banni plain in their vicinity.

Owing to the presence of vegetation, the channels are distinctly identifiable in Googleearth images as described above (Fig. 3.6). For verifying the presence of channels, topographic data from Googleearth was analysed by preparing N-S oriented cross sections across the channels (Fig. 3.7). The cross profiles clearly show a broad shallow depression confirming the formation of channels. The dense vegetation in the channels also confirms the channelization of submerging rain waters through these

channels. The geomorphic low also shows several channel like features which are broad, shallow and trending in E-W directions. In general, all channel features mapped in the Banni plain during the course of the present study are broad and shallow. The channels in the eastern fringe of the geomorphic low shows radial pattern. The channels appear to be formed by a tendency of the submerging waters to channelise and flow along the gentle gradients produced by the structurally controlled elevation variations in the Banni plain. The broad and shallow morphology of the channels indicate that they are in nascent stage. The channels may evolve into well-defined streams as the channelisation of submerging rain waters in the Banni plain continue over prolonged period of time. It is inferred that structurally controlled variations in the elevations in different parts of the Banni plain is the prime factor influencing the submergence pattern which in turn controls the moisture distribution and soil type.



**Figure 3.6** Google image showing a prominent channel feature. Red lines depict the transect of cross profiles given in Fig. 3.7.

### **The Allahbund Fault scarp**

The E-W trending Allahbund Fault was formed during the well known 1819 earthquake (Burnes 1835, Oldham 1926, Bilham, 1998). Historical documents suggest that the earthquake produced a distinct fault scarp that uplifted the northern part of the Great Rann which corresponds with the present day Bet zone (Burnes 1835, Oldham 1926). The scarp trends in roughly E-W direction and laterally extends for about 90 kms (Oldham 1926). However, presently the scarp is visibly identifiable for about 60 kms length in the central part of the extension as mapped by Oldham (1926).

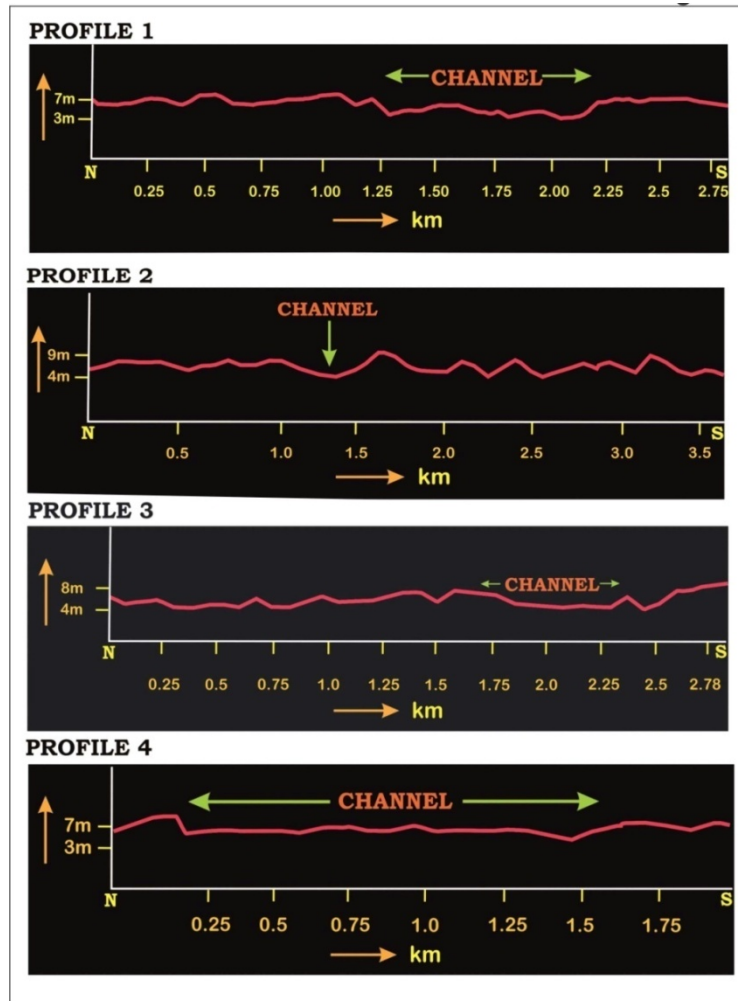


**Figure 3.7** Cross profiles across the channel feature shown in Fig. 3.6.

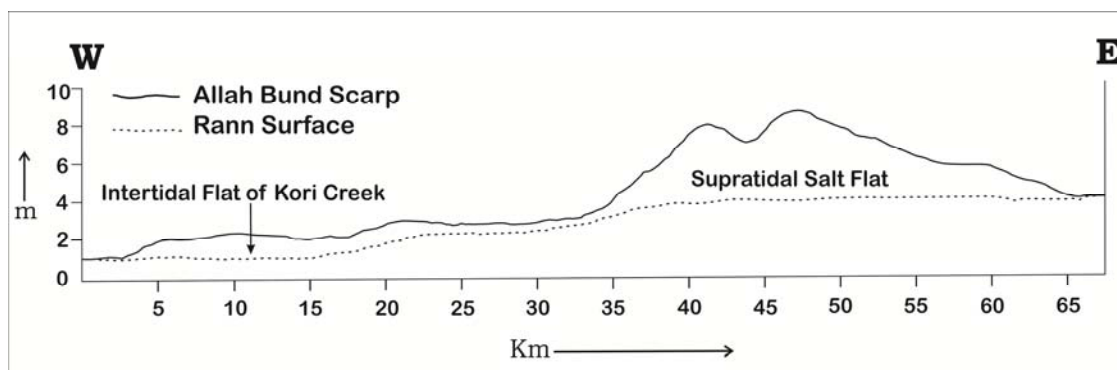


**Figure 3.8** Topographic profile drawn over the crest of the Allahbund scarp. The supratidal salt flat surface is also shown to indicate the height of the scarp. Vertical scale is highly exaggerated. The elevation data is based on the Survey of India topographical maps (survey years-1960-66).

In the westernmost part, the scarp is represented by a gentle northward rise of the ground above the intertidal flats of the Kori creek. Further eastward, the scarp gains elevation and is observed as a distinct erosional scarp (Fig. 3.8). The scarp height continues to increase eastward with the highest elevation recorded about 4-5 m from

the supra tidal salt flat in the central part (Fig. 3.6). Beyond this the scarp again gradually reduces in height and finally disappears in the flatness of the rann surface to the southeast of Shakti bet. As per the mapped trace of the scarp by Oldham (1926), the scarp continues eastward where it is believed to be represented by the southern cliffy margins of the Gainda bet, Mori bet and the Kuar bet.

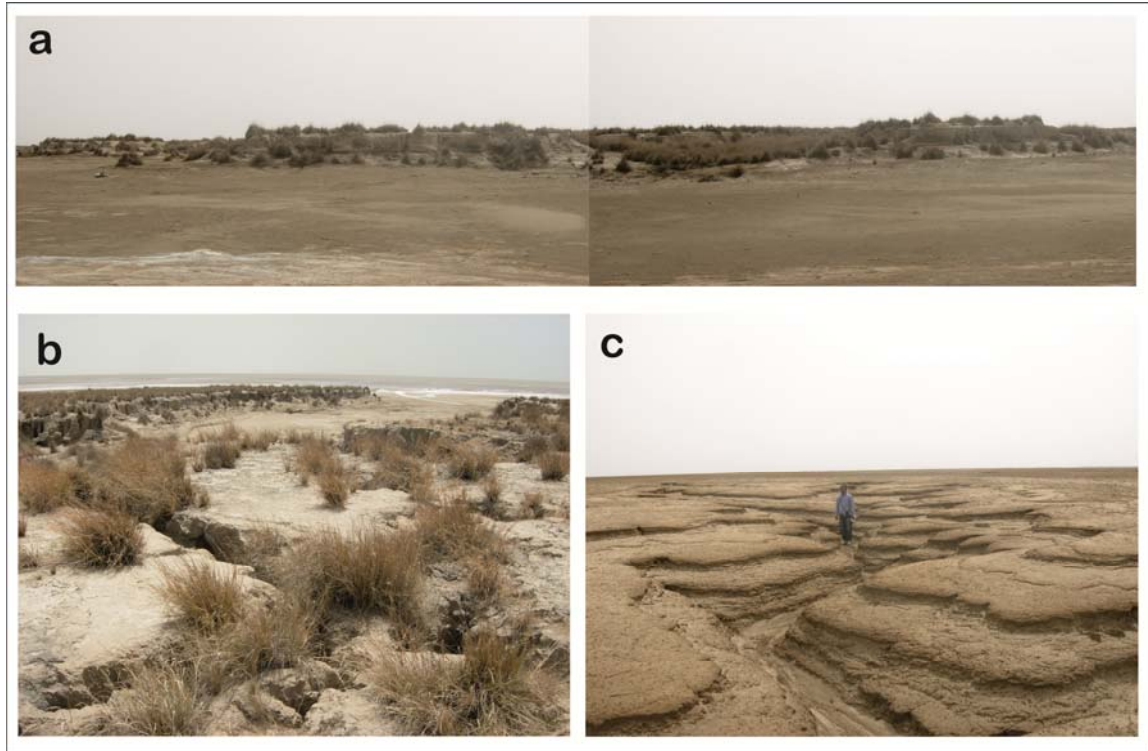


**Figure 3.9** a- View of the Allahbund scarp. Note the degraded nature of the scarp. b- View of the crest part of the Allahbund scarp. A short stream incising through the crest and merging with the supra tidal salt flat in the distant background can be seen. The surface in the foreground is formed of aeolian sediments which supports small vegetation. c- View of the gullied surface over the Allahbund scarp. Note the depth of incision in the gully. The surface here is free of aeolian sediments.

Overall, the Allahbund scarp all along its length appears as a highly degraded erosional scarp that exposes raised rann sediments in the vertical cliff sections (Fig. 3.9a). At places, the height of the scarp is accentuated by the deposition of 0.5 - 2m thick wind-blown saline silty sediments (Fig. 3.9b). This especially observed in the central part where the scarp attains highest elevation. A major significant characteristic that defines the scarp as an erosional scarp is its deeply gullied nature. The gullies are 1-3 m deep and usually form a dendritic pattern over the crest of the scarp (Fig. 3.9c). Another significant characteristic feature of the scarp is a gentle northward slope of the scarp surface which finally merges with the flat surface of the Bet zone (Fig. 3.10). The northward slope is attributed to the backtilting of the rann surface due to

upliftment along the scarp. The backtilting is however, very subtle is not recognisable in the field at many places as the elevation drop is marginal (1-2m) that occurs over the distance of few kilometres (Fig. 3.10).

### The Island Belt Fault (IBF) scarp

The north facing E-W trending linear escarpment is the most spectacular and prominent feature of the landscape that delimits the northern margin of the rocky islands of the island belt. All the rocky islands are marked by prominent steep to vertical north facing escarpments that abruptly rise above the salt encrusted surface of the rann (Fig. 3.11a, b). The escarpment shows the characteristics typical of an active fault scarp and is geomorphic expression of the Island Belt Fault (IBF) that is located further north below the rann sediments.

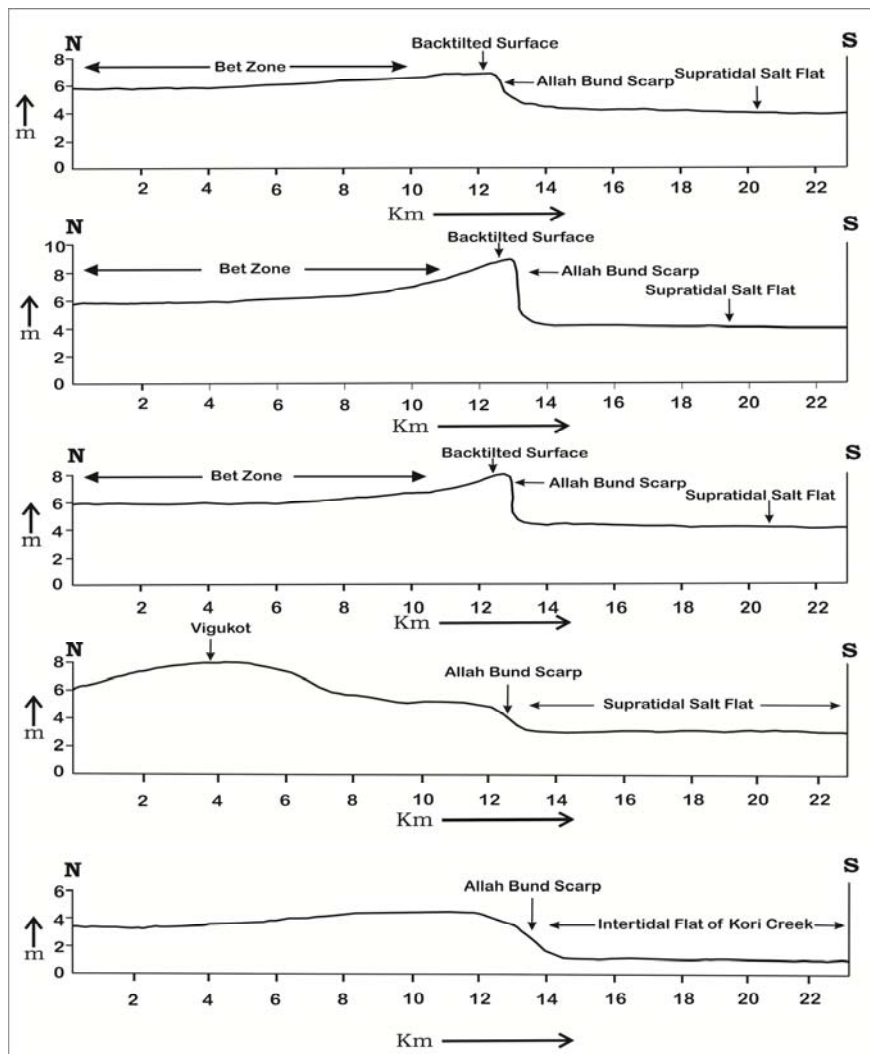


**Figure 3.10** Topographic cross sections drawn across the E-W trending Allahbund scarp. The top profile is from the western extremity while the bottom one is from the eastern extremity of the scarp. Vertical scale is highly exaggerated. The elevation data is based on the SOI topographical maps (survey years-1960-66).

The Mesozoic rocks are folded into E-W trending flexures forming the linear series of various rocky islands (Biswas 1993). The escarpment is formed in the southern limb of the anticlines while the northern limb is eroded away. The straight northern margins of the islands are attributed to the E-W trending Island Belt Fault (IBF) in the north that is presently buried below the marine sediments of the Rann. However, the nature of the escarpment varies in all the islands.



**Figure 3.11** a – Photomosaic of the northern escarpment of the Bela island. In the foreground is the rann surface. b- View of the Khadir scarp. Note the fresh nature of the escarpments.

### ***Pachham escarpment***

The Kaladungar scarp marks the northern limit of the rugged Kaladungar Hill range as well as the Pachham Island. This is represented by a steep north facing surface which abuts against the flat rann surface in the north. The scarp is the geomorphic manifestation of the Kaladungar Fault which is buried beneath the rann surface. The scarp is formed in the southern limb of the Kaladungar anticline whose northern limb has been faulted and later eroded (Biswas 1993). The scarp shows a sinuous pattern in the middle. It attains a maximum height in the centre with decreasing altitude east and westward. This decrease in altitude towards the eastern and western margin is in conformity with the doubly plunging Kaladungar anticline. Babia hill forms the highest elevation point of the Pachham Island as well as the entire Kachchh Basin. The scarp surface is characterized by the short north flowing drainages which rises from its summit and debouches in the Banni plain in the north.

The southern margin of the Kaladungar hill range which forms the back slope of the Kaladungar scarp is characterized by a gentle southward dip which later forms the northern margin of the central valley. The back slope represents the southern limb of the Kaladungar anticline. The back slope is mainly characterized by long southward flowing drainages. The slope acts as a large catchment area for the southward flowing

parallel drainages. These drainages are serving as the major feeder channel to the axial river like east flowing Pipri river and the west flowing Bandi river which drains the central valley. The drainages have carved out deep valleys in the upland part. The carving of the deep incised valleys in hard strata in an arid zone is a direct manifestation of the neotectonic uplift.

### ***Bela escarpment***

The northern escarpment of the Bela islands attains a maximum height of 246m at the centre (Fig. 3.12a). The scarp is vertical to subvertical and exposes lithologies of the Mesozoic formations comprising the island. The escarpment of the Bela island is divisible into two segments by a prominent saddle (Fig. 3.12a). The eastern part of the escarpment corresponds to the northern flank of the Mouvana dome which consists of northerly dipping Mesozoic rocks and is therefore gentler. The western part forms the main escarpment and is vertical to sub-vertical. The Mesozoic rocks exposed in the face of the escarpment dip southward that form the southern limb of the Lodrani anticline. As described earlier, the northern limb of the anticline is cut by the IBF and is buried under the rann sediments. This imparts an aspect of a cuesta scarp to this part of the Bela escarpment. However, the crest of the escarpment dips on either sides i.e. towards east and west. This is in conformity with the plunge directions of the E-W trending Lodrani anticline. Throughout its extent from north of Bela to the eastern fringe of the island, most part of the vertical extent of the escarpment presents a undissected wall like feature typical of scarps that have maintained their youthfulness due to uplift. However, at the base, features of marine erosion carved out by the sea that occupied the rann surface until late Holocene, are found. These features are described later in the chapter. The crest of the escarpment forms the main drainage divide which effectively controls the southward courses of the majority of the drainages. However, the northward flowing Nilangadh river has carved out a deep gorge that has been formed along a N-S trending transverse fault. The formation of the gorge and the wall like escarpment testifies to the youthful nature of the overall landscape of the Bela island.

### ***Khadir escarpment***

As is the case with Bela island, the northern margin of the Khadir island is also characterized by a vertical to sub-vertical north facing and E-W striking escarpment. However, unlike Bela escarpment, the Khadir escarpment is continuous and extends from the eastern margin to the western margin of the island (Fig. 3.12b). The

escarpment shows maximum elevation of in the central part and loses elevation towards east and west. In plan view, the escarpment is of arcuate shape with the concave side facing the rann in the north. The escarpment has been developed in the southern limb of Khadir anticline whereas the northern limb has completely eroded off.

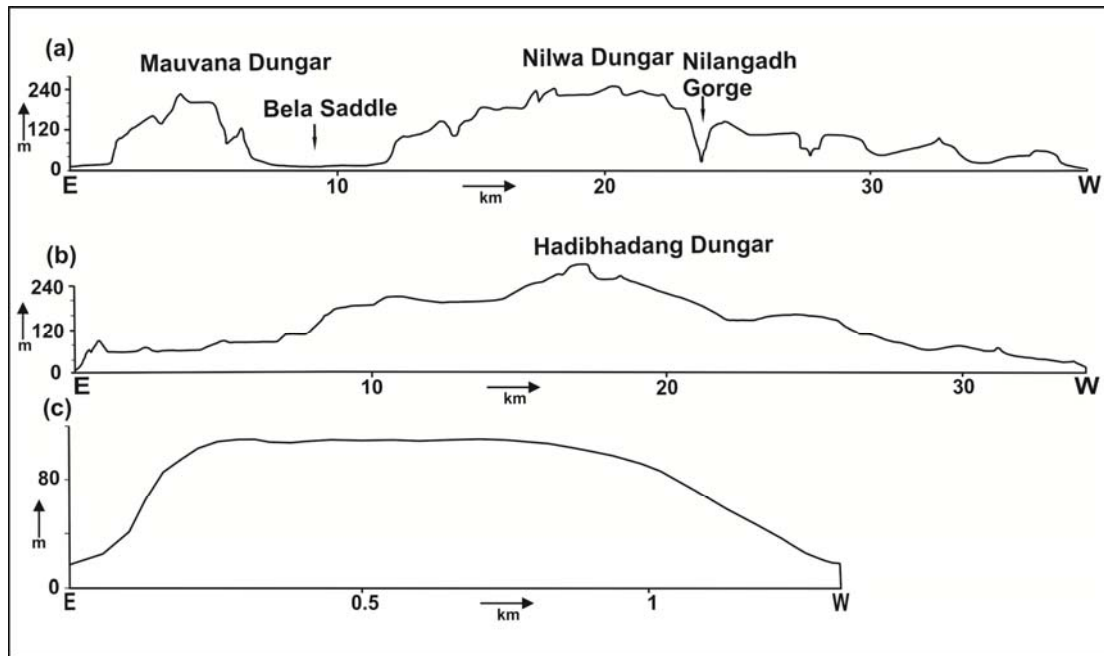


**Figure 3.12** E-W topographic profiles drawn over the crest of the northern escarpments of (a) Bela, (b) Khadir and (c) Bhanjada islands.

The IBF is not exposed anywhere and is presumably buried below the rann sediments in front of the escarpment. This has resulted in a cuesta like morphology of the Khadir island. The succession of Mesozoic formations exposed in the Khadir escarpment, are correlatable with those exposed in the Bela escarpment (Biswas 1993). The escarpment forms major drainage divide which effectively divides the drainage in south flowing north flowing drainages. In general, the Khadir escarpment is steeper and presents a relatively more youthful aspect than the Bela escarpment. However, the base of the escarpment is wider which have given rise to the streams arising from the escarpment face and flowing towards the north to met the rann surface. This is attributed to the compact lithology of the conglomerates of Cheriya bet Formation which form the oldest Mesozoic sediments of the Kachchh basin. All along the base of the scarp marine depositional and erosional landforms are found which were formed during the Holocene when the rann was occupied by shallow sea.

### ***Bhanjada escarpment***

The Bhanjada island is the smallest island of the entire island belt. It consists of igneous intrusive rocks due to which it displays a rugged mountainous topography that

is at variance with the Bela and Khadir islands which are made up of south dipping Mesozoic and Tertiary rocks. However, the northern margin of the Bhanjada island is also marked by a E-W trending north facing escarpment which suggests that it is also produced as a consequence of faulting along the IBF. The escarpment is characterized by steep face which gentler than Bela and Khadir escarpments. Moreover, the crest of the escarpment is approximately at the same level from east to west (Fig. 3.12c) whereas the Bela and Khadir escarpment dip towards the east and west which is attributed to the plunge of the respective anticlines as described earlier. The eastern and southeastern margin of the Bhanjada island is marked by the raised intertidal flats comparable to those found on the western margin of the Khadir Island.

### **GEOMORPHIC EVIDENCE OF UPLIFT ALONG THE ISLAND BELT**

The various sandy islands rising few metres above the rann surface with cliffy margins provide the most obvious geomorphic evidence of the tectonic uplift in recent times. However, the existence of the shallow sea around the rocky islands of Bela, Khadir, Bhanjada, Kuar bet and Mori bet islands has resulted in the development of marine depositional and erosional features (Fig. 3.13, 3.14) which provide evidence in respect of the uplift of these islands during the last ~2 ka.

#### **Raised Rann sediments along island margins**

The fringes of the Bela, Khadir and Bhanjada islands, including the base of the northern escarpments show a thin linear zone of raised discontinuous flat depositional surfaces consisting of 2 - 6m of Holocene marine deposits (Fig. 3.13). At most places, these flat surfaces gradually merge with the rann surface. However, these surfaces raise upto 4 - 6m above ranns towards the landward side. These are composed of sediments that were deposited during the period when the rann surface was submerged under a shallow sea upto ~2ka.

The base is marked by 20 - 30cm thick pebbly to cobbly gravel which unconformably overlies the Mesozoic sedimentary and igneous intrusive rocks in Khadir and Bhanjada islands respectively. The rest of the sections comprise in general laminated clayey silts. The uniform lithology of clayey silt is broken by the presence of several 2-10 cm thick fine sand layers. The geomorphic setting and the nature of the sediments point to the deposition of these sediments in intertidal environment. The upper part (~1.5m) of the section at Khadir shows broad shallow channel fill structures that also consist of laminated clayey silts. This could be representing the tidal channels

that were formed as a consequence of the withdrawal of the sea and widening of the intertidal zone (Chouksey et al. 2010). OSL dating these sediments have indicated that they were deposited during the Holocene (Khonde et al. 2011). Detailed results of the studies carried out and chronology of these sediments are described later.



**Figure 3.13** a- Distant view of the western margin of the Khadir island. In the foreground is the rann surface. b- Close view of the exposed section of the raised inter-tidal sediments. c- Flat terraced surface of the raised intertidal sediments. In the background is the Bhanjada island. d- View of the terraced surface of raised intertidal sediments at the eastern margin of the Bhanjada island.

### **Marine Erosional Features**

Marine erosional features are found to occur at the base of the north facing escarpments of the islands. These features are observed along the base of the northern escarpments where the Mesozoic rocks are not overlapped by the Holocene marine deposits. These erosional features are attributed to the erosive action of the sea which existed up to about ~2ka. The various erosional features observed are notches, rocky

platforms and sea caves (Fig. 3.14). Marine notches are described as grooves formed in bedrock of coasts near sea level due to either abrasion and/ or dissolution (Pirazzoli 1986, Rust & Kershaw 2000). In the tectonically active rocky coasts, marine notches are the precise indicator of rates and pattern of uplift (Rust & Kershaw, 2000). The notches are seen intermittently along the toe of the scarp which were possibly the sheltered zones. The notches show typical morphology as described by Pirazzoli (1986). The notches are seen at two levels. The lower notch occurs at a height of ~2m above the rann surface while the upper notch is found at ~4m. The occurrence of lower notch is consistent and widespread. However, the occurrence of the upper notch is discontinuous and less prominent. However, it is found to occur at the same level at all places. The two levels of notches clearly suggest uplift of the islands in two phases during middle to late Holocene time.



**Figure 3.14** a- View of a sea cave at the northern margin of Bela island (Loc. North of Kuda). b- Close view of the lower notch in Bela island (Loc. North of Kuda).

Flat rocky platforms are also found to occur at the base of the escarpments. The rocky platforms have developed over the Mesozoic rocks. The platforms are easily recognizable as wide flat rocky surfaces occurring at a height of ~4 m above the rann surface. Sea caves of various dimensions are also observed. In general, the formation of these erosional features is attributed to the Holocene sea that occupied the rann surface. The occurrence of these features above the rann surface indicates uplift of the islands along the IBF. The uplift occurred during middle to late Holocene in two phases as indicated by the two levels of notches. An uplift of at least 6m is envisaged since middle Holocene to present.

### **NEOTECTONIC UPLIFT**

Based on the distinct geomorphic characteristics and variable submergence pattern, it is inferred here, that the emergence of the rann surface may have occurred gradually due to differential tectonic activity along the various subsurface intrabasin faults in the recent past which led to the formation of the distinct morphologic units viz. the Banni plain, the Bet zone and the supra tidal salt flat. The Banni plain astrides the subsurface Median high and is separated from the rest of the Rann basin by the Banni Fault to the north (Biswas 1974). Similarly, the Bet zone is delimited by the Allahbund Fault to its south (Roy and Merh 1981). The close association of these units with faults suggest differential tectonic activity along subsurface faults within the Great Rann basin may have played a major role in the emergence of various morphologic units at different times. Based on elevation and present day submergence characteristics, the Banni plain appears to be the first to emerge followed by the Bet zone, the inner saline flat and the supra tidal salt flat, which still gets submerged by marine waters regularly.

Various coastal geomorphic features are seen at the toe of the northern escarpments of Bela and Khadir islands which are attributed to the paleo-sea which occupied the rann until ~ 2ka. Erosional rocky platforms occur discontinuously at an elevation of 2-4m above the rann surface all along the base of the Bela and Khadir escarpments. Two levels of notches designated as upper and lower notches are also observed at a height of 4m and 2m respectively. Notches are generally formed in the sheltered site away from the wave action (Rust & Kershaw 2000). The preservation of two levels of notches can be account of rapid uplift (Cooper et al. 2005). Sea caves have also been noticed all along the base of the escarpments.

Raised marine terraces consisting of sediments deposited in inter tidal conditions are documented from the western margin of the Khadir island and eastern margin of the Bhanjada island. The cliff sections of these terraces expose 5 - 6m of rann sediments. The sediments overlie the Mesozoic rocks and dominantly comprise laminated clayey silts. The presence of channel fill deposits in the upper part of the section at Khadir island suggests existence of shallow tidal channels in the intertidal zone. The formation of the terraces is attributed to tectonic uplift during late Holocene. Tectonic tilting of the islands during this period is testified by the southward decrease in the elevation of these terraces which ultimately merge with the rann surface.

### PRESENT DAY ENVIRONMENT OF THE BET ZONE

Amongst all the geomorphic domains of the Great Rann basin, described in previous chapter, the Bet Zone is marked by a characteristic micro-geomorphic diversity and complex marine/fresh water inundations during monsoonal season. The uplift along the Allahbund fault has led to the formation of several bays that punctuate the flat rann surface to form undulating topography. Moreover, the eastern extremity of the Bet zone is basically a part of the Indus delta where, according to historical records, a distributary of Indus River used to meet the Kori creek before the 1819 Allahbund earthquake (Oldham, 1826). Also, influx of fresh water from south flowing streams (seasonal) acts as a critical factor in controlling environmental conditions that also makes it a distinct geomorphic entity (Khone et.al. In Press). Understanding of modern confluence of the marine and fresh waters may act as an analogue for the past settings. Sedimentological and micropalaeontological studies on the surface sediments at various locations can serve as a tool to identify the marine-fresh water influence pattern in the northwestern rann. With this background, investigation on the surface sediments of the Bet zone was carried out. The present study covers two transects along roughly E-W and N-S direction throughout the extent of the Bet zone of Great Rann of Kachchh (Fig. 4.1).

#### SAMPLING AND LABORATORY METHODS-

The sampling was done along two transects- ESE-WNW (Transect -1) and N-S (Transect -2). Stations 1-11 fall along the Transect -1 while 12-17 forms the Transect -2 (Fig. 4.1, 4.2). The top surface was deliberately avoided to filter out excessive salt content and the aeolian activity. About 200g of sediment sample was collected from each station which was later analyzed for grain size parameters and foraminiferal studies. All samples were collected during the peak summer season in month of May 2011 when the rann surface was completely dry.

#### Grain size analysis

All the collected sediment samples show visibly fine grained nature of the sediments therefore, the grain size analysis was attempted through standard pipette

method following Folk (1974). The method is basically based on the Stock's law and settling velocity principle. The sediments were classified into sand, silt and clay fractions. Their proportions were determined and relative abundance calculated (Table 4.1; Fig. 4.3).

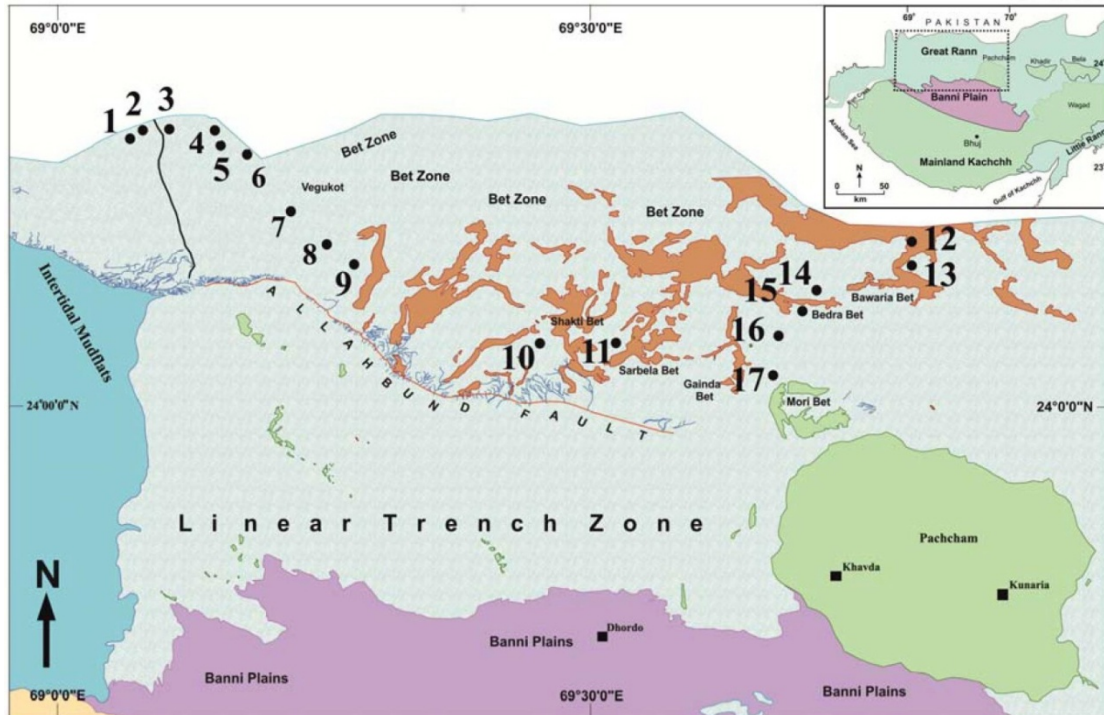


**Figure 4.1** Geomorphic map of the Bet Zone of Great Rann of Kachchh with spatial distribution of sampling stations along two transects. Transect-1 is ESE-WNW oriented transect along the southern margin of Bet Zone. Transect-2 is roughly N-S oriented transect running across the eastern margin of the Bet Zone.

### Foraminiferal Studies

Sediment volume of about ~15g of each sample was wet sieved through the standard ASTM (American Standards for Testing Materials) 63 micron sieve and >63 micron fraction was collected for foraminiferal recovery. The collected sediments were homogenized by coning and quartering followed by separation of foraminiferal tests by conventional picking under stereoscopic stereo zoom binocular microscope. As there was no coarse fraction the upper limit for the sand content was not used and simply >63micron fraction directly used for picking foraminifera. The collected foraminiferal tests were identified with the help of standard references for the modern environments up to species level (Loeblich and Tappan, 1988, Murray 2006, Walton and Sloan, 1990, Carboni and Bella 1996, Hayward and Holis, 1994).

## **SEDIMENT CHARACTERISTICS**

### **Transect 1**

This transect runs almost parallel to the wavy southern margin of the Bet zone marked by the Allahbund fault scarp and is oriented roughly in ESE-WNW direction (Fig. 4.1, 4.2a). The sediment grain size indicates the nature and energy of the depositional environment at the particular locality under which the sediments were laid down. The sediment transport and grain size appears to be primarily controlled by the micro-geomorphic settings in the Bet Zone. The broad open flow zones between the bets, sheltered zones and local depressions play significant role in grain size distribution and sorting during marine water flooding. Based on the micro-geomorphic settings and inundation waters the selective sorting of the transported grains takes place that is also seen in the grain size distribution along these zones (Fig. 4.3a). Overall, the sediments of the Bet zone are sandy-silty to clayey-silty in nature with only few locations where sand content is increased. A station wise grain size distribution and controlling factors are given in the following paragraph.

The sediments from station 1-5 fall close to a local depression occupied by south flowing river channels. Marginal sites to this depression show more silty-clayey sediments whereas the sites falling in central depression (station 2-4) are characterized by increased sand content up to ~50% (Table 4.1, Fig. 4.3a). This is due to a large channel passes through its middle part that contains sand in large proportion. This sandy fraction comprises mainly quartz, mica, and few dark coloured minerals. These sediments show moderate sorting with sub angular grains indicating its moderate transport from the northern part of the rann in Pakistan or through the margin of the Thar Desert. The observed variations in sediment characteristics are in conformity with the slightly different micro-geomorphological setting of the western part of the Bet zone described earlier.

Further eastward, station 6 to 11, the sand proportion is observed to significantly decrease with relative increase silt and clay. In fact, the sand content is almost negligible that remains below 2% at stations 6 to 10. Silt dominates the grain size contributing more than 80% while the clay fraction varies from 8-19% which is controlled by the varying energy conditions in different micro-geomorphic settings. An increase in sandy fraction up to ~10% is seen at the last station where the silt & clay contributes 71% & 19%

respectively (Table 4.1, Fig. 4.3a). This increased sand proportion is on account of relatively steep southward slope that allows more water flow with higher energy causing increased sandy influx from upland to the site.

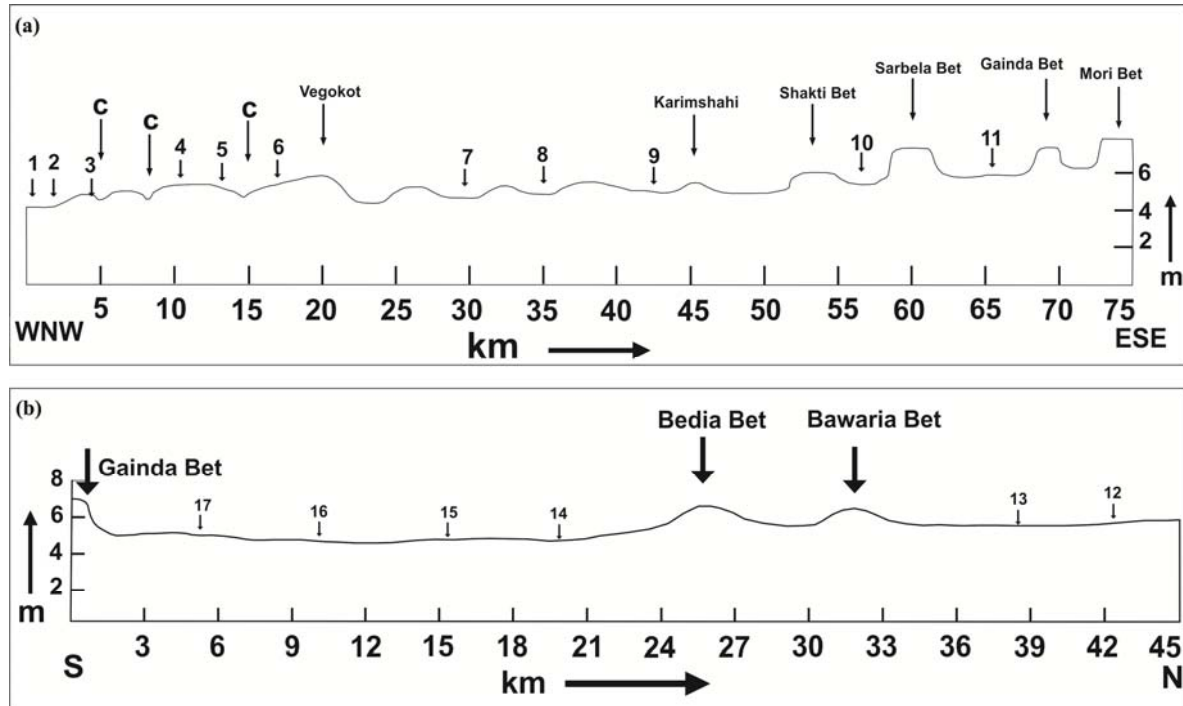


**Figure 4.2** Topographic profiles along the two transects. a) Transect-1 and b) Transect-2. The profiles drawn are based on the elevation variations data from the Survey of India topographic maps. Note the elevation variations i.e. microgeomorphic variations of the respective sampling sites as shown in figure.

## Transect 2

The second transect is oriented roughly in N-S direction that covers six stations from 12 to 17 along the eastern margin of the Bet zone (Fig. 4.1, 4.2b). The sampling stations falls in a low lying area which is prone to marine flooding on account of strong winds during SW monsoon and also at times flooding occurs due to the strong highest high tides. To avoid the seasonal reworking effects the samples were taken far from the margin of this depressed zone. The nature of the sediments along this transect is primarily dominated by the silty sediments followed by the clay fraction whereas the sand remains <10% (Table 4.1, Fig. 4.3b). Occasionally it increases up to 10% at two locations which are near to the small channel systems in the northern part. The increase in the sand content is observed near the consistent channels that follows the relatively steeper slopes on ground and carries more sand fraction in moderate to low energy conditions (Fig. 4.3b).

The silt remains the dominant size fraction throughout by contributing 70-91% of the total sediments whereas the clay fraction varies from 5-22% (Table 4.1, Fig. 4.3b).

**Table. 4.1** Table showing the grain size variation in the surface sediment samples along two transects in the Bet Zone of Great Rann of Kachchh, Western India.

Station No.	Sand %	Silt%	Clay %
1	11.51	51.71	36.78
2	17.14	52.62	30.24
3	48.63	32.64	18.73
4	13.92	55.84	30.24
5	3.89	87.47	8.64
6	0.267	82.22	17.51
7	0.334	87.76	11.9
8	9.9	71.59	18.51
9	15.03	78.46	6.51
10	1.026	81.19	17.78
11	9.9	71.59	18.51
12	1.742	81.95	16.31
13	0.971	80.52	18.51
14	9.49	83.86	6.64
15	0.51	72.31	27.18
16	1.42	74.74	23.84
17	9.3	82.39	8.31

Overall, from the grain size characteristics it appears that the sediments were deposited by submerging waters in 'ponded' conditions owing to negligible gradient. The sand and silt sediment fraction is dominated by micaceous minerals. Transport of these sediments is possible through the low energy submergence by the sea water during monsoon. Eastward and southward of the Transect -2 lies the easternmost part of the

inland supra tidal salt flat which forms local depressions and is consequently liable to submergence by sea water that remains for several weeks to months.

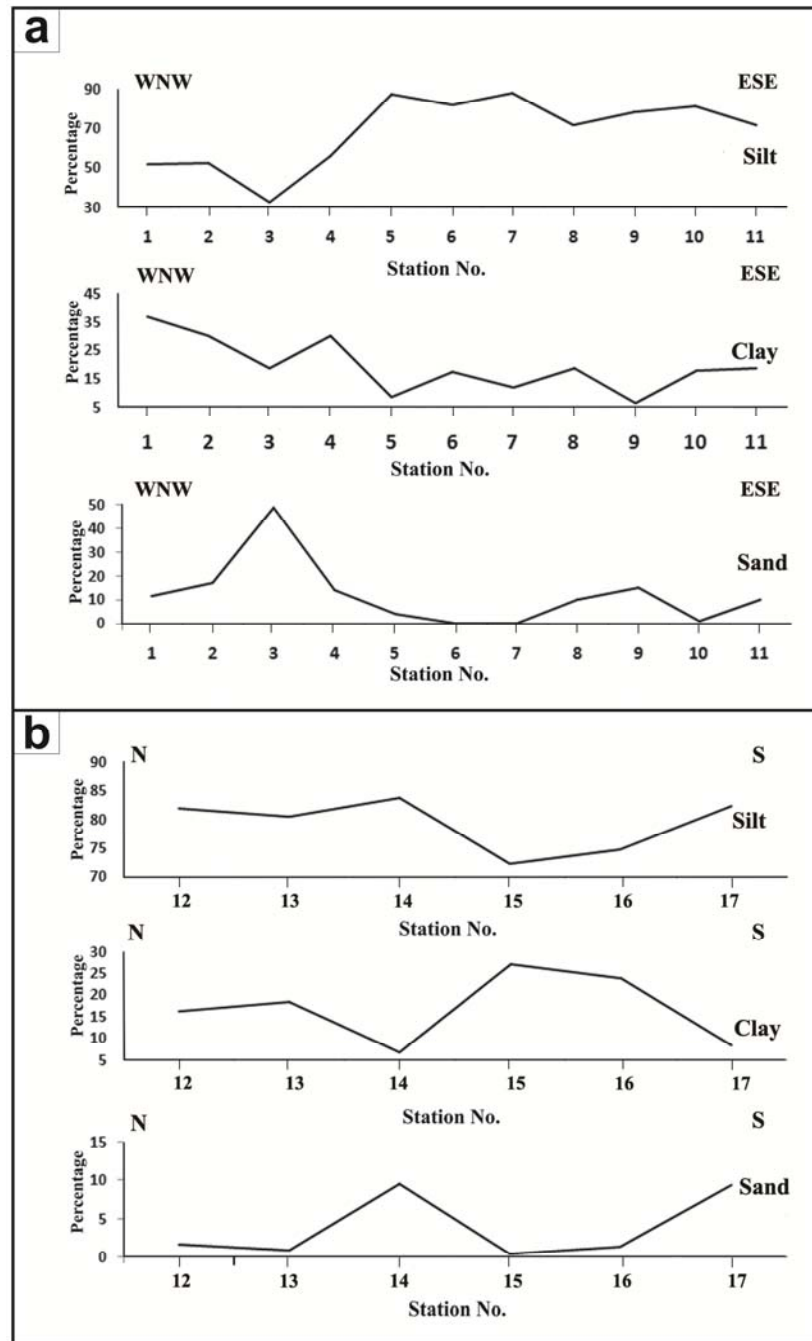


**Figure 4.3** Grain Size distribution at the sampling stations along two transects a) Transect-1 and b) Transect-2. Note that the sand proportions increases at the stations directly in contact with the inundating waters whereas the silty to clayey sediments belongs to the sheltered areas (low lying areas, depressions).

## FORAMINIFERAL ASSEMBLAGE

The foraminiferal assemblage recovered from the sediments along the two transects comprise twelve genera such as *Ammonia*, *Elphidium*, *Bolivina*, *Nonian*, *Bulimina*, *Cibicides*, *Helenina*, *Brizalina*, *Globigerinella*, *Globigerina*, *Globorotaloides* and *Gallitellia* (Table 4.2). The benthic foraminifera recorded includes: *Ammonia beccarii*, *A. tepida*, *A. parkinsoniana*, *Elphidium excavatum*, *Elphidium discoidale*, *Elphidium* sp., *Bolivina spathulata*, *Nonian asterizans*, *Bulimina marginata*, *Cibicides refulgens*, *Helenina anderseni*, *Brizalina striatula*. A few planktonic species were also recovered belonging to several species such as- *Globigerinella* sp., *Globigerina bulloides*, *Globorotaloides* sp. and *Gallitellia* sp. The SEM (Scanning Electron Microscope) image of each species is given as Fig. 4.4. A taxonomic account for the recovered species in surface sediments is given under-

### Systematic Taxonomy And Ecology

Phylum: Protozoa

Order: Foraminiferida (Eichwald, 1830)

Suborder: Rotaliina (Delage & Herouard, 1896)

Superfamily: Rotaliidae (Ehrenberg, 1839)

Subfamily: Ammoniinae (Saidova, 1981)

Genus: *Ammonia* (Brunich, 1771)

**Species: *Ammonia beccarii* (Linne, 1758)**

**Description:** Test trochospiral, biconvex, with 6-10 chambers in last whorl and rounded periphery. The sutures limbate on spiral side slightly raised whereas umbilical side sutures are depressed and ornamentation along with umbilicus with tubercles which may coalesce to form a central boss.

**Species: *Ammonia tepida* (Cushman)**

**Description:** Test low trochospiral, biconvex, large umbilical fissure with granular ornamentation. Sutures depressed, straight to radial with slight curvature. Periphery rounded.

**Species: *Ammonia parkinsoniana* (d'Orbigny, 1839)**

**Description:** Test trochospiral to low trochospiral, 6-9 chambers, biconvex with depressed sutures on umbilical side. Sutures are ornamented with the granular crystals, sometimes highly ornamented whereas the raised sutures on spiral side are noted.

**Remarks:** Lower Miocene to Holocene. Cosmopolitan. Ammonia group shows large variations in the test architecture and ornamentation. The identified species are based on broad divisions of typical not in the more refine form of formae. It's typical widespread in marginal marine environments worldwide, salinity 10-31, marsh to subtidal; tolerates through variable salinity and oxygen conditions. Well documented through the shallow waters of west coast of India.

Superfamily: Nonionacea (Schultze, 1854)

Family: Nonionidae (Schultze, 1854)

Subfamily: Nonioninae (Schultze, 1854)

Genus: Nonion (Monthfort, 1854)

**Species: Nonian asterizans (Eichtel & Moll)**

**Description:** Test compressed, low trochospiral, ovate to circular in outline. Umbilici partially to completely filled with pustules on the somewhat crenulate inner margins of the chambers. Sutures slightly curved, depressed near the umbilici. Overall rounded to sub-rounded periphery.

**Remarks:** U. Cretaceous to Holocene. Cosmopolitan. Infaunal, mud and silt loving, salinity 30-35, typically documented along the shelf regions and may transported to shallow waters.

Family: Elphidiidae (Galloway, 1933)

Subfamily: Elphidiinae (Galloway, 1933)

Genus: Elphidium (DE Montfort, 1808)

**Species: Elphidium discoidale (d'Orbigny)**

**Description:** Test medium size, biconvex, completely involute, broadly rounded periphery, and chambers many, distinct retral processes occurring as only band. Aperture composed of several small opening at the base of the apertural face.

**Remarks:** Lower Eocene to Holocene. Cosmopolitan. Epifaunal, prefers sand, survives through salinity 30-70 and typical for the brakish-hypersaline marshes and lagoons.

**Table 4.2** Table showing the dataset of recovered foraminifera along two transects for sampling stations 1-17.

**Species: Elphidium excavatum (Terquem)**

Station. No.	<i>A. beccarii</i>	<i>A. tepida</i>	<i>A. parkinsoniana</i>	<i>A. juvenile</i>	<i>E. excavatum</i>	<i>E. discoidale</i>	<i>E. species</i>	<i>N. asterizans</i>	<i>N. species</i>	<i>Globorotaloides sp.</i>	<i>Globigerinella sp.</i>	<i>G. bulloides</i>	<i>Gallitella sp.</i>	<i>Bolivina spathulata</i>	<i>Brizalina astriatula</i>	<i>Bulimina</i>	<i>C. refulgens</i>	<i>H. anderseni</i>	Total
1	205	14	11	82	8	2	0	1	0	0	0	0	0	0	0	0	0	0	323
2	285	31	9	47	4	1	0	2	0	1	0	0	0	0	0	0	0	0	380
3	155	9	5	15	2	1	1	1	0	0	0	0	0	0	0	0	0	0	189
4	130	6	0	9	19	13	4	13	0	11	0	1	0	0	0	0	0	1	207
5	233	7	3	6	9	5	8	10	3	1	0	1	0	0	0	0	0	0	286
6	120	6	3	8	0	0	0	0	1	0	0	0	0	0	0	0	0	0	138
7	109	3	0	25	11	2	0	2	1	4	0	2	0	0	0	0	0	0	159
8	178	4	0	12	19	5	2	3	8	9	0	9	0	6	1	3	0	5	264
9	188	7	0	6	35	6	1	8	1	4	1	9	2	1	1	0	2	3	275
10	257	7	0	4	12	5	3	16	4	0	0	0	0	0	0	0	0	5	313
11	147	3	0	10	30	5	1	9	3	5	1	3	0	1	2	4	1	0	225
12	195	4	0	30	31	5	6	29	8	1	1	2	2	0	0	0	2	4	320
13	92	2	0	16	10	13	4	6	0	14	0	11	8	8	8	1	2	0	195
14	241	16	3	26	20	5	4	5	1	3	0	0	2	3	2	1	5	5	342
15	164	16	9	13	12	3	2	4	2	0	0	0	0	0	0	0	0	0	225
16	230	11	0	19	13	6	3	10	0	0	0	0	0	0	0	0	0	3	295
17	218	18	3	12	10	7	6	6	1	3	0	0	0	0	0	0	0	0	284

**Description:** Test medium sized, oval to lenticular in shape, incised sutures form interocular spaces, periphery carinate, wall calcareous, finely perforate, bilamellar, septal flap partly or completely covering previous septa as the new chamber is formed.

**Remarks:** Lower Eocene to Holocene. Cosmopolitan. Infaunal, common with variable sand content in sediments, salinity 15-31, intertidal to subtidal in estuaries, lagoons to continental shelves/slope.

Superfamily: Buliminacea (Jones, 1875)

Family: Buliminidae, (Jones, 1875)

Subfamily: Buliminane (Rhumbler, 1895)

Genus: Bulimina (d'Orbigny)

**Species: Bulimina marginata (d'Orbigny 1826)**

**Description:** Test is cone shaped subcylindrical, triserially arranged characterized by distinct septa and calcareous wall. Coarsely perforate and is moderately smooth but lower margin is marked by short blunt spines.

**Remarks:** Paleocene to Holocene; Cosmopolitan fauna, reported from the shallow marine environments of west coast of India (Nisha N.R., 2002 PhD Thesis, unpublished). Positive correlation with TOC% and negative correlation with coarse sand, Opportunist.

Superfamily Bolivinaea (Glaessner, 1937)

Family: Bolivinidae (Glaessner, 1937)

Subfamily: Bolivininae (Glaessner, 1937)

Genus: Bolivina (d'Orbigny, 1839)

**Species: Bolivina spathulata (Williamson)**

**Description:** Test is triangular to oval shaped characterize by broad chambers and biserial throughout. Pores are seen on the test with irregular/obscured surface of the wall.

**Remarks:** Upper Cretaceous to Holocene; cosmopolitan form. Infaunal-epifaunal, prefers muddy sediments, survives dysoxia.

Genus: Brizalina (O.G. Costa, 1856)

**Species: Brizalina striatula (Cushman, 1992)**

**Description:** Test elongated biserial in nature with acute periphery. Narrow imperforate longitudinal costae most prominently seen on early half of the test.

**Remarks:** Upper Cretaceous to Holocene. Cosmopolitan. Common in bays and lagoons. Probably shelf species which extends into more marine marginal parts.

Superfamily: Rosalinacea (Reiss, 1963)

Family: Heleninidae (Loeblich & Tappan, 1988)

Genus: Helenina (Saundersm 1961)

**Species: Helenina anderseni (Warren)**

**Description:** Tests characterized by low trochospiral to planispiral, all flattened chambers enlarging gradually, sutures curved, oblique, depressed to the spiral side. Whereas on

opposite side sutures nearly radial, straight to slightly curved, depressed with slightly lobulate periphery.

**Remarks:** Holocene. Reported from estuarine environments, marshes, lagoons and typically reported from brackish environments (Gennari et.al 2011)

Superfamily: Planorbulinacea (Schwager, 1877)

Family: Cibicididae (Cushman)

Subfamily: Cibicidinae (Cushman)

Genus: Cibicides (Monthfort)

**Species: Cibicides refulgens de Montfort, 1808**

**Description:** Test low trochospiral to planoconvex, spiral side flat, thick sutures, strongly convex on umbilical side with depressed sutures.

**Remarks:** Paleocene to Holocene. Cosmopolitan. Epifaunal, prefers high energy environments where it attaches to hard substrates.

Superfamily: Globigerinacea

Family: Globigerinidae

**Species: Globigerina bulloides (d'Orbigny)**

**Description:** Test globose, trochospirally enrolled, chambers ovate to spherical but not elongate. Three to five chambers in final whorl, sutures distinct and depressed, umbilicus open. The short blunt spine remnants present resulting in a hispid wall surface.

**Remarks:** Upper Eocene to Holocene. Cosmopolitan.

**Globigerinella Sp.**

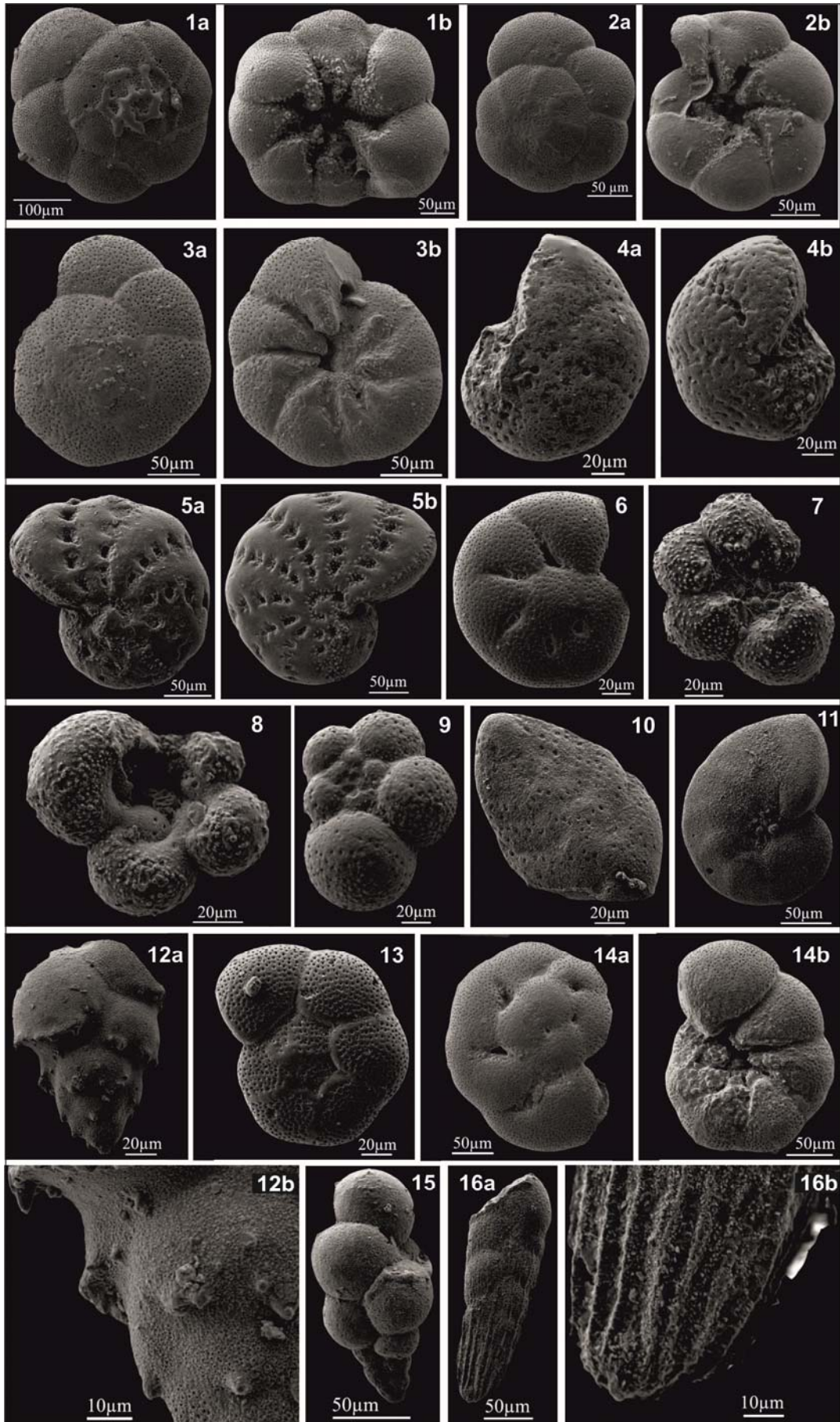
**Description:** Test moderately trochospiral, globular to ovate chambers enlarging rapidly. About 4-6 in final whorl, sutures radial, straight, depressed, peripheral outline lobulate.

**Remarks:** Type species: *Globigerina aequilateralis* Brady 1879. U. Oligocene to Holocene

**Globorotaloides Sp.**

**Description:** Test globular to subglobular and compressed; about 5-6 ovate to spherical chambers in the last whorl. Primary aperture interiomarginal.

**Remarks:** Type species: *Globorotaloides variabilis*. M. Eocene to U. Miocene, tropical-subtropical, cosmopolitan.



### **Eponides Sp.**

**Description:** A low trochospiral coil of about 6-8 chambers in last whorl, with prominent curved sutures and limbate on umbilical side continuing into peripheral keel. Broad low interiomarginal aperture extends from umbilicus to periphery.

### **Gallitellia Sp.**

**Description:** Test elongate, chambers globular and enlarging rapidly as added. Sutures deeply depressed, margins lobulate; aperture simply rounded and umbilical arch at the base of the final chamber.

**Remarks:** Type species: *Gallitellia vivans* Cushman 1934. Pleistocene to Holocene.

### **Trochammina sp.**

**Description:** Test free, trochispiral, chambers increasing gradually in size as added. Sutures radial, periphery rounded-subrounded, wall finely agglutinated, imperforate. Umbilical-extra umbilical arch with narrowed bordering lip.

**Remarks:** Carboniferous to Holocene, cosmopolitan, Reported from coastal areas of India, brackish.

The recovered foraminiferal assemblage in the surface rann sediments in northwestern portion is dominated by the species belongs to genus *Ammonia*. The species of *Ammonia* genus are very robust and can survive through considerably large changes in physico-chemical parameters as compared with the other genera species (Murray, 2006). It is also known for having large number of morphotypes of each species and ecophenotypism (Walton and Sloan, 1990; Carboni and Bella 1996, Hayward 2004). In the present study, a simple classification is adopted to separate all the species into three major typical type species i.e. of *Ammonia tepida*, *A. beccarii* and *A. parkinsoniana* as the present exercise is limited up to identification the overall assemblage in the Bet Zone and to note its response to the rapidly changing “temporary/seasonal environment”.

## **SPATIAL DISTRIBUTION OF FORAMINIFERA**

### **Transect-I**

The westernmost stations 1-3 show more than 95% of *Ammonia* genera (Fig. 4.5e), mainly classified into three type species viz., *Ammonia beccarii* (63-83%), *Ammonia tepida* (4-8%) and *Ammonia parkinsoniana* (~2.5-3-5%) (Fig. 4.5a-c). The remaining

assemblage is represented by *Elphidium excavatum*, *E. discoideale* (1-3%) and *Nonian* species (Fig. 4.6). The juvenile forms of *ammonia* are notably high in proportion contributing ~25% of the total population at station 1 and gradually decreasing to >5% at station 5 (Fig. 4.5d). Station 1-2 are from the depression in the westernmost part of transect which is also drained by a river from the north. This means that the conditions change from open marine influenced to slightly fresh water influenced. The reflection of this change in the foraminiferal assemblage is marked by increase in *A. tepida* from station 1-2, decrease in *A. parkinsoniana* and *A. juveniles* (Fig. 4.5b-d). But at station 3 *A. beccarii* increases with decreasing *A. tepida* and *A. juveniles* whereas, *A. parkinsoniana* appears unaffected with more variation in surface conditions (Fig. 4.5a-c).

Station 4 is away from the depression and is marked by decreased abundance of *Ammonia* to 70% whereas the *Elphidium excavatum* and *E. discoideale* increases to 7% and 10% respectively (Fig. 4.6a-b). This shows the inverse relationship between *ammonia* and *elphidium* species. This station is located at relatively higher elevation than the previous stations which relates with increased salinity and silty substrate preferred by *elphidium* species (Fig. 4.3 and Fig. 4.6). The planktonic foraminifers belonging to *Globigerina bulloides*, *Globorotaloides sp.* contributing almost 6% of the total population recovered from station 4 (Fig. 4.6d-e). The planktonics may have been transported through repeated marine flooding. At station 5 & 6, *A. beccarii*, *A. tepida*, *A. parkinsoniana* increases to overall 99% of the total assemblage while *E. excavatum* & *E. discoideale* decrease to zero at station 6 (Fig. 4.6a-b).

Further east, at stations 7-11 also, the foraminiferal assemblage is dominated by *ammonia* species but *A. parkinsoniana* is absent. The proportion of *A. beccarii* and *A. tepida* remains constant except at station 10 where it increases considerably to 82%. The inverse relationship of *A. beccarii* & *A. tepida* with *E. excavatum* and *E. discoideale* is observed at these stations also i.e. increase in *ammonia* species accompanied by decrease in *elphidium* species (Fig. 4.5e and Fig. 4.6c). At station 7 drastic increase in the juvenile forms is observed contributing ~15% of the total population. The planktonic foraminifera *G. bulloides* and *Globorotaloides sp.* are present at all these stations except station 10 (Fig. 4.6d-f). The maximum planktonics were recovered from stations 8 & 9. These sites fall in a depressed area which is more readily submerged by marine flooding. Station 10

on the other hand lies behind the elevated area which is explains the absence of the transported planktonic foraminifera, reduced *elphidium* and increased *A. beccarii*.

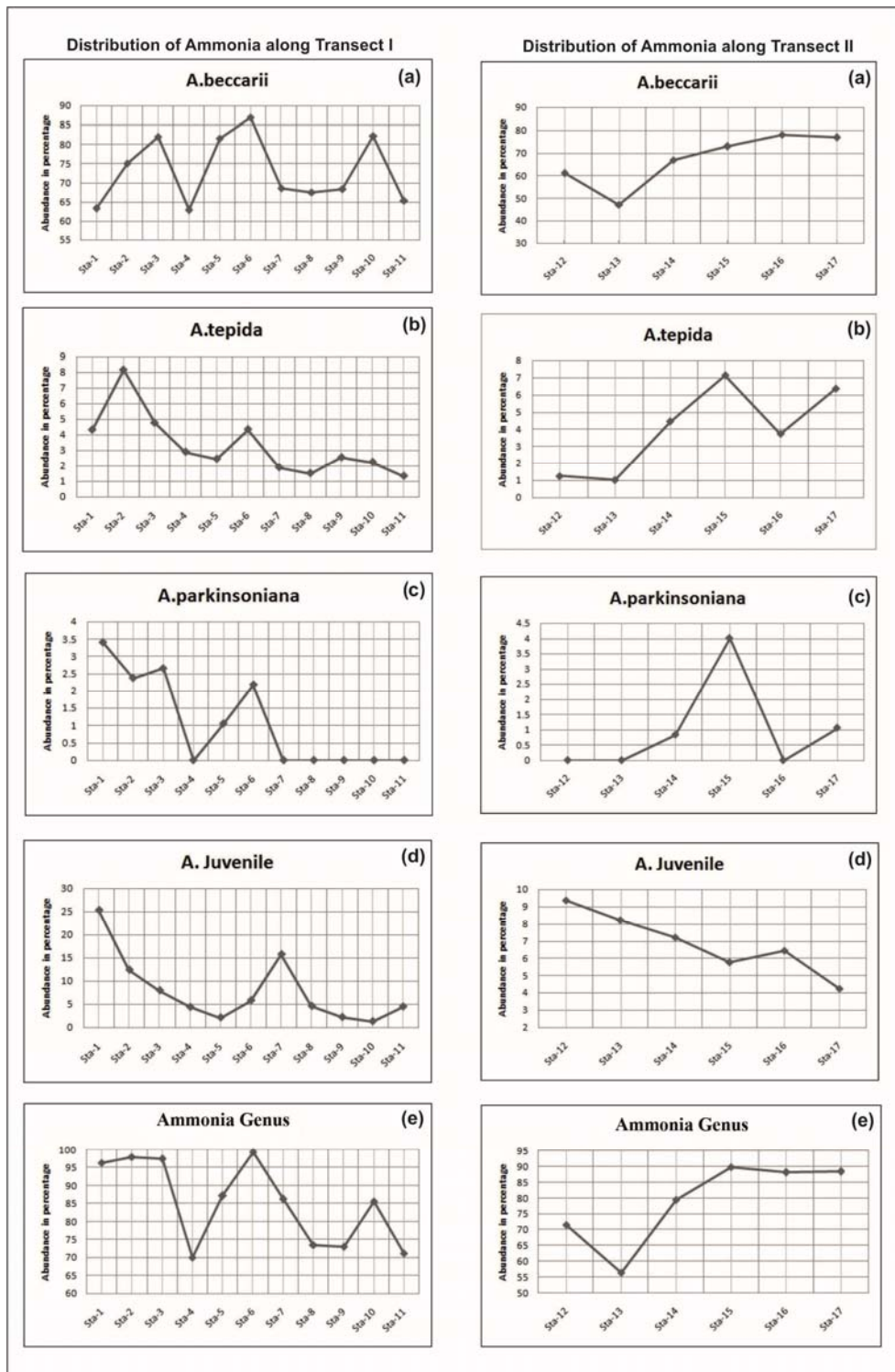


**Figure 4.5** Graph showing spatial distribution of Ammonia genus along the two transects.

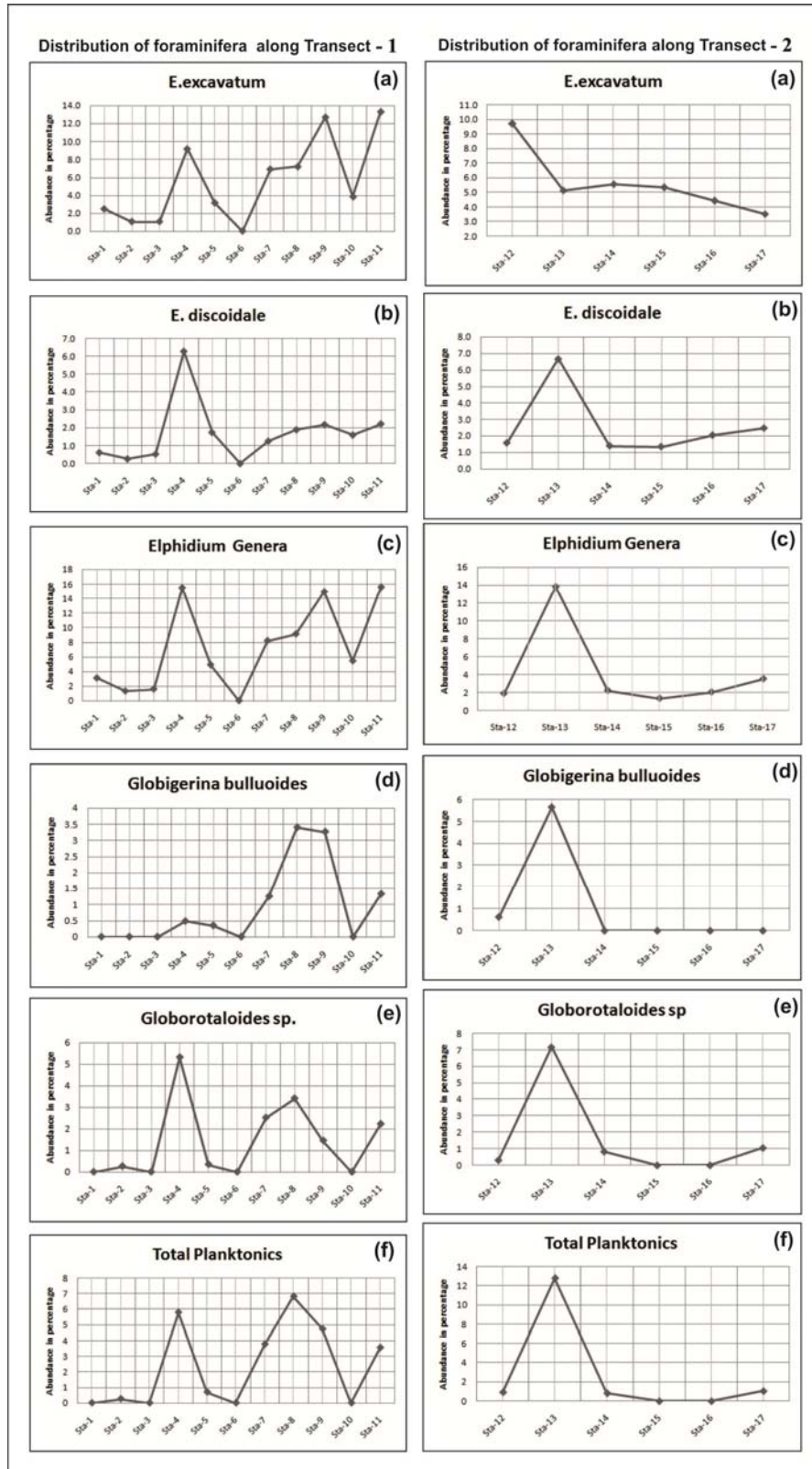


**Figure 4.6** Graphs showing spatial distribution of foraminifera along the two transects

## Transect 2

The overall foraminiferal assemblage along the roughly N-S trending transect 2 largely remains similar with the previously described transect 1 (Table 4.2). Station 12-14 shows dominance of *Ammonia beccarii* followed by *A. tepida* while *A. parkinsoniana* is absent at station 12 & 13 but present at 14 (~1%). Station 13 however shows a relative decrease in the ammonia species and increase of *E. excavatum* and *E. discoideale* (Fig. 4.6a-b). *A.* juveniles are also observed maximum at station 12 which gradually decrease towards successively northward stations (Fig. 4.5d). The planktonic foraminifera recorded maximum at the station 13 (Fig. 4.6d-f). The inverse relation of *ammonia* and *elphidium* is noted in this transect also. This variation in the *ammonia*, *elphidium* and presence of the planktonic foraminifera at station 13 is on account of the microgeomorphic setting of the site (Fig. 4.2; Fig. 4.5; 4.6). The station falls within a sheltered zone where the low energy water further loses its energy. As the site is slightly elevated and forms a small obstacle to further northward movement of submerging waters, the transported sediments and microfossils are laid down on the elevated surface. This has resulted in increased sand proportion at this station and relatively increased proportion of planktonic foraminifera as compared to stations 12 & 14 (Fig. 4.6f).

Stations 15-17 show more or less consistent occurrence of the *A. beccarii* (70-80%) but *A. tepida* (7-6.5%) and *A. parkinsoniana* are almost absent at station 16 (Fig. 4.5a-c). The decrease of the *ammonia* is interestingly marked by the increased proportion of *A.* juveniles though the overall dominance of the ammonia species is consistent. *E. excavatum* & *E. discoideale* on the other hand does not contribute more than 4% together and remain in minor proportion (Fig. 4.5; Fig. 4.6; Table 4.2). Planktonic foraminifera are recovered only from station 17 but in negligible amount. Overall, *ammonia* and *elphidium* are found to be of significance while other is of negligible importance at these stations.

## PRESENT DAY ENVIRONMENTAL CONDITIONS

The Bet zone reveals heterogeneous micro-geomorphic environments within the overall supratidal environment of the Great Rann of Kachchh. The grain size parameters, micro-geomorphic variations and microfaunal content in the study area characterize the modern environments in rapidly changing “temporary seasonal environment”.

During the SW monsoon, the mixed marine inundated waters (marine flooding and rain waters) in the rann remains for several months creating a “temporary seasonal environment” that gradually dries within 4-6 months due to evaporation after monsoon season. The marine flooding water occurs on account of the strong southwestern winds that carries living microfauna (foraminifera) into the area. The transported foraminifera get distributed to various pockets into the inundated region. Due to fresh water mixing the environment becomes more stressful for the typical marine organisms like foraminifera. Thereafter, drying of these waters takes place that results in increasing salinity conditions which exerts additional ecological stress the micro-organisms. This “seasonal ecological niche” after few months of inundation vanishes completely resulting in dying of all the transported organisms into the region. In such environments, not all the carried survives but only a few tolerant forms can survive. Secondly, the micro-geomorphic variations due to presence of several bays, elevated areas, seasonal channels and local depressions creates the environment laterally distinct and provides various micro-environments for the organisms. On account of the interplay of fresh-marine interaction and micro-geomorphic characteristics there is significant difference in the rann settings and open coastal environments.

As compared with the modern coastal foraminiferal assemblage of the Gulf of Kachchh, the Bet Zone results into less diverse foraminiferal assemblage and contains tiny tests as compared with open coastal settings such as in GOK (Rajshekhar et al. 2004, Nigam 2000). As explained in the text that there are several factors which add ecological stress on the transported foraminifera from the coastal waters into the rann. The diversity therefore limited to the few tolerant taxa which can survive through such large scale and abrupt changes in the environmental parameters (Murray 2006, Sen Gupta 1999, Boltovsky 1976). A station wise distribution of the foraminiferal assemblage and its significance is discussed below.

The foraminiferal assemblage at stations 1-3 are dominated by *Ammonia beccarii* with a decrease in juvenile forms and fluctuating abundance of *A. tepida* and *A. parkinsoniana* respectively (Fig. 4. 4a-4c of transect 1). These species are well documented from the shallow marine to intertidal sediments (Murray, 2006). They are also known to tolerate large variations in the salinity conditions as encountered in the Bet

zone (Hayward and Hollis 1994, Zaninetti 1982) as well as other environmental parameters such as temperature, oxygen and TOC (Murray, 2006). The decrease in the juveniles from station 1-3 may on account of south flowing rivers exerting stress on the juveniles due to mixing of fresh water with inundating sea water. Of the stations 4-6, only station 4 contains the planktonic foraminifera and increased abundance of *Elphidium* species (*E. excavatum* and *E. discoildale*) that are commonly reported from the marshy, lagoonal shallow marine environments (Alve and Murray 1999).

From stations 7-11, the dominating *Ammonia-Elphidium* assemblage is accompanied by *Nonian* (15%), *Globorotalids* (1.5%) and others taxa such as *Bolovina*, *Brizalina*, *Globigerinella*, *Bulimina*, *Cibicides*, *Halenina* and *Galletelia* which individually contribute below 2% (Fig. 4.5, 4.6 of transect 1). In general, the *Ammonia-Elphidium-Nonian* assemblage dominates throughout transect 1. The other species are transported in the region by marine waters but cannot thrive due to environmental stress and therefore remains in subordinate proportion of total assemblage. Increased abundance of planktic foraminifera is attributed to marine flooding.

The *Ammonia-Elphidium* species dominate the foraminiferal assemblage along N-S oriented transect 2. The northernmost stations 12-13 of this transect show high abundance of *Ammonia-Elphidium-Nonian*, whereas in the southern stations 14-17, *Ammonia-Elphidium* is abundant with observed reduction in *Nonian* species. Station 13 shows the maximum occurrence of the planktonic foraminifera (Fig. 4.6d-f of transect 2). This correlates with the increased sand proportion at this station.

The marginal marine environments are characterized by the rapid changes in the physico-chemical conditions such as nutrients, salinity, oxygen and energy, which create stressed habitats for the foraminifera (Sen Gupta 2002, Debenay et. al., 2000). The predominance of the *Ammonia* and *Elphidium* species in the sediments is noted in the Bet zone that is consistent with the varying hypersaline to brackish submerging waters. The seasonal and episodic nature of the supra-tidal environment marks this region as unique ecosystem, which controls the overall assemblage of foraminifera that are sensitive to the ecological stress. Together with the presence of several bays and variations in elevation of the Bet zone results in the formation of several microenvironments in the overall supra-tidal environment. Such monodominant occurrence of the *Ammonia* has been documented

in earlier studies from raised Holocene sediments along the margins of Khadir, Bhanjada and Kuar bet islands of Great Rann of Kachchh (Khonde et. al. 2011). The west coast marginal marine environments also comprise *Ammonia* bearing assemblage (Nigam and Khare 1999, Nigam and Chaturvedi 2000) that testify to the transport of the microfauna into the Great Rann during sea water ingression.

The Bet Zone of the Great Rann of Kachchh exhibits various microgeomorphic domains due to the presence of islands (bets), elevated surfaces, seasonal streams/river channels, local depressions and pools. The grain size studies show the fine grained nature of the surface sediments mainly silt to silty clay except at or near the river/stream channels where the sand content relatively increases. The benthic foraminiferal population in this seasonally changing environment is characterized by mainly two assemblages *Ammonia-Elphidium* assemblage and *Ammonia-Elphidium-Nonian* assemblage. The benthic assemblage is represented by *Ammonia beccarii*, *A. tepida*, *A. parkinsoniana*, *Elphidium excavatum*, *Elphidium discoidale*, *Bolivina spathulata*, *Nonian asterizans*, *Bulimina marginata*, *Cibicides refulgens*, *Helenina anderseni*, *Brizalina striatula* whereas the planktic foraminifera includes *Globigerinella* sp., *Globigerina bulloides*, *Globorotaloides* sp. and *Gallitellia* sp. The presence of reworked, planktic foraminiferal tests suggests transport from the Arabian Sea to the Bet zone on account of the strong SW monsoon winds. The modern foraminiferal assemblages described from the active coastal systems along the Gulf of Kachchh in the south, reveal significantly higher diversity than present study area (Nigam and Chaturvedi 2000, Rajshekhar 2004). However, such higher diversity near the open ocean gets reduced in the Great Rann due to the typical hypersaline conditions, submergence patterns, mixing by fresh water (runoff, fresh water influx), and the microenvironments created by variations in the elevation of the Rann surface. The diversity is limited to the few tolerant taxa which can survive through such large scale changes in the environmental parameters (Boltovsky 1976, Murray 2006, Sen Gupta 2002). Overall, the Bet zone is an excellent site for studying the foraminiferal response to the rapidly changing physico-chemical parameters in short time span. A detailed laboratory and field monitoring of these parameters and foraminiferal population throughout complete cycle can be helpful to understand the response pattern of various species with respect to the correlative factors.

**Figure 4.4** SEM photographs of the recovered foraminiferal assemblage.

1. *Ammonia beccarii* (Linne, 1758): 1a.Spiral view; 1b. Umbilical view.
2. *Ammonia tepida* (Cushman); 2a.Spiral view; 2b. Umbilical view.
3. *Ammonia parkinsoniana* (d'Orbigny, 1839); 3a.Spiral view; 3b. Umbilical view.
4. *Elphidium excavatum* (Terquem) 4a.Spiral view; 4b. Umbilical view.
5. *Elphidium discoidale* (d'Orbigny) 5a.Spiral view; 5b. Umbilical view.
6. *Elphidium sp.*
7. *Globigerinella sp.*
8. *Glogigerina bulloides* (d'Orbigny).
9. *Globorotaloides sp.*
10. *Bolivina spathulata* (Williamson).
11. *Nonian asterizans* (Eichtel & Moll).
- 12a. *Bulimina marginata* (d'Orbigny 1826); 12b. A close view showing short blunt spines
13. *Cibicides refulgens* (de Montfort, 1808).
14. *Helenina anderseni* (Warren) 14a. Spiral view; 14b. Umbilical view.
15. *Gallitellia Sp.*
- 16a. *Brizalina striatula* (Cushman, 1992); 16b. A close view showing the longitudinal coaste.

### RAISED RANN SEDIMENTS ALONG ISLAND MARGINS: PALAEOENVIRONMENTAL IMPLICATIONS

#### GEOMORPHIC SETTING

The raised rann sediments are found in the form a raised surface, few meters above the present day rann, all around the fringes of the various rocky islands. The raised rann sediments are particularly well exposed in incised cliff sections at the western margin of the Khadir, eastern margin of the Bhanjada and the southern margin of the Kuar bet island. The vast, monotonous region of rann is discontinued by the presence E-W trending discrete blocks of large Mesozoic and Neogene islands along the IBF (Island Belt Fault) namely Pachchham, Khadir, Bela and Chorar. All islands are characterized by steep north facing escarpments which mark the geomorphic expression of E-W trending Island Belt Fault (IBF) that lies buried under the rann sediments further north (Biswas 1993). A strong structural control on the landscape of these islands and evidences of active tilting along these islands in the recent past has been suggested by Chowksey et.al. (2010). Margins of these large islands have provided the space for the sediment accumulation in the sheltered zones whereas erosional processes have developed the typical coastal erosional features like- sea caves, water marks and tidal notches (Maurya et.al. 2009, Chowksey 2010). The present chapter deals with the sediment characteristics, palaeoenvironmental conditions and time of sediment deposition of these raised rann sediments.

The raised rann sediments found attached to the fringes of the rocky islands of Khadir, Bhanjada and Kuar bet in the central part of the Great rann basin (Fig. 5.1). These sediment sequences are laterally extensive in nature and gradually sloping away from the island finally merging in the rann surface. The incised vertical cliffs comprising these sequences are found at the western margin of the Khadir, eastern margin of the Bhanjada and the southern margin of the Kuar bet island respectively (Fig. 5.2). The thickness of cliffs is around ~4-6m forming flat terraced surfaces whose continuity is broken by deep erosional gullies. All the three exposed cliff sections of the rann sediments in Khadir,

Bhanjada and Kuar bet islands were selected for the present study (Fig. 5.2). Vertical litholog of the sections were prepared and their sedimentary characteristics were noted by observing the entire length of the cliffs. For sampling, the cliff sections were trenched 1 - 1.5m into the cliffs to eliminate the effect of contamination due to exposure to present conditions including the ~1 m deep saline waters that flushes basal part of the sections during periods of inundation of the rann surface. All the three sections were sampled at ~5 cm interval for micropalaeontological, sedimentological, and mineralogical studies.

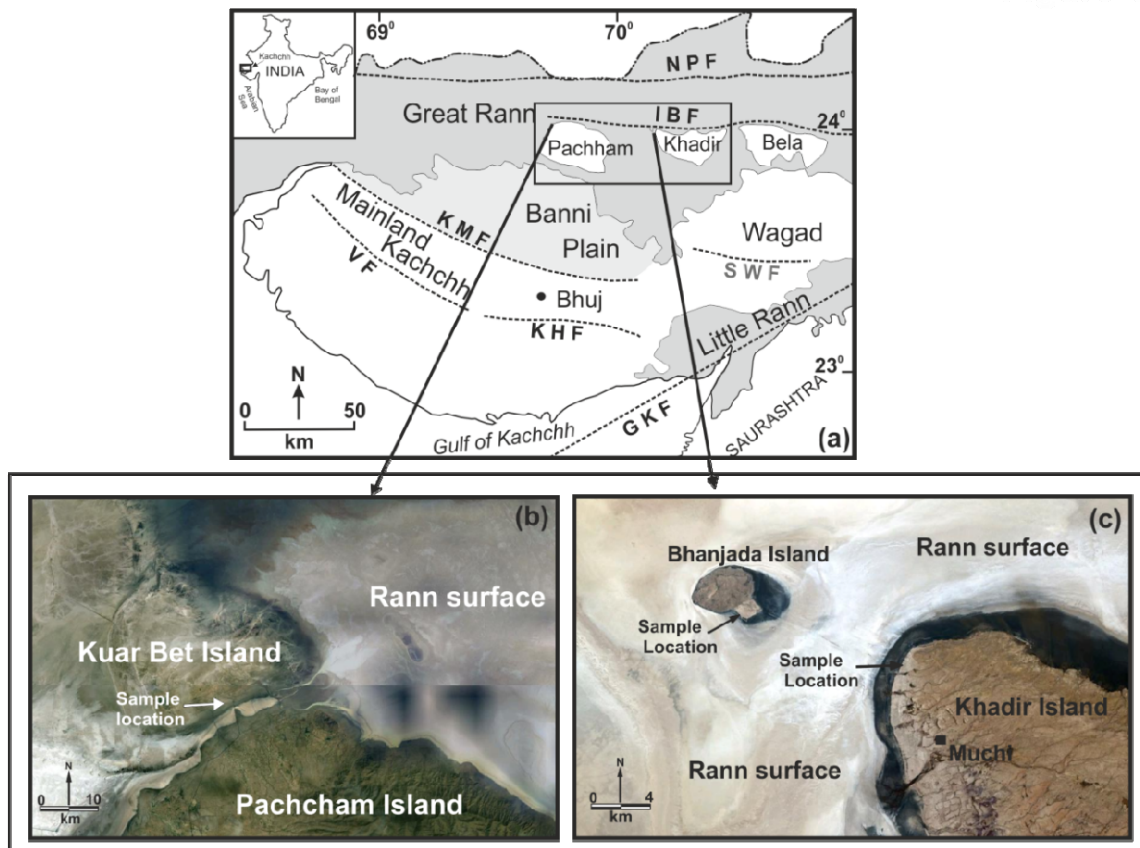


**Figure 5.1** *a*, Map of Kachchh basin showing the fault-controlled geomorphic set-up. Note the vast extent of the Great Rann forming the northern part of the basin. Unshaded areas are occupied by Mesozoic and Tertiary rocks. Boxed area shows the rocky islands of Pachcham and Khadir within the Great Rann. (Inset) Location map. *b*, Satellite image of the northwestern part of Khadir and Bhanjada islands showing the location of the sections studied (source: [www.googleearth.com](http://www.googleearth.com)). *c*, Satellite image of the northwestern part of Pachcham and Kuar Bet island showing the location of the sections studied (source: [www.googleearth.com](http://www.googleearth.com)).

## **SEDIMENTARY CHARACTERISTICS**

### **Khadir island section**

The Khadir cliff section occurs along the western margin of the Khadir island (Fig. 5.1b). The section abruptly rises from the salt encrusted rann surface in the northwestern tip of the island and abuts against the Mesozoic and Tertiary rocks inlandward (Fig. 5.2a). The sequence forms a narrow terraced surface that slopes down southwards finally merging with the rann surface. The southward tilt of the surface is in conformity with the tilt block structure of the island that also indicates active tilting during the Holocene time (Chowksey *et al.*, 2010). The maximum thickness is ~5m near Muchhi at the northwestern tip of the island where they directly rest over the Mesozoic rocks with ~20cm thick pebbly gravel at the base. The overlying sediments show a remarkable homogeneity in terms of grain size along with a strong horizontal stratification. Lithologically, the sediments range from silty sand to sandy silts with clay as minor component (Fig. 5.3).

Though visually the sediments appear uniform, the sedimentological and mineralogical studies of the samples under microscope reveal subtle variations vertically through the section. The top part of the sequence (0m to ~2m depth) is compact in nature and characterized by presence of thin laminations. Grain size is very fine and mainly contains grains of quartz, mica, few dark coloured minerals and salts. The quartz is angular to subangular in nature and so is the case with other minerals except the salts. Muscovite mica dominates the flaky mica group yet few biotites are also observed. The white coloured salt grains are lenticular to discoidal in shape. The biotic component of the sediments includes foraminifera, ostracoda, few gastropods and occasionally the pteropod shells. This zone is characterized by the highest abundance of the foraminiferal tests per unit sample described later in the text. Underlying these sediments, the horizontally stratified alternate layers of sandy silts and silty sands occur from ~2 - 4m depth. This zone is distinguished by the increased grain size as compared to the overlying sediments. The overall mineralogy remains same and grains show angular to subangular nature with moderate sorting. Here in this zone, along with the discoidal gypsum grains, few nodular salts are also seen (Fig. 5.4a and 5.4b). The bioforms are relatively less abundant. Third zone is from below ~4m depth upto the base of the sequence. Grain size of these sediments is slightly coarser though the overall textural and mineralogical characteristics

remain the same. However, few small dispersed rock fragments from locally derived rocks of Mesozoic and Neogene rocks sequences are observed in this part. Amongst salts, gypsum appears in crystallized form forming rosettes and large disc agglumates indicating the evaporative conditions. The biotic component is negligible and rapidly decreases downward to reach a completely barren part in the lower portion. The bottom ~0.5 m thick massive clay is devoid of any bioforms and contains gypsum crystals in large proportion. The clay is underlain by basal gravel.

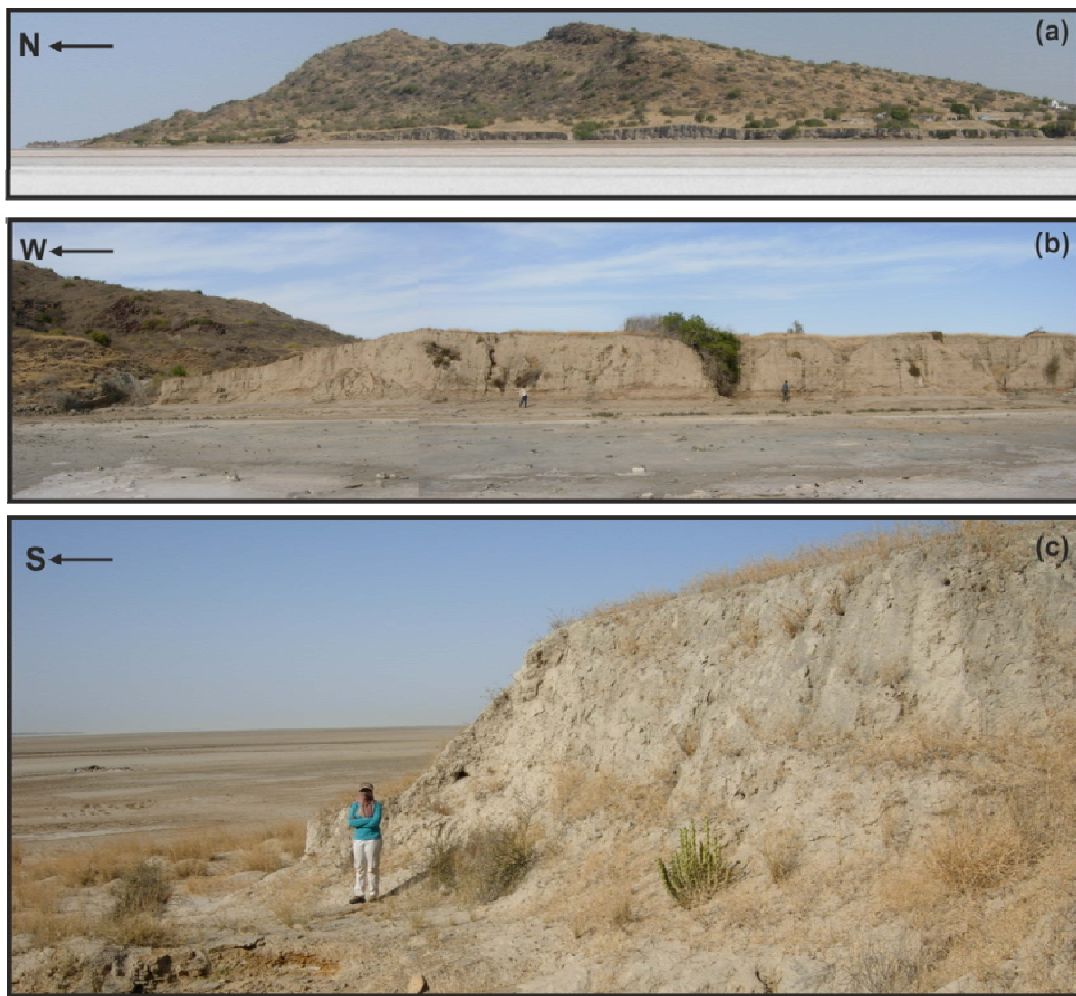


**Figure 5.2.** *a*, View of the northwestern margin of the Khadir island. The foreground is the salt-encrusted rann surface and vertical cliff section of the raised rann sediments at the base of the island. *b*, View of the southern cliff face of raised rann sediments rising above the rann surface at eastern fringe of the Bhanjada island. Part of the rocky island is visible to the left. *c*, View of the raised rann sediments at southern margin of the Kuar Bet island. Rann surface is seen in the background.

### **Bhanjada island section**

The Bhanjada island is a small, rocky, oval shaped island situated in west to the Khadir that comprises of basic intrusive igneous rocks. It abruptly rises above the rann surface at ~4km far from the Khadir island (Biswas 1993) and is separated by a stretch of salt encrusted rann surface (Fig. 5.1b). The present sequence forms a terraced surface that is attached to the eastern margin of the Bhanjada island (Fig. 5.1b). This surface covers eastern to southwestern periphery of the island whereas rest of the peripheral region of the oval shaped island is characterized by rocky outcrops. The surface however is uneven owing to formation of small channels, rills and gullies meeting the rann. Continuous vertical cliff sections are seen rising to average 3 - 4m above the rann surface. Maximum exposed thickness of ~6m is found preserved along the southern margin of the rectangular terraced surface (Fig. 5.2b). Visually, the sediment succession shows uniform characteristics with strong horizontal stratification and appears similar to the Khadir island section. Lithologically, the succession comprises alternate layers of silty sands and sandy silts with salt grains (Fig. 5.3).

Microscopic examinations of the samples reveal presence of quartz, salts and locally derived dark minerals and small proportion of the rock fragments. The sequence is divisible into two zones based on the sediment characteristics. The upper zone upto the depth of ~1m consists of well sorted fine silty sand. The quartz grains are subangular in nature whereas the dark minerals are elongated. Micas comprise dominantly muscovite and less amount of the biotite. Salt grains are of discoidal shape with infrequent lenticular grains as compared with the Khadir sequence (Fig. 5.4a). The bioforms observed include foraminifers, ostracods, gastropods, and occasional pteropods. Below this the entire section consists of horizontally stratified silty sand with thin layers of very fine sand. However, the sediments are relatively coarser and show moderate sorting.

Salts of discoidal and lenticular shape are present with gypsum rosettes and discoidal agglumates (Fig. 5.4a and 5.4b). The bioforms are similar to that of the Khadir island section but show greater consistency vertically through the sequence. The sediments overlie a basal gravel horizon whose clasts are derived from local igneous intrusive rocks that make up the Bhanjada island.

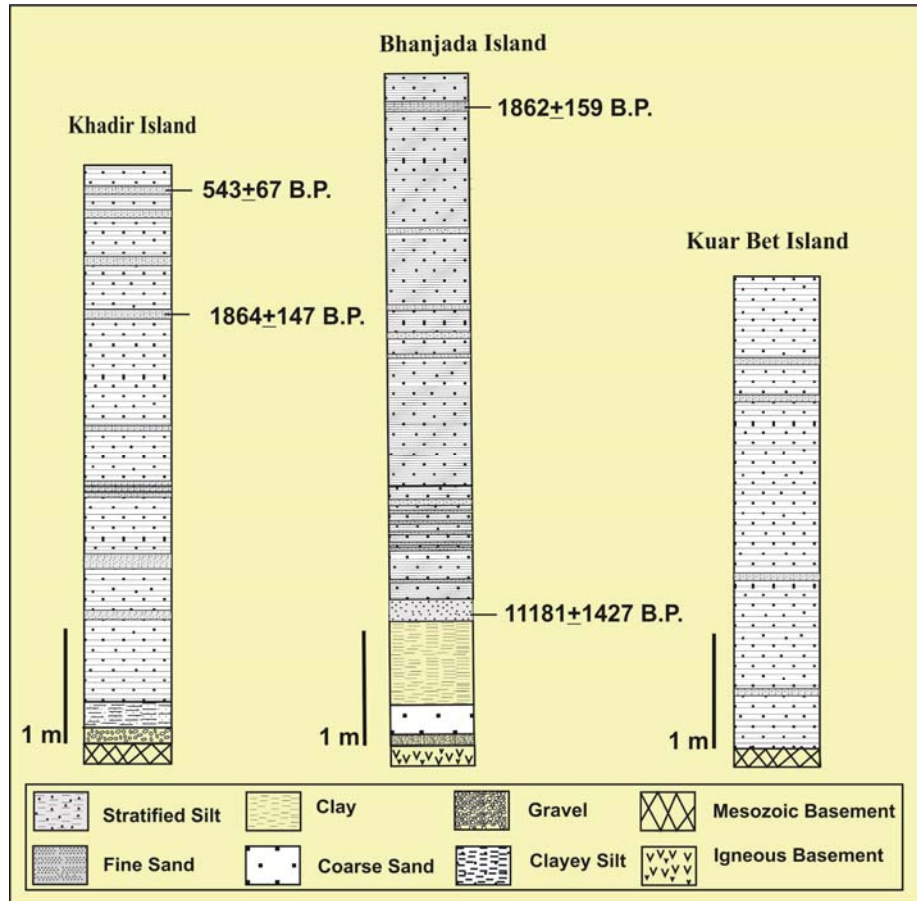


**Figure 5.3** Lithologs of the raised rann sediments in Khadir, Bhanjada and Kuar Bet islands in the Great Rann. Note the dominantly fine-grained lithology and the similarity in gross lithology in all the three islands. OSL dates obtained are also shown.

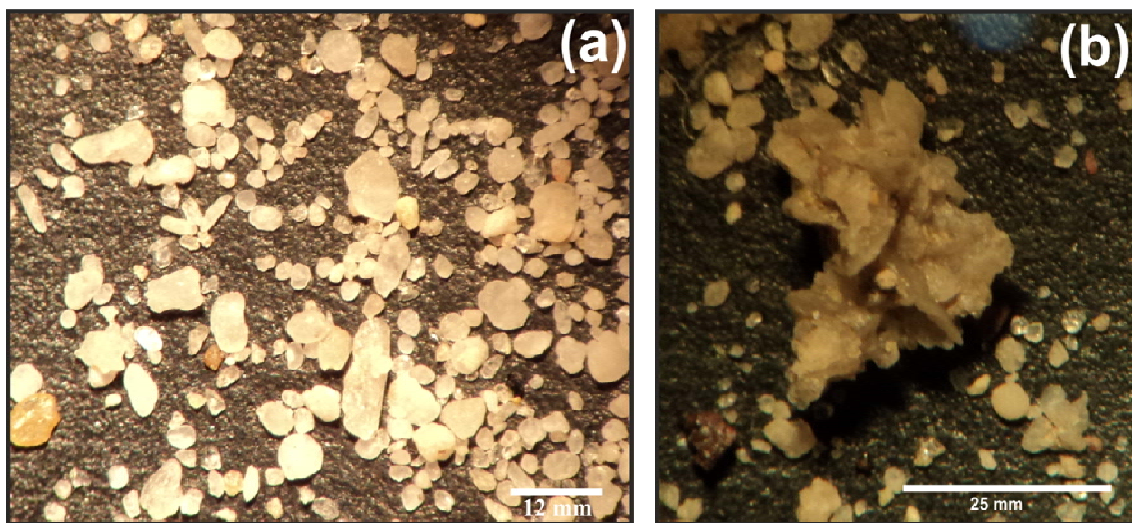


**Figure 5.4** *a*, Photomicrograph of the sediments showing discoidal and nodular gypsum crystals. *b*, Photomicrograph showing discoidal gypsum forming large agglomerates in the sediments.

### **Kuar bet island section**

Kuar Bet is located northwest of the Pachcham island (Fig. 1c). A narrow stretch (~1.5km) of the salt encrusted surface of the Great rann separates the Kuar bet from the Pachcham island. The raised rann sediments form ~5m high vertical cliffs dissected by gullies along the southern margin of the Kuar bet island (Fig. 5.2c). This sediment sequence overlies the older Mesozoic sedimentary rocks. The sediments consist of horizontally stratified sandy silts and silty sands similar to the earlier sequences at Khadir and Bhanjada islands (Fig. 5.3). A marginal variation in grain size and sorting is observed in present cliff section. Mineralogically, the sediments comprise quartz, mica with muscovite as dominant mineral and salt grains of discoidal and nodular shape. In the basal part of the section, microscopic agglumates of the discoidal salts forming various shapes like elongate branched tubes are observed. Locally derived fine lithic fragments of the older Mesozoic rocks are commonly seen. The biotic content includes foraminifers, ostracods, pteropods, gastropods with varying abundance. The proportion of the pteropods however notably more as compared with the other two sequences described earlier. The size of the gastropods and pteropods is also observed to increase in the Kuar bet sequence on account of its vicinity to the typical marine waters in the past.

### **CHRONOLOGY**

The Khadir and Bhanjada island sections were dated using Optically Stimulated Luminescence (OSL) technique. In Khadir island section, the samples were collected at 0.20 m and 1.80 m depths, while at Bhanjada island section, the samples were collected at 0.20 m and 4.75 m depth (Table 5.1). The dating was carried out at Wadia Institute of Himalayan Geology (WIHG), Dehradun. The two samples from Khadir island section at 0.20 m and 1.80 m depths yielded ages of  $543 \pm 67$  B.P. and  $1864 \pm 147$  B.P. respectively (Table 1). Samples from Bhanjada island section at 0.20 m and 4.75 m depths yielded ages of  $1862 \pm 159$  years B.P. and  $11181 \pm 1427$  years B.P. respectively (Table 5.1). The OSL dates suggest uninterrupted sedimentation around the margins of the rocky islands in the Great Rann throughout the Holocene times up to ~500 yrs B.P.

**Table 5.1** Table showing single aliquot regeneration OSL ages and data for raised sediments from Khadir and Bhanjada bet islands.

Sr. No.	Location	Depth	Obtained dates	U (ppm)	Th (ppm)	Potassium K%	Eq. dose (De) Gy	Dose rate Gy/ka
01	Khadir island	0.2 m	543± 67	0.4	7	1.13	1.0±0.1	1.9±0.1
02	Khadir island	1.8m	1864± 147	1.84	4	0.76	3.0±0.16	1.6±0.1
03	Bhanjada island	0.2m	1862± 159	4.68	12	1.04	5.6±0.4	3.0±0.2
04	Bhanjada island	4.75m	11181± 1427	0.32	3	0.95	15.9±1.7	1.4±0.1

### MICROPALAEONTOLOGICAL STUDIES

For sampling, the cliff sections were trenched ~1 - 1.5m into the cliffs to eliminate the effect of contamination due to exposure to present conditions including the ~1m deep saline waters that flushes basal part of the sections during periods of inundation of the rann surface. The step trench of the section was then subjected to close sampling at ~5cm interval for micropalaeontological, sedimentological, and mineralogical studies. For micropalaeontological studies, selected samples were processed by following standard conventional methodology described by Murray (2006). Almost 300 foraminiferal tests were picked from most of the samples from most of the samples. The generic level identification was attempted by using standard references (Loeblich and Tappan, 1988). In the following paragraphs, the results of micropalaeontological analyses and its palaeoenvironmental implications is discussed.

#### Khadir island section

The foraminifers were handpicked from the samples and studied under microscope following standard procedures (Murray 2006). The genera identified from the Khadir island section include *Ammonia*, *Trochamina*, *Anomalinoidea*, *Elphidium*, *Nonian* and *Epistominella*. The overall foraminiferal assemblage of the sequence indicates deposition in shallow marine environment. The vertical distribution of the foraminifera throughout section were also calculated which shows the significant variations in the abundance of foraminifera per unit sample. Three zones are identified viz. the maximum abundance zone, fluctuating abundance zone and third, the barren zone which is almost devoid of any fresh foraminiferal tests (Fig. 5.5).

The fluctuations in the abundance of foraminifera are found to correlate with the sedimentary characteristics described earlier. The first zone (0 - ~2m down) is characterized by the fine grained sediments and yields the maximum foraminiferal tests that ranges more than 8000/g and minimum up to 2000/g of processed sediments (>63 micron fraction). All the recovered test belongs to the spherical rounded foraminifera whereas; there was no elongate or lenticular foraminifer in the samples. The morphological features are well preserved but the size of the tests is less as compared with the typical present day coastal foraminifera along the Kachchh coast (Rajshekhara et al. 2004, Nigam and Chaturvedi, 2000). Some broken tests are also recovered in some samples but the proportion is rare.

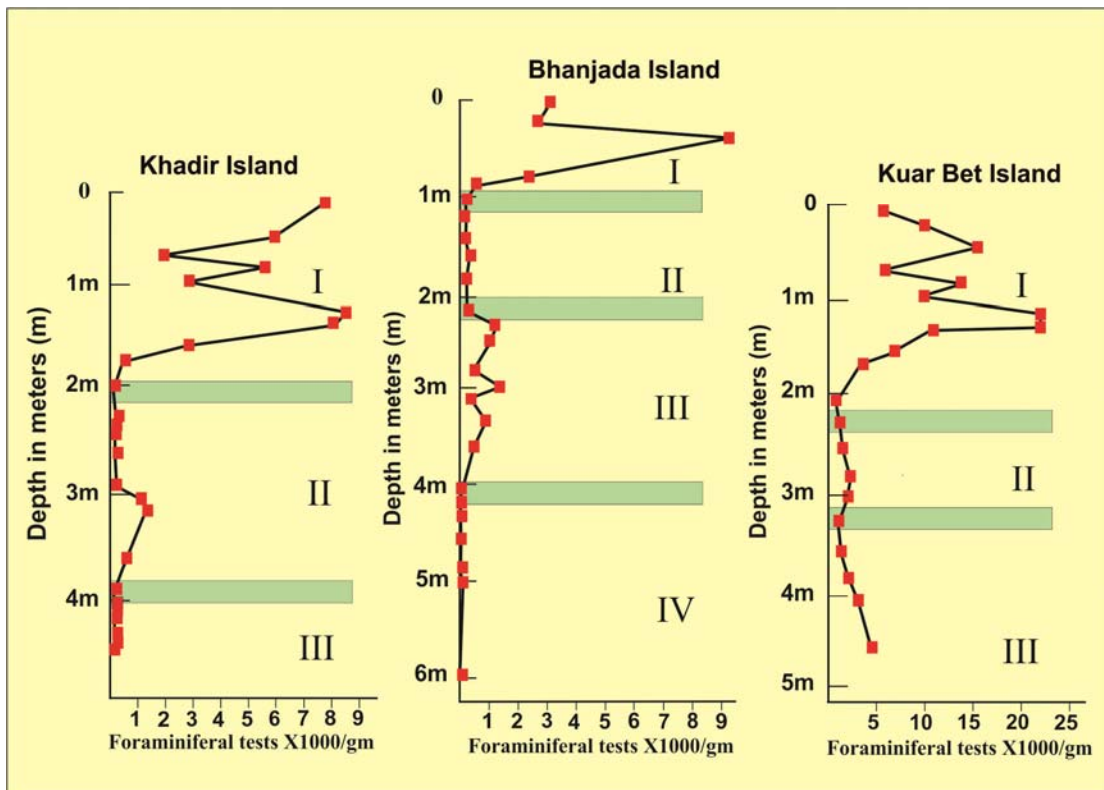


**Figure 5.5** Graphs showing vertical distribution and abundance zones of foraminiferal tests throughout the cliff sections at Khadir, Bhanjada and Kuar Bet islands.

The intermediate abundance zone (~2-3.5 m) is characterized by the decreased foraminiferal yield per unit sample (Fig. 5.5). This zone also shows mixing of the older foraminiferal tests with in situ tests. These older tests, derived from marine Tertiary rocks exposed inland, are relatively large sized and are reworked as indicated by loss of morphological characters and pinkish to brownish red in colour of the test. The loss of

morphological features is clearly evident while observing under the microscope. Relative abundance of these older, reworked foraminifera remains consistently less than the in situ, fresh foraminifera. The third zone (below 3.5m) is almost devoid of the in situ foraminiferal tests but very few older foraminifers continue to occur (Fig. 5.5). This zone is, therefore, identified as the barren zone that is devoid of any fresh foraminiferal tests in the samples.

### **Bhanjada island section**

The foraminiferal assemblage recovered from the Bhanjada island section includes *Ammonia*, *Trochamina*, *Anomalinoidea*, *Elphidium*, *Nonian* and *Epistominella*. Other bioforms observed includes the ostracods, few gastropods, and pteropods. *Ammonia* is the most dominant genera here as the case with the sediments of Khadir island described above. The assemblage is indicative of shallow marine depositional environment. The variations in vertical distribution of foraminifera in the Bhanjada island section are significant. Based on this, the sediment succession is divisible into four zones of abundance namely, the zone of maximum abundance, the zone of intermediate abundance, the zone of fluctuating abundance and the zone of minimum abundance (Fig. 5.5). In contrast with the Khadir sequence, the foraminifera continued to occur till the lower part of the section. The topmost zone is the zone of maximum abundance (0 - 1m) which shows highest number (9000) of tests per gram of the sediment. In this respect, this zone is comparable to the upper zone of the Khadir island section. The second zone is the zone of intermediate abundance (1 - 2m depth) which shows less than thousand tests per gram of the sediments (Figure 5.5). The third zone (2-4m depth) shows the large scale fluctuations per unit sample and therefore named as the zone of fluctuating abundance. This zone shows variations in the foraminiferal count from few hundred to ~2 thousand tests per gram sediment. In lower portion of this zone, occurrence of the few older foraminiferal tests is noted. These older, reworked foraminifera appear similar with those found in Khadir island sequence. The proportion of older and broken tests is increased as compared with the earlier Khadir sequence. These (older) tests are rounded on account of reworking and the morphological features are poorly preserved. Since the Bhanjada island is made entirely of igneous rocks, the older foraminifera are obviously derived from the same Tertiary lithologies that are exposed in the nearby areas which have contributed to the

Khadir island sequence. In situ foraminifers are small in size but their morphology is well preserved. Below ~4m is the zone of minimum abundance. Here, the abundance of in situ foraminiferal tests is reduced but they continue to occur in association with the older foraminifera. The generic assemblage is similar to the Khadir island section. The similarity of the sediments and foraminiferal assemblage of the Khadir and Bhanjada islands points to identical depositional environments, which is also corroborated by the identical geomorphic settings to the sediments.

### **Kuar bet island section**

The Kuar bet island section was also studied for its foraminiferal content. The foraminiferal assemblage recovered comprise *Ammonia*, *Trochamina*, *Anomalinoidea*, *Elphidium*, *Nonion* and *Epistominella*. *Ammonia* continues to remain the dominant genera in the Kuar bet section as well. Although, overall assemblage is comparable with the Khadir and Bhanjada island sections; the overall abundance of the other genera is relatively increased in association with *Ammonia*. The tests are morphologically well preserved and characterized by increased size of the tests compared with the other two studied sequence. Based on relative abundance, the Kuar bet section is vertically divisible into three zones – the upper zone (0 - 2.5m), zone of fluctuating abundance, the middle (2.5 - 3.5m) zone of intermediate abundance and the lower zone (below 3.5m depth) is the zone of increasing abundance (Fig. 5.5). The foraminifers indicate conditions similar to those existing at the margins of the Khadir and Bhanjada islands, though, the increased size of the tests and the relatively increased abundance of genera other than *Ammonia* suggests the existence of relatively favourable conditions.

### **PALAEOENVIRONMENTAL IMPLICATIONS**

The geomorphic setting of the sediments and the fact that the rann surface is a now dried up palaeo-sea floor suggests that the sediments were deposited during Holocene along the shorelines of the rocky islands. The sediment succession comprises horizontally stratified sandy silts and silty sands with minor variations in grain size (Fig. 5.3). Mineralogically, the sediments contain mainly quartz, mica (muscovite), salts and few dark minerals. Salts occur in fairly large proportion in all the three sediment sections. The salts are obviously derived from the marine waters that previously occupied the rann surface as there is no source for salts on the rocky islands. The salts comprise mainly

discoidal and nodular grains of gypsum typically formed in marine marginal settings (Fig. 5.4). Overall, the salt rich sediments suggest prevalence of hyper-saline conditions during their deposition. Salt rich sediments with similar textural characteristics in modern day marginal marine settings are reported from several places like the Abu Dhabi sabkha (Bulter 1969, Cann et.al. 2004, Warren 2006).

The foraminiferal assemblage recovered from the three island sections is remarkably similar which strongly point to the existence of more or less similar environmental conditions along the margins of the islands. The observed genera belong to typical shallow marine environment (Murray 2006). *Ammonia* is found to be consistently dominant vertically through the sediment succession in all the three sections studied. Relative abundance of the genera shows that *Ammonia* contributes up to 80-85% of the total recovered foraminifera. The monodominant nature of the *Ammonia* is not uncommon and is encountered from various environmental settings (Phleger, 1970; Walton and Sloan, 1990; Ahuva Almogi-Labin *et al.* 1992, Wenrich *et. al.* 2007). It is considered as one of the most tolerant foraminifera to the fluctuating salinities (euhaline) and can tolerate fluctuating temperature conditions (Boltovskoy *et. al.* 1991, Scott *et. al.* 1976; Wenrich *et. al.* 2007). In specific environmental settings, the monodominant occurrence of *Ammonia* is not uncommon and is known from many pockets around the globe (Walton and Sloan 1990). It also shown to survive through wide range of temperatures (Brooks 1967) and is also known to be tolerant to wide range of salinity conditions (Scott *et.al.* 1976, Bradshaw 1961, Murray 2006). *Trochamina* is another genus commonly found in marine marginal environments (Hayward, 1993; 1994) and is also recorded from salt marshes (Patterson *et. al.*, 2004; Horton and Murray 2007, Gehrels and Newman 2004). The survival of *Trochamina* through low oxygenated condition is also well documented (Moodley 1992, Sen Gupta and Platon 2006). *Elphidium* and *Nonian* are also known from the high salinity regimes (Cann and De Decker 1981, Cann *et. al.* 2000a, 2000b).

The overall foraminiferal assemblage and vertical variations in the abundance suggests hyper-saline to brackish conditions in the vicinity of the islands in the Great Rann. The sediment characteristics also advocate the existence of the hypersalinity conditions during the deposition of these sediments indicated by the presence of salts in abundant proportion. The nodular and rosetts forms in a peculiar hypersaline conditions

that can be seen in present day sebkha environments like Abu Dhabi and Persian Gulf (Warren 2006). The vertical variation in abundance of the foraminifera through the sediment successions is significant (Fig. 5.5). The foraminiferal abundance in all the three sequences show specific pattern of increasing and decreasing forams per unit sample. Based on the abundance pattern of the foraminifera per unit sample several zones are identified. The wide variations in abundance patterns of the foraminifers is attributed to changes in the salinity conditions. The salinity changes cannot be ruled out as there is a strong possibility of periods of enhanced fresh water influx from the adjacent landmass. Second, is the largely homogeneous nature and absence of discordant sedimentary depositional feature or any abrupt termination or change in the nature of the sediments and the foraminiferal assemblage suggests that the conditions remained uniform with short term fluctuations from brackish to hypersaline. These conditions persisted along the island margins for a long period of time during the Holocene.

The chronological data suggests an average sedimentation rate of  $\sim 1.22$  mm/year for the Khadir Island and  $\sim 0.48$  for the Bhanjada Island. The lower rate of sedimentation at Bhanjada Island is in conformity with the fact the eastern margin formed a sheltered or a shadow zone when the shallow gulf occupied the Great Rann which was connected to the Arabian sea in the west. This is comparable with the present day conditions in the Gulf of Kachchh in the southern part of the Kachchh where the sediments coming from the Arabian Sea in the west are distributed along its northern and southern coastlines (Chauhan 1994). Assuming a similar setting in the Great Rann, it is obvious that the eastern margin of the Bhanjada Island was located in the shadow zone that resulted in low rate of sedimentation. The sedimentation at Bhanjada Island terminated at around 1860 yr B.P. However, no major shift in environmental conditions is indicated by the micropalaeontological data from the Khadir Island where the sedimentation continued up to  $\sim 500$  yr B.P. It is inferred that the geomorphic setting of the sediment starved eastern margin of the Bhanjada Island is primarily responsible for the early termination of sedimentation, rather than a change in environmental conditions. The elevation difference of the sediment successions in the Bhanjada and Khadir islands is attributed to the differential post-depositional uplift along the Island Belt Fault (IBF) and associated cross faults (Biswas and Khattri 2002).

The OSL dates obtained are in conformity with historical accounts that describe ships reaching up to a port called Verawow in Nagar Parker hills located at the northern margin of the Great Rann, which was abandoned about ~500 years as the sea dried out (Frere, 1870). This suggests the existence of a shallow but navigable sea that was responsible for the deposition of sediments along the shores of the rocky islands until ~500 years before present. The salt encrusted rann surface itself is regarded as an uplifted paleo-sea floor as evidenced by several earthquakes in the region during the last 400 years (Burnes 1835, Glennie and Evans 1976, Merh, 2005). Recent studies have documented raised notches and other marine erosional features at ~2-6m above the rann surface at the base of the north facing escarpments of the Khadir, Bela, and Bhanjada islands (Chowksey *et al.* 2010). The occurrence of rann sediments along the fringes of the rocky islands, described in the present study, at 5-6 m above the salt encrusted rann surface is attributed to tectonic uplift of the islands along the Island Belt Fault during the last ~500 years. The development of vertical cliff sections and deep erosional gullies formed over these sediments testifies the tectonic uplift in the region.

### TEXTURAL CLASSIFICATION AND LITHOSTRATIGRAPHY OF THE CORE SEDIMENTS

The present chapter deals with the subsurface sediment characteristics, wide scale palaeoenvironmental conditions and development of lithostratigraphic framework of the Great Rann of Kachchh basin based on the two sediment cores (Fig. 6.1; 6.2). Two continuous cores, one from the central part of basin (~60m depth) and the other from the marginal part of the basin in Banni plain (~51m) were raised. The cores were drilled by considering that, the central and marginal parts of the Great Rann basin would provide a basin wide record to reconstruct palaeoenvironmental conditions, provenance of the rann sediments and its geological evolution throughout Holocene times. South marginal core in Banni plain can be assessed to estimate the role of the southern hillocks in the sediment budget of the rann basin. A detail account on the regional geomorphic set-up is given in Chapter 3. The site selection criteria and core processing is given in Chapter 4. A brief description of scientific drilling, coring exercise and subsurface sediment characteristics with palaeoenvironmental conditions existed in the rann basin is given below.

#### CORE DRILLING

Two continuous sediment cores were raised (Fig. 6.1) to investigate the subsurface sediment of the Great Rann basin. The Dhordo core of ~60m depth was raised from the southern fringe of the salt encrusted surface occurring to the north of Dhordo village near Pachham island. This site falls in the central part of the Great Rann basin which is frequently inundated by marine waters coming from the east. (Fig.6.1). The Berada core of ~51m depth was raised from the Banni plain and is closer to the rocky mainland Kachchh in the south. The site located to the NE of Berada village that falls in the Banni plain which forms the southern marginal part of the Great Rann basin and is free of present day marine influence (Fig. 6.1). The cores were raised by rotary drilling in sealed PVC pipes. X-ray images of all cores were obtained to study the sedimentary characteristics of the sediments in undisturbed conditions. This was followed by splitting of cores. The split sections of cores were visually examined for their physical and sedimentary characteristics

(Fig. 6.3; 6.4). One half of both the cores were sampled at 2cm interval while the other half has been preserved in sub-zero temperatures at Department of Geology, The M. S. University of Baroda.

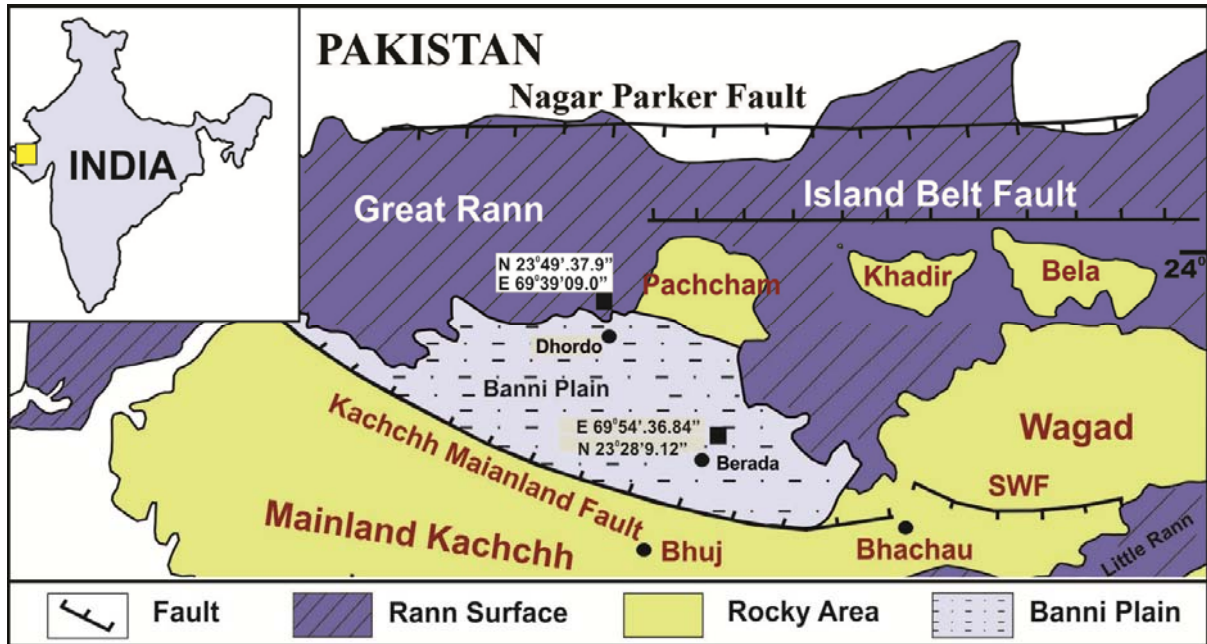


**Figure 6.1** Geomorphic map of the Great Rann of Kachchh basin with major faults. Locations of the two drilled cores are shown as solid squares.

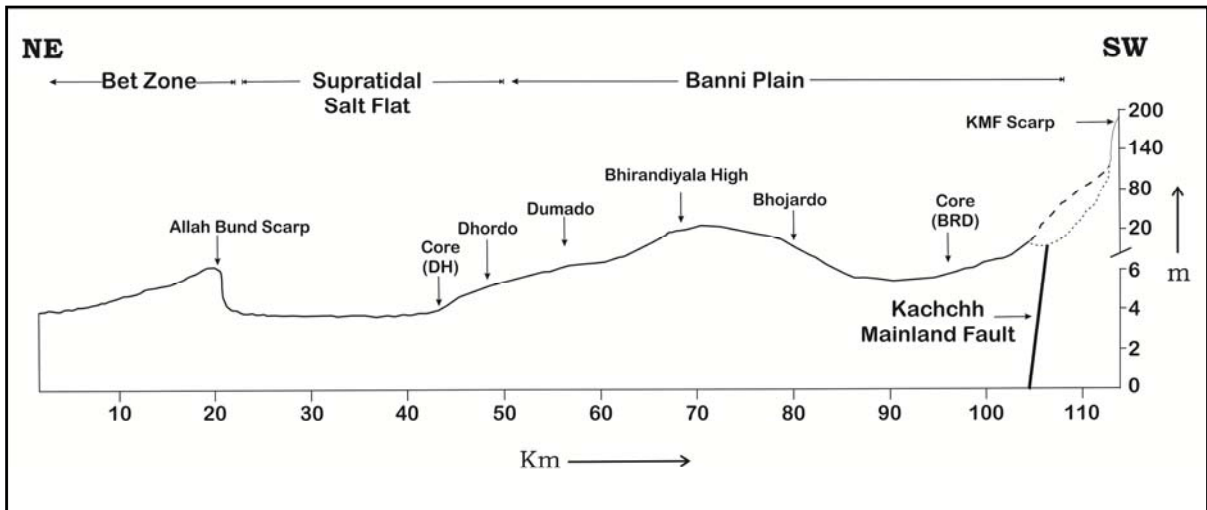


**Figure 6.2** Topographic section along the line covering core locations in the Great Rann of Kachchh basin. Vertical scale is highly exaggerated. Note the locations of the cores (DH and BRD) with respect to the basin and the distance between two.

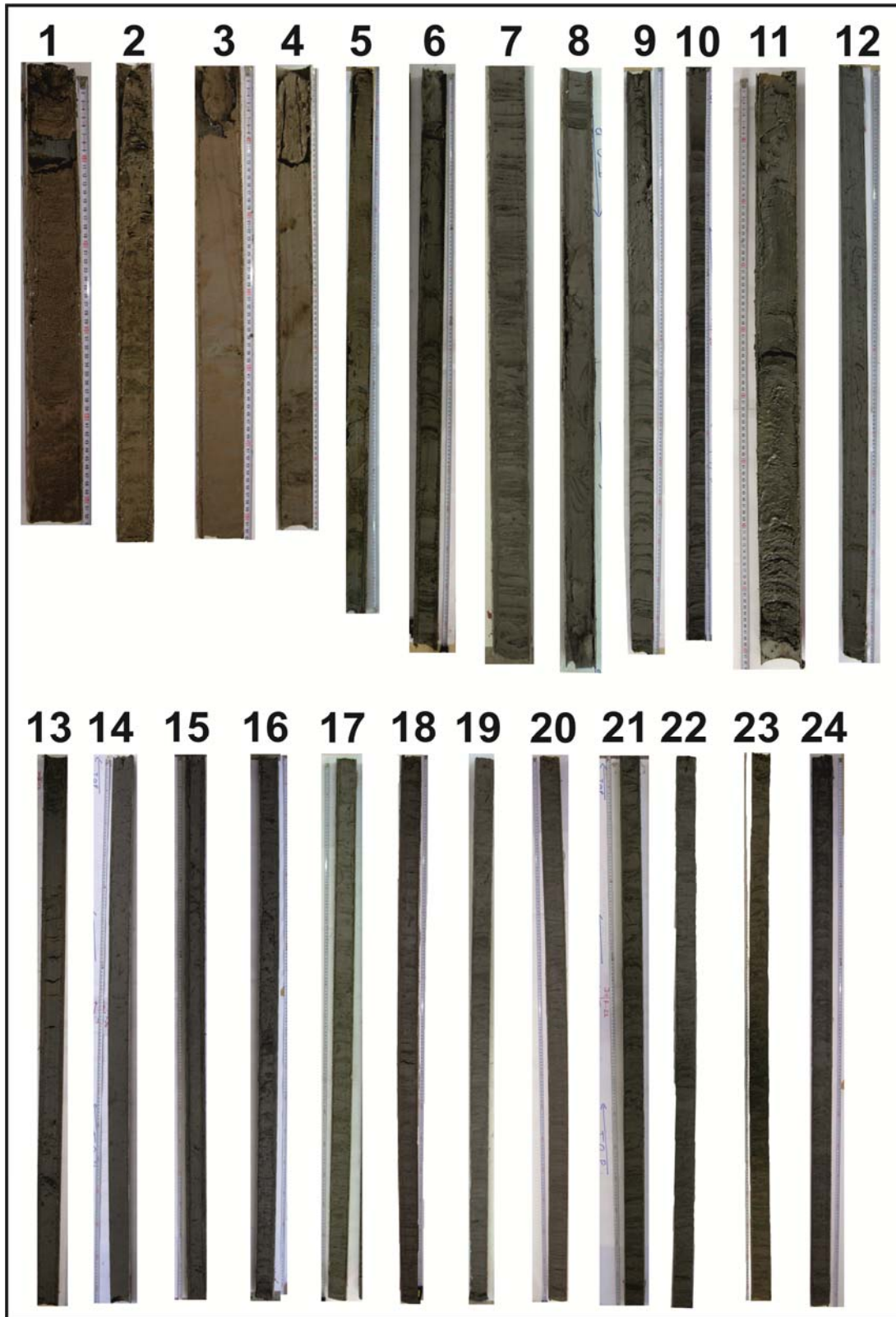


**Figure 6.3** Photographs of the split core pipes of Dhordo Core raised from north of Pachham Island, Great Rann of Kachchh basin. Note the excellent recovery of the sediments.

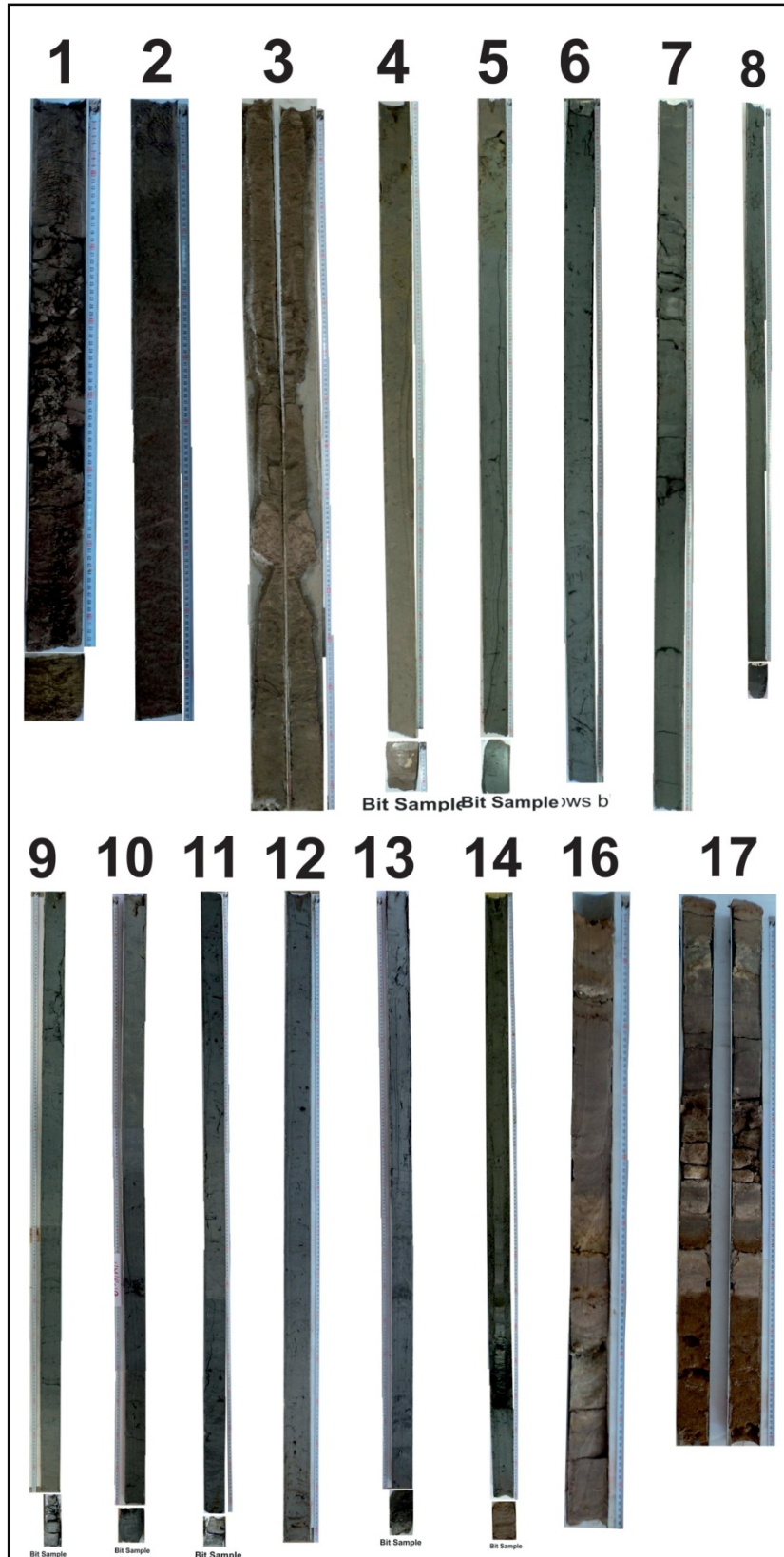


**Figure 6.4** Photographs of the split core pipes of Berada Core raised from Banni plain of Great Rann basin. Note the excellent recovery of the sediments.

## RADIOCARBON DATING

Age determinations by  $^{14}\text{C}$  Accelerated Mass Spectrometry method was undertaken on raw sediment samples and Mollusk shells at NSF Arizona AMS facility (The University of Arizona) using their standard protocol. Calibration of the raw data to age years BP was completed using the calibration data set by Stuiver et al. (1998).

**Table 6.1** Table showing the samples from Dhordo and Berada Cores dated using  $^{14}\text{C}$  dating by AMS method.

S. No.	Lab. No.	Sample ID	Depth (m)	Material	d13C	F	$^{14}\text{C}$ age BP	Cal. Age (yr) Marine. 09
<b>Dhordo core</b>								
1	AA96716	DH/AMS/3	25.78	Shell	-0.2 0.4369	$\pm 0.0025$	6,652 $\pm$ 45	6985 $\pm$ 54
2	AA96717	DH/AMS/4	45.00	Bulk sediment	-20.0 0.1801	$\pm 0.0016$	13,772 $\pm$ 73	16340 $\pm$ 79
3	AA96718	DH/AMS/5	60.13	Bulk sediment	-20.7 0.1522	$\pm 0.0015$	15,123 $\pm$ 81	17700 $\pm$ 86
<b>Berada core</b>								
1	AA96721	BRD/AMS/3	19.2	Shells	-3.9 0.4259	$\pm 0.0025$	6,856 $\pm$ 45	7235 $\pm$ 54
2	AA96722	BRD/AMS/4	32.78	Shell	-7.2 0.3405	$\pm 0.0022$	8,654 $\pm$ 51	8491 $\pm$ 59
3	AA96723	BRD/AMS/5	38.88	Bulk sediment	-27.8 0.3250	$\pm 0.0021$	9,029 $\pm$ 53	9515 $\pm$ 61

### Age Model

The Great Rann basin has accumulated a huge sediment pile since the post glacial times as indicated by the bottom most dating horizon in Dhordo Core at ~60m depth that yield age ~17ka BP (Fig. 6.5). This clearly indicates the rann basin started accumulating sediments as a rapid response to the changing climate after LGM. Based on the present chronologic control, the sedimentation rate in the central rann basin appears as highest ~11.3mm/year during the Late Pleistocene times (17.7 to 16.3ka B.P.). The rate of sedimentation was high ~17.4 mm/year even during the Early Holocene times as indicated by the Berada core in the south marginal rann (9.5 to 8.4ka BP). Thereafter further reduction in the sediment flux is observed during the Mid Holocene times in the marginal Berada core i.e. ~7.3mm/year whereas the central portion shows further lower in sedimentation ~2mm/year during Mid Holocene times. During the Late Holocene times

relative increase in the central and as well as the marginal parts of the rann basin is suggested.

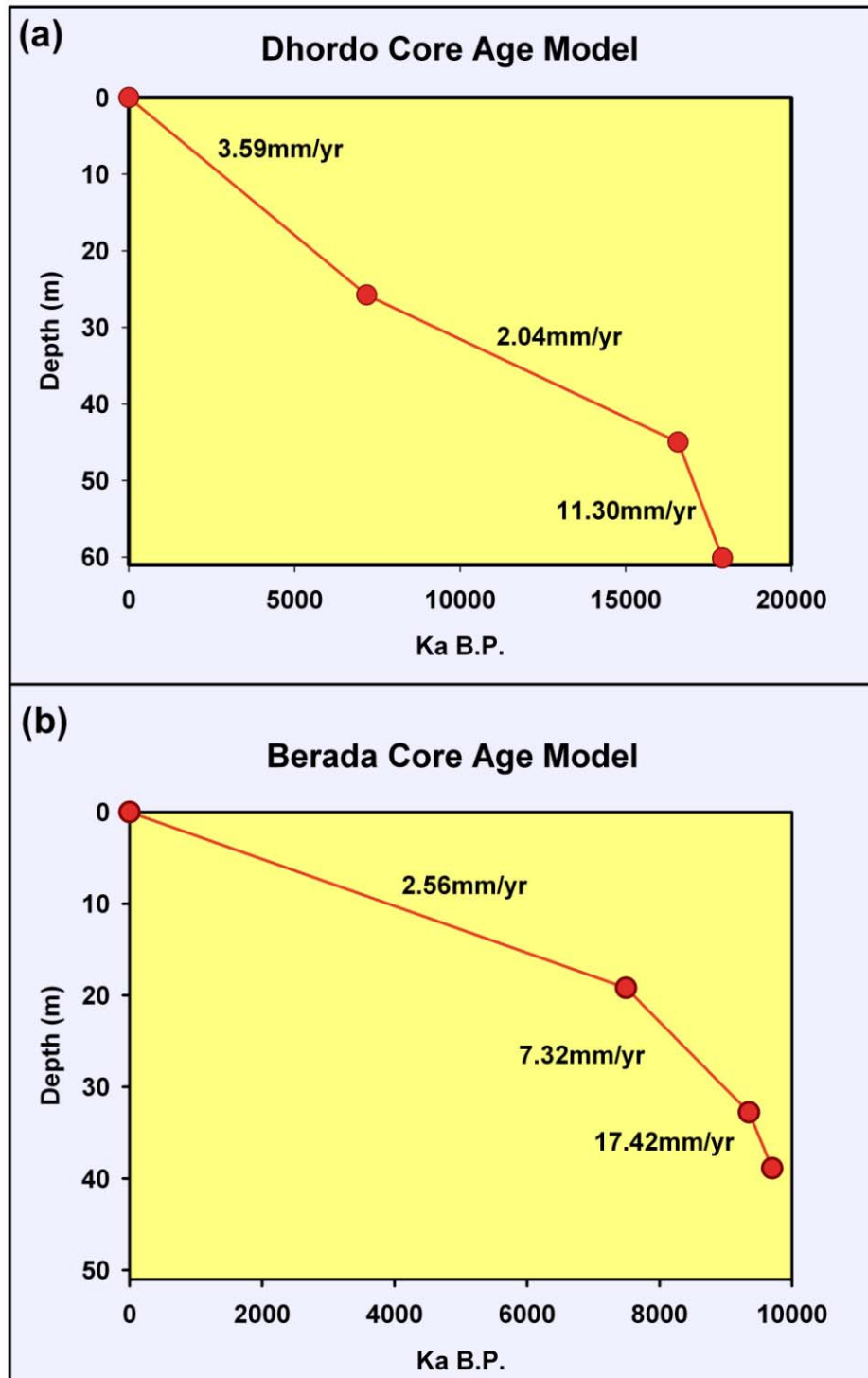


**Figure 6.5** Age Model for the Great Rann of Kachchh sedimentation during past ~17ka BP based on six  $^{14}\text{C}$  dating horizons from both the cores (Dhordo and Berada cores).

## **STRATIGRAPHY OF THE CORES**

Both cores showed remarkable dominance of fine grained clay and silt rich lithologies. Therefore, detailed textural analysis to lithologically characterize the cores was found necessary. About 64 samples from Dhordo core and about 57 samples from the Berada core were subjected to textural analysis. Relative silt-clay-sand contents were determined. These were used in conjunction with the visual observations of the core to subdivide the cores into various lithological units. Lithostratigraphic units delineated mainly based on textural characteristics and visual observations, generated on the two cores is described here. Their possible implications for lithostratigraphic development and palaeoenvironmental conditions in the Great Rann basin are also discussed. A total of 06 samples were dated using AMS technique. The AMS dating was carried out at the NSF Arizona AMS Facility, The University of Arizona, USA.

### **Dhordo core**

The Dhordo core is subdivided into 16 lithounits (Fig. 6.6). The units are distinguished on the basis of physical characteristics, grain size distribution, textural characteristics and X-ray radiographs. The distinctive characteristics of the units delineated are described bottom upwards (Table 6.2). The Unit-1 (60.40 - 53m depth) comprises a thick sequence of dark grayish colored, clayey silts forming bottommost part of the core. The unit is also marked by fine laminations of silt rich sediments. Occurrence of overall silt dominated clayey sediments indicates uniform depositional conditions whereas fine silty lamina indicates spells of increased flux from the source region. Preliminary micropalaeontological analysis of samples show presence of shallow benthic foraminifera which confirms the deposition of sediments in marine environment. AMS dating of a sediment sample from of 60.13m and 45.00m depth have yielded age of  $17,700 \pm 86$  and  $16,340 \pm 79$  Ka BP (Fig. 6.5; Table 6.1). This suggests that marine sedimentation in the Great Rann basin was initiated before ~15 ka BP.

The Unit-2 (53-43 m depth) also comprises a thick sequence of finely laminated clayey silts which is similar to the underlying unit. However, the unit is distinguished by the presence of increased frequency of thin silt-rich laminae that alternate with clayey silt layers. Sand is practically absent throughout this unit. The overall depositional environment appears to be similar to that of Unit-1 with increased but periodic influx of

silt from the source regions. This unit also show presence of shallow marine microfauna. AMS dating of a sediment sample from of 45 m depth have yielded an age of 16,340±79 yr BP (Fig. 6.6). Overall, the two bottommost units (1 & 2) together indicate uninterrupted sedimentation under uniform depositional conditions.

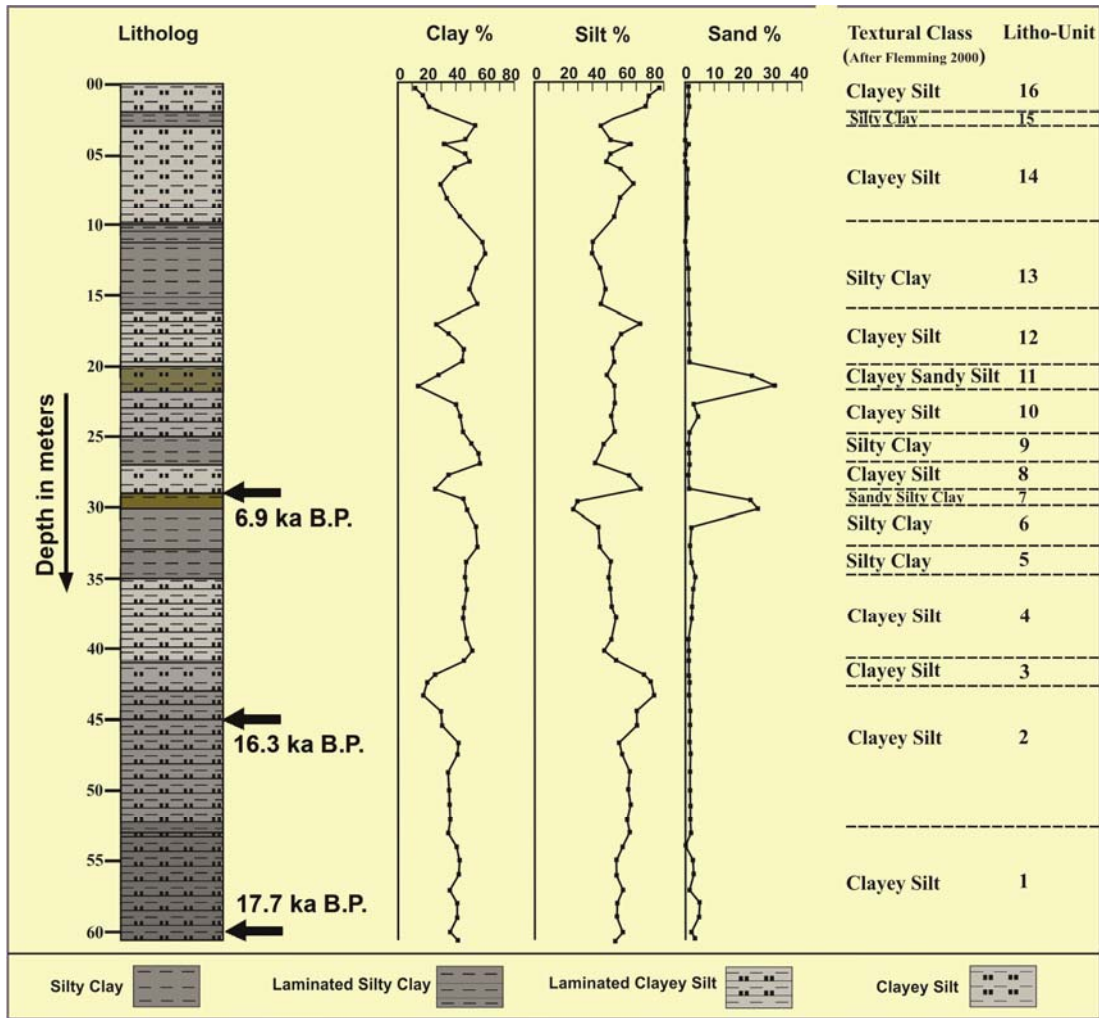


**Figure 6.6** The downcore grain size variations in Dhordo Core is shown in the form of graphs with their textural classes following Flemming 2000.

The Unit-3 (43 - 41m depth) consists of laminated silty clays with thin silt-rich layers. The unit shows sudden increase in silt proportion up to ~80% which distinguishes it from the underlying units. The relative increase in silt may be suggestive of significant increase in sediment input. The all pervasive presence of laminations through the base of the core to the present unit indicate turbulence-free conditions within the overall realm of shallow marine environment as suggested by the presence of benthic foraminifera.

The Unit-4 (41 - 35m depth) consists of massive brownish to greyish coloured clayey silts. The silt –rich layers are also present. Though, lithologically the unit is similar, the absence of laminations distinguishes it from the underlying units. The sand content also shows a marginal increase. Shallow marine foraminifera observed in the few test samples analysed indicate continuation of identical depositional conditions.

**Table. 6.2** Summary of textural characteristics of the various lithounits of the Dhordo core.

Lithological Unit	Depth in meters	Lithology/ textural Class	Textural characteristics of Individual lithounit
16	0 - 2	Clayey Silt	Earthy Brown coloured, laminated silts with scattered salt crystals. Gypsum crystals present.
15	2 - 3	Silty Clay	Light brown, massive silty clay. Mottling in shades of ash gray color noted throughout the unit.
4	3 - 10	Clayey Silt	Brown to Grayish green coloured clayey silt. Mottling is also observed in shades of brown and ash colour.
13	10 - 16	Silty Clay	Dark greenish silty clay with fine silt layers.
12	16- 20	Clayey Silt	Bluish green sticky clayey silt with silt layers.
11	20 - 22	Clayey Sandy Silt	Greenish clayey sandy silt with very fine silt layers.
10	22 - 25	Clayey Silt	Dark gray clayey silt with occasional silty layers. Scattered organic particles present throughout.
9	25 -27	Silty Clay	Bluish gray silty clayey sediments. Broken as well as complete bivalve and gastropod shells present.
8	27 - 29	Clayey Silt	Greenish massive clayey silt. Laminations are absent throughout this unit. Broken bivalve shells are present occasionally.
7	29 – 30	Sandy Silty Clay	Greenish sandy silty clay. Characterized by relative decrease in silt and increase in sand proportion.
6	30 - 33	Silty Clay	Greenish silty clay.
5	33 - 35	Silty Clay	Greenish clay with silt lamina is seen.
4	35 - 41	Clayey Silt	Massive Brownish to greenish clayey silt with occasional silt layers.
3	41 - 43	Clayey Silt	Dark brownish clayey silt with some thin silt lamina The sediment is massive in nature.
2	41 - 53	Clayey Silt	Dark gray coloured clayey silty sediments. Characterized by high frequency of Silt layers throughout this unit.
1	53 - 60	Clayey Silt	Dark gray coloured clayey silty sediments with silt layers.

The Unit-5 (35 - 33m depth) is characterised by a relative increase in clay content in comparison to the underlying Unit-4. The gross lithology of the unit is found to be silty clay with a negligible sand content (<5%). The sediments show greenish colour with thin silty layers. This unit is also characterised by the presence of shallow marine microfauna.

The Unit-6 (33 - 30m depth) comprises massive greenish coloured clayey silts. The unit is distinguished from the lower unit on the basis of significant increase in silt content to >80%. The concomitant decrease of clay content to <20% is also significant (Fig. 6.6; Table 6.2). The sand continues to remain unimportant (<5%). The sediment indicates silt-rich sediments from the surrounding source areas. The microfaunal content indicates shallow marine environment. However, the high content of silt may be indicative of slightly shallower conditions during the deposition of the sediments. However, this needs to be confirmed by further detailed studies.

The Unit-7 (30 - 29m depth) is texturally classified as sandy silty clay. The clay content is observed to increase with respect to the underlying unit. The silt content is drastically reduced to <30%. A consequent increase of sand content to ~25% is seen (Fig. 6.6). The unit is distinguished mainly on the basis of increased content of sand in the otherwise dominantly silty-clayey sediments comprising the core. On a tentative basis the increased sand content may be suggestive of further shallowing up of the basin. However this needs to be supported by detailed multi-proxy data to be generated on the core.

The Unit-8 (29 - 27m depth) comprises mainly clayey silts. The unit is characterised by a sharp increase in the silt content to ~70% with a corresponding decrease in the clay content (Fig. 6.6). The sediments show massive nature and contain shallow marine microfauna. The nature of the sediments suggest a relative deepening of the basin after the shallowing phase indicated by the underlying units (7 & 6). Towards the upper part of the unit, few segregated masses of small broken shells of bivalves and gastropods are observed.

The Unit-9 (27 - 25m depth) consists of massive silty clays with negligible amount of sand. The unit is characterised by a significant increase in clay content with corresponding decrease of silt content as compared to the underlying unit. A significant feature of the unit is the presence of broken and complete shells. The broken shells are mostly of bivalves and gastropods. The complete shells are very few and are identified as

Arca sp. The broken shells suggest turbulent conditions at or close to the site of the core. Few samples tested for the microfauna have shown the presence of shallow marine microfauna. AMS dating of shell sample from 25.78 m depth have yielded an age of 6,985 ± 54 yr BP (Fig. 6.6). The Unit-10 (25 - 22m depth) consists of clayey silt. The unit shows marginal increase of sand content towards the top, however, it does not exceed 5%. The unit shows massive nature with several thin silt-rich layers. The unit is also characterised by randomly distributed black coloured particles presumably comprising organic matter rich material. The overall depositional environment appears to have remained unchanged since the deposition of the underlying Unit-9.

The Unit-11 (22 - 20m depth) lithologically consists of sandy silt with clay as minor component. The silt content is >50% while the sand content is >20%. The reduction of clay content to <15% is very significant. The sediments are of massive nature and the lithological uniformity is maintained throughout the unit. The unit indicates increased influx of sand with dominance of silt into the basin for a relatively short period of time. Preliminary analysis of few test samples show the presence of shallow marine microfauna.

The Unit-12 (20 - 16m depth) comprises bluish green coloured sticky clayey silts. The sand content is reduced to <1% in contrast to the underlying unit (Fig. 6.6). The silt content remains dominant, however, it increases significantly to >70%. Similarly the clay content also increases to ~25%. The sediments suggest a relative deepening of the basin during the deposition of this unit, few samples analysed have yielded shallow marine foraminifera.

The Unit-13 (16 - 10m depth) lithologically consists of greenish coloured silty clays (Fig. 6.6). The unit also shows thin silt-rich layers alternating with silty clays. The unit is distinguished by high amount of clay (~60%). Rest of the sediment component is silt with sand in negligible amount (<1%). The stratified character in different parts of the unit is imparted by the presence of thin silt-rich layers. The gross lithology of the unit suggests a depositional environment comparable to the underlying unit.

The Unit-14 (10 - 3m depth) lithologically consists of clayey silts and is texturally similar throughout the length of the unit. The silt content varies from 50-65%, while the clay content varies from 30-49% The sand content remains negligible. The unit is divisible into three sub-units based on the colour of the sediments. The bottom part of the unit (~3

m thick) comprises greenish green coloured massive sediments. The middle part (~2m thick) comprises alternate bands of ash coloured and brown coloured sediments giving the sub-unit a distinct banded appearance. The unit appears to indicate significant shallowing of the basin in short phases. The top part of the unit (~2m thick) consists of ash coloured sediments with iron-rich mottles distributed randomly. Overall, the unit appears to indicate significant and rapid changes in the depositional conditions. These changes could be in the form of alternate shallowing and relative deepening of the basin. Few randomly picked samples from the unit and analysed have shown the presence of shallow marine microfauna.

The Unit-15 (3 - 2m depth) lithologically comprises brown coloured massive silty clays. The clay content is ~55% with ~45% silt (Fig. 6.6). The unit is lithologically consistent and is characterised by a distinctive earthy brown colour. The colour of the unit is similar to the surficial sediments of the Rann. The unit appears to indicate further shallowing up of the basin, a trend that is visible in the underlying unit as well. The unit contains scattered gypsum crystals which points to significant shallowing of the basin. This unit may be the equivalent of the gypsum-rich layer reported from the shallow subsurface in the vicinity of the rocky Pachchham island. Preliminary micropalaeontological analysis of few samples from this unit have yielded shallow marine foraminifera. However, the size of the foraminifera was found to be significantly reduced. This could be due to stressful conditions that may have been triggered by shallowing of the basin as a consequence of the gradual withdrawal of the sea. The stressful conditions may also have been produced by increasing dominance or mixing of freshwater with the sea water as is the case in the present day surface environment of the Rann. Overall, the unit suggests a definite transitional phase from the fully marine conditions to present conditions existing in the Ranns.

The Unit-16 (1 - 0m depth) visually appears similar to the underlying unit owing to its earthy brown colour and massive nature. However, the gross lithology is found to be clayey silt. A sharp increase of silt content to >80% with concomitant decrease in clay content to <20% distinguishes it from the underlying unit (Fig. 6.6). The sand content remains negligible (1-2%). In general, the unit may be considered to represent the transition to present day conditions. Foraminifera with significantly reduced size are

observed in few samples analysed from this unit indicating stressful conditions comparable to the present conditions. However, further multidisciplinary studies are required to precisely characterise the transition phase represented by the upper two units of the core.

### **Berada core**

The entire ~50 m length of the Berada core is subdivided into 13 lithounits (Fig. 6.7). The major lithologic characteristics of the various units delineated are described bottom upwards (Table 6.3). The Unit-1 (51 - 47.5m depth) forms the bottommost part of the core and consist of unconsolidated brown coloured coarse sands. The sand comprises highly angular and unsorted grains. The sand content is very high with silt as minor component. The clay content is negligible. Mineralogically, the sand consists dominantly of quartz followed by feldspars. The general textural characteristics of the sand suggest fluvial origin. The angular and unsorted nature of the sand suggests a proximal source of the sediments. The most likely source of the sand deposits is the rocky mainland Kachchh to the south that exposes Mesozoic sandstones and limestones. Recent studies have documented dominantly coarse-grained (colluvio-fluvial) Quaternary sediments in the front of the KMF scarps marking the northern margin of the mainland (Chowksey et al., 2011). The sand deposits in the bottom of the core are possibly the northward extension these deposits. The unit shows sharp contact with the underlying unit. The clay content varies from 50-55% while silt forms the rest of the sediment component (Fig. 6.7). Sand is significantly absent in this unit. Preliminary analysis of samples for microfauna revealed the presence of shallow marine microfauna indicating marine origin of this unit. The unit, therefore marks the submergence of the basin by a transgressive sea.

The Unit-3 (42.5 - 40m depth) consists of unconsolidated brownish white coloured coarse sands. The sand is lithologically similar to Unit-1 and consists of angular to unsorted grains. The unit appears to be of fluvial origin. The angular and unsorted sand grains suggest close proximity of the source which is most likely the rocky mainland in the south. The unit probably marks a brief phase of regression of the sea with a consequent extension of the fluvial deposition from the mainland toward north into the Rann basin. The upper part of the unit comprises pebbly sands which contains pebble sized clasts of Mesozoic rocks.

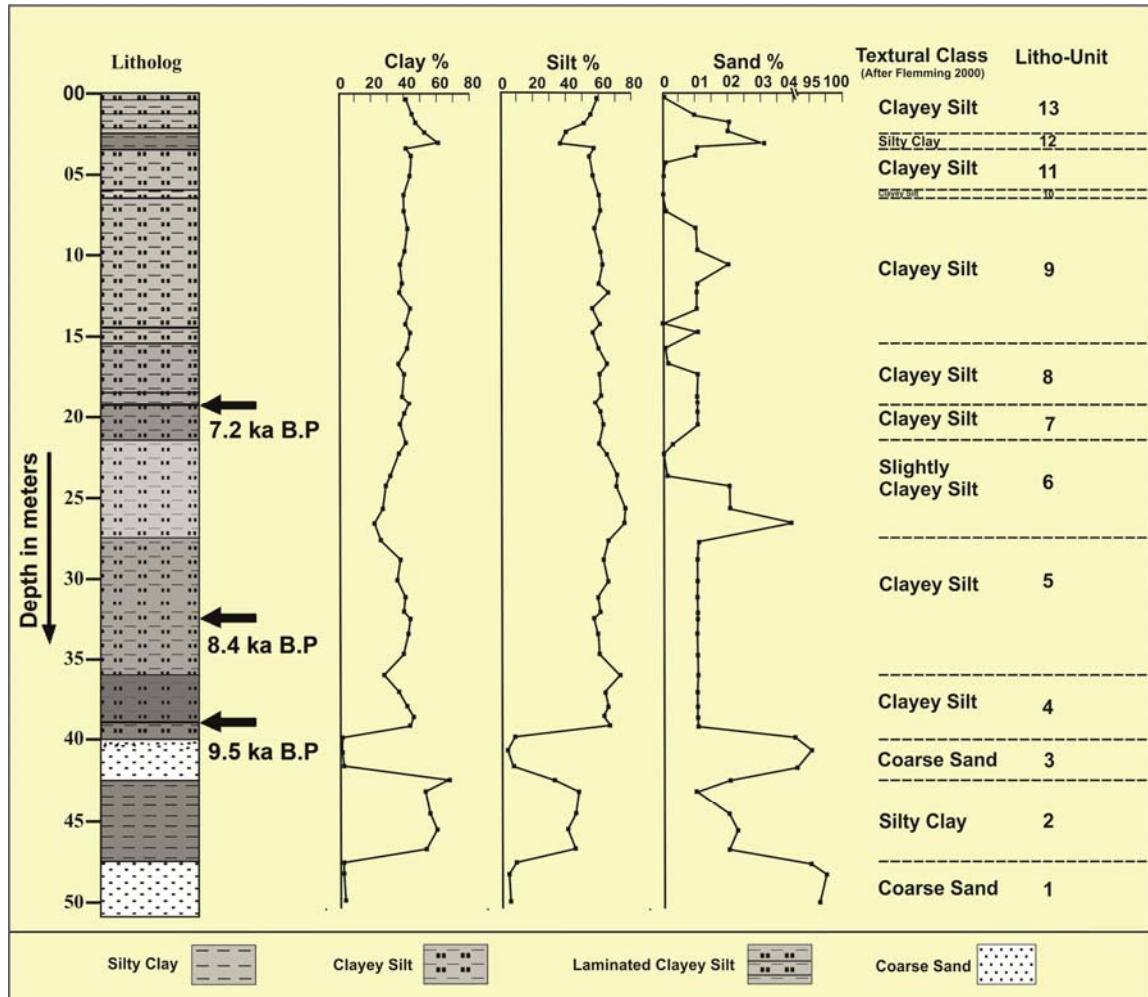


**Figure 6.7.** The downcore grain size variations in Berada Core is shown in the form of graphs with their textural classes following Flemming 2000.

The Unit-4 (40 - 36m depth) consists of massive clayey silts. The silt content is >70% while the clay content is <30%. The sand content is negligible (<1%). The unit marks a sharp lithological contrast with the underlying unit that consists of fluvial sands (Fig. 6.7; Table 6.3). Preliminary analysis showed the presence of shallow marine microfauna. A notable feature of the unit is the occurrence of small broken and complete shells of gastropods and bivalves in a zone starting from ~39.5 - 37.5m depth. The shell remains are irregularly distributed and do not form clusters. The complete shells are exclusively of small gastropods. The other significant feature of the unit is the presence of a 1.5cm thick organic matter rich layer at ~39m depth. The layer appears to be of peat composition as the organic matter examined under microscope revealed the presence of undecomposed plant matter. The peat layer indicates a marginal near-coastal environment.

This unit, therefore, marks a renewed phase of marine transgression into the Rann basin that overlapped the underlying fluvial deposits.

**Table. 6.2** Summary of textural characteristics of the various lithounits of the Berada

<b>Lithological unit</b>	<b>Depth in meters</b>	<b>Lithology/ Textural Class</b>	<b>Textural characteristics of individual lithounits</b>
13	0-2.5	Clayey Silt	Brown coloured laminated silt with clay sediments. Scattered gypsum crystals.
12	2.5-3.5	Silty Clay	Light brown coloured silty clay sediments with high mica content.
11	3.5-6	Clayey Silt	Light brown coloured massive, loose silt with less clay proportion.
10	6-6.5	Clayey Silt	Greenish colour clayey silt with increased mica content.
9	6.5-15.5	Clayey Silt	Bluish green clayey silt with scattered black organic particles. 2cm thick organic rich layer at ~15m depth.
8	15.5-18.5	Clayey Silt	Massive light greenish gray coloured clayey silt. Scattered broken shells of bivalves present throughout.
7	18.5-21.5	Clayey Silt	Greenish gray massive clayey silt with scattered organic particles .A thick organic rich layer noted at ~19m depth.
6	21.5-27.5	Slightly Clayey Silt	Massive dark greenish gray colored silt rich sediments with low clay proportion. Scattered organic particles present throughout.
5	27.5-36	Clayey Silt	Light greyish green coloured massive clayey silty sediments. Scattered occurrence of Bivalve and Gastropod shells with organic particles. Cirithids abundant.
4	36-40	Clayey Silt	Massive dark brownish to gray colored clayey silt with broken shells.
3	40-42.5	Coarse Sand	Yellow coloured loose, angular, unsorted, coarse sand of fluvial origin. Upper portion of the unit is marked by pebbles.
2	42.5-47.5	Silty Clay	Semi compacted silty clayey sediments. Topmost thin layer is of moderately sorted ferruginous semicompacted sand followed by intercalations of ash coloured and yellowish coloured silty layers.
1	47.5-51.11	Coarse Sand	Brown coloured loose, angular, unsorted coarse sand of fluvial origin.

AMS dating of the peat sample from 38.88 m depth has yielded an age of  $9515 \pm 61$  yr BP (Fig. 6.7). This suggests that by  $\sim 9$ ka BP, the marginal parts of the Great Rann, including the Banni region, were also completely submerged by sea.

The Unit-5 (36 - 27.5m depth) comprises a monotonous sequence of clayey silts. The unit is distinguished by its greyish green colour and randomly distributed and scattered small gastropod shells along the length of the unit. Lithologically, the unit consists of silts (55 - 65%) and clay (35-40%). The sand content is negligible. This unit is also characterised by the presence of shallow marine foraminifera. The unit indicates continuous sedimentation under uniform depositional conditions for a long period of time. The uniform character of the sediments suggests a relative deeper basin than during the deposition of the underlying unit that marks the initiation of the marine transgressive phase. The  $^{14}\text{C}$  age at 32.78m yielded an age of  $8,491 \pm 59$  yr BP (Table 6.1).

The Unit-6 (27.5 - 21.5m depth) consists of a continuous uniform lithological composition that is texturally classified as clayey silt. The unit shows dark greenish grey colour which is at variance with the underlying unit consisting of similar lithology. The unit is also distinguished from the underlying unit by a significant reduction in clay content. The clay content is 20% in the lower part and increases to about 35% in the upper part (Fig. 6.7). Correspondingly, the silt content is higher ( $\sim 65\%$ ) in the lower part and gradually decreases to about 55% in the upper part. The sand content is  $<5\%$ . The upper part of the unit shows the presence of mud clast that correlates with the increased influx of clay. Black coloured organic matter rich particles are scattered vertically throughout the unit. A major part of the unit indicates a uniform depositional environment similar to the underlying unit. However, the presence of mud clast in the upper part suggests shallowing up of the basin.

The Unit-7 (21.5 - 18.5m depth) comprises massive greyish coloured clayey silts. Lithologically and texturally it is similar to the underlying unit, however, it is distinguished due the presence of organic material. The organic material is present in the form of scattered black coloured particles and few millimeter thick organic matter rich layers. The unit is also significant as it shows the occurrence of a thin layer that is rich in broken shells. The broken shells mostly appear to belong to bivalves. An overall similar

depositional conditions with increased input of organic matter is inferred during the deposition of this unit.

The Unit-8 (18.5 - 15.5m depth) consists of massive light greenish coloured clayey silts with few thin silt-rich layers. The unit is distinguished because of its light colour and randomly distributed pieces of broken shells of bivalves. The broken shells are more abundant in the upper 1.5 m thick zone of the unit. Preliminary analysis of few test samples have yielded shallow marine microfauna. The overall, depositional environment appears to have remained same, however, the presence of broken shells may be an indicator of relatively shallower conditions with some turbulence. AMS dating of shells from of 19.20 m depth have yielded an age of  $7,235 \pm 54$ yr BP (Fig. 6.6).

The Unit-9 (15.5 - 6.5m depth) comprises a thick monotonous sequence of massive bluish green coloured clayey silt. The silt and clay contents remain remarkably uniform throughout the unit with a ratio of 60:40. The unit shows scattered occurrences of black coloured organic matter rich particles. Micropalaeontological analysis of few samples on a preliminary level have revealed the presence of shallow marine benthic foraminifera. The unit was probably deposited in a relative basin as compared to the underlying units. The conditions persisted for a long period of time. The Unit-10 (6.5 - 6m depth) consists of massive clayey silt with a distinctive green colour. Texturally the unit is similar to the underlying unit. The microfaunal content is also similar to the underlying units. However, its distinctive colour may be indicative of a brief change in depositional conditions or in the nature of sediment influx. Further detailed studies are essential for deducing the change indicated by this unit. The Unit-11 (6 - 3.5m depth) comprises clayey silts and compositionally similar to the underlying Units 10 & 9. The unit is separated out on the basis of the thin distinctive underlying Unit-10. The unit shows a marginal increase in clay content and shows presence of shallow marine microfauna.

The Unit-12 (3.5 - 2.5m depth) is characterised by increased content of clay. The unit is lithologically classified as silty clay. The clay content is increased to >60% while silt content is <40%. The sand content marginally increases to about 3% (Fig. 6.6; Table 6.3). No major deviation in depositional conditions is indicated by this unit. The Unit-13 (2.5 - 0m depth) consists of laminated brown coloured clayey silt. The silt content shows an increasing trend towards the top of the unit. The lower part of the unit showed

dispersed grains of gypsum which correlates with similar characteristics in the upper part (unit-15) of the Dhordo core and also the gypsum layer observed in the shallow subsurface in the vicinity of Pachchham island (Glennie and Evans, 1976). Few samples tested for microfaunal content have shown the presence of small sized shallow marine foraminifera. However, the marine microfauna is absent in the top ~1 m of the unit. The unit represents the transitional phase from marine to present non marine conditions. Lithologically and texturally the upper part of this unit is comparable to the topmost unit of the Dhordo core.

The lithological similarity of the Dhordo and Berada cores is very striking even though they are located more than 50km apart. Both cores are dominantly composed of fine grained lithology ranging from clayey silts to silty clays (Figure 6.6, 6.7). The persistence of the fine grained lithology in both the cores is amazing. About 46 m (~75%) of the total length of the Dhordo core consists of clayey silts while silty clays form the rest of the core. The clayey silt comprise about 39 m (~76%) of the total length of the Berada core while silty clay forms only about 6 m of the total length of the core. This indicates an overwhelming domination of clayey silts in the sedimentary basin fill of the Rann. The overall lithological composition of the cores appear to be in conformity with the geomorphological setting of the Rann that suggests that it was an embayed shallow gulf in the past.

Based on the AMS date of  $17,700 \pm 86$  yr BP obtained from Dhordo core at a depth of 60.13m, it is inferred that the central part of the Great Rann basin corresponding to the present day supra tidal salt flat, was submerged by a shallow sea by ~15 ka. However, the submergence of the entire basin appears to have taken place gradually. The AMS date of  $9,515 \pm 61$  yr BP obtained from the Berada core at 38.88 m depth suggests that marginal parts including the present day Banni plain were submerged by ~9ka BP. Since then, continuous marine sedimentation took place through the Holocene under shallow marine conditions.

### FORAMINIFERAL STUDIES ON CORE SEDIMENTS

The present chapter describes the foraminiferal studies carried out on the two cores raised from Dhordo and Berada regions of the Great Rann of Kachchh basin. The prime objective of this exercise was to identify the palaeoenvironments as reflected in the subsurface sediments of the Great Rann basin. Foraminifera are small protists that are typical of marine environments. Their presence right from the coastal, intertidal to deep waters yields specific assemblages that help in reconstructing the palaeoenvironmental conditions of geological past (Murray 1991). The wide spread abundance and precise applicability makes them one of the most studied microfossils. Since there is no previous information on the subsurface sediments of the Great Rann, the study of foraminifera occurring in the two cores is significant mainly for two reasons. The first reason is that, such a study is important for scientifically validating the long standing hypothesis that the Great Rann marks the site of a palaeo-gulf that existed for a long period of time and the second reason is to provide evidence in respect of temporal variations in the depositional conditions of the sediments as revealed by the cores.

The Dhordo core (60m depth) and Berada core (50m depth) represent the central and the southern marginal part of the Great Rann basin. In Dhordo core 16 such lithounits were identified whereas the Berada core is divisible into 13 lithounits. To build a broad framework of the palaeoenvironmental changes through the entire length of these cores, representative samples were taken from each lithounit for both the cores. As discussed in the previous chapter, the available chronological data suggests that the Dhordo core dates back ~18 ka BP while the interpreted marine section of the Berada core dates back to ~10 ka BP. The following paragraphs include the detailed results and interpretation of the foraminiferal studies of the Great Rann sediments including their systematic taxonomy and palaeoenvironmental implications.

#### FORAMINIFERAL ASSEMBLAGE

The foraminiferal studies on the two cores Dhordo and Berada yield a diverse assemblage of the foraminifera in the Great Rann of Kachchh basin. The foraminiferal assemblage comprises a total of 30 genera of benthic and planktic species (Table 7.1 and

7.2). The benthic assemblage comprises of *Ammonia*, *Calcarina*, *Elphidium*, *Haynesina*, *Taxyella*, *Cibicides*, *Criboelphidium*, *Cycloforina*, *Oridorsalis*, *Nonian*, *Nonionoides*, *Nonionella*, *Bolivina*, *Brizalina*, *Lagena*, *Hopkinsina*, *Quinqueloculina*, *Miliola*, *Miliolinella*, *Spirillina*, *Textularia*, *Triloculina*, *Uvigerina* and planktonic forms includes *Gallitellia*, *Globigerinella*, *Globorotaloides*. The species identification attempted yielded 35 species comprising *Ammonia beccarii*, *Ammonia tepida*, *Ammonia parkinsoniana*, *Calcarina cancar*, *Elphidium crispum*, *E. williamsoni*, *E. excavatum*, *Haynesina depressula*, *Criboelphidium ocenansis*, *Nonian commue*, *Nonionoides gratelaupi*, *Nonionella labradorica*, *N. atlantica*, *Bolivina variabilis*, *B. pseudoplicata*, *Brizalina spathulata*, *Lagena striata*, *L. levis*, *Hopkinsina pacifica*, *Quinqueloculina limbata*, *Q. oblonga*, *Q. seminulum*, *Q. aspera*, *Spirulina sp.* *Triloculina lavegata*, *T. tricarinata*, *T. oblonga*, *Oolina sp.*, *Uvigerina sp.* *Spirulinid sp.*, *Cycloforina*, *Cibicides sp.*, *Oridorsalis sp.*, *Spiroloculina sp.*, *Milliamina fusca* and planktonic species include three taxa- *Globorotaloides sp.*, *Globigerinella sp.* and *Gallitellia vivans*.

## SYSTEMATIC TAXONOMY

Phylum: Protozoa

Order Foraminiferida Eichwald, 1830

Suborder: Rotaliina Delage & Herouard, 1896

Superfamily: Rotaliidae Ehrenberg, 1839

Subfamily: Ammoniinae Saidova, 1981

Genus: *Ammonia* Brunich, 1771

**Species: *Ammonia beccarii* (Linne, 1758)**

**Description:** Test trochospiral, biconvex, with 6-10 chambers in last whorl and rounded periphery. The sutures limbate on spiral side slightly raised whereas umbilical side sutures are depressed and ornamentation along with umbilicus with tubercles which may coalesce to form a central boss.

**Species: *Ammonia tepida* (Cushman)**

**Description:** Test low trochospiral, biconvex, large umbilical fissure with granular ornamentation. Sutures depressed, straight to radial with slight curvature, periphery rounded.

**Species: *Ammonia parkinsoniana* (d'Orbigny, 1839)**

**Description:** Test high to low trochospiral, 6-9 chambers, biconvex with depressed sutures on umbilical side. Sutures are ornamented with the granular crystals, sometimes highly ornamented whereas the raised sutures on spiral side are noted.

**Remarks:** Early Miocene to Holocene. Cosmopolitan. *Ammonia* group shows large variations in the test architecture and ornamentation. This group is characteristic of marginal marine environments, marsh to subtidal zones worldwide, and tolerates a wide range of salinity (10-31‰) and oxygen conditions. *Ammonia* species are well documented from the shallow waters of west coast of India (Nigam and Chaturvedi 2000, Nigam and Khare 1999).

Calcarena D'Orbigny

**Species:** *Calcarina cancar*

**Description:** Test large, up to 2mm in diameter, lenticular, biconvex, commonly with a few many heavy and blunt to splayed or bifurcating radial spines, five to six whorls.

**Remarks:** Pliocene to Holocene.

Family: Elphidiidae Galloway, 1933

Subfamily: Elphidiinae Galloway, 1933

Genus: Elphidium DE Montfort, 1808

**Species:** *Elphidium crispum* (Terquem)

**Description:** Test medium size to large, biconvex, completely involute, broadly rounded periphery, and many chambers, distinct retral processes occurring as only band. aperture consists of a row of pores arranged in a curved line at the base of the apertural face.

**Remarks:** Lower Eocene to Holocene. Cosmopolitan. Epifaunal, prefers sandy substrate, survives in wide range of salinity condition (30-70 unit ‰) and abundant in brackish-hypersaline marshes and lagoons.

**Species:** *Elphidium excavatum* (Terquem)

**Description:** Test medium sized, oval to lenticular in shape, incised sutures form interocular spaces, periphery carinate, wall calcareous, finely perforate, bilamellar, septal flap partly or completely covering previous septa as the new chamber is formed.

**Remarks:** Early Eocene to Holocene. Cosmopolitan. Infaunal, common in sandy substrate with variable sand content, salinity 15-31‰, intertidal to subtidal in estuaries, lagoons to continental shelf/slope.

**Species:** *Elphidium williamsoni* (Haynes)

**Description:** Test slightly compressed, planispiral, subcircular. Peripheral outline lobulate especially in last chambers, peripheral margin subangular in earlier chambers and becoming more rounded in the last chamber. 10-12, curved, pored chambers in fully grown tests.

Genus: *Criboelphidium* (Cushman and Bronnimann, 1948)

**Species:** *Criboelphidium oceanansis*

**Description:** Test planispiral and involute with rounded noncarinate periphery, eight to eleven inflated chambers in the final whorl, umbilicus with boss, surface rough, wall of earlier chambers thickened by later lamination.

**Remarks:** Miocene to Holocene. Cosmopolitan.

Superfamily: Nonionacea (Schultze, 1854)

Family: Nonionidae (Schultze, 1854)

Genus: *Haynesina* (Banner and Culver, 1978)

**Species:** *Haynesina depressula* (Cushman)

**Description:** Test planispiral, bilaterally symmetrical, involute and biumbonate, four to six chambers per whorl, increasing gradually, rounded periphery, radial curved sutures, surface of the umbilical area covered by granules, aperture largely obscured by granules.

**Remarks:** Upper Pliocene to Holocene.

Superfamily: Nonionacea Schultze, 1854

Family: Nonionidae Schultze, 1854

Subfamily: Nonioninae Schultze, 1854

Genus: *Nonion* SE Monthfort, 1854

**Species:** *Nonion commune* (d'Orbigny, 1839)

**Description:** Test compressed, low trochospiral, ovate to circular in outline. Umbilicus partially to completely filled with pustules on the somewhat crenulate inner margins of the

chambers. Sutures slightly curved, depressed near the umbilicus. Overall rounded to sub-rounded periphery.

**Remarks:** Late Cretaceous to Holocene. Cosmopolitan. Infaunal, mud and silt loving, salinity 30-35‰, typically documented along the shelf regions (Nisha 2002).

#### **Nonionoides Saidoves, 1975**

**Species:** *Nonionoides grateloupi* (d'Orbigny, 1836)

**Description:** Test slightly asymmetrical and weakly trochospiral, with evolute spiral side, chambers are usually constant in height but gradually increasing breadth that result in auriculate test outline.

**Remarks:** Holocene, Sublittoral.

#### **Nonionella Voloshinova, 1958**

**Species:** *Nonionella labradorica* Dawson, 1860

**Description:** Test trochospiral in the early stage, later nearly planispiral and involute, chambers enlarging rapidly as added, periphery subangular to rounded. Surface smooth other than postules, finely perforate.

**Remarks:** Miocene to Holocene, cosmopolitan.

**Species:** *Nonionella atlantica* Cushman, 1947

**Description:** Test slightly compressed in a low trochospiral coil, rounded periphery, spiral side partially evolute around the umbilical boss, numerous chambers are seen, whorls progressively enlarging.

**Remarks:** Upper Cretaceous to Holocene. Cosmopolitan.

#### ***Globigerinella Sp.***

**Description:** This planktic foraminiferal taxon is characterized by its test moderately trochospiral, globular to ovate chambers enlarging rapidly. About 4-6 in final whorl, sutures radial, straight, depressed, peripheral outline lobulate .

**Remarks:** Late Oligocene to Holocene

#### ***Globorotaloides Sp.***

**Description:** Test of this planktic foraminifera is globular to subglobular and compressed; about 5-6 ovate to spherical chambers in the last whorl. Primary aperture interiomarginal.

**Remarks:** Middle Eocene to Holocene , tropical-subtropical, cosmopolitan.

Superfamily: Bolivinaea, (Glaessener, 1937)

Family: Bolivinidae, (Glaessener, 1937)

Genus: Bolivina, (d'Orbigny, 1839)

**Species: *Bolivina variabilis* Williamson, 1858**

**Description:** Test elongate, ovoid to triangular in outline, somewhat compressed, chambers broad and low, biserial throughout, the final chamber is rarely in central portion, perforate, surface ornamented with irregularly anastomosing costae.

**Remarks:** Pliocene to Holocene.

**Species: *Bolivina pseudoplicata* Heron-Allen and Earland, 1913**

**Description:** Test elongate, triangular in shape, compressed, biserial, surface rough, irregular rough, anastomosing coasts.

**Remarks:** Pliocene to Holocene.

Superfamily Bolivinaea Glaessner, 1937

Family: Bolivinidae Glaessner, 1937

Subfamily: Bolivininae Glaessner, 1937

Genus: Bolivina d'Orbigny, 1839

**Species: *Bolivina spathulata* (Williamson)**

**Description:** Test is triangular to oval shaped characterized by broad chambers and biserial chamber arrangement throughout. Pores are seen on the test with irregular/obscured surface of the wall.

**Remarks:** Late Cretaceous to Holocene; cosmopolitan form. Infaunal to epifaunal, prefers muddy sediments. This taxon has preference for low-oxygen condition.

***Lagena* sp. Popescu, 1983**

**Description:** Test unilocular, flask like, compressed periphery, broadly carinate, surface smooth with occasionally striated, aperture round to oval, terminal the end of the distinct neck.

**Remarks:** Middle Miocene to Holocene.

**Species: *Lagena levis***

**Description:** Test unilocular, flask shaped, globular to oblate, broadly carine, smooth surface.

**Species: *Legina striata* d'Orbigny 1839**

**Description:** Test unilocular, flask shaped, globular to oblate, characterized by striate or ribs like structure.

**Genus: *Hopkinsina* Howe and Wallace, 1932**

**Species:** Elongate narrow chambers, slightly inflated, increasing size with added chambers, early stage triserial and later becomes biserial, perforate, surface longitudinally striated with low coaste.

**Remarks:** Eocene to Holocene. Cosmopolitan.

**Genus: *Gallitellia* Loeblich and Tappan, 1986**

**Species: *Gallitellia vivans***

**Description:** Test elongate, chambers globular and enlarging rapidly as added. Sutures deeply depressed, margins lobulate; aperture simply rounded and umbilical arch at the base of the final chamber.

**Remarks:** Type species: *Gallitellia vivans* Cushman 1934. Pleistocene to Holocene. . This planktonic species is reported from the Quaternary sediments exposed in the gulf of Cambay (Ghosh et. al. 2008).

Suborder: Millollna (Delage and Herouard, 1896)

Family : Hauerinidae Schwager, 1876

Subfamily: Hauerininae Schwager, 1876

Genus : Quinquelocullna d'Orbigny, 1826

**Species: *Quinqueloculina seminulum***

**Description:** Test oval when viewed laterally, but triangular from the ends, longer than broad, surface smooth, periphery rounded, aperture rounded with a conspicuous tooth.

**Remarks:** Cretaceous to Recent

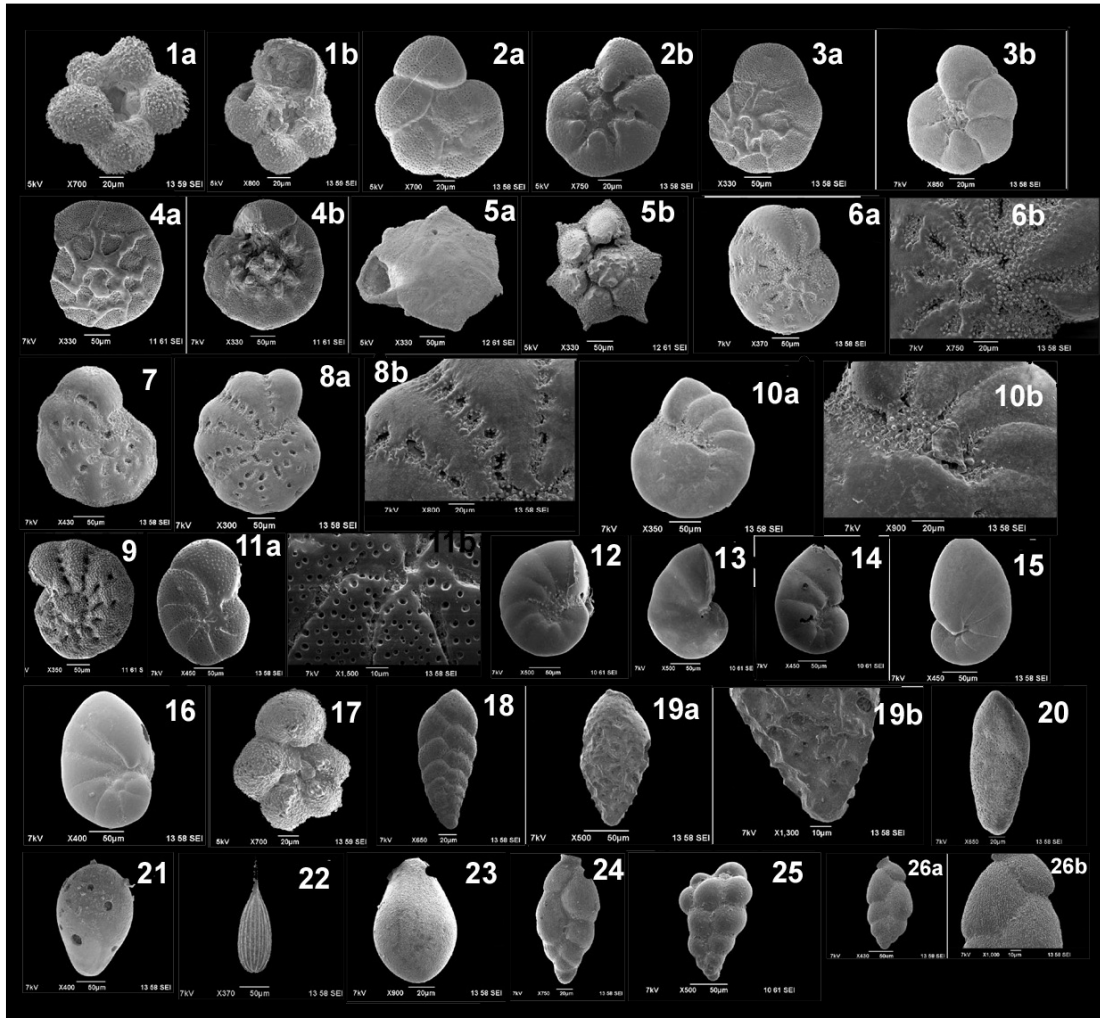


**Figure 7.1** Plate showing the foraminiferal assemblage recovered from Dhordo and Berada cores 1a, 1b. *Globorotaloid* sp.; 2. *Ammonia parkinsoniana* 2a. Spiral view 2b. Umbilical view; 3. *Ammonia tepida*. 3a. Spiral view 3b. Umbilical view; 4. *Ammonia beccarii* 4a. Spiral view 4b. Umbilical view; 5. *Calcarina calcar*; 6a. *Elphidium excavatum*, 6b. Close view showing the umbilicus and granules along the sutures. 7. *Elphidium clavatum*; 8a. *Elphidium williamsoni*, 8b. Close view; *Criboelphidium ocanensis*; 10a. *Haynesina depressula*, 10b. Close view showing the postules. 11a *Nonian* sp. 11b. Close view showing the smooth surface of the species; 12. *Nonian commune*; 13. *Nonionella* sp.; 14. *Nonionella atlantica*; 15. *Nonionella labradorica*; 16. *Nonionoides grateleupi*; 17. *Globorotaloides* sp.; 18. *Bolivina variabilis*; 19a. *Bolivina pseudoplicata*, 19b. Close view of showing the anastomosing pattern costae; 20. *Brizalina spathulata*; 21. *Lagena* sp.; 22. *Lagena striata*; 23. *Lagena levis*; 24. *Hopensinella pacifica*; 25. *Gallitellia vivans*; 26a. *Uvigerina* sp. 26b. Close view showing the parallel striata or ribs.



**Figure 7.2** SEM images of the recovered foraminifera from the Dhordo and Berada Cores  
 1. *Triloculina tricarinata*; 2. *Miliolina australis*; 3. *Milonella grata*; 4. *Quinqueloculina seminula*; 5. *Quinqueloculina levigata*; 6. *Quinqueloculina oblonga*; 7. *Triloculina levigata*; 8. *Cycloforina*; 9. *Quinqueloculina sp.*; 10. *Miliamina fusca*; 11. *Triloculina oblonga*; 12 *Fursenkonia sp.*; 13. *Triloculina sp.*; 14. *Spiroculina sp.*

**Species: *Quinquiliculina limbata***

**Description:** Tests elongated oblate in the overall form, aperture ovate, flush with surface.

**Species: *Quinquiliculina oblonga***

**Description:** Test ovate in outline, early chambers quinquiloculinate depending on degree of overall of other successive chambers.

**Species: *Quinquiliculina laevigata***

**Species: *Quinquiliculina aspera***

**Species: *Triloculina oblonga* Montagu**

Test longer than broad, surface ornamented with closely set delicate distinct longitudinal costae; sutures depressed, aperture circular with a tooth.

Subfamily : Miliolinellinae Vella, 1957

Genus : Triloculina d'Orbigny, 1826

**Species: *Triloculina laevigata* d'Orbigny, 1826**

**Description:** Test ovate in outline, rounded to ovate in section, periphery rounded, chambers half than the coil length, final chamber largely covered by apertural flap.

**Species: *Triloculina tricarinata* d'Orbigny, 1826**

**Description:** Test ovate, equilaterally triangular or subtriangular, the three chambers are clearly visible.

***Fursenkoina sp.***

**Description:** Test biserial, early chambers added less than 180 degrees apart, resulting in sigmoid or twisted biserial appearance.

**Remarks:** U. Cretaceous to Holocene

***Oolina sp.***

**Description:** Test unilocular, globular to ovate, surface smooth or very finely striated.

***Uvigerina Sp.***

Test generally small, chambers are triserially arranged in the early stage then becomes biserial. Chambers large and globular, wall finely perforate, aperture short, tubular with a slight neck.

***Spirulinid sp.***

**Description:** Spiral, planispiral, appears similar to *Spiroloculina*.

***Spiroculina sp.***

Test 1 % to 2 times as long as broad, concave with the central part of the periphery the thickest part, chambers rapidly increasing in size and thickness as added, The peripheral margins of the early chambers persisting as raised ridges

***Cycloforina sp.***

**Description:** Test quinquiloculine, always five chambers visible from the exterior chambers one half of the coil in length, added against the previous whorl without a separate chamber floor.

**PALAEOENVIRONMENTAL CHANGES IN THE DHORDO CORE**

The foraminiferal assemblage in the Dhordo core shows significant variations in the overall abundance pattern down core. The mostly benthic forms dominate all over the record amongst which the genus *ammonia* dominates in most of the samples followed by *Elphidium* species and *Nonian* species. Based on the abundance patterns, the core is divided into four zones (Fig. 7.3-7.5).

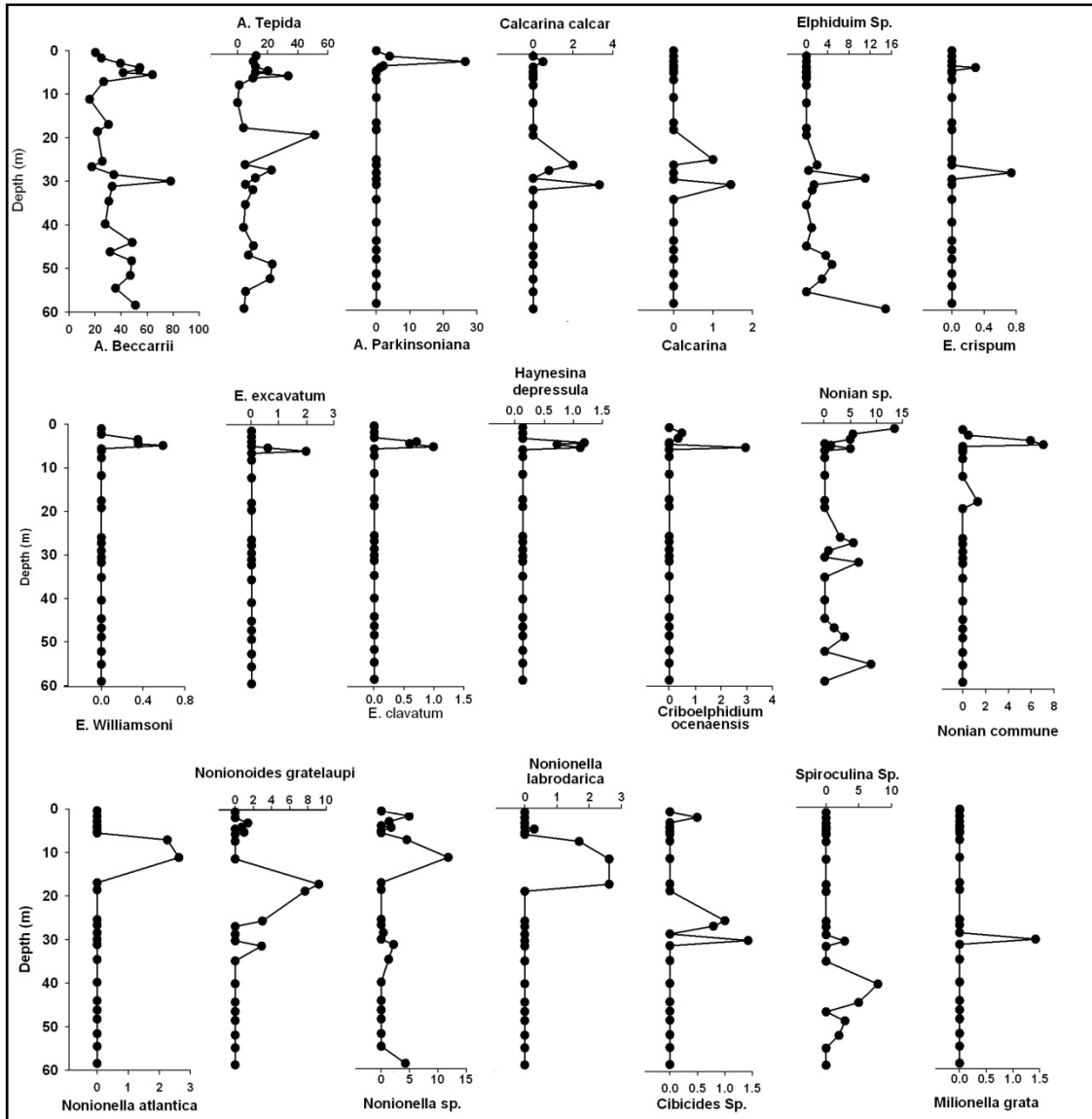


Figure 7.3 Graphs showing down core variations of foraminiferal species in Dhordo Core.

### Zone-I (60 - 31m depth)

The bottom most zone of the Dhordo core dominates by *Ammonia* genus which contributes more than 70% of the total assemblage. The bottom upward foraminiferal distribution shows that *A. beccarii* and *A. tepida* together dominate the assemblage. The bottom upward variation in the ammonia species shows maximum abundance between 55-48 m that is followed by the relative decrease in its proportion. In these depths *Quinqueloculina seminula* marks its high abundance (~10-25%), *Triloculina sp.* (2-20%) and *Brizalina spathulata* (~1-6%). *Elphidium sp.* also seen to increase between during this interval contributing 2-4% except the bottommost sample that contributes in a very high

proportion (~15%) (Fig. 7.3-7.5; Table 7.1). The rest of the species remain in subordinate proportions. Other species of *Nonian* and *B. variabilis* contributes in considerable proportion in only few samples. Above 48m to 31m a decrease in total abundance of *ammonia* is observed. This reduction affected mostly to the *A. tepida* as compare to the *A. beccarii*. In contrast to this *Quinqueloculina seminula* (10-30%), *Q. oblonga* (3-7%) and *Q. laevigata* (1-5%) are markedly increased in their proportion that remains consistent throughout this zone. Other species *Bolivina variabilis* and *B. spathulata* also increase in this zone (Fig. 7.3-7.5; Table 7.1).

The *Ammonia* is the most dominant genus throughout the core which is also clearly seen in this zone. It is known as the most tolerant and robust foraminifera that can survive through large fluctuations in ecological parameters like salinity, temperature, oxygen and nutrient supply (Boltovsky 1976, Murray 2006, Sen Gupta 2002). The other dominant species are *Q. seminulum* and *B. spathulata* in this zone. *Q. seminula* is a typical shelf species and is known to colonize even in the estuarine settings (Murray, 2006). The association of *Ammonia* group with the *Quinqueloculina seminulum* is found to increase in the brackish to high saline conditions (9-40) during the seasonal variability on seasonal records in coastal areas of Santona, Spain (Cearreta 1988, 1989). *Triloculina sp.* is observed to dominate in the marine hyposaline conditions that prefer the low organic matter (Murray 1991). However, *B. spathulata* is observed as one of the first foraminiferal species that survived in first marine excursion in Marmara Sea (McHugh et.al. 2008). These workers found *Brizalina spp.* along with the *Ammonia* group as a confirmatory evidence for the typical marine settings in the area. The upper part between 48-30 m depths is characterized by the reduction in overall *Ammonia* species and increase in the *Quinqueloculina seminula*, *Q. oblonga*, *Q. laevigata* along with the increased proportion of *Bolivina variabilis* and *B. spathulata* (Fig. 7.3-7.5). The other dominant assemblage of the *Q. seminula* is reported from variety of near shore environments such as marshes, backshore, wave-dominated and estuarine settings (Laprida et.al. 2011, Martin 2000, Murray 2006). Studies on modern samples show that *Q. oblonga* is controlled largely by salinity conditions and its increased proportion can be considered as a normal marine salinity conditions (Jane E. Swallow 2000).

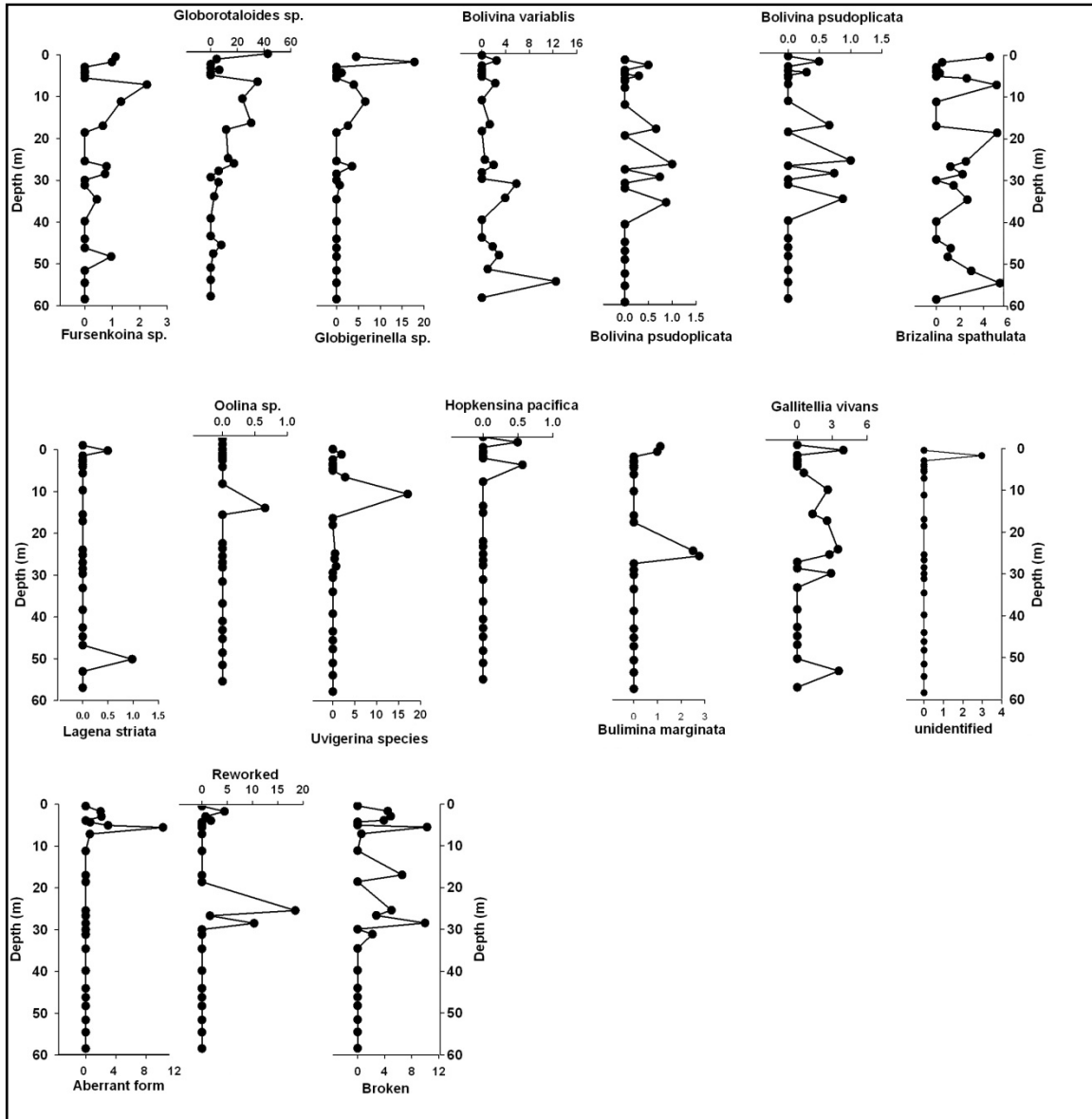


**Figure 7.4** Graphs showing down core variations of foraminiferal species in Dhordo Core.

Based on the vertical variations this zone is characterized the two characteristic assemblages- 1) *Ammonia-Quiniquiloculina-Triloculina-Brizalina* for the lower part between 60 - 48m depth and 2) *Ammonia-Quiniquiloculina-Bolovina* assemblage between 48-31 m depth. The foraminiferal abundance is observed to increase from bottom to top suggesting favourable conditions for conditions for their survival. The deposition of these sediments started around ~18ka BP which indicates the early submergence of the central Great Rann basin in response to the post glacial sea level rise. The lower zone foraminiferal assemblage of *Ammonia-Quiniquiloculina-Brizalina* is indicative of the

initial phase of the marine incursion into the basin forming brackish to shallow marine conditions whereas the upper part assemblage of *Ammonia-Quinuiloculina-Bolivina* assemblage suggests the prevalence of the shallow water marine conditions.

### Zone-II (31 - 25m depth)

This zone is characterized by the large scale changes in the overall assemblage. *Ammonia* found to further decrease by ~20% of the total assemblage. Many species appear in this zone such as *Calcarina calcer*, *Nonian sp.*, *Nonionoides sp.*, *Nonionella sp.*, *Cibicides sp.*, *Bulimina marginata*, and planktonics include *Globigerinella*, *Globorotalia sp.* and *Gallitellia vivans* (Fig. 7.3-7.5; Table 7.1) A decrease on the *Quinuiloculina* is also noted. Another marked feature of this unit is the occurrence of the large proportion of broken and reworked foraminifera between ~20 - 30m depth. The *Ammonia* specimens abruptly increase in their overall size by several times and also appear as reworked or redistributed. This marks a significant change in the environmental conditions.

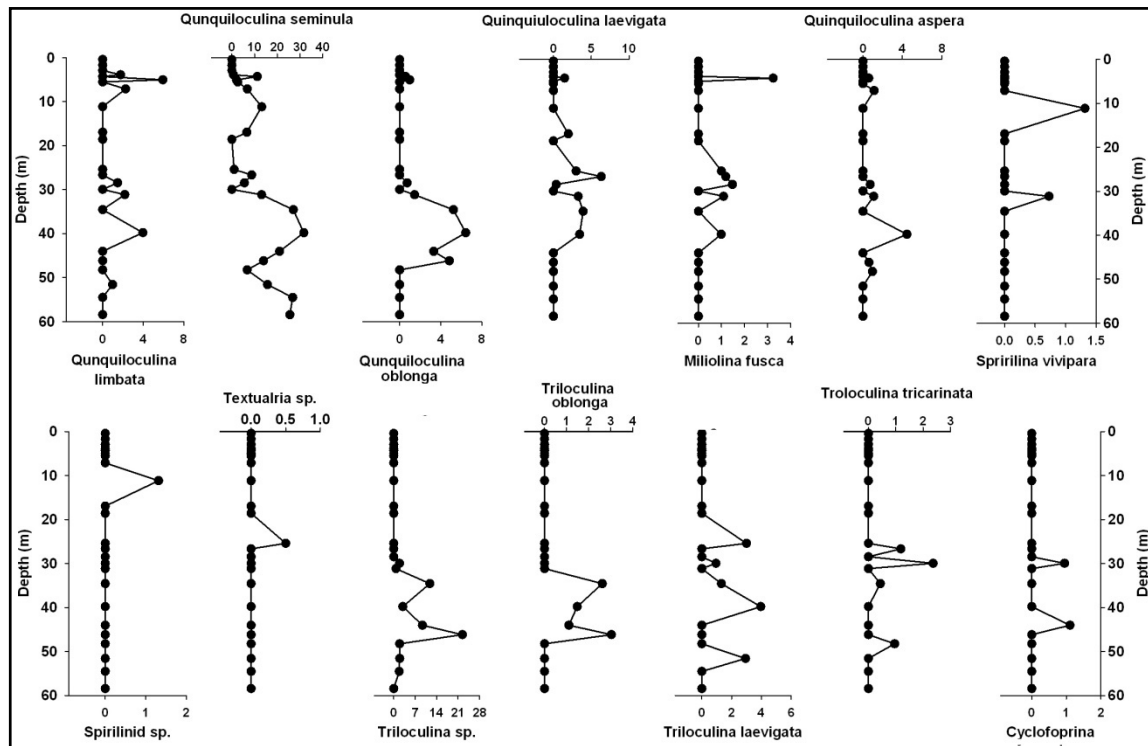


**Figure 7.5** Graphs showing down core variations of foraminiferal species in Dhordo Core.

The appearance of the broken and reworked specimens in significant amount suggests the high energy conditions and reworking (~25% of the total assemblage). The same is in conformity by the appearance of hard substrate loving *Calcarina* species

(Murray, 2006). Increased grain size of the sediments in this zone suggests strong fluctuations from the shallow marine to continentally influenced settings on account of the terrestrial organic matter input into the basin (Fig. 7.2). Interestingly, the species diversity and overall abundance of foraminifera is maximum in this zone. *Globorotaloides* sp. (~10%), *Brizalina spathulata* (5), *Gallitellia vivans* (4%), *Nonian* (6%), *Nonionoides* (9%) and *Nonionella* (8%), whereas rest of the species contribute in minor proportion (Fig. 7.3-7.5, Table 7.1).

This zone is characterized by *Ammonia-Globorotaloides-Nonionoides* assemblage. The high diversity in this zone may on account of the foraminiferal transport through the Arabian Sea and the broken and reworked foraminifera suggest redistribution of the sediments. This also may be on account of the increase in strength of fluvial systems due to strong monsoonal conditions. The strong monsoonal winds may also cause the strong vertical mixing of the sediments in offshore which may be carried into the Great Rann rann due to high tidal influence. These interpretations are consistent with the other studies described in the subsequent chapters. However, a high resolution foraminiferal study along with good chronological controls is required to understand the environmental changes in this zone.

### **Zone-III (25 - 8m depth)**

In this zone, the *Ammonia beccarii* reduces further whereas *A. tepida* is absent throughout. The proportion of the few reworked specimens are found to continue to occur. The planktonic foraminifera like *Globorotaloides*, *Gallitellia vivans* and *Globigerinella* sp. contributes in the highest proportion followed by the *Nonian*, *Ninionella*, *Nonionoides* and *Furkensisiana* species (Fig. 7.3-7.5; Table 7.1). The planktonic component in this zone is found to be dominant. Other species like *Bolovina pseudoplicatam* *Brizalina spathulata*, *Bolovina marginata* are also present but vary rapidly.

The association of the *Ammonia-Nonionella* group, *Nonionella* are known from the coastal marine environments and also where the fresh-marine influence is seen (Murray 2006). The *Nonionella* sp. is considered as the opportunists that can also survive the low oxygenated conditions and low nutrient conditions (Murray 2006). These above facts points towards the mixed marine environments during the Mid-Holocene time. This is also

indicated by the C/N ratios in this interval of Dhordo core included in succeeding chapter. The overall species diversity reduces in this zone from bottom to top.

#### **Zone-IV (8 - 0m depth)**

In the topmost part of the Dhordo Core, the *Ammonia* species dominates again contributing more than 80% of the total assemblage. The occurrences are found to be - *Ammonia beccarii* (60%), *A. tepida* (10%) and *A. parkinsoniana* (~5%) (Fig. 7.3-7.5; Table 7.1). Other species like *Brizalina* sp., *Bolovina* sp., *Elphidium* sp., *Fursenkonia* sp. also appears along with *Nonion* sp., *Nonionella* sp. and *Quinqueloculina* sp. Planktonics including *Goloborotalia* sp., *Gallitellia vivans* are also present (Fig. 7.3-7.5). This unit is mostly dominated by the *Ammonia-Nonion-Elphidium* species. The similar assemblage is also observed during the surface sediment studies along the Bet Zone in northwestern rann and described in a previous chapter. The dominance of *Ammonia* species is a characteristic feature of this region in modern environment due to stressful conditions. The top most zone indicates the typical shallow marine conditions existed during the deposition as also indicated by the lowest abundance and diversity of the foraminifera in these sediments. However, the top most zone is marked by marine regressive phase that indicates withdrawal of the marine waters from Great Rann of Kachchh during recent past.

### **PALAEOENVIRONMENTAL CHANGES IN THE BERADA CORE**

On the basis of the abundance patterns, the Berada core is divided in three zones that suggest variations in the environmental conditions.

#### **Zone-I (50 - 36m depth)**

The marine transgression in Berada core is indicated during the Early Holocene times (~10ka BP). The bottom most samples in this zone mainly comprises of the older, reworked foraminifera. The fresh foraminifera recovered are found to primarily belong to the *Ammonia* and *Elphidium* genera (Fig. 7.6; Table 7.2).

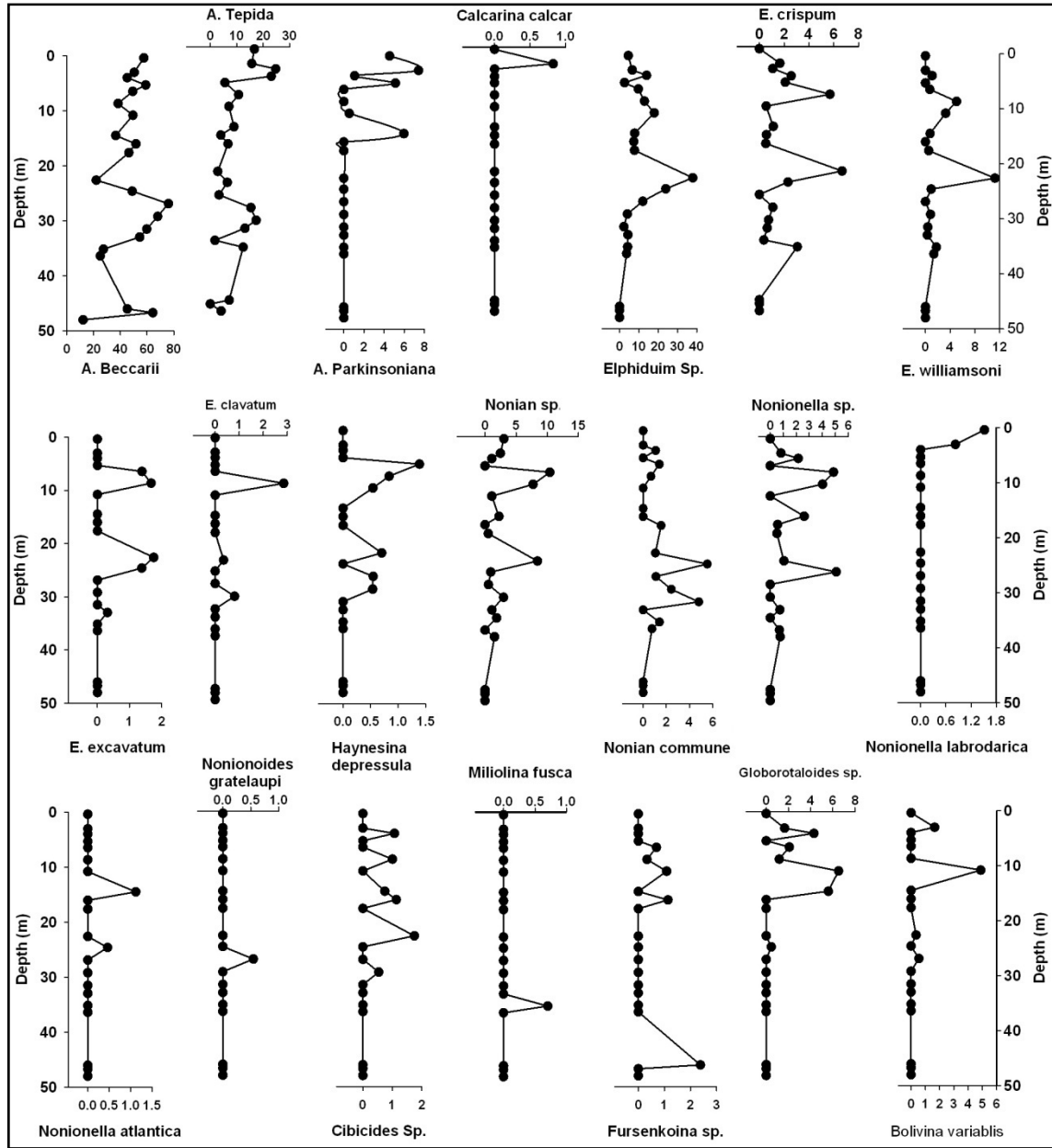


**Figure 7.6** Graphs showing down core variations of foraminiferal species in Berada Core.

**Zone-II (36 - 19m depth)**

This zone comprises fresh foraminifera that includes dominantly *A. beccarii* (30-80%), *A. tepida* (0-20%), *Elphidium sp.* (0-40%), *E. crispum* (0-8%), *E. williamsoni* (0-12%), *Quinqueloculina sp.* (0-5%), *Q. limbata* (0-2%) *N. commue* (0-6%), *Nonioan sp.* (0-2%), *Nonionella* (0-5%), *B. spathulata* (0-4%) (Fig. 7.6; 7.7; Table 7.2). The reworked or older foraminifera are completely absent. The lower most part of this zone is characterized by the predominant *A. beccarii* followed by *Elphidium* and *Quinqueloculina* genus (Fig.

7.3). The species diversity also ranges between 10-15 throughout this unit indicating the favourable environmental conditions for the survival of foraminifera.

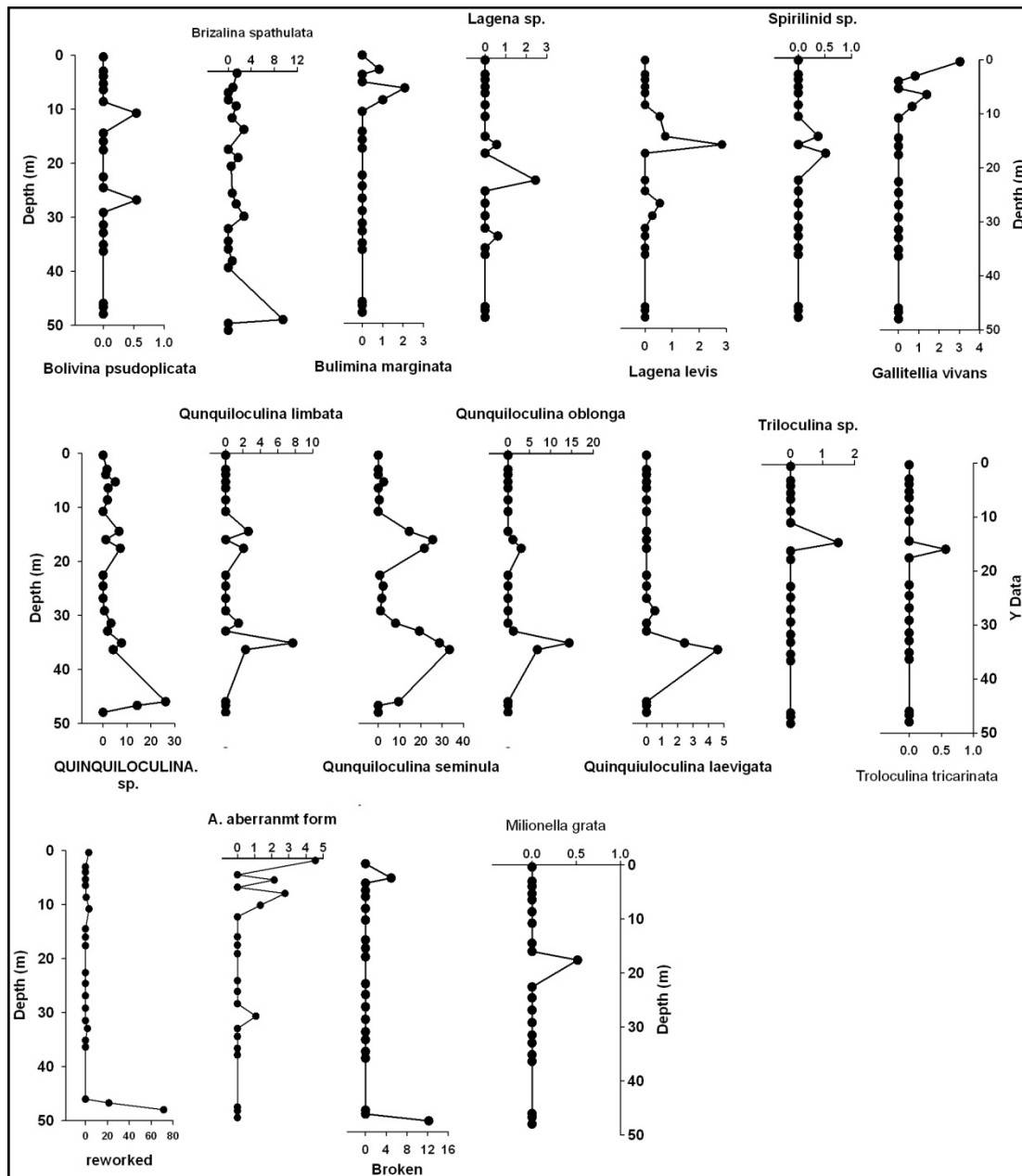


**Figure 7.7** Graphs showing down core variations of foraminiferal species in Berada Core.

The *Ammonia-Elphidium* association is common in shallow marine environments (Murray, 2006, Sen Gupta, 1999). Being the second most dominant genus in the core along with the dominant composition of *Quinqueloculina* sp. indicates brackish to shallow marine conditions of the initial transgressive phase (Murray 1991, Murray 2006, Phipps et.al. 2010). The *Elphidium* and *Quinqueloculina* species with the *Ammonia* genus are also

commonly found in modern coastal regions along the Gulf of Kachchh (Rajshekhkar et.al. 2004, Nigam and Chaturvedi 2004). This particular unit encompasses the Early Holocene time from 9.5- 6.5ka B.P. Therefore it is inferred that during the Early Holocene times Banni region was under the marine settings that is also supported by C/N ratio data and the foraminiferal assemblage in the marginal part is denoted by the *Ammonia-Elphidium-Quinqueloculina* species (Fig. 7.4).

### **Zone-III (19 - 0m depth)**

The topmost unit of this core yields more or less similar fauna assemblage to that of the lower zone but characteristically differs in the abundance pattern. The genus *Ammonia* dominates in this unit also by contributing more than 60-85% of the total assemblage. The presence of *A. parkinsoniana* is also observed throughout this unit. Three species represent the genus *Ammonia* in this zone i.e. *A. beccarii* (50-60%), *A. tepida* (5-20%), *A. parkinsoniana* (0-6%). In contrast with the lower zone, the second dominant contributing element is found to be *Quinqueloculina seminulum* (0-30%) followed by *Elphidium* (10-20%). *Nonian* sp. (0-10%), *Nonionella* (0-6%), *Globorotaloides* (0-7%), *B. variabilis* (0-6%) respectively (Fig. 7.3; Table 7.2). The drastically increased abundance of the *Quinqueloculina* species along with the *Elphidium-Nonian* indicates the brackish to marine conditions whereas the increased abundance of *Nonionella* sp indicates the increased fresh water influx into the basin. This is well constrained in C/N ratios described in later chapter. The largely fluctuating species diversity in this zone may be on account of the rapidly changing environmental conditions that led to the domination of only the tolerant taxa.

**Table 7.1** Table showing the foraminiferal abundance (in percentage) in the Dhordo Core.

Sr. No.	1	2	3	4	5	6	7	8	9	10	11	12	13	14	15	16	17	18	19	20	21	22	23	24
Depth (m)	0.44	1.70	2.92	3.90	4.30	5.04	5.52	7.12	11.16	16.96	18.58	25.42	26.66	28.46	29.95	31.15	34.57	39.79	44.03	46.17	48.24	51.59	54.52	58.43
<i>A. beccarii</i>	20.2	24.8	39.5	54.4	54.0	41.6	64.1	26.6	15.8	30.3	21.8	25.5	17.4	34.3	78.2	33.1	30.6	27.7	48.6	31.5	48.1	47.1	0.0	0.0
<i>A. tepida</i>	12.4	10.4	11.9	20.1	11.8	33.7	10.3	1.1	0.0	3.9	51.3	5.0	22.5	11.8	5.2	10.2	5.2	4.0	10.5	7.3	23.1	21.6	0.0	0.0
<i>A. parkinsoniana</i>	0.0	4.0	26.6	2.1	1.2	0.0	0.0	0.0	0.0	0.0	0.0	0.0	0.0	0.0	0.0	0.0	0.0	0.0	0.0	0.0	0.0	0.0	0.0	0.0
<i>A. aberrant</i> <i>form</i>	0.0	2.0	2.1	0.0	0.6	3.0	10.3	0.6	0.0	0.0	0.0	0.0	0.0	0.0	0.0	0.0	0.0	0.0	0.0	0.0	0.0	0.0	0.0	0.0
<i>Calcarina calcar</i>	0.0	0.5	0.0	0.0	0.0	0.0	0.0	0.0	0.0	0.0	0.0	2.0	0.8	0.0	3.3	0.0	0.0	0.0	0.0	0.0	0.0	0.0	0.0	0.0
<i>Calcarina</i>	0.0	0.0	0.0	0.0	0.0	0.0	0.0	0.0	0.0	0.0	0.0	1.0	0.0	0.0	0.0	1.5	0.0	0.0	0.0	0.0	0.0	0.0	0.0	0.0
<i>Elphidium</i> Sp.	0.0	0.0	0.0	0.0	0.0	0.0	0.0	0.0	0.0	0.0	0.0	2.0	0.4	11.1	1.4	1.1	0.0	1.0	0.0	3.6	4.8	2.9	0.0	0.0
<i>E. crispum</i>	0.0	0.0	0.0	0.0	0.3	0.0	0.0	0.0	0.0	0.0	0.0	0.0	0.0	0.7	0.0	0.0	0.0	0.0	0.0	0.0	0.0	0.0	0.0	0.0
<i>E. williamsoni</i>	0.0	0.0	0.3	0.4	0.6	0.0	0.0	0.0	0.0	0.0	0.0	0.0	0.0	0.0	0.0	0.0	0.0	0.0	0.0	0.0	0.0	0.0	0.0	0.0
<i>E. excavatum</i>	0.0	0.0	0.0	0.0	0.6	2.0	0.0	0.0	0.0	0.0	0.0	0.0	0.0	0.0	0.0	0.0	0.0	0.0	0.0	0.0	0.0	0.0	0.0	0.0
<i>E. clavatum</i>	0.0	0.0	0.0	0.7	0.6	1.0	0.0	0.0	0.0	0.0	0.0	0.0	0.0	0.0	0.0	0.0	0.0	0.0	0.0	0.0	0.0	0.0	0.0	0.0
<i>Haynesina depressula</i>	0.0	0.0	0.0	1.1	0.6	1.0	0.0	0.0	0.0	0.0	0.0	0.0	0.0	0.0	0.0	0.0	0.0	0.0	0.0	0.0	0.0	0.0	0.0	0.0
<i>Taxyella fontcaudensis</i>	0.0	0.0	0.0	5.3	1.2	0.0	0.0	0.0	0.0	0.0	0.0	1.5	0.0	0.0	0.0	0.0	0.0	0.0	0.0	0.0	0.0	0.0	8.9	0.0
<i>Criboelphidium ocenaensi</i>	0.0	0.5	0.3	0.0	0.0	3.0	0.0	0.0	0.0	0.0	0.0	0.0	0.0	0.0	0.0	0.0	0.0	0.0	0.0	0.0	0.0	0.0	0.0	0.0
<i>Nonian</i> sp.	13.5	5.4	4.9	0.0	1.2	5.0	0.0	0.0	0.0	0.0	0.0	3.0	5.5	0.7	0.0	6.5	0.0	0.0	0.0	1.8	3.8	0.0	0.0	0.0
<i>Nonionoides gratelaupi</i>	0.0	0.0	1.4	0.7	0.0	1.0	0.0	0.0	0.0	9.2	7.7	3.0	0.0	0.0	0.0	2.9	0.0	0.0	0.0	0.0	0.0	0.0	0.0	4.3
<i>Nonian commune</i>	0.0	0.5	5.9	7.1	0.0	0.0	0.0	0.0	0.0	1.3	0.0	0.0	0.0	0.0	0.0	0.0	0.0	0.0	0.0	0.0	0.0	0.0	0.0	0.0
<i>Nonionella</i> sp.	0.0	5.0	1.4	0.0	1.8	0.0	0.0	4.5	11.8	0.0	0.0	0.0	0.0	0.4	0.0	2.2	1.3	0.0	0.0	0.0	0.0	0.0	0.0	0.0
<i>Nonionella labrodarica</i>	0.0	0.0	0.0	0.0	0.3	0.0	0.0	1.7	2.6	2.6	0.0	0.0	0.0	0.0	0.0	0.0	0.0	0.0	0.0	0.0	0.0	0.0	0.0	0.0
<i>Nonionella atlantica</i>	0.0	0.0	0.0	0.0	0.0	0.0	0.0	2.3	2.6	0.0	0.0	0.0	0.0	0.0	0.0	0.0	0.0	0.0	0.0	0.0	0.0	0.0	0.0	0.0
<i>Globorotaloides</i> sp.	42.7	4.5	0.0	0.0	6.5	0.0	0.0	35.0	23.7	30.3	11.5	13.0	17.4	5.9	0.0	5.8	2.6	0.0	0.0	7.9	1.9	0.0	12.5	0.0

<b>Globigerinella sp.</b>	4.5	17.8	0.0	0.0	1.2	0.0	0.0	4.0	6.6	2.6	0.0	0.0	3.6	0.0	0.0	0.7	0.0	0.0	0.0	0.0	0.0	0.0	5.4	0.0
<b>Bolivina variabilis</b>	0.0	2.5	0.0	0.0	0.0	0.0	0.0	2.3	0.0	1.3	0.0	0.5	2.0	0.0	0.0	5.8	3.9	0.0	0.0	1.8	2.9	1.0	0.0	0.0
<b>Brizalina spathulata</b>	4.5	0.5	0.0	0.0	0.3	0.0	2.6	5.1	0.0	0.0	5.1	2.5	1.2	2.2	0.0	1.5	2.6	0.0	0.0	1.2	1.0	2.9	0.0	0.0
<b>Bolivina pseuduplicata</b>	0.0	0.5	0.0	0.0	0.3	0.0	0.0	0.0	0.0	0.7	0.0	1.0	0.0	0.7	0.0	0.0	0.9	0.0	0.0	0.0	0.0	0.0	0.0	0.0
<b>Fursenkoina sp.</b>	1.1	1.0	0.0	0.0	0.0	0.0	0.0	2.3	1.3	0.7	0.0	0.0	0.8	0.7	0.0	0.0	0.4	0.0	0.0	0.0	1.0	0.0	0.0	0.0
<b>Lagena sp.</b>	0.0	0.0	0.0	0.0	0.0	0.0	0.0	0.0	0.0	0.0	0.0	0.0	0.0	0.0	0.0	0.0	0.0	0.0	0.0	0.0	0.0	0.0	0.0	0.0
<b>Lagena levis</b>	0.0	0.0	0.0	0.0	0.0	0.0	0.0	0.0	0.0	0.0	0.0	0.0	0.0	0.0	0.0	0.0	0.0	0.0	0.0	0.0	0.0	0.0	0.0	0.0
<b>Lagena striata</b>	0.0	0.5	0.0	0.0	0.0	0.0	0.0	0.0	0.0	0.0	0.0	0.0	0.0	0.0	0.0	0.0	0.0	0.0	0.0	0.0	0.0	1.0	0.0	0.0
<b>Oolina sp.</b>	0.0	0.0	0.0	0.0	0.0	0.0	0.0	0.0	0.0	0.7	0.0	0.0	0.0	0.0	0.0	0.0	0.0	0.0	0.0	0.0	0.0	0.0	0.0	0.0
<b>Uvigerina species</b>	0.0	2.0	0.0	0.0	0.0	0.0	0.0	2.8	17.1	0.0	0.0	0.5	0.4	0.7	0.0	0.0	0.0	0.0	0.0	0.0	0.0	0.0	0.0	0.0
<b>Hopkinsina pacifica</b>	0.0	0.5	0.0	0.0	0.0	0.0	0.0	0.6	0.0	0.0	0.0	0.0	0.0	0.0	0.0	0.0	0.0	0.0	0.0	0.0	0.0	0.0	3.6	0.0
<b>Bulimina marginata</b>	1.1	1.0	0.0	0.0	0.0	0.0	0.0	0.0	0.0	0.0	0.0	2.5	2.8	0.0	0.0	0.0	0.0	0.0	0.0	0.0	0.0	0.0	0.0	0.0
<b>Gallitellia vivans</b>	0.0	4.0	0.0	0.0	0.0	0.0	0.0	0.6	2.6	1.3	2.6	3.5	2.8	0.0	0.0	2.9	0.0	0.0	0.0	0.0	0.0	0.0	0.0	0.0
<b>Cibicides Sp.</b>	0.0	0.5	0.0	0.0	0.0	0.0	0.0	0.0	0.0	0.0	0.0	1.0	0.8	0.0	1.4	0.0	0.0	0.0	0.0	0.0	0.0	0.0	0.0	0.0
<b>Unidentified</b>	0.0	3.0	0.0	0.0	0.0	0.0	0.0	0.0	0.0	0.0	0.0	0.0	0.0	0.0	0.0	0.0	0.0	0.0	0.0	0.0	0.0	0.0	0.0	0.0
<b>Quinquiloculina sp.</b>	0.0	0.0	0.0	0.0	0.0	0.0	0.0	0.0	0.0	0.0	0.0	0.0	0.0	0.0	0.0	0.0	0.0	0.0	0.0	0.0	0.0	0.0	26.8	25.5
<b>Qunquiloculina limbata</b>	0.0	0.0	0.0	1.8	0.0	5.9	0.0	2.3	0.0	0.0	0.0	0.0	0.0	1.5	0.0	2.2	0.0	4.0	0.0	0.0	0.0	1.0	0.0	0.0
<b>Qunquiloculina seminula</b>	0.0	0.0	0.0	0.7	11.2	2.0	2.6	6.8	13.2	6.6	0.0	1.0	8.7	5.5	0.0	13.1	27.1	31.7	21.0	13.9	6.7	15.7	0.0	0.0
<b>Qunquiloculina oblonga</b>	0.0	0.0	0.0	0.0	0.6	1.0	0.0	0.0	0.0	0.0	0.0	0.0	0.0	0.7	0.0	1.5	5.2	6.4	3.3	4.8	0.0	0.0	0.0	0.0
<b>Quinquiloculina laevigata</b>	0.0	0.0	0.0	0.0	1.5	0.0	0.0	0.0	0.0	2.0	0.0	3.0	6.3	0.4	0.0	3.3	3.9	3.5	0.0	0.0	0.0	0.0	0.0	0.0
<b>Miliolina fusca</b>	0.0	0.0	0.0	0.0	3.2	0.0	0.0	0.0	0.0	0.0	0.0	1.0	1.2	1.5	0.0	1.1	0.0	1.0	0.0	0.0	0.0	0.0	0.0	0.0
<b>Quinquiloculina aspera</b>	0.0	0.0	0.0	0.0	0.6	0.0	0.0	1.1	0.0	0.0	0.0	0.0	0.0	0.7	0.0	1.1	0.0	4.5	0.0	0.6	1.0	0.0	0.0	0.0
<b>Spirilina vivipara</b>	0.0	0.0	0.0	0.0	0.0	0.0	0.0	0.0	1.3	0.0	0.0	0.0	0.0	0.0	0.0	0.7	0.0	0.0	0.0	0.0	0.0	0.0	0.0	0.0

<b>Spirilinid sp.</b>	0.0	0.0	0.0	0.0	0.0	0.0	0.0	0.0	1.3	0.0	0.0	0.0	0.0	0.0	0.0	0.0	0.0	0.0	0.0	0.0	0.0	0.0	0.0	0.0	0.0
<b>Textualria sp.</b>	0.0	0.0	0.0	0.0	0.0	0.0	0.0	0.0	0.0	0.0	0.0	0.5	0.0	0.0	0.0	0.0	0.0	0.0	0.0	0.0	0.0	0.0	0.0	1.8	0.0
<b>Oridorsalins Sp.</b>	0.0	0.0	0.0	0.0	0.0	0.0	0.0	0.0	0.0	0.0	0.0	0.5	0.0	0.0	0.0	0.0	0.0	0.0	0.0	0.0	0.0	0.0	0.0	0.0	0.0
<b>Triloculina sp.</b>	0.0	0.0	0.0	0.0	0.0	0.0	0.0	0.0	0.0	0.0	0.0	0.0	0.0	0.0	1.9	0.7	11.8	3.0	9.4	22.4	1.9	2.0	0.0	0.0	0.0
<b>Triloculina oblonga</b>	0.0	0.0	0.0	0.0	0.0	0.0	0.0	0.0	0.0	0.0	0.0	0.0	0.0	0.0	0.0	0.0	2.6	1.5	1.1	3.0	0.0	0.0	0.0	0.0	0.0
<b>Triloculina laevigata</b>	0.0	0.0	0.0	0.0	0.0	0.0	0.0	0.0	0.0	0.0	0.0	3.0	0.0	0.0	0.9	0.0	1.3	4.0	0.0	0.0	0.0	2.9	0.0	0.0	0.0
<b>Troloculina tricarinata</b>	0.0	0.0	0.0	0.0	0.0	0.0	0.0	0.0	0.0	0.0	0.0	0.0	1.2	0.0	2.4	0.0	0.4	0.0	0.0	0.0	1.0	0.0	0.0	0.0	0.0
<b>Cyclofoprina</b>	0.0	0.0	0.0	0.0	0.0	0.0	0.0	0.0	0.0	0.0	0.0	0.0	0.0	0.0	0.9	0.0	0.0	0.0	1.1	0.0	0.0	0.0	0.0	0.0	0.0
<b>Spiroculina Sp.</b>	0.0	0.0	0.0	0.0	0.0	0.0	0.0	0.0	0.0	0.0	0.0	0.0	0.0	0.0	2.8	0.0	0.0	7.9	5.0	0.0	2.9	2.0			
<b>Milionella grata</b>	0.0	0.0	0.0	0.0	0.0	0.0	0.0	0.0	0.0	0.0	0.0	0.0	0.0	0.0	1.4	0.0	0.0	0.0	0.0	0.0	0.0	0.0	0.0		
<b>Broken</b>	0.0	4.5	4.9	3.9	0.0	0.0	10.3	0.6	0.0	6.6	0.0	5.0	2.8	10.0	0.0	2.2	0.0	0.0	0.0	0.0	0.0	0.0	0.0	0.0	14.9
<b>Reworked</b>	0.0	4.5	0.7	1.8	0.0	0.0	0.0	0.0	0.0	0.0	0.0	18.5	1.6	10.3	0.0	0.0	0.0	0.0	0.0	0.0	0.0	0.0	0.0	0.0	0.0

**Table 7.2** Table showing the foraminiferal abundance (in percentage) in Berada Core.

Sr. No.	1	2	3	4	5	6	7	8	9	10	11	12	13	14	15	16	17	18	19	20	21
Depth (m)	0.36	3.00	3.96	5.30	6.45	8.65	10.79	14.48	16.00	17.60	22.59	24.59	26.86	29.18	31.48	32.94	35.14	36.36	46.00	46.70	47.98
<i>A. beccarii</i>	57.58	50.41	45.16	58.97	49.31	38.36	49.46	36.57	51.70	46.39	22.11	48.85	75.96	67.92	59.78	54.52	27.37	25.05	45.24	64.29	12.24
<i>A. tepida</i>	16.67	15.70	24.73	23.08	5.56	10.72	7.07	8.96	3.98	6.70	2.81	6.45	3.28	15.36	17.34	13.08	1.75	12.43	7.14	0.00	4.08
<i>A. parkinsoniana</i>	4.55	7.44	1.08	5.13	0.00	0.00	0.54	5.97	0.00	0.00	0.00	0.00	0.00	0.00	0.00	0.00	0.00	0.00	0.00	0.00	0.00
<i>Calcarina calcar</i>	0.00	0.83	0.00	0.00	0.00	0.00	0.00	0.00	0.00	0.00	0.00	0.00	0.00	0.00	0.00	0.00	0.00	0.00	0.00	0.00	0.00
<i>Calcarina</i>	0.00	0.00	0.00	0.00	0.00	0.00	0.00	0.00	0.00	0.00	0.00	0.00	0.00	0.00	0.00	0.00	0.00	0.00	0.00	0.00	0.00
<i>A. aberrant</i> <i>form</i>	4.55	0.00	2.15	0.00	2.78	1.34	0.00	0.00	0.00	0.00	0.00	0.00	0.00	1.08	0.00	0.00	0.00	0.00	0.00	0.00	0.00
<i>reworked</i>	3.03	0.00	0.00	0.00	0.00	0.67	3.26	0.00	0.00	0.00	0.00	0.00	0.00	0.00	0.00	1.87	0.00	0.00	0.00	21.43	71.43
<i>Elphidium Sp.</i>	4.55	6.61	13.98	2.56	9.72	12.90	17.93	7.84	7.39	7.73	37.89	23.96	12.02	4.04	2.21	4.36	4.21	3.63	0.00	0.00	0.00
<i>E. crispum</i>	0.00	1.65	1.08	2.56	2.08	5.70	0.54	1.12	0.57	0.52	6.67	2.30	0.00	1.08	0.74	0.62	0.35	3.06	0.00	0.00	
<i>E. williamsoni</i>	0.00	0.00	1.08	0.00	0.69	5.03	3.26	0.75	0.00	0.52	11.23	0.92	0.00	0.81	0.37	0.31	1.75	1.34	0.00	0.00	0.00
<i>E. excavatum</i>	0.00	0.00	0.00	0.00	1.39	1.68	0.00	0.00	0.00	0.00	1.75	1.38	0.00	0.00	0.00	0.31	0.00	0.00	0.00	0.00	0.00
<i>E. clavatum</i>	0.00	0.00	0.00	0.00	0.00	2.85	0.00	0.00	0.00	0.00	0.35	0.00	0.00	0.81	0.00	0.00	0.00	0.00	0.00	0.00	0.00
<i>Haynesina depressula</i>	0.00	0.00	0.00	0.00	1.39	0.84	0.54	0.00	0.00	0.00	0.70	0.00	0.55	0.54	0.00	0.00	0.00	0.00	0.00	0.00	0.00
<i>Taxyella fontcaudensis</i>	0.00	0.00	0.00	0.00	0.00	0.00	0.00	0.00	0.00	0.00	0.00	0.00	0.00	0.00	0.00	0.00	0.00	0.00	0.00	0.00	0.00
<i>Criboelphidium ocaensis</i>	0.00	0.00	0.00	0.00	0.00	0.00	0.00	0.00	0.00	0.00	0.00	0.00	0.00	0.00	0.00	0.00	0.00	0.00	0.00	0.00	0.00
<i>Nonian sp.</i>	3.03	2.48	1.08	0.00	10.42	7.71	1.09	2.24	0.00	0.52	8.42	0.92	0.55	2.96	1.11	1.87	0.00	1.53	0.00	0.00	0.00
<i>Nonionoides gratelaupi</i>	0.00	0.00	0.00	0.00	0.00	0.00	0.00	0.00	0.00	0.00	0.00	0.00	0.55	0.00	0.00	0.00	0.00	0.00	0.00	0.00	0.00
<i>Nonian commune</i>	0.00	0.00	1.08	0.00	1.39	0.67	0.00	0.00	0.00	1.55	1.05	5.53	1.09	2.43	4.80	0.00	1.40	0.76	0.00	0.00	0.00
<i>Nonionella sp.</i>	0.00	0.83	2.15	0.00	4.86	4.02	0.00	2.61	0.57	0.52	1.05	5.07	0.00	0.00	0.74	0.00	0.70	0.76	0.00	0.00	0.00
<i>Nonionella labrodarica</i>	1.52	0.83	0.00	0.00	0.00	0.00	0.00	0.00	0.00	0.00	0.00	0.00	0.00	0.00	0.00	0.00	0.00	0.00	0.00	0.00	0.00
<i>Nonionella atlantica</i>	0.00	0.00	0.00	0.00	0.00	0.00	0.00	1.12	0.00	0.00	0.00	0.46	0.00	0.00	0.00	0.00	0.00	0.00	0.00	0.00	

<b>Globorotaloides sp.</b>	0.00	1.65	4.30	0.00	2.08	1.17	6.52	5.60	0.00	0.00	0.00	0.46	0.00	0.00	0.00	0.00	0.00	0.00	0.00	0.00	0.00
<b>Globigerinella sp.</b>	0.00	0.00	0.00	0.00	0.00	0.00	0.00	0.00	0.00	0.00	0.00	0.00	0.00	0.00	0.00	0.00	0.00	0.00	0.00	0.00	0.00
<b>Bolivina variabilis</b>	0.00	1.65	0.00	0.00	0.00	0.00	4.89	0.00	0.00	0.00	0.35	0.00	0.55	0.00	0.00	0.00	0.00	0.00	0.00	0.00	0.00
<b>Brizalina spathulata</b>	1.52	0.83	0.00	0.00	1.39	0.67	2.72	0.00	1.70	0.52	0.70	1.38	2.73	0.00	0.00	0.00	0.70	0.00	9.52	0.00	0.00
<b>Bolivina psudoplicata</b>	0.00	0.00	0.00	0.00	0.00	0.00	0.54	0.00	0.00	0.00	0.00	0.00	0.55	0.00	0.00	0.00	0.00	0.00	0.00	0.00	0.00
<b>Fursenkoina sp.</b>	0.00	0.00	0.00	0.00	0.69	0.34	1.09	0.00	1.14	0.00	0.00	0.00	0.00	0.00	0.00	0.00	0.00	0.00	2.38	0.00	0.00
<b>Lagena sp.</b>	0.00	0.00	0.00	0.00	0.00	0.00	0.00	0.00	0.57	0.00	2.46	0.00	0.00	0.00	0.00	0.62	0.00	0.00	0.00	0.00	0.00
<b>Lagena levis</b>	0.00	0.00	0.00	0.00	0.00	0.00	0.54	0.75	2.84	0.00	0.00	0.00	0.55	0.27	0.00	0.00	0.00	0.00	0.00	0.00	0.00
<b>Lagena striata</b>	0.00	0.00	0.00	0.00	0.00	0.00	0.00	0.00	0.00	0.00	0.00	0.00	0.00	0.00	0.00	0.00	0.00	0.00	0.00	0.00	0.00
<b>Oolina sp.</b>	0.00	0.00	0.00	0.00	0.00	0.00	0.00	0.00	0.00	0.00	0.00	0.00	0.00	0.00	0.00	0.00	0.00	0.00	0.00	0.00	0.00
<b>Uvigerina species</b>	0.00	0.83	0.00	0.00	0.69	0.34	0.00	0.00	0.00	0.00	0.00	0.00	0.00	0.00	0.00	0.00	0.00	0.00	0.00	0.00	0.00
<b>Hopkinsina pacifica</b>	0.00	0.00	0.00	0.00	0.00	0.00	0.00	0.00	0.00	0.00	0.00	0.00	0.00	0.00	0.00	0.00	0.00	0.00	0.00	0.00	0.00
<b>Bulimina marginata</b>	0.00	0.83	0.00	0.00	2.08	1.01	0.00	0.00	0.00	0.00	0.00	0.00	0.00	0.00	0.00	0.00	0.00	0.00	0.00	0.00	0.00
<b>Gallitellia vivans</b>	3.03	0.83	0.00	0.00	1.39	0.67	0.00	0.00	0.00	0.00	0.00	0.00	0.00	0.00	0.00	0.00	0.00	0.00	0.00	0.00	0.00
<b>Cibicides Sp.</b>	0.00	0.00	1.08	0.00	0.00	1.01	0.00	0.75	1.14	0.00	1.75	0.00	0.00	0.54	0.00	0.00	0.00	0.00	0.00	0.00	0.00
<b>unidentified</b>	0.00	0.00	0.00	0.00	0.00	0.00	0.00	0.00	0.00	0.00	0.00	0.00	0.00	0.00	0.00	0.00	0.00	0.00	0.00	0.00	0.00
<b>Quinquiloculina. Sp.</b>	0.00	1.65	1.08	5.13	2.08	1.84	0.00	6.72	1.14	7.22	0.00	0.00	0.00	0.54	3.32	1.87	7.72	4.21	26.19	14.29	0.00
<b>Qunquiloculina limbata</b>	0.00	0.00	0.00	0.00	0.00	0.00	0.00	2.61	0.00	2.06	0.00	0.00	0.00	0.00	1.48	0.00	7.72	2.29	0.00	0.00	0.00
<b>Qunquiloculina seminula</b>	0.00	0.00	0.00	2.56	0.00	0.50	0.00	14.55	25.57	21.65	0.70	2.30	1.64	1.08	8.12	19.31	28.77	33.46	9.52	0.00	0.00
<b>Qunquiloculina oblonga</b>	0.00	0.00	0.00	0.00	0.00	0.00	0.00	0.00	1.14	3.09	0.00	0.00	0.00	0.00	0.00	1.25	14.39	6.88	0.00	0.00	0.00
<b>Quinquiloculina laevigata</b>	0.00	0.00	0.00	0.00	0.00	0.00	0.00	0.00	0.00	0.00	0.00	0.00	0.00	0.54	0.00	0.00	2.46	4.59	0.00	0.00	0.00
<b>Miliolina fusca</b>	0.00	0.00	0.00	0.00	0.00	0.00	0.00	0.00	0.00	0.00	0.00	0.00	0.00	0.00	0.00	0.00	0.70	0.00	0.00	0.00	0.00
<b>Quinquiloculina aspera</b>	0.00	0.00	0.00	0.00	0.00	0.00	0.00	0.00	0.00	0.00	0.00	0.00	0.00	0.00	0.00	0.00	0.00	0.00	0.00	0.00	0.00

<b>Spirulina <i>vivipara</i></b>	0.00	0.00	0.00	0.00	0.00	0.00	0.00	0.00	0.00	0.00	0.00	0.00	0.00	0.00	0.00	0.00	0.00	0.00	0.00	0.00	0.00
<b>Spirulinid sp.</b>	0.00	0.00	0.00	0.00	0.00	0.00	0.00	0.37	0.00	0.52	0.00	0.00	0.00	0.00	0.00	0.00	0.00	0.00	0.00	0.00	0.00
<b>Textualria sp.</b>	0.00	0.00	0.00	0.00	0.00	0.00	0.00	0.00	0.00	0.00	0.00	0.00	0.00	0.00	0.00	0.00	0.00	0.00	0.00	0.00	0.00
<b>Oridorsalins sp.</b>	0.00	0.00	0.00	0.00	0.00	0.00	0.00	0.00	0.00	0.00	0.00	0.00	0.00	0.00	0.00	0.00	0.00	0.00	0.00	0.00	0.00
<b>Triloculina sp.</b>	0.00	0.00	0.00	0.00	0.00	0.00	0.00	1.49	0.00	0.00	0.00	0.00	0.00	0.00	0.00	0.00	0.00	0.00	0.00	0.00	0.00
<b>Triloculina <i>oblonga</i></b>	0.00	0.00	0.00	0.00	0.00	0.00	0.00	0.00	0.00	0.00	0.00	0.00	0.00	0.00	0.00	0.00	0.00	0.00	0.00	0.00	0.00
<b>Triloculina <i>laevigata</i></b>	0.00	0.00	0.00	0.00	0.00	0.00	0.00	0.00	0.00	0.00	0.00	0.00	0.00	0.00	0.00	0.00	0.00	0.00	0.00	0.00	0.00
<b>Troloculina <i>tricarinata</i></b>	0.00	0.00	0.00	0.00	0.00	0.00	0.00	0.00	0.57	0.00	0.00	0.00	0.00	0.00	0.00	0.00	0.00	0.00	0.00	0.00	0.00
<b>Cyclofoprina</b>	0.00	0.00	0.00	0.00	0.00	0.00	0.00	0.00	0.00	0.00	0.00	0.00	0.00	0.00	0.00	0.00	0.00	0.00	0.00	0.00	0.00
<b>Spiroculina sp.</b>	0.00	0.00	0.00	0.00	0.00	0.00	0.00	0.00	0.00	0.00	0.00	0.00	0.00	0.00	0.00	0.00	0.00	0.00	0.00	0.00	0.00
<b>Milionella <i>grata</i></b>	0.00	0.00	0.00	0.00	0.00	0.00	0.00	0.00	0.00	0.52	0.00	0.00	0.00	0.00	0.00	0.00	0.00	0.00	0.00	0.00	0.00

### MAJOR AND TRACE ELEMENT STUDIES ON CORES

The data included in the previous chapters indicate that the Great Rann was a large marginal marine basin which formed a major depocenter at the western continental margin of India at least since the last ~18 ka. The basin accumulated huge thickness of sediments under shallow marine conditions with moderate to high sedimentation rates. Both the cores, show dominantly fine grained sediments in the central as well as marginal parts of the basin. Detailed geochemical studies on the core samples was carried out to understand the nature of the sediments deposited in the basin. The present chapter includes the details of these studies carried out with a view to reconstruct- the land-marine interaction, palaeoenvironmental conditions and terrestrial input throughout the post-LGM time. The elemental geochemical proxies included are organic C, N, C/N ratio, major and trace elements present in the Dhordo and Berada cores.

#### ELEMENTAL PROXIES

The relative abundance of many major and trace elements and their ratios are identified to vary with the erosional processes, sediment transport, grain size, productivity and bottom water conditions. A brief introduction of the proxies used and their application is as below.

#### **Biogenic proxies ( $C_{Org}$ , $N_{TOTAL}$ , $CaCO_3$ )**

The organic carbon ( $C_{Org}$ ) and total nitrogen ( $N_{TOTAL}$ ) are used as proxies for overhead primary surface productivity in the marine sediments. Primarily  $C_{Org}$  and  $N_{TOTAL}$  are derived from the debris of surface biogenic components undergoes rapid deposition (Muller and Suess 1979). However, an assumption is to be made that there are no other post depositional processes that altered their proportions. The oxic waters on the other hand can alter their proportion that may lead to oxidization of top few cm sediments that interacted with oxic waters. On temporal scale, the change in the overhead surface productivity can be seen as the relative variations concentration of these  $C_{Org}$  and  $N_{TOTAL}$ .

Similarly for the surface primary productivity,  $\text{CaCO}_3$ , Sr and Ba content are used to decipher the relative changes on temporal scales (Reichert 1997). In this case if the carbonates derived from the shallower settings then it may not reflect the true signature of the productivity, instead it may have additional carbonates from the continental input (Sirocko 1993). Therefore, the  $\text{CaCO}_3$  can be used with the other elemental proxies such as Sr and Ba content in the sediments (Dymond et.al. 1992).

### **Land Marine Interaction (C/N Ratio)**

The elemental ratio of Carbon and Nitrogen (C/N) is a primary, fast proxy for the marginal basins like Great Rann of Kachchh. It provides the dominance of the marine Vs terrestrial environment through the temporal scale. C/N ratio is well studied along with the  $\delta^{13}\text{C}$  for tracking the source of organic carbon (Lamb et.al. 2006). The C/N ratio is very useful indicator in deciphering mixing of terrestrial and marine plant input in the salt marshes and estuarine settings (Middleburg et.al. 1997) However, there are intricacies involved if the organic matter decomposes or undergoes oxidization (Mayers 1996). Basically, the freshly deposited organic matter derived from typical marine phytoplanktons ranges between 6-9 whereas the terrestrial plants (vascular plants) derived organic matter shows C/N around 15 or more (Bordowskiy et.al. 1965, Mackenzie 1980). In Arabian Sea the C/N ratio is found to vary between  $8\pm 2$  as documented by Reichart (1997) and Bhushan et.al. (2001).

### **Terrestrial Inputs (Major elements)**

The major elements such as Al, Ca Mg, Fe and K are considered as a terrestrial influx proxy as these elements are typically released during the weathering from rocks. Also, these elements largely remain unaffected by the post depositional oxidation-reduction processes (Agnihotri 2001). Fe takes part on the oxidation-reduction processes but considering its high concentration but its minute proportion may change in the typical marginal settings that cannot change its overall proportion significantly (Agnihotri 2001). Therefore, the downcore records of these elements can be used to as terrestrial input proxies and therefore are also useful to denote the monsoonal pattern. The Al normalized ratios of major elements can also be used in understanding the weathering history of the source rocks such as K/Al, Mg/Al are used to denote the degree of leaching in the hinterland regions (Limmer et.al. 2012).

### **Nutrient proxies (Cu, Ni, Zn, Co, Cd, Pb, Ba, Sr)**

Nutrients are essential components for the productivity in the marine basins. There are two nutrient sources for the productivity changes i.e. increase and/or decrease in overall productivity on temporal scales. i) Through terrestrial inputs via river influx, and ii) By Upwelling of the deposited nutrients. Rivers flowing into the basin carries the important nutrients from the terrestrial realm generated on account of the weathering and erosive processes. Cu, Ni, Zn, Co, Cd, Pb, Ba, and Sr are considered as the nutrients for productivity in the aquatic basins. Ba is powerful indicators of the surface productivity changes as it has one oxidation state. However, it also requires enough pore water sulphate concentration to ensure the absence of reducing conditions (Eagle et.al. 2003). Similarly, in oxic environments Ni, Cu, Zn can be useful for deciphering the nutrient conditions (Tribovillard et. al. 2006). Cd is generally released with the organic matter and therefore may correlate with the total organic carbon in the marine sediments (Piper and Parkins 2004). Other elements like Co, Cd and Sr can also serve as a micronutrient proxy.

### **Palaeo-Redox Proxies**

The trace element distribution is largely controlled by the redox conditions and are reliable proxies for the reconstructing the palaeodepositional conditions. The oxic to anoxic conditions can be deciphered through the relative changes in the Mn concentrations because it gets enriched in oxidizing zone whereas it gets mobilized during the reducing conditions. Contrastingly, Cr found to be depleted in oxic zone and anti-correlated with the Mn proportions (Dean et. al. 1997). Similarly, the ratio of Ni/Co is been used as redox index of which the high values indicates reducing conditions (Dill 1986). Jones and Manning (1997) proposed the ranges for distinguishing oxic to anoxic conditions in several catagories such as-i.e. Ni/Co ratio <5 indicates oxic conditions, 5-7 denotes dysoxic conditions >7 means anoxic conditions.

## **RESULTS AND INTERPRETATION - DHORDO CORE**

### **Major Elements**

The major elements Al, Ca, Fe, Mg, and K show significant variations in the Dhordo core from bottom upwards (Table 8.1). These elements are considered as indicators of detritus input. Amongst these Al, K and Mg are primarily associated with aluminosilicates (Backman et.al. 2006, Lim et.al. 2006).

**Table 8.1** Downcore variations in Major and Trace elements (Al normalized) in Dhordo core.

Sr. No	Depth (m)	Major Elements normalized with Al					Trace elements normalized with Al												
		AL	Ca/Al	Fe/Al	Mg/Al	K/Al	Li/Al	Cr/Al	Mn/Al	Ni/Al	Co/Al	Cu/Al	Zn/Al	Sr/Al	Cd/Al	Ba/Al	Pb/Al	Bi/Al	
1	0.48	4.75	0.93	0.57	0.34	-	-	-	-	-	-	-	-	-	-	-	-	-	
2	1.72	5.53	0.83	0.60	0.33	-	-	-	-	-	-	-	-	-	-	-	-	-	
3	2.94	6.72	0.50	0.77	0.31	-	-	-	-	-	-	-	-	-	-	-	-	-	
4	3.93	6.38	0.62	0.74	0.32	-	-	-	-	-	-	-	-	-	-	-	-	-	
5	4.29	6.03	0.71	0.63	0.35	-	-	-	-	-	-	-	-	-	-	-	-	-	
6	5.02	6.08	0.66	0.67	0.29	-	-	-	-	-	-	-	-	-	-	-	-	-	
7	5.54	6.8	0.61	0.66	0.28	-	-	-	-	-	-	-	-	-	-	-	-	-	
8	7.1	5.86	0.80	0.61	0.30	0.35	8.70	17.26	140.37	9.16	4.34	6.17	20.34	40.59	1.68	63.54	6.37	8.82	
9	11.18	6.01	0.82	0.65	0.28	0.36	8.84	17.67	145.36	9.59	4.39	6.44	20.23	40.74	1.61	63.19	6.08	8.31	
10	14.48	6.2	0.75	0.67	0.29	0.37	9.29	18.18	155.27	10.19	4.50	7.02	20.34	38.57	1.54	60.67	6.25	8.29	
11	16.96	6.43	0.69	0.63	0.28	0.36	8.94	17.58	143.73	9.73	4.30	6.70	19.61	36.95	1.50	60.54	5.94	7.91	
12	18.61	6.68	0.65	0.70	0.28	0.36	8.80	18.80	147.90	10.23	4.18	7.10	22.69	34.31	1.49	63.48	6.53	7.67	
13	20.52	6.34	0.71	0.63	0.27	0.35	9.25	18.74	140.70	10.51	4.30	30.38	39.34	38.05	1.48	60.25	5.79	7.94	
14	21.22	4.42	0.90	0.52	0.24	0.36	8.07	17.90	136.56	8.57	4.81	5.08	22.43	50.92	2.20	74.76	8.85	10.87	
15	23.34	6.53	0.69	0.67	0.28	0.37	9.25	18.28	138.83	10.09	4.37	14.82	25.88	37.81	1.42	57.98	5.15	7.83	
16	25.38	6.19	0.80	0.66	0.28	0.34	8.60	18.58	129.48	10.60	4.33	29.16	36.37	42.06	1.53	56.96	5.77	8.27	
17	26.64	6.27	0.73	0.64	0.27	0.40	10.04	18.42	154.03	10.40	4.59	7.00	21.43	40.47	1.54	62.34	6.23	8.14	
18	28.44	6.47	0.74	0.65	0.27	0.38	9.26	19.70	141.56	10.46	4.40	14.39	27.55	37.83	1.53	63.26	5.80	7.91	
19	29.93	6.58	0.76	0.67	0.28	0.36	8.70	18.04	128.34	10.47	4.24	21.96	30.60	37.70	1.43	57.77	5.32	7.77	
20	31.13	6.86	0.73	0.64	0.29	0.37	9.02	18.25	136.65	9.99	4.22	6.99	20.83	36.38	1.44	62.81	6.29	7.47	
21	34.55	6.74	0.77	0.65	0.28	0.37	9.26	18.19	148.29	10.40	4.36	15.47	26.27	37.29	1.41	58.67	5.47	7.64	
22	36.67	6.22	0.76	0.65	0.27	0.35	8.56	19.06	139.15	10.56	4.38	7.19	23.21	36.03	1.58	65.74	6.73	8.27	
23	39.77	6.18	0.80	0.67	0.28	0.37	9.11	19.47	150.32	11.15	4.54	15.05	27.50	37.29	1.49	63.36	6.37	8.43	
24	42.91	6.22	0.79	0.65	0.26	0.37	8.82	18.65	149.12	10.05	4.45	7.36	21.93	38.04	1.61	69.96	7.28	8.11	
25	44.01	8.98	0.58	0.48	0.21	0.25	6.06	12.14	107.96	6.73	3.10	4.86	14.85	26.17	1.08	44.97	4.40	5.67	
26	46.15	6.18	0.79	0.64	0.26	0.34	8.49	17.02	143.13	9.76	4.37	6.74	19.92	36.39	1.60	60.53	6.50	8.17	
27	48.22	6.51	0.79	0.68	0.26	0.35	8.49	16.11	140.69	9.21	4.28	6.52	18.84	35.28	1.41	60.90	5.44	7.80	
28	51.57	6.47	0.79	0.63	0.28	0.36	8.67	17.60	146.22	9.63	4.31	6.90	20.32	36.99	1.51	65.07	6.31	7.84	
29	54.5	6.5	0.79	0.63	0.27	0.36	8.45	16.88	137.24	9.51	4.21	6.94	19.29	37.30	1.52	65.16	6.33	7.87	
30	58.45	6.25	0.82	0.66	0.28	0.35	8.67	17.96	141.04	10.12	4.33	20.62	30.28	36.90	1.51	61.46	5.38	8.17	

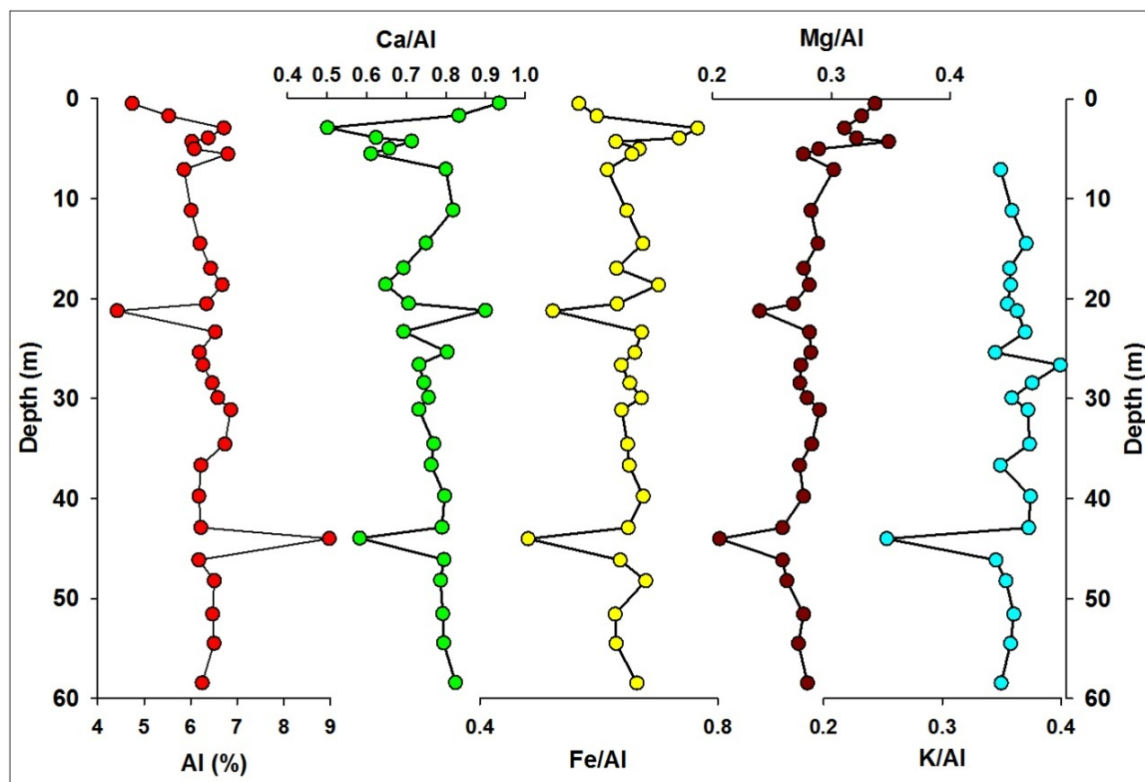


**Figure 8.1** Down core variations in Al and other 'Al normalized' major elements from Dhordo core.

In Dhordo core Al is correlated with the Fe (0.74), K (0.58), Mg (0.56) whereas poor correlation of Al with Ca is seen (0.31). Similarly, positive correlation of Mg/Al versus K/Al (0.65) and Fe/Al versus K/Al (0.64) is observed (Table 8.1; Fig. 8.1). Based on distribution of major elements, the Dhordo core is divisible into three zones indicating the change in environment and nature of detrital flux into the central rann basin.

#### ***Zone-I (~60m to ~21m)***

This bottommost zone of the Dhordo core is further divisible into two subzones i.e. Lower subzone- ~60 - 45m depth and Upper subzone 45-21m depth (Fig. 8.1).

Lower Subzone (60 - 45m depth) - Al remains more or less stable during this phase (except at ~45m depth) whereas the Fe/Al and K/Al ratio shows small changes in this bottom most part of this zone. The relatively increased Fe/Al ratio the uppermost part is noted. Overall stability in the major elements is abruptly interrupted at ~45m that is reflected in almost all other elements. The strong positive peak observed in Al whereas, at the same horizon rest of the ratio proxies show negative shift. Also, Ca/Al, Fe/Al, Mg/Al and K/Al shows slightly higher values than the average of their entire core records (Fig.

8.1; Table 8.1). However more or less stable ratios indicate that there are no significant changes (large scale increase or decrease in terrestrial flux) during ~17.7 to ~16.3ka.

Upper Subzone (~45 to ~22m) - In this zone the Al remains stable in the lower portion that increases slightly towards the upper half of the zone. Ca/Al and Fe/Al shows inverse relation from bottom to top in this zone, whereas Mg/Al remains stable and does not vary much (Fig. 8.1). K/Al shows significant positive shift compared to Zone-I. Mg/Al on the other hand remains stable and do not vary much. In this subzone, the K/Al indicates significant increase in the terrestrial influx from the hinterland source (Fig. 8.1; Table 8.1). Radiometrically, this zone encompasses a large span from terminal Pleistocene-Early Holocene -Mid Holocene times. The K/Al and Mg/Al ratios are in conformity with the clay mineralogical studies suggesting the strengthening monsoonal conditions during deposition of these sediments (described in earlier chapter). These results are also in conformity with earlier studies from the continental archives of NW India and Arabian Sea (Enzel et.al. 1999, Thamban et.al. 2002).

#### ***Zone-II (~22 - 8m depth)***

This zone is characterized by significant increase in Ca/Al, minor increase in Mg/Al and slight negative slope of Fe/Al and Al content in the bulk sediment sample. The K/Al ratio on the other hand varies with negative sloping upwards. The significant increases in the Ca/Al ratio values are inverse with the Fe/Al values is noted, whereas, negative slope of K/Al ratio values upward in this zone (Fig. 8.1). Therefore, the elemental ratios in this zone suggests relatively reduced terrestrial input to the basin since post 6.9ka years before present. The clay mineralogical evidence by physical Vs chemical weathering proxies (S+K/I+C) also suggests reduced physical weathering conditions in the hinterland regions. The reason for the abruptly increased Ca/Al ratio values may be on account of the increased biological productivity.

#### ***Zone-III (~8-0 m depth)***

The uppermost zone of Dhordo core shows most fluctuating changes in all the elements and Al normalized ratios. Largest positive shifts in Al, Fe/Al, Mg/Al are noted whereas the Ca/Al shows the inverse relation by reducing (Fig. 8.1; Table 8.1). Topmost samples again vary in opposite direction in all ratios. The environmental processes are significant here in this zone as they represent the shallowing and drying phase of the

basin. The increased Fe/Al and Mg/Al in large proportions essentially points towards the enrichment of these elements in the form of detritus may be due to the fresh water influx. Sedimentologically, the upper part of the Dhordo core is characterized by the fine grained sediments that are dominated by the mica minerals. The abundance of the micaceous minerals may leach the Mg, Fe, Al in large quantities that may have yielded high values in these elements. The mica accumulation increased during the deposition of these sediments may on account of the filled up basin. The resulting reduced low energy conditions and sheltered zone of rann basin would have accumulated the micas through suspension. The reduced Ca/Al varies in contrasting manner as compared with the other elemental ratios. This may be due to the relatively much higher micas as compared with the other minerals in this zone that does not contain Ca in large proportions.

#### **C/N Ratios (Land-Marine Interaction)**

This ratio reflects the ratio of aquatic organic matter compared to the terrestrial organic matter (Meyers and Lallier-Vergas 1999). The typical marine organic matter shows the C/N ratio values between 5-6 while it gets increased as the fresh water influx (terrestrial sourced organic matter carried by rivers) and reaches 15 and more for the typical terrestrial vascular plants (Borbowskiy 1965, Hedges et.al. 1986). In Dhordo core C/N ratio fluctuates from 4 to 78 indicating the typical marine to terrestrial origin of the organic matter in the sediments. The minimum value occurs in the topmost portion 4.4 at ~ 2.4m below rann surface whereas, the highest values occurs ~20.70 to 21.80m downcore showing wide variation (Table 8.2; Fig. 8.2).

**Table 8.2** Downcore variations in CaCO<sub>3</sub> &, N%, C% and C/N ratio in Dhordo core.

Sr. No.	Sample ID	Depth (m)	CaCO <sub>3</sub> %	N%	C%	C/N
1	DH-1-8	0.16	11.31	0.02	0.15	7.25
2	DH-1-24	0.48	9.76	0.01	0.13	20.45
3	DH-1-37	0.74	12.16	0.01	0.08	5.84
4	DH-2-20	1.40	11.82	0.02	0.12	5.67
5	DH-2-36	1.72	10.43	0.01	0.20	13.91
6	DH-3-10	2.40	9.88	0.05	0.20	4.38
7	DH-3-37	2.94	8.59	0.03	0.35	11.51
8	DH-3-50	3.20	10.48	0.06	0.32	5.21
9	DH-4-26	3.93	9.09	0.03	0.25	8.57
10	DH-4-44	4.29	9.96	0.03	0.26	9.68
11	DH-5-22	5.02	6.24	0.03	0.35	12.19
12	DH-5-48	5.54	8.93	0.03	0.34	10.92

13	DH-5-81	6.20	13.00	0.02	0.15	8.25
14	DH-6-35	7.10	11.04	0.02	0.34	14.39
15	DH-6-85	8.10	12.96	0.04	0.37	10.60
16	DH-6-135	9.10	12.51	0.03	0.30	11.16
17	DH-7-18	10.30	13.20	0.03	0.30	9.23
18	DH-7-62	11.18	11.59	0.03	0.35	12.40
19	DH-7-78	11.50	13.28	0.04	0.37	8.17
20	DH-7-110	12.14	13.24	0.04	0.31	8.38
21	DH-8-13	13.50	13.15	0.03	0.30	9.46
22	DH-8-62	14.48	11.64	0.03	0.43	14.88
23	DH-8-103	15.30	13.42	0.03	0.40	13.79
24	DH-9-38	16.96	11.00	0.03	0.48	16.10
25	DH-9-60	17.40	13.37	0.02	0.22	10.16
26	DH-10-21	18.61	10.75	0.03	0.42	13.89
27	DH-10-60	19.39	12.64	0.02	0.21	9.51
28	DH-11-15	20.52	10.25	0.02	0.34	15.04
29	DH-11-24	20.70	11.54	0.01	0.12	15.63
30	DH-11-29	20.80	10.81	0.00	0.06	21.23
31	DH-11-39	21.00	8.60	0.00	0.17	
32	DH-11.48	21.18	10.33	0.01	0.07	12.40
33	DH-11.79	21.80	10.65	0.01	0.59	
34	DH-12-12	22.90	12.53	0.03	0.36	10.25
35	DH-12-64	23.94	10.80	0.03	0.48	18.82
36	DH-13-24	25.38	11.58	0.03	0.45	14.47
37	DH-14-29	26.64	11.09	0.03	0.42	14.23
38	DH-14-119	28.44	12.19	0.03	0.50	16.80
39	DH-15-29	29.93	12.23	0.03	0.45	15.68
40	DH-15-89	31.13	10.74	0.03	0.45	14.38
41	DH-16-42	33.21	13.91	0.03	0.28	9.26
42	DH-16-103	34.43	13.96	0.03	0.32	10.59
43	DH-16-109	34.55	13.00	0.03	0.45	15.68
44	DH-17-72	36.67	12.76	0.03	0.54	19.70
45	DH-17-113	37.49	14.25	0.03	0.31	10.09
46	DH-18-79	39.77	10.92	0.03	0.55	21.46
47	DH-18-120	40.59	13.87	0.03	0.32	11.79
48	DH-19-74	42.91	12.08	0.02	0.39	18.67
49	DH-19-103	43.49	13.86	0.03	0.29	11.30
50	DH-19-129	44.01	11.20	0.04	0.45	11.50
51	DH-20-79	46.15	12.09	0.02	0.36	16.06
52	DH-20-112	46.81	13.99	0.03	0.35	11.80
53	DH-20-136	47.29	14.63	0.03	0.33	11.32
54	DH-21-29	48.22	11.94	0.03	0.87	34.55
55	DH-21-48	48.60	13.57	0.04	0.40	9.10
56	DH-21-78	49.20	14.01	0.04	0.39	8.98
57	DH-22-49	51.57	9.61	0.02	0.45	18.15
58	DH-23-39	54.50	12.80	0.02	0.37	15.32
59	DH-23-74	55.20	14.67	0.04	0.36	9.04
60	DH-23-144	56.60	14.56	0.04	0.38	9.27
61	DH-24-51	58.45	13.05	0.02	0.35	15.91

### Zone-I (60 - 21m)

The lowermost part (60 to ~ 21 m) shows that the values are in between the typical marine to the continental C/N values i.e. 9-34 (Fig. 8.2; Table 8.2). The lower portion (60-50m) of this zone shows fluctuations between 9 - 15 indicating the marine and terrestrial spells. Similarly at ~48m depth large peak in C/N ratio jumps to 35 that is also seen in the abruptly increased organic carbon content indicating the terrestrial flux. The age of these sediments is between 17.7-16.5ka. From 48 to 33m depths, the C-N ratio fluctuates widely between the 10 -20 that may indicate the regular intervals of terrestrial punctuations during the deposition of these sediments (Mayers 1994). The increased terrestrial organic matter is correlated with the major element data and clay mineralogical studies suggesting the developing monsoonal conditions after the terminal monsoonal conditions towards the Mid-Holocene times. The topmost part of this zone at ~23-21m is consistently yields the high C/N ratio values including the highest C/N values throughout the core i.e. 78 (Fig. 8.2). The  $^{14}\text{C}$  radiocarbon dating gives ~6.9ka ~25m indicating the high terrestrial flux into the rann basin during Mid-Holocene times. The increased grain size in this zone testifies to the above interpretation of increased flux into the basin.

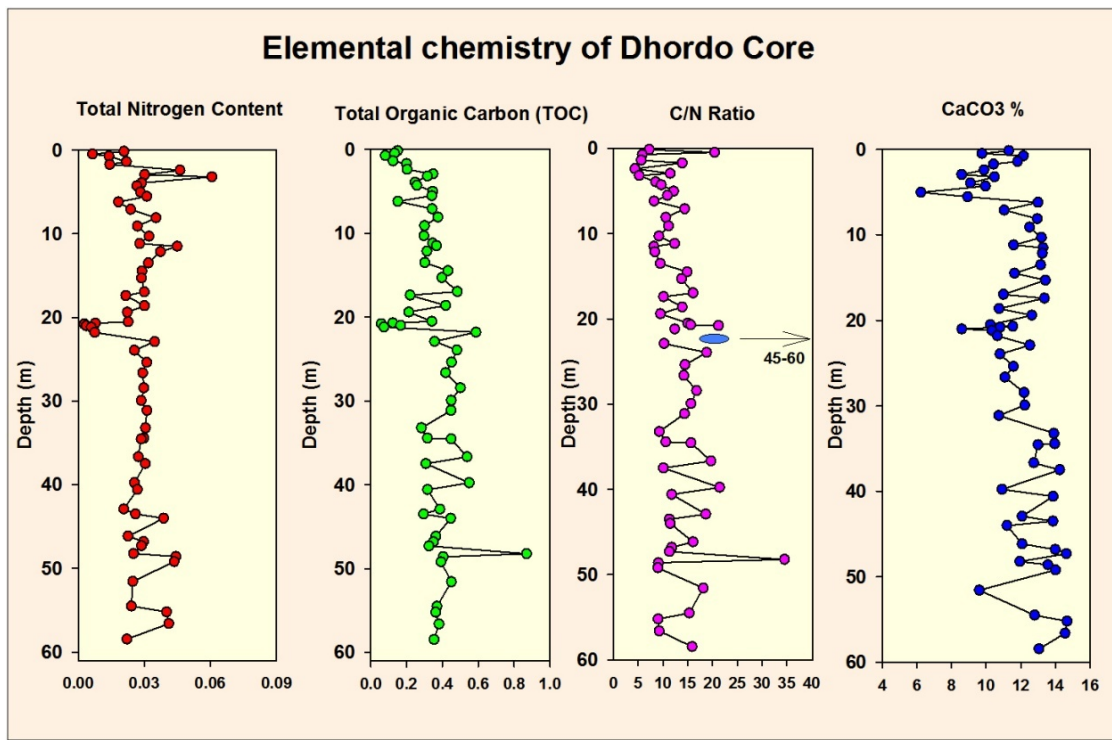


**Figure 8.2** Downcore variations in N, C, C/N ratio and CaCO<sub>3</sub> content in Dhordo core.

### ***Zone-II (20 - 8m depth)***

In this middle zone C/N ratio decreases from the bottom to top from 21-9 (Fig. 8.2). The bottom part contains mixed marine values around 10-12 with few intervals of increased terrestrial flux whereas in upper part C/N values gets reduced indicating the environmental shift towards the marine dominant settings or reduced terrestrial influx into the rann. Interestingly, the clay mineral ratio proxies, elemental data and Sr-Nd isotopic studies also suggest the decreased terrestrial inputs during this time. The Sr-Nd isotopic studies revealed the gradual decline of the major river system post 6.9ka that was contributing sediments to the rann basin. These changes are more likely to have occurred due to the climatic aridity event during the post Mid-Holocene times as shown by the earlier studies (Enzel et.al. 1999, Prasad et.al. 2006, Thamban et.al. 2002, von Rad et.al. 1999) and same is evident on broad scales in present dataset.

### ***Zone-III (8 - 0m depth)***

The topmost zone is characterized by the lowermost C/N ratio throughout the core record around 4 at 2.4m and rest of the values occasionally exceeds 9 indicating the dominantly marine derived organic matter in the topmost zone (Fig. 8.2). Though there are two intervals where it shows terrestrial values that can be due to the increased input of land derived materials. This zone also witnessed the regression of the marine water column during the recent past that may leading the mixture of land derived particles.

### **C/N ratio and CaCO<sub>3</sub>**

The average value of organic carbon in Dhordo core is ~0.3 % (range 0.06-0.8%). Organic carbon remains more or less stable from the 60 - 21m and fluctuates within a narrow range. Above 21m it decreases upwards with overall negative slope towards top of the core. The top ~8m of the core section shows a relatively rapid decrease in the organic carbon content. The maxima occurs at the ~48m and minimum values are near ~21m depth (Fig. 8.2; Table 8.2). These high values are associated with the increased C/N ratio values indicating the increased terrestrial flux of organic matter during the deposition of these sediments. The increased grain size during these intervals is in conformity with the interpretations. The CaCO<sub>3</sub> concentrations range between 6.2 to 14.7 weight percent in the sediments. At bottom of the core, it shows high values that steeply decrease from ~55 to 50m above which it fluctuates in wide range between 50-30m. From 30 to 8m depth

CaCO<sub>3</sub> remains relatively high with restricted narrow range fluctuations. The lower values peaks are generally associated with the high C/N ratio at ~50 and ~20m depths however the minimum values at ~6m is associated with highest peak of total nitrogen content (Fig. 8.2). The C/N values at this level show the typical marine value. The total organic carbon and CaCO<sub>3</sub> values do not show any significant correlation (0.08). The comparison of CaCO<sub>3</sub>, organic carbon weight percentage and C/N ratio values in Dhordo core indicates that change terrestrial influx after terminal Pleistocene (~16ka) to Early Holocene times (50-30m) is associated with the decrease in CaCO<sub>3</sub> content with negative correlation (-0.56). This relation suggests the decrease productivity during the increased fresh water flux into the basin and vice versa. Similarly, the strong negative correlation between the C/N ratio and organic carbon weight percentage is observed in between 20-8m depth and weak correlations (0.34) is noted in 0- 8 meter depths.

### **Trace Elements**

The major and trace elements serves as indicators of the palaeoenvironmental processes such as land-marine interactions, nutrient and productivity conditions, oxidizing-reducing conditions during the deposition of these sediments. Based on the present dataset the studied Dhordo core shows changes in palaeoenvironmental conditions as described below.

#### ***Palaeo-redox conditions***

The Cu, Mn, Co and Ni concentrations in marine sediments reflect the redox conditions of bottom waters (Broecker and Peng 1982, Calvert and Pedersen 1993, Dean et.al. 1994). The downcore variations of Cu, Mn, Co and Ni in the Dhordo core vary from 12.14-19.70, 107-96-155.27, 6.73-11.15 and 4.86-30.38 respectively. The Cr-Ni and Cr-Mn shows high correlation coefficients (0.90, 0.67) in throughout the core, however, Cr-Cu shows relatively poor correlation (0.36). Cr/Al, Co/Al ratio remains in a narrow range whereas minor variations seen in Mn/Al and Ni/Al show minor positive shift after ~45m depth (Fig. 8.3; Table 8.1). Cu/Al also remains in narrow range except 40-20m depth where it varies significantly as also seen in Mn/Al. The overall restricted range of the redox proxies elemental concentrations indicates the more or less stable oxic conditions (Tribovillard et.al. 2006; Calvert and Pedersen 1993). The Ni/Co ratio values are fluctuating from 1.78 to 2.47 in the core record. Below 5 Ni/Co ratio also indicates the

prevailing oxic conditions prevailing during the deposition of these sediments (Jones and Manning 1997). These results are in conformity with the shallow marine settings of the Great Rann of Kachchh basin.

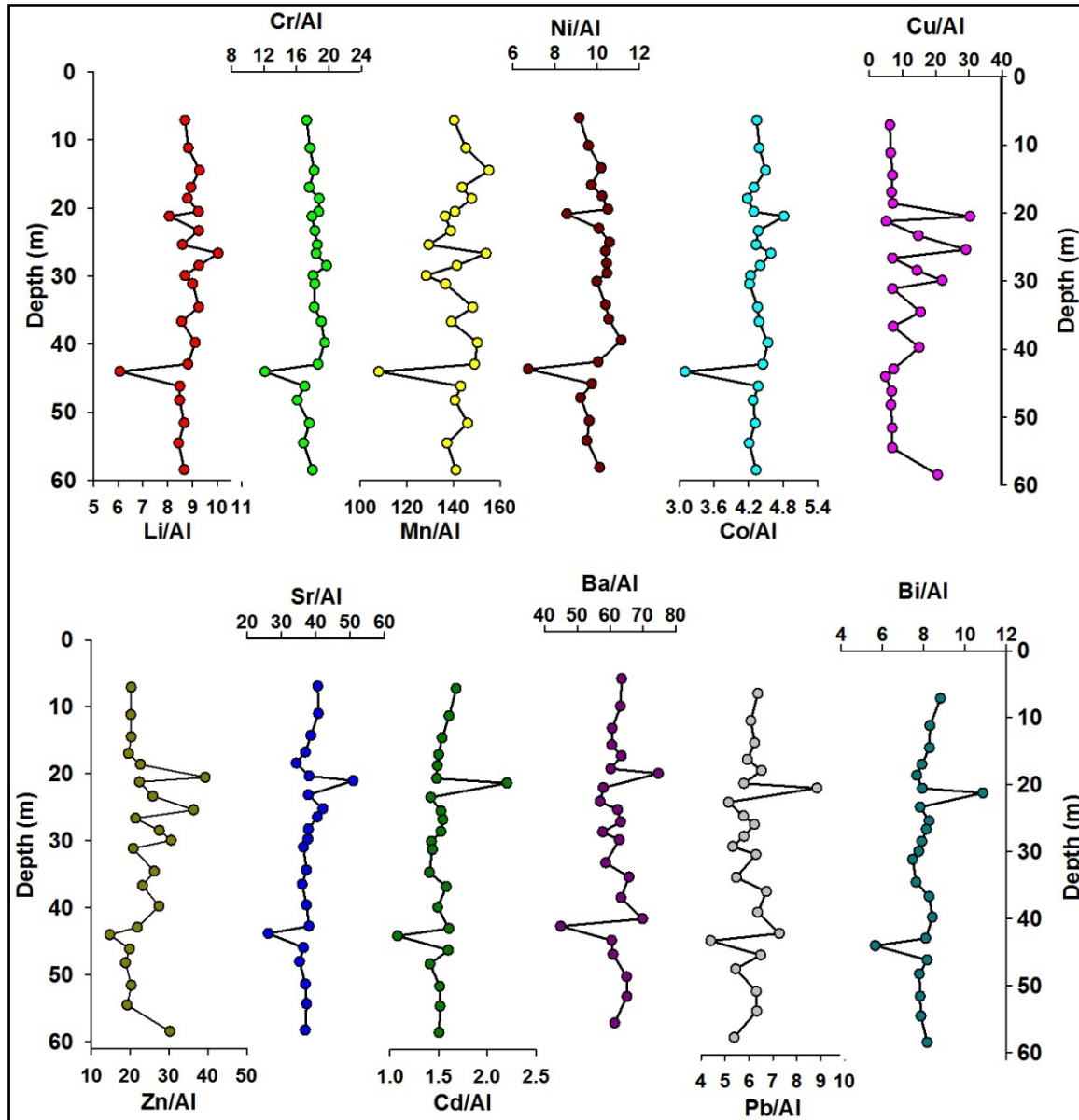


**Figure 8.3** Trace element distribution (in ppm) in Dhordo core.

### *Nutrient Conditions*

The nutrient conditions can be reconstructed using Cu, Zn, Cd, Co, Pb and Ba elements that are normalized with the aluminum concentration in the sediments. The down core variations in concentration of these elements provide the relative changes in the nutrient conditions from the nutrient-rich to nutrient-depleted conditions.

Zone-I (60-21m depth)- Lower Subzone (60-45m depth)- The trace element composition in this zone yields the most stable and restricted values in Cr/Al, Ni/Al, Co/Al, Cu/Al, Sr/Al, Cd/Al and Bi/Al indicating no significant change during the deposition of these sediments whereas few ratios such as Mn/Al, Pb/Al and Zn/Al and Ba/Al shows very minor variations in this zone (Fig. 8.3). It is important to note here that the terrestrial flux during this time frame remained unchanged during the deposition of this zone.

As mentioned above, that there are two sources for the nutrient supply into the basin i) riverine input and ii) upwelling (redistribution of the older nutrients). Therefore, it becomes important to note the terrestrial input signals during this time which would suggest the similar results what yielded here in this zone. The factor behind the minor variations in the Pb, Zn and Ba may be due to Mn-Fe cycling that can significantly alter the trace metal composition. The Mn-Fe cycling due to redox reactions can primarily influence Zn, Pb (as <sup>+2</sup> cations) (Tribovillard et.al. 2006). Upper Subzone-Zone-II (~45-20m depth)- This zone is characterized by the large scale fluctuations in Ni/Al, Cu/Al, Zn/Al, Pb/Al, Bi/Al and partly in Mn/Al, Ba/Al, the trace element ratios whereas Cr/Al, Co/Al, Sr/Al, Cd/Al does not vary and remains stable (Fig. 8.3; Table 8.1). The large scale fluctuations in many ratios indicates the spells/cycles of increased and decreased nutrients during this time. The correlatability of these results not only with the major elements in this zone but also for the clay mineral variations strongly suggests the pattern of nutrient variance during the Early to Mid Holocene times. This period was marked by the developing to strong monsoonal conditions that is deciphered by the clay mineral humidity proxies (Ill/Ch; K/Ch) that also confirmed by the terrestrial input proxies i.e. major element distributions in this zone.

Zone-II (20-8m depth) - This zone shows mostly restricted values except the Mn/Al that is showing increase to decrease in values. Sr/Al reduces slightly at ~21m depth then upward it shows slight positive slope. Cd/Al, Ba/Al, Pb/Al and Bi/Al also shows slight positive slope whereas Ni/Al goes in contrast (Fig. 8.3; Table 8.1). Such a minor change in many proxies may be insignificant. However, the other proxy records suggests the monsoonal weakening (clay mineralogy results) that restricted the riverine input to the basin (Sr-Nd Isotopic results) during the deposition of these sediments. The Zone-III (8-2m depth) is not included in this section due to the technical error.

## **RESULTS AND INTERPRETATION - BERADA CORE**

### **Major Elements**

Al and other major elements (Al normalized) vary considerably through the down core records (Table 8.3). Based on the variations the core is divided into four zones.

#### ***Zone-I (50-39 m depth)***

The lowermost zone of the Berada core comprises of significant lithological variations. The bottom most samples are from the compacted ferruginous sandstone that is intercalated by fluvial river sandy horizon (47-43m depth) showing brownish yellow to brownish red colour. The fluvial nature of the sand is clearly evident from the sedimentological studies. This zone extends up to ~39 m depth and is characterized by the highest Al content. The Ca/Al and K/Al varies in their extremes in entire core.

#### ***Zone-II (39-25 m depth)***

The bottom of this zone marks the beginning of marine sedimentation in the marginal part basin at ~9.3 ka B.P. This zone is characterized by the high values of Al and positive slopes of Fe/Al, Mg/Al and K/Al (Fig. 8.4; Table 8.3). Increase in these elements provides strong evidence for high terrestrial input into the basin. Ca/Al of the other hand shows antithetic relationship with the other element ratios marking the reduced Ca flux during the increased detrital flux. This zone represents the Early Holocene times (9.5-8.4ka BP). The clay mineral records in conformity with the above interpretation that also suggest the intensification of monsoonal conditions.

#### ***Zone-III (25-8 m depth)***

This zone again shows positive slope in the Al content in the sediments whereas the Ca/Al proportion remains almost restricted in a narrow range with minor positive slope. Fe/Al, K/Al on the other hand show large scale variations with overall negative shift near 20m and positive shift above 20m depth. The concomitant lower values of Ca/Al during the high detrital input are characteristically noted in Berada core. The top section of this zone denotes the lowering of these elemental ratios.

**Table 8.3** Downcore variations in Major and Trace elements (Al normalized) in Berada core.

Sr. No.	Depth (m)	Major Elements normalized with Al					Trace elements normalized with Al											
		AL	Ca/Al	Fe/Al	Mg/Al	K/Al	Li/Al	Cr/Al	Mn/Al	Ni/Al	Co/Al	Cu/Al	Zn/Al	Sr/Al	Cd/Al	Ba/Al	Pb/Al	Bi/Al
1	0.38	6.35	0.88	0.69	0.29	0.34	8.33	15.37	132.37	8.88	4.16	5.83	17.01	36.26	1.42	55.29	4.73	8.26
2	3.21	5.41	0.87	0.62	0.26	0.32	7.42	18.01	134.52	8.67	4.27	5.57	22.74	44.11	1.83	74.16	7.52	9.09
3	3.98	7.03	0.70	0.67	0.33	0.35	9.06	15.61	144.89	8.95	4.00	8.67	16.89	33.87	1.31	51.64	5.95	8.12
4	5.32	6.83	0.66	0.67	0.37	0.35	8.82	16.76	146.88	9.38	4.12	5.86	20.39	33.55	1.45	60.54	6.62	7.69
5	6.47	6.35	0.72	0.69	0.32	0.35	8.22	15.87	136.04	8.69	4.08	5.31	17.75	32.90	1.41	76.08	4.57	7.98
6	8.63	6.56	0.57	0.76	0.30	0.34	8.53	15.49	114.20	8.97	4.15	5.60	16.22	31.61	1.37	53.13	4.62	7.80
7	10.81	6.67	0.64	0.60	0.27	0.34	8.49	14.79	108.57	8.43	3.91	5.00	17.16	31.87	1.35	54.25	4.73	7.72
8	14.50	6.83	0.59	0.67	0.30	0.35	8.63	15.16	131.64	8.80	3.99	5.30	16.20	31.95	1.33	53.60	4.48	7.54
9	15.98	6.89	0.60	0.68	0.30	0.39	9.58	17.12	136.83	9.63	4.29	6.11	18.09	35.40	1.31	57.05	4.71	7.69
10	17.58	6.74	0.61	0.73	0.30	0.36	8.75	15.86	122.67	9.11	4.09	5.75	20.08	32.19	1.34	53.66	4.63	7.72
11	19.38	6.80	0.81	0.64	0.29	0.33	8.17	14.74	135.21	8.50	3.84	5.24	15.78	35.38	1.33	53.38	4.87	7.56
12	20.78	6.62	0.76	0.71	0.30	0.33	8.32	14.37	140.60	8.51	3.89	5.64	16.30	34.71	1.36	52.77	4.53	7.77
13	22.57	6.59	0.76	0.58	0.28	0.33	8.13	14.55	125.96	7.82	3.65	4.63	16.41	34.39	1.37	88.11	4.68	7.73
14	24.57	6.13	0.79	0.69	0.30	0.36	8.87	16.43	136.65	8.91	4.28	5.93	17.58	37.73	1.46	59.24	5.01	8.48
15	26.88	6.50	0.70	0.67	0.26	0.33	8.04	16.44	126.13	8.90	4.00	6.97	20.57	32.84	1.52	64.02	6.61	7.80
16	29.16	6.80	0.63	0.66	0.25	0.35	8.66	15.46	119.59	9.05	4.01	6.07	16.72	31.05	1.33	52.72	5.27	7.61
17	31.46	6.68	0.72	0.67	0.29	0.32	8.08	15.06	122.87	8.46	3.93	5.25	16.77	34.91	1.35	53.24	6.00	7.66
18	32.86	6.73	0.80	0.69	0.28	0.34	8.51	15.62	138.20	8.93	4.05	6.13	16.55	36.31	1.34	53.85	4.82	7.79
19	32.96	6.84	0.78	0.71	0.27	0.33	8.27	14.96	144.35	8.85	4.03	5.58	16.84	36.09	1.32	53.14	4.86	7.60
20	35.16	6.59	0.93	0.76	0.32	0.32	8.04	14.66	131.30	8.89	4.08	5.55	17.61	41.01	1.37	54.37	4.64	7.81
21	36.38	6.21	0.88	0.63	0.28	0.33	8.20	15.09	132.02	8.58	4.02	5.41	16.90	39.31	1.45	60.40	4.85	8.22
22	37.38	6.58	0.90	0.68	0.29	0.32	7.99	14.60	133.17	8.85	4.22	5.67	16.08	39.27	1.37	56.47	4.64	7.78
23	42.92	7.75	0.33	0.62	0.23	0.43	10.11	14.64	68.18	8.80	3.99	6.34	16.66	25.89	1.16	66.18	4.64	6.74
24	43.66	5.88	1.94	0.62	0.22	0.31	7.99	13.91	93.25	8.52	3.94	6.25	15.99	48.05	1.53	62.22	4.45	8.70
25	47.18	7.46	0.42	0.64	0.19	0.32	9.44	18.37	52.14	9.28	3.75	6.74	16.00	31.38	1.20	49.65	4.15	7.12

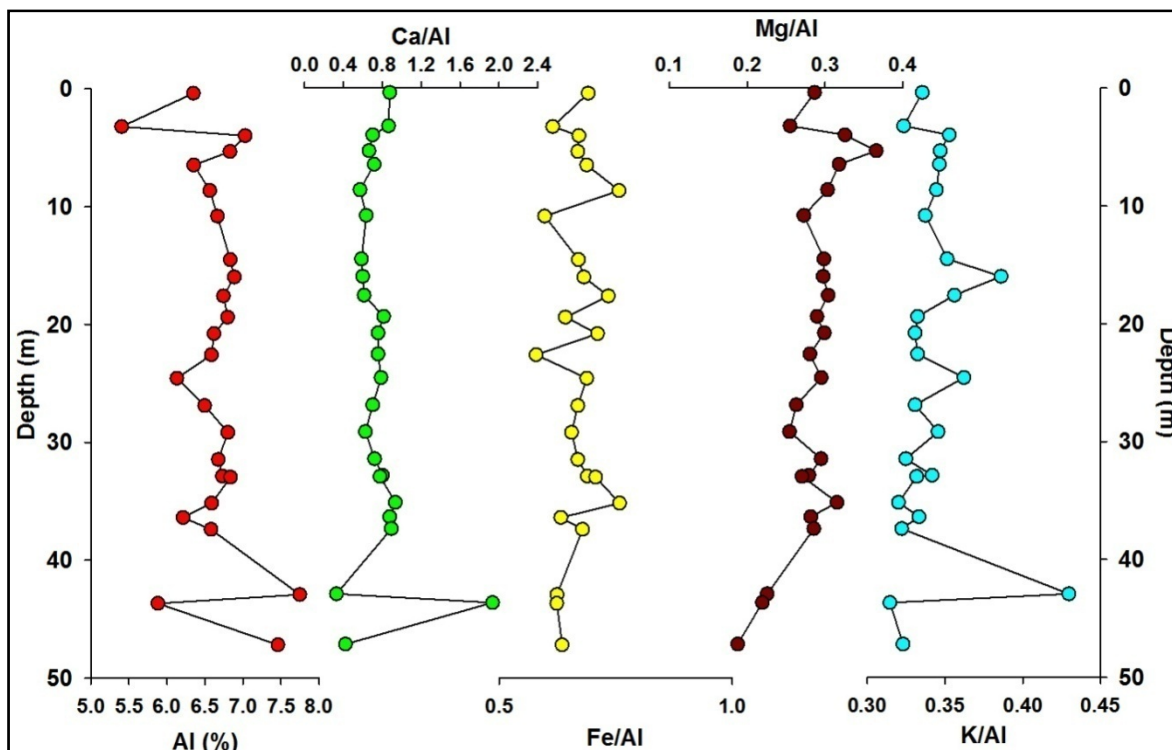


**Figure 8.4** Down core variations in the major elements (Al normalized) in Bearada core.

#### ***Zone-IV (8-0 m depth)***

The topmost zone of the Berada core shows considerable variations in the elemental composition in Al, Ca, Mg, Fe and K. This part marks the marine regressive phases during the recent times. The bottom upward variations in Al, Fe/Al, Mg/Al and K/Al show correlatable changes in the form of high values in the bottom samples whereas the in the top samples the concentrations of these elements is found to be relatively depleted. Ca/Al on the other hand shows the minute positive slope within a restricted narrow. The detrital input and associated processes is difficult to assess at the top part of the core.

#### **C/N ratios (Land-Marine interaction)**

The C/N ratios show large variations in the Berada core (Table 8.4).

**Table 8.4** Downcore variations in CaCO<sub>3</sub>%, N%, C% and C/N ratio in Berada core

Sr. No.	Depth (m)	CaCO <sub>3</sub> %	N	C	C/N
1	0.38	14.33	0.02	0.53	28.41
2	0.6	14.74	0.03	0.19	5.64
3	1.29	10.66	0.02	0.24	12.18
4	1.69	11.23	0.02	0.18	10.79

5	2.51	11.06	0.02	0.26	14.94
6	3.21	11.01	0.01	0.08	10.95
7	3.98	26.53	0.02	0.24	13.07
8	4.4	13.12	0.04	0.23	5.66
9	5.32	12.16	0.02	0.17	8.68
10	5.8	12.34	0.04	0.25	6.80
11	6.47	10.86	0.08	0.25	3.12
12	7.19	9.74	0.05	0.52	10.71
13	8.63	9.89	0.07	0.69	10.19
14	9.39	10.88	0.05	0.62	12.67
15	10.19	10.55	0.05	0.67	12.34
16	10.81	11.77	0.03	0.48	14.59
17	11.39	11.27	0.05	0.59	11.83
18	12.6	11.55	0.06	0.70	12.47
19	13.2	11.32	0.06	0.68	11.63
20	14.4	11.90	0.06	0.70	12.60
21	14.5	11.95	0.03	0.44	16.29
22	15.98	10.45	0.04	0.64	14.63
23	16.4	12.54	0.06	0.74	12.22
24	17.58	12.36	0.04	0.71	15.89
25	18.1	11.51	0.06	0.74	11.86
26	18.7	15.03	0.06	0.81	13.30
27	19.38	15.67	0.03	0.35	10.03
28	20.78	14.33	0.04	0.32	9.21
29	22.57	14.97	0.03	0.32	11.41
30	22.99	13.03	0.04	0.38	9.22
31	23.49	11.85	0.05	0.65	13.80
32	24.57	12.94	0.04	0.72	18.48
33	24.99	12.68	0.05	0.62	13.22
34	25.8	10.72	0.04	0.54	14.21
35	26.88	9.66	0.28	1.69	6.08
36	27.3	7.10	0.04	0.82	19.24
37	27.7	8.19	0.07	1.40	19.90
38	28.4	10.40	0.07	1.15	17.45
39	29.16	13.56	0.05	1.16	21.83
40	30.6	12.63	0.07	1.16	16.69
41	31.46	11.78	0.04	0.66	16.51
42	32.1	13.19	0.07	0.97	14.38
43	32.96	17.60	0.04	0.44	11.49
44	35.16	15.01	0.03	0.38	12.25
45	36.38	16.15	0.02	0.29	11.78
46	36.9	16.11	0.05	0.39	8.12
47	37.38	20.09	0.03	0.37	12.25
48	38.76	14.05	0.18	3.58	20.16
49	39	6.44	0.09	1.78	19.93
50	45.98	32.02	0.02	0.16	6.42
51	46.72	7.30	0.04	0.23	5.54
52	47.18		0.0321	0.2013	6.2693

The Berada core is divisible into four zones based on the variations in C/N ratios.

***Zone-I (50 - 39m depth)***

As described earlier the bottom (47 - 38m depth) most part of the core comprises of a fluvio-marine intercalated sediments that yield typical marine values (C/N ratio ~5) at bottom most part which is disrupted by the terrestrial fluvial influence zone yielding C/N values of ~35.

***Zone-II (39 - 25m depth)***

Above ~39m the C/N ratio again corresponds to the marine influenced settings as indicated by the C/N ratio values below 10. These sediments were deposited during the Early Holocene times (~9.5ka B.P.). During Early Holocene times the dominant marine conditions show shift towards the terrestrial values that can be seen through positively sloping C/N ratio values till ~28m depth. The monsoon strengthening is observed during the Early Holocene times as described earlier. Therefore, high fresh water runoff into the marginal rann may be the cause for such increased C/N values. In 28 - 25m depth interval, the C/N ratios abruptly decreases ~5 indicating shift towards the marine realm.

***Zone-III (25 - 8m depth)***

In this zone the C/N ratio values ranges from 10-15 with largely fluctuating conditions. The typical C/N values in marine realm ranges from 7-10 and in Arabian Sea it genererally varies from 7-11 (Agnihotri 2001). The occurrence of the C/N values in range of 10-15 with consistent fluctuations suggests the mixed-marine conditions during this time. This zone passes through Mid-Holocene times as described above.

***Zone-IV (8 - 0m depth)***

This zone starts with the typical marine C/N ratio ~5 that occurs abruptly after the mixed marine environment. These low marine values continue to occur upto ~4.4m depth indicates typical marine influenced settings (Bordovsky, 1965; Lamb et.al. 2006). The top portion of Berada core is characterized by fluctuating values between 10-15, except at 0.6 m which shows ~6 C/N ratio and topmost sample at 0.38m depth where the highest C/N ratio ~29 is recorded.

**C/N ratio and CaCO<sub>3</sub>**

In Berada core, the C/N ratio and CaCo3 are inversely correlated with each other between 38-30 m. The correlation between C/N and CaCO3 is observed to decrease from

the bottom to top of the core. In lower portion between (38 - 28m depth) it shows the strong negative correlation (-0.61). Similarly for the upper intervals (28 - 21m depth) -0.5 and (21 - 10m depth) -0.38 and (10 - 0m depth) it shows -0.16 (weakly correlated). The overall downcore record on the other hand shows very weak correlation between C/N and CaCO<sub>3</sub>. The inverse relation between these two proxies indicates the terrestrial input in the basin. Therefore looking at the CaCO<sub>3</sub> profile on broad scale the enriched CaCO<sub>3</sub> content is observed to correspond to the strong monsoonal spells during Early to Mid-Holocene times. The post Mid-Holocene aridity event is recorded by decrease in the overall CaCO<sub>3</sub> content in the sediments.

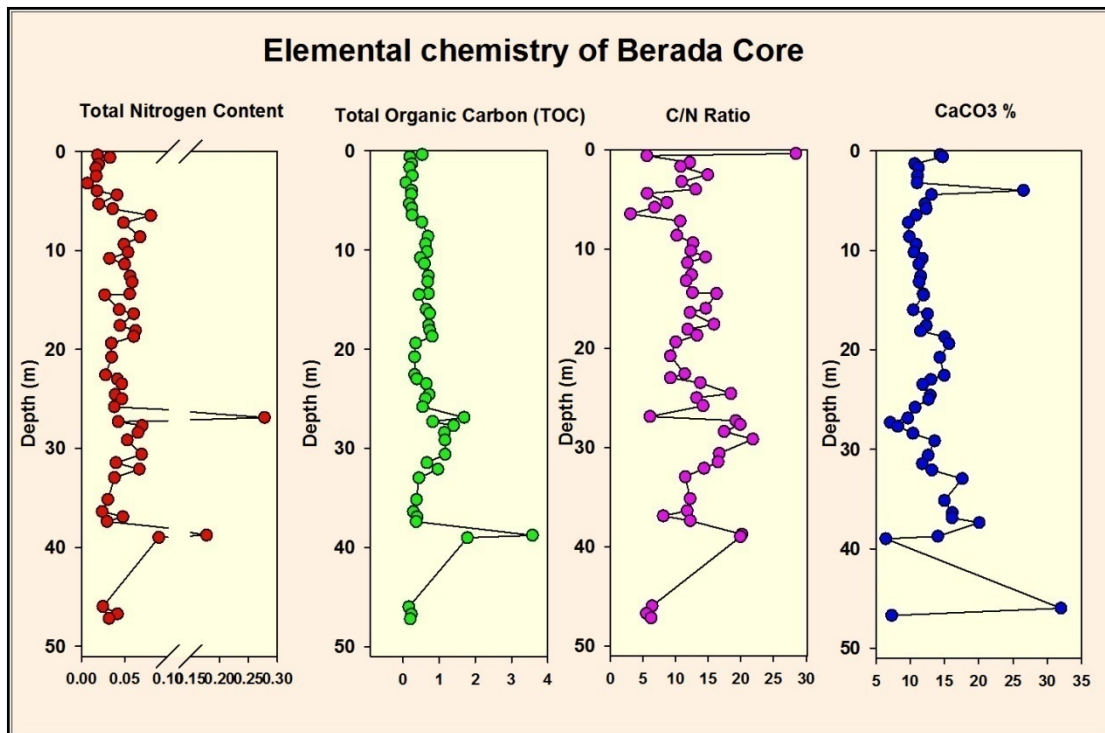


**Figure 8.5** Down core variations in the N,C, C/N ratio and CaCO<sub>3</sub> content in Berada core.

## Trace Elements

### *Palaeoredox conditions*

The downcore variations of Cr, Cu, Mn, Ni and Co in the Berada core vary from 13.91-18.37, 4.63-8.67, 52.14-146.88, 7.82-9.63 and 3.65-4.29 respectively (Fig. 8.6). The Cr-Ni, shows high correlation coefficient (0.60) in throughout the core records however Cr-Mn and Cr-Cu are weakly correlated (0.31 and 0.29). These elements are showing relative changes along the downcore records in Zn, Cr, Ni and Co on account of the

fluctuations in the environmental conditions. However, Ni/Co value throughout the down core records ranges between the 2.01-2.48 with average value 2.16 clearly indicating the oxic conditions. This is also in accordance with the central rann values that also suggest the prevailing oxic conditions throughout the sedimentary record. Berada core falls in a marginal part as compared with the central Dhordo core that is in support of the well oxygenated conditions in the basin. However, the high productivity induced anoxia is also reported Arabian Sea (Sirocko et.al. 2000 and references therein, van Rod et.al. 1999). Therefore the variations in the trace elements and their proportion in the Berada core suggest the oxic conditions throughout.

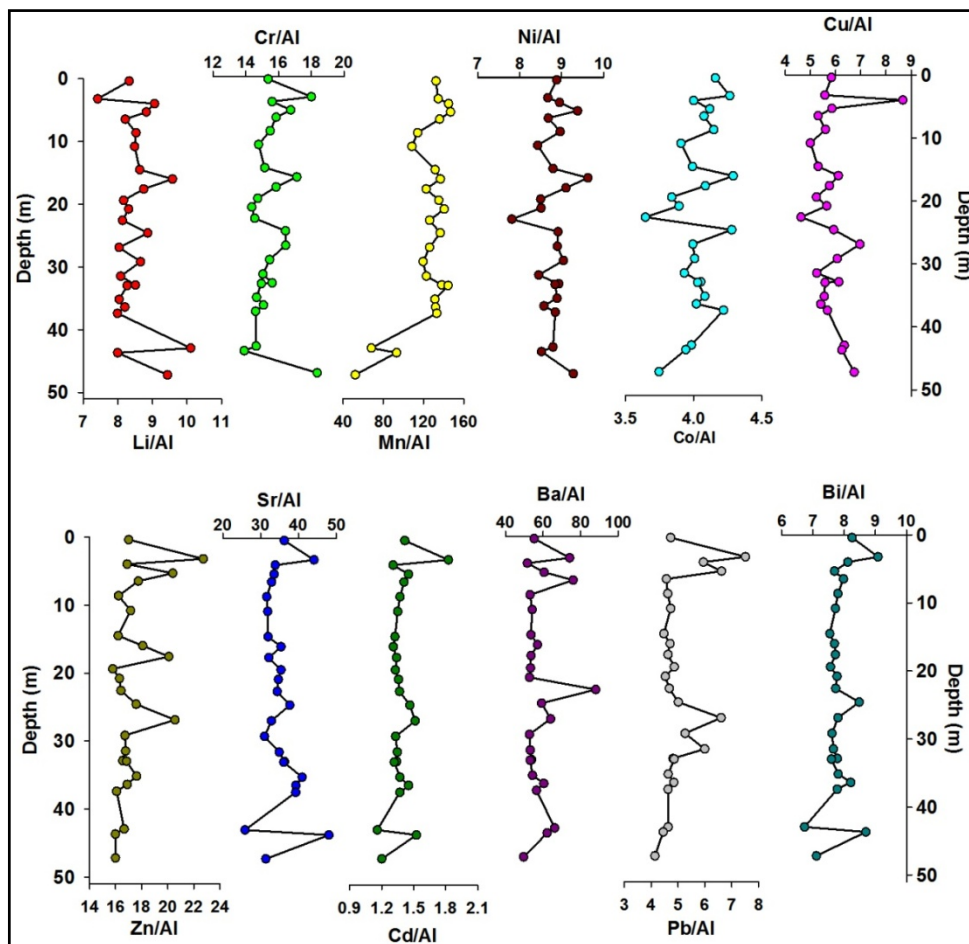


**Figure 8.6** Down core variations in the trace elements (Al normalized) in Berada core.

### *Nutrient Conditions*

In Berada core the nutrient proxies such as Cu/Al, Zn/Al, Cd/Al, Co/Al, Pb/Al and Ba/Al are analyzed for the down core variations (Fig. 8.6). Most of the elements show the narrow range of fluctuations in the record except at bottom parts.

**Zone-I (50 - 39m depth)** - As stated earlier, this zone passes through the intercalated sequence of the fluvial-marine sediments. The lower most samples Mn/Al, Co/Al, Zn/Al and Cd/Al shows the lowest values that is corroborated with the least organic carbon. This indicates the low nutrient rich waters during the deposition of these conditions. The fluvial sands comprise predominantly quartz in the overall mineralogy therefore the trace element analysis was not performed on these samples.

**Zone-II (39 - 25m depth)** - The second zone is characterized by the high values of each element proxy that is on account of the change in environmental conditions due to marine capture during the Early Holocene (9.5ka B.P.). From bottom upwards Mn/Al, Ni/Al, Zn/Al, Cd/Al and Pb/Al are restricted in a narrow range suggesting no significant changes in the nutrient influx during Early to Mid Holocene times. However Sr/Al and Cu/Al shows negative sloping values and Co/Al shows relatively increased values. The major elements Fe/Al, Mn/Al and other are indicating the increased detrital content to the site. The CaCO<sub>3</sub>% content in this zone is observed to increase in the sediments that is also positively correlated with the organic carbon indicating the increase in the productivity conditions.

**Zone-III (25 - 8m depth)** - In this zone, Ni/Al, Co/Al and Cu/Al shows increasing values suggesting the increased nutrient conditions during Mid-Holocene times. Rest of the elements remain in a narrow range that with minor variations up to ~18m depth. Above this horizon overall reduction in most of the elements is observed suggesting depleted nutrient conditions.

**Zone-IV (8 - 0m)** - Topmost zone of the Berada core yields abrupt positive shifts in all the elemental proxies including Mn/Al, Ni/Al, Co/Al, Cu/Al, Zn/Al and Ba/Al. This unit marks the wide scale fluctuations in the elemental proportions in the upper zone. The reduction in the values at bottom parts of this unit may due to the restricted fresh water influx into the region on account of the prevailing aridity condition during post Mid-Holocene times. The top section marks the withdrawal of marine waters that may lead to reworking. Overall the top part of the core shows nutrient depleted conditions.

### CLAY MINERALOGICAL STUDIES

Interaction of the nature of rock type, topography with climatic conditions that trigger weathering processes supplies the sediments from the high mountainous areas to the basins. The degree of weathering, transport mechanisms and source to sink distance creates the characteristic textural contents at various stages during the transport before deposition. The nature of sediments on temporal scale indicates the change depositional settings and overall energy of the environments. In Great Rann basin, textural studies based on core sediments reveals the dominance of fine grained sediments primarily by presence of clayey silts to silty clays that indicates the overall low energy of depositional environment. As the clay is a significant contributor in bulk grain size of rann sediments throughout, it necessitates characterization of bulk clay mineralogy to understand the source for the clay minerals in hinterland. The clay mineral assemblage is successfully used as a provenance and palaeoclimatic proxy (Kessarkar *et.al.* 2003, Thamban *et.al.* 2002) and are known to vary with the major climatic and environmental conditions throughout the glacial and sub-glacial scales (Boulay *et.al.* 2007, Wan *et.al.* 2007, Colin *et.al.* 2010) In the present study, the clay mineralogy of core sediments was used to assess the spatial and temporal changes in palaeoenvironmental conditions and provenance of the subsurface rann sediments.

#### CLAY MINERALS AS A REGIONAL PALAEO- PROXY

Clay mineralogy is widely accepted, rapid proxy for provenance of the sediments in marine, continental environments, ocean current studies and also for the palaeoclimatic studies. Nevertheless, it is necessary to take certain parameters into account in clay mineral studies such as- sediment nature, source region, oceanographic/continental settings, parent rock composition and depositional processes. Also, there are many other processes can change the overall clay mineral assemblage during or after the deposition of the sediments such as selective deposition (Degens & Ittekkot 1984), textural attributes (Gibbs, 1977, Maldonado and Stanley, 1981;), redistribution (Kolla *et. al.* 1981), flocculation (Grim 1968), and may also be due to methodic approaches of sample preparation and/or during quantification of clay minerals (Moore and Reynolds 1989).

Also, in geologically older sediments diagenetic alterations can modify the clay mineralogy of the sediments, however, in recent samples it is negligible (Grim, 1968). In addition to this, several assumptions are to be made before the clay mineral studies that are summarized in Thamban *et.al.* (2002) and Alizai *et.al.* (2012).

Considering all the above facts, the clay mineral relative abundance studies can be used to decipher the provenance of the sediments and also high resolution paleoenvironmental history in the recent geological past (Sirocko and Lange 1991, Gingele 1996, Thamban *et.al.* 2002, Wan *et.al.* 2007, Colin *et.al.* 2010). Along with the relative abundance studies the other parameters like the Illite crystallinity and Illite chemistry is helpful to study the degree of hydrolysis and leaching processes (Thamban *et.al.* 2002). Several clay mineral ratios are important for environmental reconstruction such as humidity, leaching, dry-warm phases and its relation with the climate and/or local processes of deposition (Alizai *et.al.* 2012 and references therein).

The eastern Arabian Sea clay mineral records are well documented to understand provenance and transport pathways of fine grained sediments; currents and re-distribution of the fine grained sediments (Kolla *et. al.* 1981, Konta 1985, Rao 1991, Rao and Rao, 1994, Kessarkar *et. al.* 2003) and palaeomonsoon & weathering history (Thamban *et. al.* 2002, Thamban and Rao 2005). Most of the studies deal with the surface sediments and clay mineral distribution pattern along and across the west coast of India from shallow marine (100m depth) to several hundred meters in depth. The temporal scale studies are largely from continental shelf and shelf margins of southwestern India (Thamban *et. al.* 2002, Chauhan *et. al.* 2000, Pandharinath 2009). For sediments along the west coast of India, three major source regions are identified based on the clay mineral composition: Illite, Chlorite rich sediments belongs to Indus, Smectite dominated sediments from the Deccan traps and Kaolinite-Smectite enriched sediments derived from the gneissic rocks (Kessarkar *et.al.* 2003). Offshore records from Gulf of Kachchh clay mineral signatures are also documented by several studies (Chauhan 1994, Rao and Rao 1995, Chauhan *et. al.* 2006).

To characterise the clay mineral assemblage in the Great Rann basin it is necessary to overview the clay mineral records from adjacent regions. Glennie and Evans (1976) studied the clay mineral assemblage in the upper ~1m of the Great Rann sediments at

various locations suggesting that the presence of the Illite, Chlorite and Kaolinite and Montmorillonites/Smectites suggesting the Indus and Deccan trap source to rann minerals. The clay mineral signatures of the Indus River is well documented from the offshore parts (Kolla et.al. 1981, Rao and Rao 1995) but the continental to deltaic record and clay mineral variations during Holocene period is published only recently by Alizai et.al. (2012). The clay mineralogy of marine cores from the Indus shelf and from off Karachi is documented by Limmer *et.al.* 2012. Accessing the northwestern Rann, Nara river sediments analyzed for clay minerals suggest the Illite and Smectite are more relative to Kaolinite and Smectite (Tyagi et.al. 2012). For the local sources from Mainland Kachchh clay mineral records of Middle Jurrassic formation shows the abundance of Kaolinite and Smectite (Fursich *et.al.* 2005). Clay minerals in the Aravalli derived sediments also suggest the presence of Illite and Smectite (Pandharinath *et.al.* 1999, Jain and Tondon, 2003, Sharma et al. 2010).

**Table 9.1.** List of the clay mineral ratio proxies for palaeoclimatic and environmental studies. These proxies are adopted from Biscay 1989, Gingele 1996, Colin *et.al.* 2012 and Alizai *et.al.* 2012 and references therein.

Sr. No.	Proxy	Process		
		Increase in ratio	Decrease in ratio	
1	(Smectite + Kaolinite)/ (Illite + Chlorite)	Relative Increase in physical weathering	Relative decrease in physical weathering	Chemical Vs Physical weathering Proxy
2	Kaolinite/ Smectite	Dry seasonal climate	Warm humid climate	Climate Proxy
3	Kaolinite/Illite & Kaolinite/Chlorite	Indicates enhanced humidity Increased chemical hydrolysis	Indicates reduced humidity Decreased chemical hydrolysis	Humidity Proxy & Chemical hydrolysis indicator
4	Illite/Chlorite & Smectite/ (Illite + Chlorite)	High chemical weathering	Low chemical weathering	Chemical weathering
5	Kaolinite/ (Illite+ Chlorite) & Smectite/Kaolinite	Increased leaching  Reduced leaching	Decreased leaching  Enhanced leaching	Leaching Proxies
6	Illite Crystallinity			Degree of Hydrolization
7	Illite Chemistry	Below 0.5 –Fe, Mg rich Illites Above 0.5 –Al rich Illites		Nature of Illite (Fe rich or Al rich Illites)

With this background, the first objective was to characterise the clay mineralogy of the rann sediments and identify the potential provenance regimes in the deposition of rann sediments. Another aspect was to study whether the provenance remained same or shifted in past and whether the clay mineralogy can be used as a proxy for the known climatic phases. Several clay mineral ratios are adopted that are environmentally sensitive proxies and therefore can be used as indicators of the environmental change (Table 9.1).

## **RESULTS**

The major clay minerals present in all the sediment samples are: Smectite (Sm), Illite (Ill), Kaolinite (Ka) and Chlorite (Ch). Identification of Illite, Chlorite and Kaolinite was through the distinct peaks whereas the Smectite peaks showed small deviations in the diffraction pattern. This may be due to the presence of the mixed layering within the Smectites which is also seen in flood plains and deltaic sediments of Indus system (Alizali *et. al.* 2012). It has been observed by these workers that increasing dominance of Smectite abundance tends to carry more pure Smectite peaks, whereas the low Smectite samples contain relatively more mixed-layering which resulted in irregular peak position in the results. In our samples Smectite remains present in subordinate proportion and major abundance of the clay mineral is governed by the Illite and Chlorite. Therefore, considering the low abundance of Smectites, the low interference Smectite peaks are treated as Smectites. The down core distribution of these clay minerals in both the cores is shown in Fig. 9.1 & 9.2 which clearly indicates the dominance of the Illite and Chlorite over Smectite and Kaolinite. In Dhordo core Illite shows the narrowest range of variations followed by Chlorite whereas Smectite shows wide range of variations. Berada core comprises relatively less Illite, increased Chlorite and Kaolinite as compared to Dhordo core records (Fig. 9.2a). Based on the variations in clay mineralogy, both the cores are divided into several zones.

### **Clay Mineralogy of Dhordo Core**

Samples from this ~61m deep core from the central rann basin were taken from various lithounits to demonstrate overall clay mineral evolution through time. In all, 30 samples were analysed from the Dhordo core. The results of the XRD analysis of the Dhordo core are given in Table 9.2.

**Table 9.2** Table showing clay mineral variations in Dhordo Core.

Sr. No.	Depth	Sand	Silt	Clay	Smectite	Illite	Kaolinite	Chlorite	ill. Chem.	Ill. crstlnty	S + K / I+C	Sm/ (ill+Ch)	Ka/ (ill+Ch)	Ka/ ill	Ka/ Sm	Ka/ ch	Sm/ Ka	ill/ ch
1	0.46	1	87	12	1.30	66.76	7.98	23.96	0.258	0.10	0.10	0.01	0.09	0.12	6.14	0.33	0.16	2.79
2	1.7	1	77	22	7.87	66.23	7.60	18.30	0.25	0.15	0.18	0.09	0.09	0.11	0.97	0.42	1.04	3.62
3	2.96	0	46	54	7.26	66.03	7.63	19.08	0.20	0.19	0.17	0.09	0.09	0.12	1.05	0.40	0.95	3.46
4	3.91	0	53	47	11.85	63.48	10.78	13.89	0.22	0.19	0.29	0.15	0.14	0.17	0.91	0.78	1.10	4.57
5	4.31	1	67	32	12.44	63.83	7.04	16.69	0.26	0.12	0.24	0.15	0.09	0.11	0.57	0.42	1.77	3.82
6	5.04	0	53	47	4.72	69.33	7.57	18.38	0.24	0.15	0.14	0.05	0.09	0.11	1.60	0.41	0.62	3.77
7	5.52	0	50	50	4.57	63.74	9.69	22.00	0.30	0.10	0.17	0.05	0.11	0.15	2.12	0.44	0.47	2.90
8	7.12	1	69	30	3.02	69.92	7.27	19.79	0.22	0.10	0.11	0.03	0.08	0.10	2.41	0.37	0.42	3.53
9	11.16	0	41	59	8.99	61.94	8.49	20.58	0.25	0.15	0.21	0.11	0.10	0.14	0.94	0.41	1.06	3.01
10	14.46	0.5	49.5	50	8.47	63.12	13.87	14.54	0.22	0.15	0.29	0.11	0.18	0.22	1.64	0.95	0.61	4.34
11	16.94	0.5	73	26.5	9.44	63.17	10.46	16.93	0.22	0.20	0.25	0.12	0.13	0.17	1.11	0.62	0.90	3.73
12	18.59	0.5	54	45.5	8.65	64.22	8.27	18.86	0.35	0.19	0.20	0.10	0.10	0.13	0.96	0.44	1.05	3.41
13	20.54	23	50	27	10.47	65.79	12.02	11.72	0.20	0.20	0.29	0.14	0.16	0.18	1.15	1.03	0.87	5.61
14	21.22	31	55	14	3.23	72.04	5.54	19.19	0.23	0.10	0.10	0.04	0.06	0.08	1.72	0.29	0.58	3.75
15	23.36	4	53	43	17.60	53.94	11.66	16.80	0.40	0.18	0.41	0.25	0.16	0.22	0.66	0.69	1.51	3.21
16	26.4	0.5	47.5	52	11.04	60.29	14.61	14.06	0.36	0.20	0.34	0.15	0.20	0.24	1.32	1.04	0.76	4.29
17	26.66	1	42	57	12.50	55.65	10.33	21.52	0.33	0.20	0.30	0.16	0.13	0.19	0.83	0.48	1.21	2.59
18	28.46	1	73	26	8.30	61.81	12.85	17.04	0.34	0.20	0.27	0.11	0.16	0.21	1.55	0.75	0.65	3.63
19	29.95	25	27	48	13.51	57.38	12.63	16.48	0.31	0.20	0.35	0.18	0.17	0.22	0.93	0.77	1.07	3.48
20	31.15	3	51	46	11.84	60.42	7.37	20.37	0.36	0.20	0.24	0.15	0.09	0.12	0.62	0.36	1.61	2.97
21	34.57	2	53	45	8.33	62.80	10.21	18.66	0.35	0.15	0.23	0.10	0.13	0.16	1.23	0.55	0.82	3.37
22	36.65	0.5	48.5	51	12.16	57.06	12.16	18.62	0.27	0.20	0.32	0.16	0.16	0.21	1.00	0.65	1.00	3.06
23	39.79	1	82	17	10.60	58.26	13.47	17.67	0.34	0.15	0.32	0.14	0.18	0.23	1.27	0.76	0.79	3.30
24	42.89	2	44	54	9.41	62.57	12.99	15.03	0.36	0.18	0.29	0.12	0.17	0.21	1.38	0.86	0.72	4.16
25	44.01	1	70	29	7.53	63.36	7.35	21.76	0.32	0.12	0.17	0.09	0.09	0.12	0.98	0.34	1.02	2.91
26	46.17	1	58	41	8.19	61.48	7.68	22.65	0.24	0.10	0.19	0.10	0.09	0.12	0.94	0.34	1.07	2.71
27	48.24	1	65	34	9.96	57.19	11.16	21.69	0.29	0.12	0.27	0.13	0.14	0.20	1.12	0.51	0.89	2.64
28	51.59	1	63.5	35.5	9.10	61.31	13.63	15.96	0.27	0.15	0.29	0.12	0.18	0.22	1.50	0.85	0.67	3.84
29	54.52	2	56	42	8.95	62.66	9.07	19.32	0.38	0.19	0.22	0.11	0.11	0.14	1.01	0.47	0.99	3.24
30	58.43	4	56	40	10.48	62.70	6.06	20.76	0.25	0.15	0.20	0.13	0.07	0.10	0.58	0.29	1.73	3.02

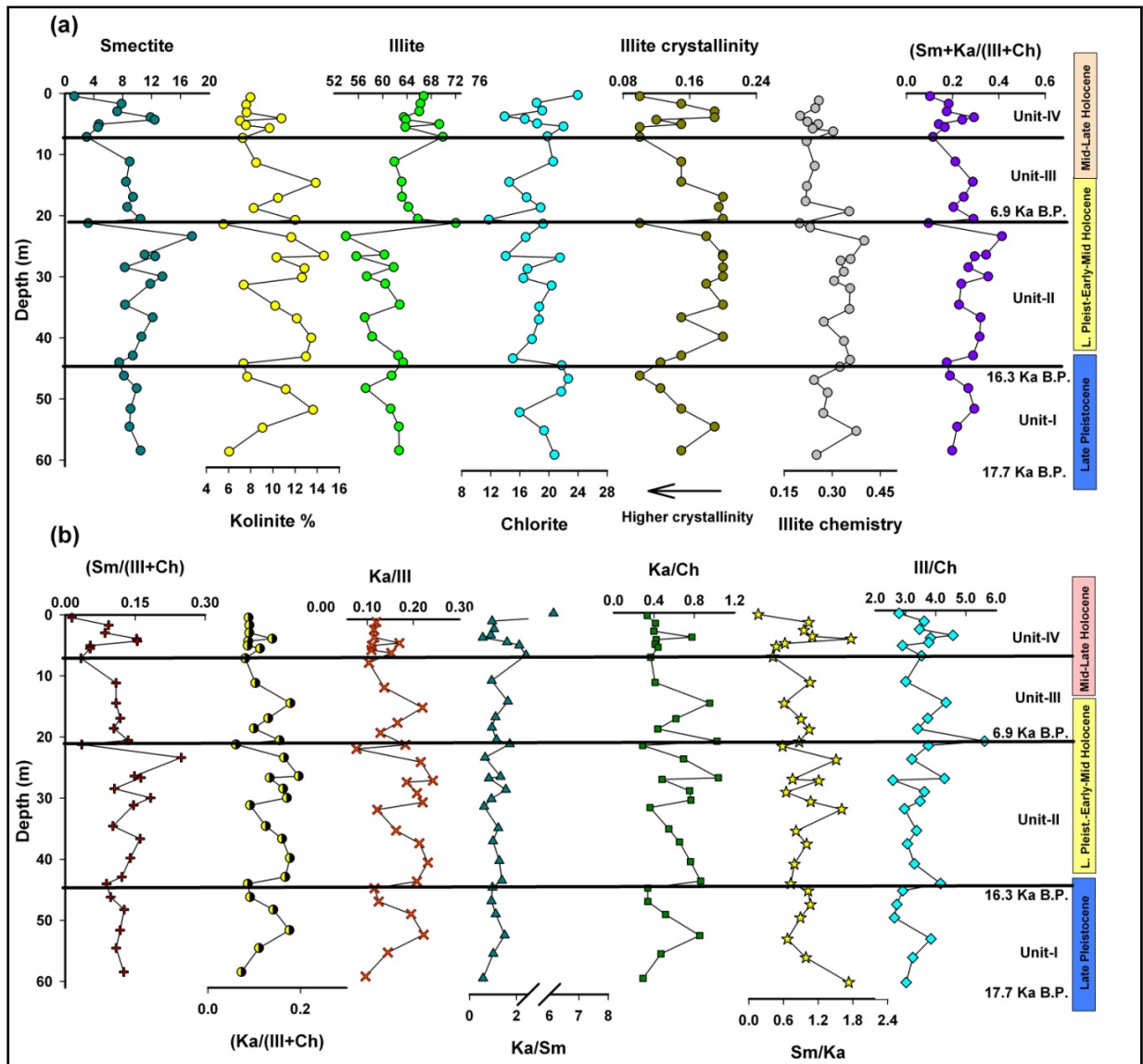


**Figure 9.1.** a) Down core variations in major Clay minerals (Smectite, Illite, Kaolinite and Chlorite), Illite Crystallinity, Illite Chemistry and (Sm+Ka)/(Ill+Ch) ratio. b) Downcore variations in environmentally sensitive clay mineral ratio proxies in Dhordo Core. The divisible zones and the overall timeframe of deposition also indicated.

The results show Illite and Chlorite as dominating clay minerals comprising 53.94-72.04% (avg. 62.62%) and 11.72-23.96% (avg. 18.41%) respectively, whereas, Smectite and Kaolinite varies from 1.3-17.6% (avg. 9.06%) and 5.54-14.61% (avg. 9.91%) suggesting its subordinate proportion (Fig. 9.1a & 9.1b). The downcore clay mineral abundance pattern, clay mineral ratio (paleo- proxies) allows us to divide Dhordo core into four zones as described below.

**Zone - I (60.40 - 44.01m)** - The bottom most part of the Dhordo core is lithologically characterised by grayish coloured clayey silty sediments with fine occasional laminations. The grain size comprises primarily silt rich sediments while sand proportion remains  $\leq 4\%$ . Mineralogically, this zone comprises of Smectite 7.53-10.48% (avg. 9.04%), Illite 57.19-63.36% (avg. 61.45%), Kaolinite 6.06-13.63% (avg. 9.16%) and Chlorite 15.96-22.65% (avg. 20.36%) as major clay minerals. An inverse relationship is observed amongst Kaolinite-Chlorite and Smectite-Illite (Fig. 9.1a; Table 9.2). Illite, Chlorite shows a cyclic decrease followed by an increasing trend in their relative abundance; however Kaolinite runs in reverse direction (Fig. 9.1a). Ka/Ill, Ka/Ch ratio shows the maximum values at 51.59m where it almost doubles within a cyclic increase followed by a decrease towards the top of this zone  $\sim 44\text{m}$  (Fig. 9.1b; Table 9.2). Radiometrically, the deposition of this zone started in latest Late Pleistocene times i.e. 17.7 ka B.P. ( $\sim 60\text{m}$  depth) whereas the upper part this zone dated as  $\sim 16.3$  ka B.P. ( $\sim 44\text{m}$  depth).

**Zone - II (44.01 - 21.22m)** - Overlying the bottommost zone is a thick greenish-bluish to dark gray coloured sediment sequence that is comparatively variable in textural properties. Sediments are silty clays to clayey silts and clayey sandy silt to sandy silty clay at places. The clay mineral abundance in this zone for Smectite, Illite, Kaolinite and Chlorite is 3.23-17.6% (avg. 10.77%); 53.94-72.04% (avg. 60.20%); 5.54-14.61% (avg. 11.26%) & 14.06-21.52% (avg. 17.77%) respectively (Fig. 9.1a; Table 9.2). This zone passes through the large time span from the Late Pleistocene to Early-Mid Holocene times ( $\sim 16.3$  to  $\sim 6.9\text{Ka}$  B.P) comprising largest sediment thickness compared to other zones. The evolving clay minerals in this time mark two distinct phases (Lower subzone & Upper subzone) of the clay mineral accumulation in rann basin through this time period.

The lower sub zone is characterised by decreasing Illite, Kaolinite and increasing Smectite and Chlorite abundance. The climate and leaching proxies [Ka/Ill, Ka/Ch, Ka/(Ill+Ch)] also registers the decreasing trend in this zone. In contrast with, the upper part of this zone records the largest fluctuations with increase in the Smectite and Kaolinite proportion whereas; the Illite shows maximum decrease reaching to its lowest abundance. The chemical weathering proxy (Sm/(Ill+Ch), humidity proxies (Ka/Ill, Ka/Ch) also follows this positive slope by increasing values with fluctuations (Fig. 9.1b). This is also supported by the high values in Illite crystallinity and chemistry.

**Zone - III (21.22 - 7.12m)** - This zone comprises of bluish-greenish sticky to plastic clayey sediments varying from silty clay to clayey silts with occasional increased sand content (Table 9.2; Fig. 9.1). The clay mineral relative abundance for Smectite 3.02-10.47% (avg. 8.17%), Illite 61.94-65.79% (avg. 64.69%), Kaolinite 7.27-13.87% (avg. 10.06%) and Chlorite 11.72-20.58% (avg. 17.07%) respectively (Fig. 9.1; Table 9.2).

The bottom most sample of this zone marks a striking increase in the sand content to 30% at 21.22m that equally reflected on clay mineralogy with an extraordinary shift in the Illite content (~72%). This sudden increase in sand content was observed in only two successive samples whereas samples above these depths remain low in sand proportion. Illite content above this level shows decreasing values of abundance but remains still much higher as compared with all older samples. Smectite remains more or less constant (~10%) whereas Kaolinite and Chlorite largely fluctuates. The clay mineral ratios involving Smectite and Kaolinite shows wide variations as the Smectite and Illite remain more or less stable (Fig. 9.1a). Illite chemistry values are more or less stable as well (except one samples) but Illite crystallinity shows decreasing upwards values indicating the less effect of hydrolization.

**Zone - IV (7.12 - 0.46m)** - The topmost zone texturally appears uniform but notable variation is marked by the sediment colour which is also reflected on the clay mineral variations. The major clay mineral variations for Smectite 1.3-12.44% (avg. 7.14%), Illite 63.48-69.33% (avg. 65.63%), Kaolinite 7.04-10.78% (avg. 8.33%) and Chlorite ranges between 13.89-23.96% (avg. 18.90%). Illite and Chlorite continues to dominate the assemblage, Kaolinite remains more or less stable (~8%) in this zone whereas subtle variations are seen in Smectite and Chlorite (Table 9.2).

### **Clay Mineralogy of Berada Core**

Berada core is ~51m deep core raised from in the marginal part of the Great Rann basin and therefore may reflect the basin wide changes in rann sedimentation as well as the local effects in the shallower part of the basin. It shows massive fluvial sands and mixed marine sands in the bottom most part (~51 - 40m) Maurya *et.al.* (2013). The basic grain size variations shows that more or less fine grained (muddy) sediments dominate in the marginal part of Great Rann basin. Details of grain size variations and textural attributes are documented in Maurya *et.al.*

(2013). In this study total 23 samples from various depths were selected for clay mineralogical studies (Table 9.3).

The relative abundance of major clay minerals is follows. Smectite 3.74-14.02% (avg. 9.0), Illite 53.48-74.21% (avg. 61.22%), Kaolinite 6.48-22.96% (avg. 10.85%) and Chlorite show 12.35-25.76% (avg. 18.92%). Based on vertical distribution of clay mineral variations, the Berada core is divisible into four broad zones.

**Zones - I (43.64 - 32.94m)** - The bottom most zone mainly comprises of light brown to grayish green coloured clayey silty sediments. This zone passes through a fluvial sequence that is sharply covered by marine sediments at 43-44m interval (Maurya *et.al.* 2013). The bottom most two samples of this zone belongs to mixed marine sediments. However, the overall relative abundance of the clay minerals observed as - Smectite (5.29-12.95%; avg. 8.30%), Illite (54.89-74.21%; avg. 63.58%), Kaolinite (6.78-22.96%; avg. 11.70%) and Chlorite (13.28-23.18%; avg. 16.42%).

**Zone -II (32.94 - 19.4m)** - Sediments of this zone are grayish to greenish in colour and texturally appear homogeneous as clayey silts. On the other hand, clay minerals show considerable variations in the relative abundance (Fig. 9.2a). Major clay minerals- Smectite (3.99-14.02%; avg. 8.21%), Illite (58.39-65.38%; avg. 62.17%), Kaolinite (6.48-13.61%; avg. 9.31%) and Chlorite (18.67-22.5%; avg. 20.32%). Illite increases upwards and Chlorite remains more or less stable with small increase whereas Smectite clearly shows a cyclic increases followed by decreasing relative abundance. The Illite crystallinity and Illite chemistry are also marked by fluctuations. The weathering, climate and leaching proxies [Sm+Ka/Ill+Ch, Ka/Ch, Ka/Ill, Ka/(Ill+Ch)] also shows considerably decreased values in phases (Fig 9.2b).

**Zone-III (19.4 - 10.79m)** - In this zone also sediments are marked by variations in colour from light greenish to bluish coloured sediments that texturally appears homogeneous. The clay mineral abundance in this zone comprises of 11.71-13.85% Smectite (avg. 12.58), 53.48-59.57% Illite (avg. 56.99), 7.57-12.58% Kaolinite (avg. 6.98) and 16.6-20.75% Chlorite with average 20.75% (Table 9.3). Mineralogically, this zone is marked by a rapid increased in Smectite, decreased Illite and Kaolinite content. The climate and leaching proxies [Ka/ill, Ka/Ch, Ka/(Ill+Ch)] also reflecting the decreased values whereas the increased content of the chemical weathering (Sm/(Ill+Ch)). The Illite chemistry and crystallinity values are also correspondingly increased with the enhanced chemical weathering (Fig. 9.2b).

**Table 9.3** Table showing clay mineral variations in Berada Core

Sr. No.	Depth	Sand	Silt	Clay	Smectite	Illite	Kaolinite	Chlorite	ill. Chem.	ill crstlnty	S + K / I+C	Sm/ (ill+Ch)	Ka/ (ill+Ch)	Ka/ ill	Ka/ Sm	Ka/ ch	Sm/ Ka	ill/ ch
1	0.4	0	59	41	3.74	66.38	11.01	18.87	0.27	0.12	0.17	0.04	0.13	0.17	2.94	0.58	0.34	3.52
2	4	1	54	45	9.06	62.45	16.14	12.35	0.24	0.22	0.34	0.12	0.22	0.26	1.78	1.31	0.56	5.06
3	5.3	0	56	44	6.85	58.2	15.62	19.33	0.34	0.20	0.29	0.09	0.20	0.27	2.28	0.81	0.44	3.01
4	6.45	0	60	40	12.36	57.39	13.96	16.29	0.31	0.20	0.36	0.17	0.19	0.24	1.13	0.86	0.89	3.52
5	8.65	1	57	42	8.65	57.69	7.9	25.76	0.33	0.19	0.20	0.10	0.09	0.14	0.91	0.31	1.09	2.24
6	10.79	2	61	37	11.71	53.48	12.58	22.23	0.21	0.09	0.32	0.15	0.17	0.24	1.07	0.57	0.93	2.41
7	14.5	0	60	40	11.83	59.57	7.57	21.03	0.14	0.19	0.24	0.15	0.09	0.13	0.64	0.36	1.56	2.83
8	16	0	59	41	12.94	55.8	8.12	23.14	0.23	0.18	0.27	0.16	0.10	0.15	0.63	0.35	1.59	2.41
9	17.6	1	60	39	13.85	59.12	10.43	16.6	0.23	0.20	0.32	0.18	0.14	0.18	0.75	0.63	1.33	3.56
10	19.4	1	57	42	5.81	58.71	12.98	22.5	0.25	0.20	0.23	0.07	0.16	0.22	2.23	0.58	0.45	2.61
11	20.8	1	62	37	10.56	64.29	6.48	18.67	0.15	0.20	0.21	0.13	0.08	0.10	0.61	0.35	1.63	3.44
12	22.59	0	64	36	8.32	65.38	7.25	19.05	0.20	0.10	0.18	0.10	0.09	0.11	0.87	0.38	1.15	3.43
13	24.59	2	70	28	7.41	64.98	6.83	20.78	0.24	0.15	0.17	0.09	0.08	0.11	0.92	0.33	1.08	3.13
14	26.86	4	75	21	3.99	61.17	13.61	21.23	0.31	0.13	0.21	0.05	0.17	0.22	3.41	0.64	0.29	2.88
15	29.18	1	62	37	7.33	62.26	10.26	20.15	0.22	0.05	0.21	0.09	0.12	0.16	1.40	0.51	0.71	3.09
16	31.48	1	59	40	14.02	58.39	7.76	19.83	0.16	0.20	0.28	0.18	0.10	0.13	0.55	0.39	1.81	2.94
17	32.94	1	56	43	6.72	54.89	22.96	15.43	0.22	0.15	0.42	0.10	0.33	0.42	3.42	1.49	0.29	3.56
18	35.14	1	60	39	11.17	64.53	8.77	15.53	0.18	0.19	0.25	0.14	0.11	0.14	0.79	0.56	1.27	4.16
19	36.36	1	72	27	7.95	59.78	9.09	23.18	0.18	0.11	0.21	0.10	0.11	0.15	1.14	0.39	0.87	2.58
20	37.4	1	63	36	12.95	62.44	7.71	16.9	0.17	0.22	0.26	0.16	0.10	0.12	0.60	0.46	1.68	3.69
21	42.94	2	32	66	5.73	74.21	6.78	13.28	0.13	0.20	0.14	0.07	0.08	0.09	1.18	0.51	0.85	5.59
22	43.64	1	47	52	5.29	65.63	14.89	14.19	0.18	0.16	0.25	0.07	0.23	0.23	2.81	1.05	0.36	4.63

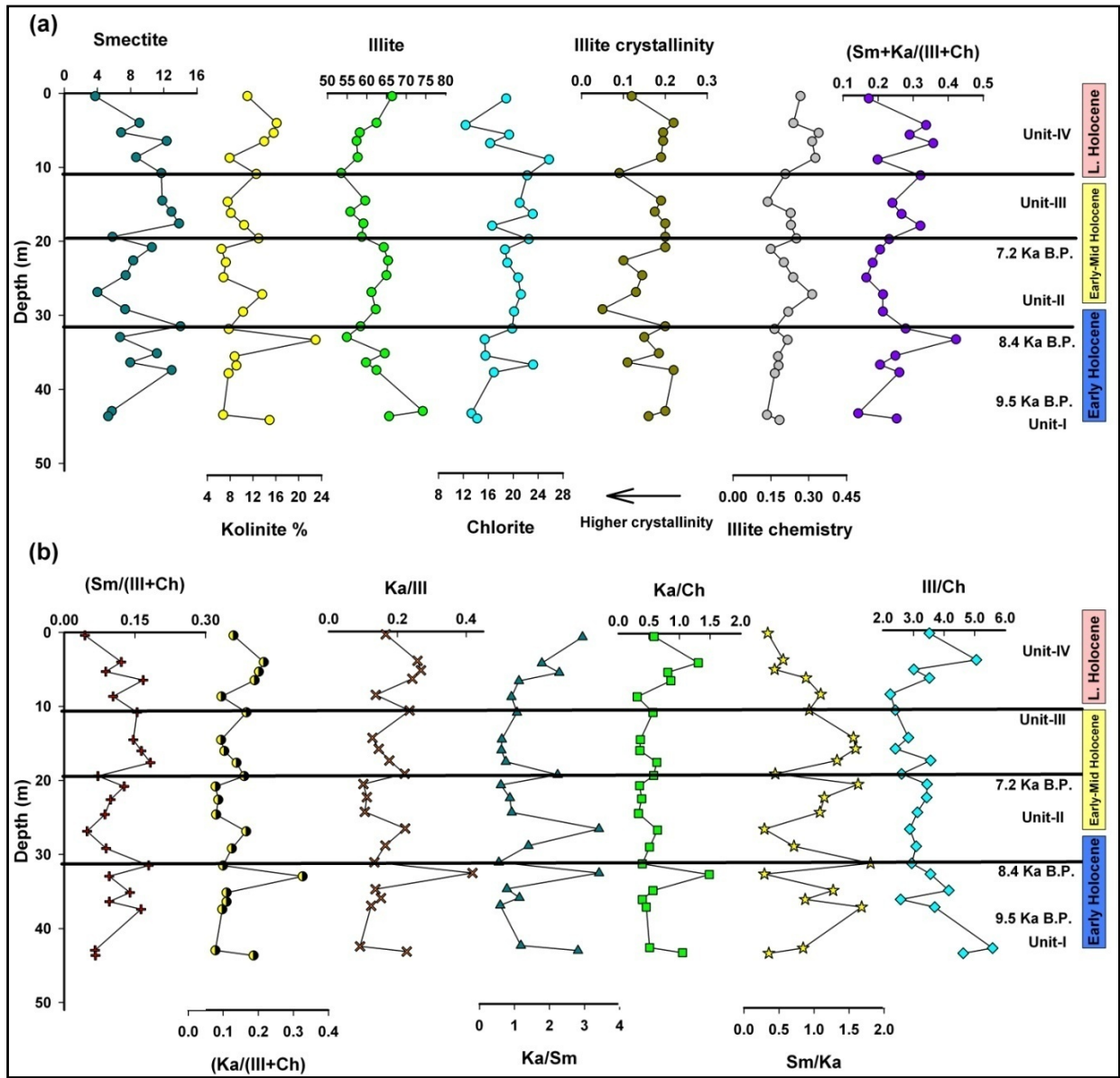


**Figure 9.2.** a) Down core variations in major Clay minerals (Smectite, Illite, Kaolinite and Chlorite), Illite Crystallinity, Illite Chemistry and (Sm+Ka)/(III+Ch) ratio. b) Downcore variations in environmentally sensitive clay mineral ratio proxies in Berada Core. The divisible zones and the overall timeframe of deposition also indicated.

**Zone-IV (10.79 - 0.40m)** - The topmost zone of Berada core is composed of silty and clayey silts are light to dark brown coloured sediments followed by the greenish to grayish coloured sediments. This zone is characterised by rapidly increasing Illite and decrease in Smectite content. Kaolinite and Chlorite shows wide fluctuations in which Chlorite decreases significantly to its lowest level (Fig. 9.2a; Table 9.3). Illite crystallinity and

chemistry values are increased suggesting the enhanced hydrolyzation conditions during the deposition of these sediments.

### **IMPLICATIONS FOR PROVENANCE OF RANN SEDIMENTS**

The Great Rann of Kachchh basin is bounded by the Aravallies and Thar Desert in its northern margins whereas the southern margin is delimited by the Kachchh Mainland hills. Historically, the tributaries of river Indus, Nara and River Saraswati flowed through the Rann of Kachchh (Geddes 1960, Wadiya 1975, Glennie and Evans 1976). Presently there are no rivers contributing significantly to the basin and during the rainy season only fresh water flows into the Great Rann from northern (Nara and other channels) and southern margin from Kachchh Mainland hills).

Provenance discrimination using clay mineralogy is well documented in the published literature (Griffin *et.al.* 1968, Morgon 1977, Singer 1984, Rao and Rao 1994). However, there is no such data available for the for rann sediments. The present study brings first records on clay mineralogical studies shows that Illite and Chlorite are most dominating minerals in rann sediments over the Smectite and Kaolinite. Formation of these clay minerals depends on several factors such as- lithology/rock type, climate and topography (Singer, 1984). It is an important fact that the Great Rann basin was connected with the Arabian Sea till recent past prior to its drying (Frere 1870, Merh 2005, Maurya *et.al.* 2009 Khonde *et. al.* 2011). Therefore, clay mineral records from surrounding continental and marine settings become significant.

The modern spatial distribution of the clay minerals in western continental shelf sediments is studied by Nair *et.al.* (1982). This study shows that the sediments from Indus river are present in large amounts in the clay fraction that overshadows over the local sources such as Deccan trap and Western Ghats marginal regions. Another attempt by Rao and Rao (1995) for the spatial clay mineral distribution along and across the western continental margin of India provided the signatures of characteristic clay mineralogy for the various geological formations along west coast of India. Three major provenance sources were identified for its characteristic clay mineralogy such as- a) Northern Arabian Sea is characterised by high Illite and Chlorite concentration that is mainly Himalayan origin b) High Smectite is supplied by the Deccan Trap basalts and c) Kaolinite and gibbsite dominant sediments are contributed from the gneissic and lateritic rocks of

Western Ghat and coastal laterites respectively. On temporal scales Thamban *et.al.* (2000) and Kessarakar *et.al.* (2003) worked on downcore variations of clay minerals for the provenance studies and denoted the influence of the Illite rich sediments transported up to off Goa coastal sediments. The continental archives Pandharinath *et.al.* (1999) reported clay mineral results from Nal Sarovar that receives sediments from the Aravalli and easternmost Kachchh. They have demonstrated the presence of Illite and Smectite in the Aravalli derived sediments. Sharma *et.al.* (2012) have also shown the presence of Smectite rich soil profiles from the plains of Rajasthan region.

It is evident from these studies that the western coastal Indian margin of Arabian Sea is dominated by the Indus derived Illites in the offshore. Illites and Chlorites are typical physical weathering products from high altitudinal regions (Chamley 1989). Therefore, a high abundance of these minerals in rann sediments point towards the Himalayan born sediment input in the rann basin. Such high amount Illite and presence of Chlorites is also seen throughout the Indus system right from its flood plains in Eastern Panjab of Pakistan to the Indus delta at Keti Bander and also from offshore records (Alizai *et.al.* 2012 Limmer *et.al.* 2012). Despite the similarity of Illite abundance in Rann and Indus sediments; there are some remarkable differences of rann clay assemblage as compared with typical Indus sediments. A comparison of all major clay mineral groups from important sites in and around the Great Rann is given in Table 9.4 and Fig. 9.3.

**Table 9.4.** Comparison of relative abundance of clay mineral in core sediments of Great Rann with surrounding regions

Location of the core/samples/ trench	Smectite %	Illite %	Kaolinite %	Chlorite %	Reference
Dhordo core (central rann basin)	1-18	54-72	6-15	12-24	Present study
Berada core (margin of rann basin)	4-14	54-74	7-23	12-26	Present study
Rann sediments- top 2.6 m (Shakti bet)	1-12	56-70	2-21	8-37	Tyagi <i>et.al.</i> (2012)
Nara Region	27-74	20-58	1-4	4-13	Alizai <i>et.al.</i> (2012)
Indus Delta region (Keti Bander)	35-54	34-52	1-5	7-12	Alizai <i>et.al.</i> (2012)
Marot Core (Eastern Punjab)	27-64	25-60	2-6	4-11	Alizai <i>et.al.</i> (2012)
Tilwala (EPR)	25-65	24-66	1-6	5-12	Alizai <i>et.al.</i> (2012)
Fort Abbas trench	47-57	32-45	3-5	6-8	Alizai <i>et.al.</i> (2012)
Fort Derawar	39-57	38-50	2-5	7-11	Alizai <i>et.al.</i> (2012)

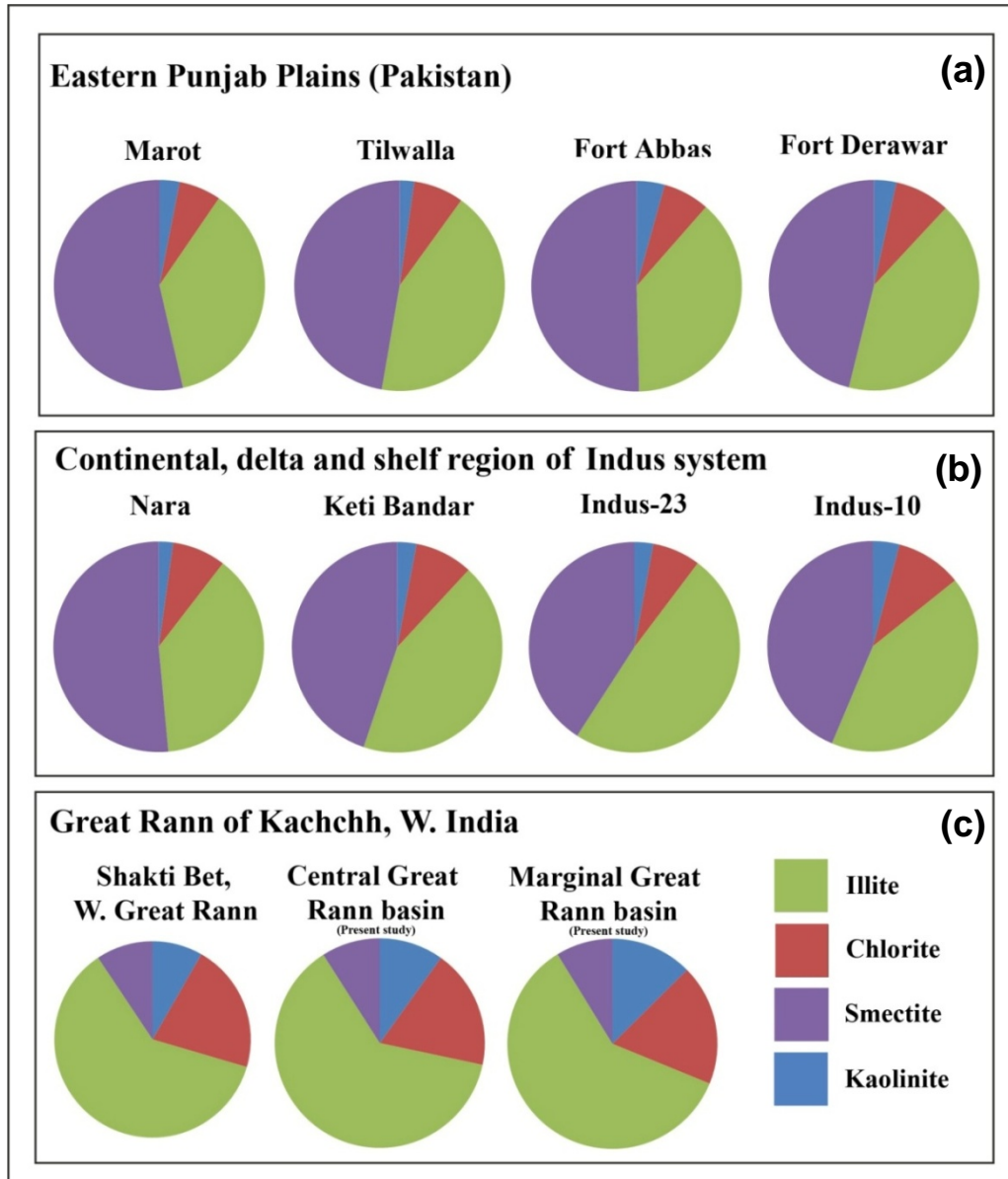


**Figure 9.3.** Clay mineral characteristics of Indus river system from its flood plains, river mouth (delta) and shelf region compared with Great Rann basin, Kachchh. a) The Eastern Punjab (Pakistan) flood plains near Behwalpur region comprising Marot, Tilwalla cores and Fort Abbas and Derawar trenches in flood plains covering from ~49Ka to recent (Alizai *et.al.* 2012). b) The clay mineralogy of from the present day confluence of the eastern and western tributaries of Indus river that represents the older river sediments essentially of Himalayan origin but not necessarily of river Nara (Alizai *et.al.* 2012), Keti Bander core is from the Indus delta region near to the river mouth (Alizai *et .al.* 2012) and Indus-23, Indus-10 core records are from north of Indus canyon and off Karachi (Pakistan) respectively (Limmer *et.al.* 2012). C) Clay mineral data of rann sediments near Shakti bet (Tyagi *et.al.* 2012) western great rann and present study i.e. Central and Marginal Great Rann of Kachchh basin.

It is evident from Table 9.4 and Fig. 9.3 that the rann sediments are consistently more abundant in Illite and Chlorites as compared with the Indus sediments. The dominance of the Illites in rann sediments can be related with the Himalayan source but another Illite source is alluvial plains in Rajasthan i.e. Aravallies (Pandharinath *et.al.* 1999, Sharma *et.al.* 2010). Therefore, to check with the typical Himalayan source, the Illite crystallinity and chemistry values are taken into account. The variation in the degree of Illite crystallinity depends on the degree of hydrolization. The Illite chemistry varies from Fe-Mg rich to Al rich Illites with increasing leaching effects (Chamley *et.al.* 1989). This leaching effects and crystal widening is expected more in the alluvial plains of Rajasthan (Aravalli source) as the weathering processes are more prone to change degree of crystallinity and chemistry (Thiry 2000). The Illite chemistry record at both core sites shows low values indicating Fe-Mg rich Illites that means fresh Illite deposition (Fig. 9.1a and 9.2a). This is also in conformity with the overall low values of Indus Illites where the degree of hydrolization is relatively less as indicated by Fe-Mg rich Illites (Alizai *et.al.* 2012, Limmer *et.al.* 2012). The evidence of increased hydrolization effects on Indus derived Illites comes from off Maharashtra and Goa where Al-rich Illites are common on account of leaching of Fe-Mg cations and Al rich Illites in the marine sediments (Thamban *et.al.* 2002). Therefore, the Illites in Great Rann appear more of Himalayan derived in nature.

Another point is the rann sediments are rich in Illite and Chlorites and less in Smectites and more Kaolinite as compared with the Indus sediments. Such differences are significant while looking in to the provenance of the sediments and may help in understanding fine scale input from other sources. Also, there is consistency in higher Smectites in Indus records whereas rann sediments are consistently low in Smectites abundance (Table 9.4; Fig. 9.3). This large difference in the Smectite abundance may be due to Smectite producing lithologies in the eastern Panjab and northeastern regions of Pakistan. Also the ophiolites in the Pakistan-Makarn region contain Smectites that may have been carried with the alongshore currents to the near coastal regions (Alizai *et.al.* 2012, Limmer *et.al.* 2012). Smectites are typically formed in the warm-dry climates and are characteristic products of volcanic rocks such as Basalts in the west coast of India (Rao and Rao 1994). In the rann basin the source of the smecties appears from the local

patchy volcanic and from the river Nara that previously contributed sediments to the rann and may also be related with the tributaries that drained through the northwestern Smectite rich lithologies (Alizai *et.al.* 2012). This is in conformity with suggestion by Glennie and Evans (1976) that many other rivers were falling into the Indus course or joining Nara have contributed the sediments to the basin. Tyagi *et.al.* (2012) also speculated Deccan basalts and Nara River as a source for the raised rann sediments based on limited clay mineralogical data in northwestern rann. Moreover, the present day seasonal inundation of Arabian Sea water into rann suggests another possibility of Smectite transport in rann through the alongshore currents when rann was connected with the Arabian Sea. Though, if it is the case, the dominance of Smectite that we observe in Indus system might have reflected in rann sediments too. Therefore the contribution via alongshore currents appears less and may never acted as a sole source for Smectites. Interestingly, the onshore Indus system and records from offshore Karachi and north to the Indus canyon (Indus-10 & 23) shows the characteristically high Smectites (Fig. 9.3). An overall increase in Illites percentage is also observed from northwest to southeast from Pakistan towards Rann (Fig. 9.3). Thus, the decrease in Smectite therefore plays a significant role in changing the relative abundance in the clay mineralogy from Indus system to Great Rann of Kachchh.

Chlorite is also a key indicator of physical weathering in cold, arid climate (Biscay, 1965; Singer, 1984). Both the Dhordo (central) and Berada (south marginal) cores comprises Chlorite proportion  $\sim 18\%$  which is almost three folds that to onshore records of Indus system and two fold with the offshore records (Fig. 9.4) (Alizai *et.al.* 2012, Limmer *et.al.* 2012). The south flowing river Nara and Panjab flood plains essentially contains less Chlorites, therefore, there might be some mixing of Chlorite rich source before Nara debouches in Rann basin or other tributaries of Indus from northwestern part. Another possibility is the drainages from northeastern part might have contributed originally Himalayan derived Chlorites to the basin through Luni and/or other northeastern rivers. Yet the northeastern drainages largely comes from the Aravallies source that does not contain large Chlorite contents in its soil (Sharma *et. al.* 2012). Therefore, a detail characterization of the hinterland/source regions in the upstream is required to prove which part has contributed the higher Chlorite content in the rann sediments.

The dominant Chlorite and Illites in the rann sediments strongly points towards the distal Himalayan source for rann sediments as compared with the local/proximal Kachchh Mainland Hills and/or Aravallies. Though, the considerable proportion of Kaolinite undoubtedly comes from the proximal sources as the exposed lithologies of Kachchh Mainland Hills are abundant in Kaolinite (Biswas 1993, Fursich *et.al.* 2005). This is also supported by the increased Kaolinite content in the marginal regions that are more prone to the Kaolinite source (Fig. 9.4a). Also, the Kaolinite are relatively more in Berada core as compared to Dhordo and more northern sediments near Shakti bet (Tyagi *et.al.* 2012).

Overall, mostly the provenance of the Great Rann basin can be inferred that the major contribution comes from the Himalayan derived sediments which strongly masks the peninsular, local and proximal sources (Smectite and Kaolinite) such as the Aravalli, and Mainland Kachchh. Kaolinite is abundant in the exposed older formations of Mainland Kachchh (Biswas 1993, Fursich *et.al.* 2005). The source for the Smectite on the other hand may be south flowing rivers like Nara (Tyagi *et.al.* 2012), and/or defunct tributaries once flowed into rann and also small inputs from Aravallis (Singh *et.al.* 2010).

## **PALAEOENVIRONMENTAL IMPLICATIONS**

The temporal scale variations in clay minerals and clay mineral ratio proxies shows significant changes based on which both the cores are divisible into several phases. The available chronology on the cores suggest that the central part of rann basin was already accumulating sediments in marine settings whereas the south marginal part of the basin has received marine sediments during early Holocene times i.e. 9.5ka B. P. (Maurya *et. al.* 2013). The temporal palaeoenvironmental significance of both the core sites is discussed.

### **Dhordo core**

**Zone – I** - Zone- I of Dhordo core (60.13 - 44.04m) is characterised by significant variations in the clay minerals that are also visible through changes in environment sensitive proxies. The relative decrease in Illite and Chlorite is observed in bottom part of this zone that collaborates with the increasing Kaolinite and more or less consistent Smectite (Fig. 9.1). The humidity proxies (Ka/Ch & Ka/Ill) show the cyclic increase followed by a decreasing values bottom upward (Fig. 9.1b). A fourfold increase in the

Ka/Ch ratio (Humidity proxy) is recorded at ~51.6m depth as compared with the lowest value (Fig. 9.1b). These persistent high values in humidity proxies are indicative of increased humidity in the hinterland regions (Thamban *et.al.* 2002). The depositional age of these sediments ranges between ~17.7 to 16.3ka B.P. (Fig. 9.1). Such evidences of such Late Pleistocene monsoon intensification that punctuated the generally weak monsoon are also recorded from continental margin off Goa based on clay mineral records during ~28 & 22ka B.P. (Thamban *et.al.* 2002). The leaching proxies (Ka/(Ill+Ch); (Sm/Ka) and weathering proxies (Sm + Ka/Ill + Ch) are also indicates increase and coherent changes in leaching and weathering in source regions. Furthermore, the Sm/Ka Vs Illite crytallinity and Ka/(Ill+Ch) Vs Illite crytallinity plots points towards the warm wet climate with moderate to high leaching (Fig. 9.4a and 5a). The higher degree of crytallinity in these graphs (Fig. 9.1b, 9.4a and 9.5a) shows low hydrolization during the deposition of these minerals that may points toward the rapid deposition of the sediments. Similarly, a high resolution multi proxy record of laminated sediments from off Pakistan margin also revealed such abrupt events of spells of intensifying monsoon during the ~29-27ka & 23-17ka B.P. (von Rad *et. al.* 1999).

**Zone-II** - This zone (44.01 - 21.22m) encompasses the Late-Pleistocene-Early Holocene towards Mid-Holocene times from ~45m depth (16,340±79 years B.P.) to 27.78m depth (6, 985±54 years B.P.) in Dhordo core. Continuation with the underlying zone, this zone can be described into two broad zones. The first zone from bottom of this zone is characterised by increased Smectite and Chlorite (rapid increase) and decrease in Illite and Kaolinite (rapid decrease) whereas; the upper zone is characterised by fluctuations in all the clay mineral assemblage (Fig. 9.1a). A constituent high values in Ka/Ch & Ka/Ill (climate proxies) observed in bottom part of this zone as compared with the underlying sequence (44.01 - 34.5m depth). These variations in the ratios are in conformity with the other paleoclimatic studies stating that the strengthening monsoonal condition during Late-Pleistocene- Early Holocene times as a rapid response to the post glacial climate change (van Campo *et.al.* 1982, Sirocko *et.al.* 1993, Overpeak *et.al.* 1996, van Rod 1999, Thmaban *et.al.* 2001, 2002). On the other hand, the upper zone of this zone is characterised by high values in climate and weathering proxies that are interrupted by negative fluctuations which is also reflected in overall clay mineral abundances (Fig. 9.1).

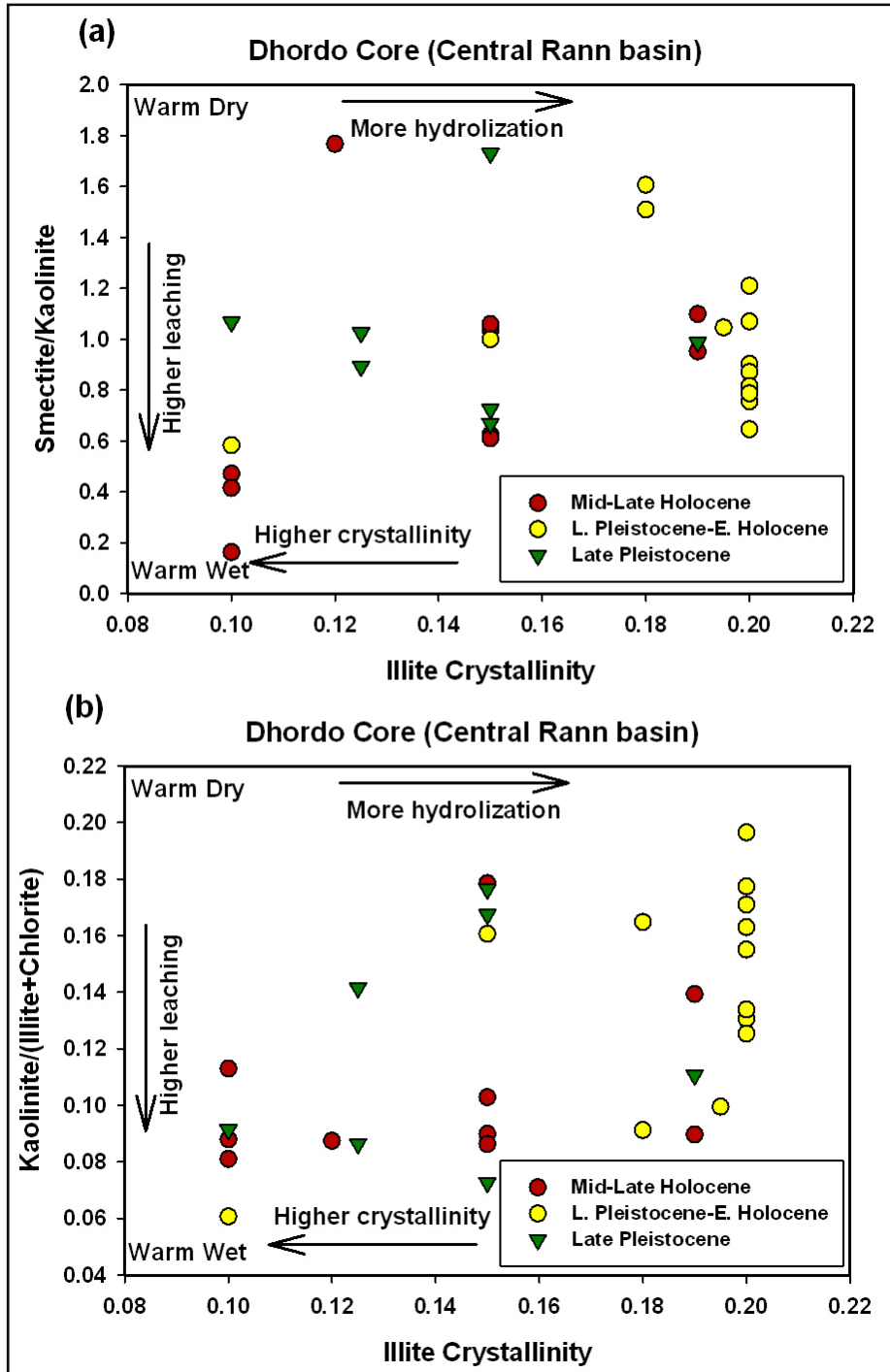


**Figure 9.4** Plots showing Illite crystallinity Vs Chemical weathering proxies for the individual time frames for Dhordo Core samples. (a) Smectite/(Illite+Chlorite) Vs Illite crystallinity, and (b) Kaolinite/(Illite+Chlorite) Vs Illite crystallinity. Note that the L. Pleistocene values are more sparsely arranged, L. Pleistocene to E. Holocene values shows lowered degree of Illite crystallinity with increased hydrolization processes; whereas; Mid-Late Holocene values are more or less indicating higher leaching and variable degree Illite crystallinity.

These interruptions may be indicative of the non-steady conditions that caused the negative shifts in generally positive high values in the humidity, leaching and chemical weathering proxies (Fig. 9.1a and 9.1b). The developing monsoonal conditions during 13-6 ka are evident through various studies whereas, the Holocene maxima is also suggested around 7-9 ka B.P. (Prell *et.al.* 1986, van Campo *et.al.* 1986, Naidu and Malmgren 1996, Thamban *et.al.* 2002). The radiocarbon age in the uppermost part of this zone dated back to 6.9 ka which corroborates with the earlier records (Fig. 9.1). Another testimony is higher degree of hydrolyzation and poor crystallinity in Illites for the lower zone samples of this zone suggesting the warm wet conditions, whereas, the upper zone is advocating generally warm humid climate interrupted by dry spells (Fig. 9.4a and 9.5a). Ka/Sm does not respond to these changes because the relative percentage of Smectite and Kaolinite is almost comparable in their abundances (Alizai *et.al.* 2012) (Table 9.2 and Fig. 9.1b).

Overall, these environmental proxies advocate the humid phase in between 16.3 ka B. P. to Early Holocene times. Another, humid climate phase that is punctuated by dry spells is recorded in the upper part of this zone that may be during Early to Mid Holocene times. The overall clay mineral proxies record the strengthened monsoonal condition during the Early Holocene towards Mid Holocene times by its maxima prior to 6.9ka B.P. as evidenced by the largest positive shifts in the values at ~24-28m depth (Fig. 9.1a and 8.1b). The present dataset differs with the records from off Goa that shows low intensity monsoon prevailed during ~13 - 9ka B.P. and monsoon strengthening started only after ~9ka B.P. (Thamban *et.al.* 2002).

**Zone-III** - Clay mineralogically, this zone (21.22 - 7.12m) is characterised by abrupt rise in Illite percentage while Smectite remain more or less stable and Kaolinite and Chlorite shows fluctuating abundance throughout the zone (Fig. 9.1a). This abrupt change in Illite is coeval with the coarser sediment flux in the area that may be pointing some event as sand content increases to 31% ~23.3 20.5m depth.

The clay mineral ratios for humidity proxies (Ka/Ch; Ka/Ill) show lower values except only one sample at ~14.4m (Fig. 9.2a). The low constant values in Sm/(Ill+Ch) ratio, and Ka/(Ill+Ch) shows low values (except one sample ~14.4m) indicating relatively less chemical weathering and weathering (Fig. 9.1b). The chemical weathering can be correlated with the precipitation in the region on temporal scales (Chamley 1989).

Therefore, these results are suggestive of the overall weakening monsoonal conditions with decreased humidity in the region (Thamban *et.al.* 2002). This interpretation is in conformity with the earlier studies from adjacent regions suggesting the weakening monsoonal condition since ~6ka B.P. (Enzel *et.al.* 1999, Prasad *et.al.* 2006, Deo *et.al.* 2011 and Alizali *et.al.* 2012).

**Zone-IV** - In Zone-IV (7.12 - 0.4m), the abundance of Smectite is mirrored by Chlorite with increasing values at lower half and decreasing values in upper half. The same pattern is followed by Illite crystallinity and chemistry values indicating the increased hydrolization at ~4m depth. The chemical weathering proxies Sm/(Ill+ch) and Ill/Ch indicates the increased chemical weathering in middle of this zone whereas the leaching and hydrolization proxies are in contrast suggesting the reduced leaching and degree of hydrolization in this portion (Fig. 9.1b). Even if we consider this phase as an individual spell of increased humidity conditions in the region and more or less the clay mineral records suggests the weaker monsoon with more of dry spells in climate during the Late Holocene times. Moreover, it is noteworthy here to point out that during the drying of the rann basin has seen marine regression phases and therefore the palaeoclimatic it is not necessary that the clay minerals in this particular zone are reflecting true signatures. It is also possible that largely the sediments of this zone are reworked and re-distributed during the regressive cycles.

#### **Berada Core**

**Zone-I (43.64 - 32.94m)** – The ~51m deep Berada core in its bottom most part consist of fluvial sands which are sandwiched by a small phase of marine ingressions (Maurya *et.al.* 2013). Two representative samples from these older marine sediments analyzed (~43 - 44m depth) whereas the overlying fluvial sediments are devoid of clay fraction. As mentioned above, overlying samples are from the persistent marine record above these fluvial sandwiched horizons. In marginal parts also the clay mineralogy is dominated by Illite, Chlorite whereas Smectite and Kaolinite remain present in relatively low proportions (Fig. 9.2a). Here the fluctuations are seen in the clay mineral abundance which may not essentially reflect of the climatic signature as the marine ingressions and regression phases primarily redistribute or influence the true signatures. Crystallinity values indicating lowering the degree of crystallinity whereas the positive slope of the

chemistry values indicates the tendency of cation loosing on account of hydrolysis (Adate *et.al.* 2000; Alizai *et.al.* 2012).

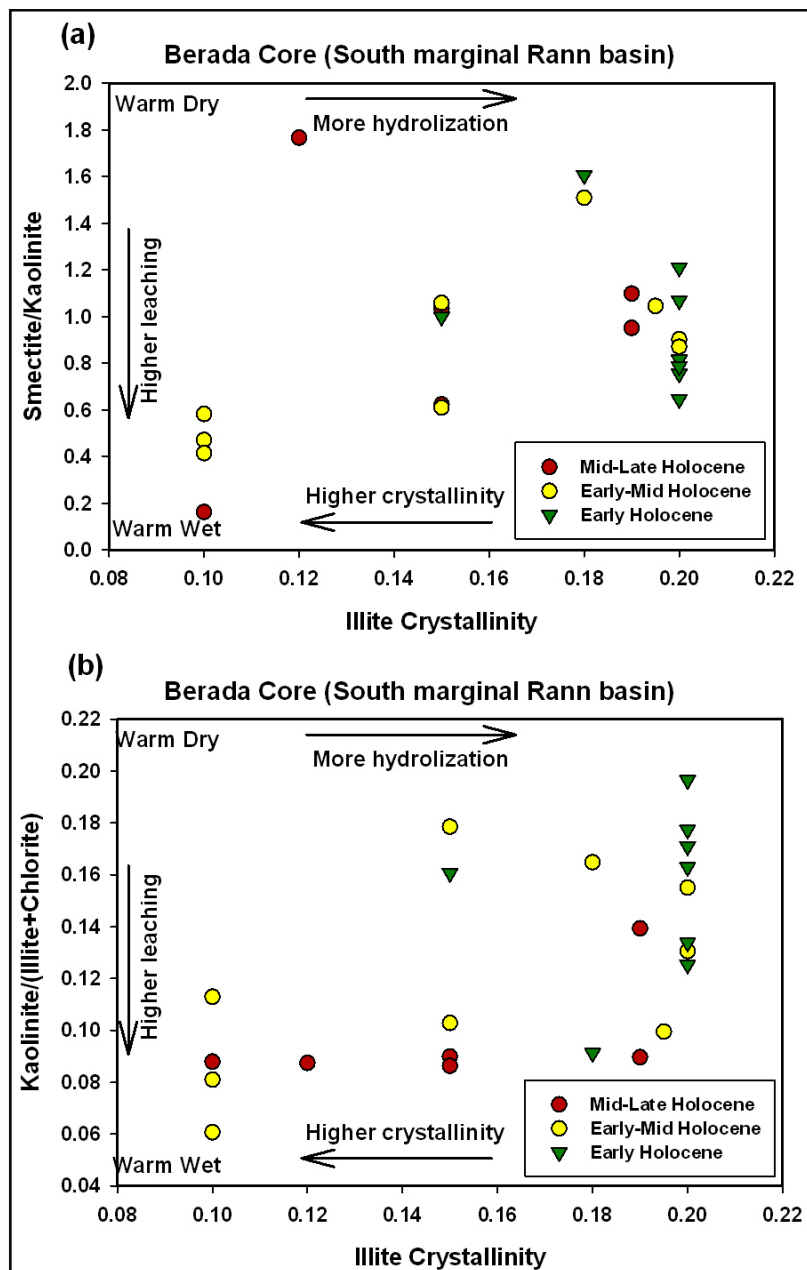


**Figure 9.5.** Plots showing Illite crystallinity Vs Chemical weathering proxies for the individual time frames for Dhordo Core samples. (a) Smectite/(Illite+Chlorite) Vs Illite crystallinity, and (b) Kaolinite/(Illite+Chlorite) Vs Illite crystallinity. Note that the E. Holocene values shows lowered degree of Illite crystallinity with increased hydrolyzation processes; Early-Mid Holocene values are more sparse and shows evidences of high-lower degree of hydrolyzation processes; whereas; Mid-Late Holocene values essentially shows higher order of leaching processes.

**Zone-II (32.94 - 19.4m)** - In this zone Illite and Chlorite abundance shows increase up in section, whereas, Smectite and Kaolinite shows antithetic relations from bottom to top of the section (Fig. 9.2a). The increased Kaolinite content is marked in bottom part of the zone when Smectite proportion is low and opposite trend in upper part of the zone. The Sm/ka ratio therefore suggests the enhanced leaching at the middle part (27 - 28m depth) of the graph (Fig. 9.2b).

The clay mineral ratio for climate proxies (Ka/Ch; Ka/Ill) show relatively humid phase in the bottom of the section whereas upper part of the zone shows lowered values indicating falling humidity and increased dry arid climate as also evident by increase in Smectite proportion (Fig. 9.2a and 9.2b). The Illite chemistry values are also roughly following this trend suggesting the decreased effects of hydrolysis in the upper part as compared with the lower part of the zone (Fig. 9.2a). These records pointing towards the strengthened monsoonal conditions between 8.4 to 7.2 ka with relatively changed environmental conditions at the bottom and top of the sections. Leaching and chemical weathering proxies are also in conformity with these signatures suggesting phase of strengthening monsoonal pattern after ~8.4ka B.P (Fig. 9.2a and 9.2b). Therefore, the Early Holocene strengthening monsoon signatures are also visible in the marginal parts of the basin that are seen from central portion of rann. Additionally, the time age control here in this case allows us to know the timings of intensification more precisely between 8.4 to 7.2 ka B. P.

**Zone-III (19.4 - 10.79m)** - This zone was deposited during pre-Mid Holocene times that records characteristic clay mineralogy showing extraordinary increased Smectite content and reduced Kaolinite and Illite abundance (Fig. 9.2a). Smectite is a typical weathering product of dry, arid climate indicating the increasing aridity in the region (Thiry, 2000). The chemical weathering proxy (Sm/(Ill+Ch) and leaching proxy (Ka/(Ill+Ch) together indicating the high chemical weathering and reduced leaching (Fig. 9.4b and 9.5b) are indicative of dry seasonal climatic conditions (Alizai *et.al.* 2012). Also, the climate proxies (Ka/Ch, Ka/Ill and Ka/Sm) together indicate dry seasonal climatic conditions prevailing during the deposition of these sediments (Chamley 1989, Thamban *et.al.* 2002). The recorded loss of the humid climate to seasonal dry period appears after 7ka BP, yet

the exact time is to be determined through more chronologic data. However the documented timing of aridity in Thar Desert records ~5.5 ka B.P. (Enzel *et.al.* 1999).

**Zone-IV (10.79 - 0.40m)** - The topmost zone of the Berada core is characterised by significant changes in the clay mineral records. Remarkable changes include the upward increase in Illite, and Kaolinite content whereas Smectite and Kaolinite shows decreased values to its lowest throughout the core (Fig. 9.2a). Climate proxies show (Ka/Ill, Ka/Ch) enhanced humid conditions, relatively increased values Sm/Ka ratio suggests enhanced leaching conditions which is also supported by the high values of Illite crystallinity and chemistry (Fig 9.2a and 9.2b). Ill/Ch ratio also suggests the increased chemical weathering during the deposition of these sediments (Fig 9.2b). Prior to interpret the results for this zone it is to be noted that on account of marine regression there might be significant changes in the sediment distribution, re-distribution in this region. Therefore, the sediments in the upper parts of the core may not reflect the true palaeoclimatic signatures.

### Sr-Nd ISOTOPIC STUDIES ON CORE SEDIMENTS

The present chapter deals with the provenance reconstructions of the Great Rann sediments. Identifying and characterization provenance of the sediment is one of the prime factors in understanding the overall evolution of a sedimentary basin. The Great Rann of Kachchh graben has accumulated huge amount of sediments since Late Pleistocene till it's drying in historical times. An attempt is made to understand the provenance of the rann basin, characterization of the hinterland sources and their transport pathways. The present study aims to characterize Sr-Nd isotopic composition of rann sediments with a view to find answers to the following questions-

- 1) From where the rann sediments are primarily derived?
- 2) What was the role of Kachchh hillocks and Aravallies in provenance evolution?
- 3) Was there any such large river system existed that supplied sediments to rann and to validate whether the much debated "mythical" Saraswati/Ghaggar river was responsible for the filling up of the Great Rann basin? And
- 4) Whether, the source of the rann sediments ever changed since LGM?

#### PROVENANCE STUDIES

Several tools are available for indentifying the source rock characteristics and erosion patterns in the hinterland regions. The most rapid proxy for such studies is clay mineral assemblage in the basin. Considering the minimum effect of the neoformed clay minerals, quantifying clay mineral assemblage is relatively easy and fast proxy for the provenance reconstructions. A large amount of published literature is available in this respect since late sixties. Clay mineralogy is successfully used as provenance proxy along the western coast of India and Arabian Sea (Rao and Rao, 1994; Kessarkar et.al. 2003; Chauhan et.al. 2006; Alizai et.al. 2012). However, there are several intricacies involved in the clay mineral quantification and certain post depositional processes that may change the overall clay mineral abundance/distributions. A detailed evaluation on this is discussed in

earlier chapter. Also, there are limitations in specifically characterizing the provenance discrimination on finer scale.

Other proxies for provenance characterization are- mineralogical assemblage (Alizai et.al. 2011), REE (LREE & HREE) pattern and dating specific minerals like feldspars, zircons, mica using Ar-Ar dating and U-Pb dating (McDaniel et.al., 1994; Clift et.al. 2001). One such powerful tool is the Sr-Nd isotopic studies of specific fraction or in bulk sediments depending on the purpose and type of sediments are to be studied. It is widely accepted as a precise provenance tracer in characterizing source, quantifying erosion rates and also in ocean water current circulation studies. There are several studies from Bay of Bengal and Arabian Sea documenting changes in erosion patterns, transport pathways and shift in the provenance for the accumulating sediments (France-Lanord et.al. 1993, Colin et.al. 1999, Clift et.al. 2002, Kessarkar et.al. 2003, Ahmed et.al. 2005, Singh et.al. 2008, Liu et.al. 2005, Clift et.al. 2008). In addition, there are few studies from the Indus river system (Clift et.al. 2008, Clift et.al. 2010), Thar Desert and their source (Tripathi et.al. 2004, Saini et.al. 2010; 2011, Tripathi et.al. 2013) Kachchh Volcanics (Sen et.al. 2009) and Aravallies using Sr-Nd isotopic composition. Therefore, due to its applicability and suitability, the temporal variations in Sr-Nd isotopes were carried out on the core samples for tracking the sources of the Great Rann sediments.

## **PROVENANCE TRACKING OF THE GREAT RANN SEDIMENTS**

The detailed methodology adopted for the sample processing, Sr and Nd extraction and isotopic measurements along with other technical details is discussed in Chapter 2. The Strontium and Neodymium isotopic compositions and their variations in the silicate fractions in the rann sediments from two shallow cores (Dhrodo and Berada) are given in Table 10.1 and 10.2 respectively. Detailed information of the sample depth, isotopic concentration and ratio is given in these tables. By virtue of its geographic location, the Great Rann basin is primarily expected to be characterised by multiple sediment sources. At present, only Nara river and Luni river exist which flow into the Great Rann in the northwestern and northeastern part. The eastern margin shows several rivers like Banas, Saraswati and Rupen river that arise in the Aravalli ranges. Several small rivers flow into the Rann from the Kachchh mainland in the south. However, all rivers except, Nara river are strongly ephemeral and are not known to carry significant amount of sediment loads.

**Table 10.1** Downcore variations in the  $^{87}\text{Sr}/^{86}\text{Sr}$  and Sr (ppm) isotopic concentration in the Dhordo and Berada Core in Great Rann basin of Kachchh, and rivers draining from the Aravallis.

<b>Sr No.</b>	<b>Sample ID</b>	<b>Depth (m)</b>	<b><math>^{87}\text{Sr}/^{86}\text{Sr}</math> (Corr.)</b>	<b>Sr (ppm)</b>	<b>Std Err. <math>^{87}\text{Sr}/^{86}\text{Sr}</math></b>	<b>Std Err. Sr ppm</b>
01	DH-1-24	0.48	0.728006	140.35	0.0014	0.0065
02	DH-2-36	1.72	0.727946	121.22	0.0013	0.0051
03	DH-3-37	2.94	0.725449	99.33	0.0012	0.0039
04	DH-4-26	3.93	0.725854	97.41	0.0014	0.0061
05	DH-4-44	4.29	0.726797	105.47	0.0014	0.0050
06	DH-5-22	5.02	0.726484	100.23	0.0015	0.0078
07	DH-5-48	5.54	0.726849	100.26	0.0009	0.0029
08	DH-6-35	7.1	0.727716	120.27	0.0009	0.0028
09	DH-7-62	11.18	0.727097	117.72	0.0009	0.0042
10	DH-8-62	14.48	0.726502	111.47	0.0014	0.0031
11	DH-9-38	16.96	0.726320	112.25	0.0015	0.0039
12	DH-10-21	18.61	0.726340	101.91	0.0015	0.0054
13	DH-11-15	20.52	0.728226	117.25	0.0016	0.0060
14	DH-11-49	21.2	0.730531	148.40	0.0011	0.0060
15	DH-12-64	23.34	0.728269	101.74	0.0020	0.0113
16	DH-13-24	25.38	0.728236	98.40	0.0019	0.0059
17	DH-14-29	26.64	0.730023	107.46	0.0009	0.0031
18	DH-14-119	28.44	0.729822	106.99	0.0018	0.0073
19	DH-15-29	29.93	0.730340	108.24	0.0014	0.0053
20	DH-15-89	31.13	0.730340	108.24	0.0014	0.0053
21	DH-17-72	36.67	0.731281	112.06	0.0009	0.0041
22	DH-18-79	39.77	0.732244	106.06	0.0008	0.0033
23	DH-19-74	42.91	0.732095	125.83	0.0010	0.0039
24	DH-19-129	44.01	0.732493	109.12	0.0014	0.0053
25	DH-20-79	46.15	0.730941	109.83	0.0013	0.0038
26	DH-21-29	48.22	0.731680	109.28	0.0018	0.0060

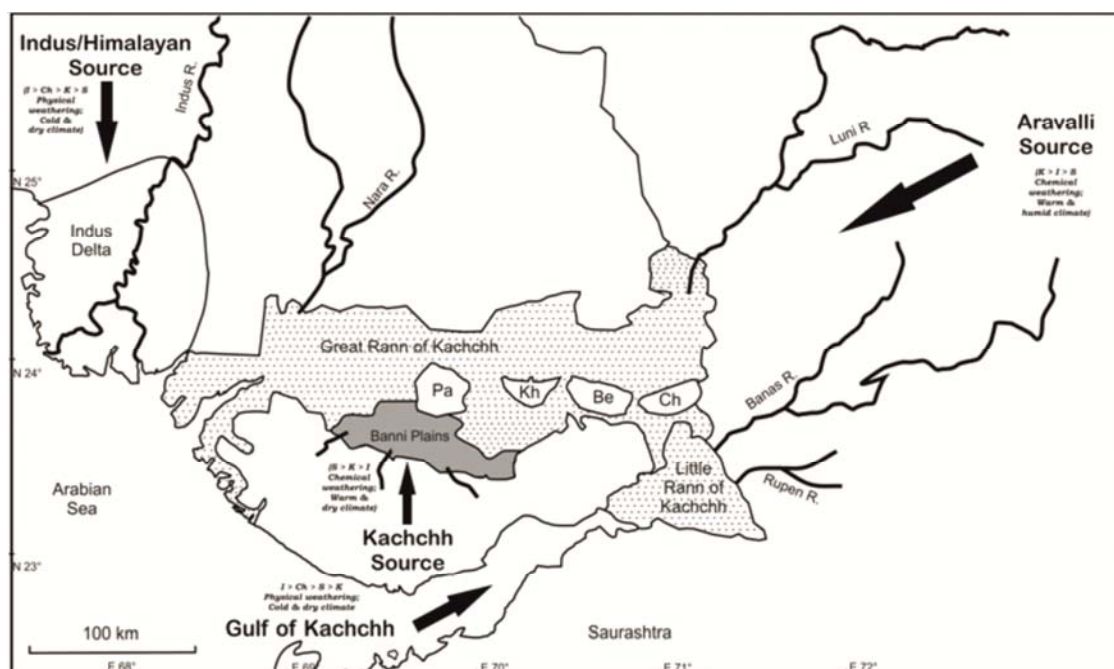
<b>27</b>	DH-22-49	51.57	0.731885	107.09	0.0017	0.0075
<b>28</b>	DH-23-39	54.5	0.730690	114.45	0.0012	0.0064
<b>29</b>	DH-24-51	58.45	0.730690	114.45	0.0012	0.0064
<b>30</b>	BRD-1-19	0.38	0.727538	106.84	0.0011	0.0041
<b>31</b>	BRD-3-48	3.21	0.727798	142.11	0.0009	0.0053
<b>32</b>	BRD-4-19	3.98	0.728257	109.12	0.0014	0.0053
<b>33</b>	BRD-4-86	5.32	0.728938	107.24	0.0014	0.0048
<b>34</b>	BRD-5-26	6.47	0.729601	108.43	0.0012	0.0052
<b>35</b>	BRD-5-134	8.63	0.729593	107.35	0.0014	0.0047
<b>36</b>	BRD-6-76	10.81	0.729793	105.89	0.0022	0.0115
<b>37</b>	BRD-7-106	14.5	0.729790	100.56	0.0017	0.0198
<b>38</b>	BRD-8-29	15.98	0.729671	102.11	0.0020	0.0085
<b>39</b>	BRD-8-109	17.58	0.730343	101.12	0.0010	0.0033
<b>40</b>	BRD-9-49	19.38	0.730625	96.86	0.0017	0.0053
<b>41</b>	BRD-10-139	24.57	0.732193	107.97	0.0008	0.0041
<b>42</b>	BRD-11-76	26.88	0.731435	107.90	0.0010	0.0039
<b>43</b>	BRD-12-19	29.16	0.730561	95.73	0.0011	0.0033
<b>44</b>	BRD-12-134	32.86	0.730625	96.86	0.0017	0.0053
<b>45</b>	BRD-13-26	32.96	0.728418	108.02	0.0008	0.0028
<b>46</b>	BRD-13-136	35.16	0.729996	101.47	0.0016	0.0036
<b>47</b>	BRD-14-16	36.38	0.731193	113.92	0.0015	0.0062
<b>48</b>	BRD-14-66	37.38	0.725077	102.70	0.0028	0.0080
<b>49</b>	BRD-16-19	42.92	0.730722	107.92	0.0011	0.0049
<b>50</b>	BRD-16-56	43.66	0.725320	87.22	0.0031	0.0092
<b>51</b>	BRD-17-16	47.18	0.725086	96.74	0.0020	0.0080
<b>52</b>	LUNI	Channel	0.730103	131.19	0.0009	0.0029
<b>53</b>	RUPEN	Channel	0.731141	83.97	0.0008	0.0026
<b>54</b>	SARASWATI	Channel	0.734564	57.80	0.0012	0.0034
<b>55</b>	BANAS	Channel	0.745289	53.04	0.0008	0.0019

**Table 10.2** Downcore variations in the  $^{143}\text{Nd}/^{144}\text{Nd}$ ,  $\epsilon\text{Nd}$  and Nd (ppm) isotopic concentration in the Dhordo and Berada Core in Great Rann basin of Kachchh, and rivers draining from the Aravallis.

Sr No.	Sample ID	Depth (m)	$^{144}\text{Nd}/^{143}\text{Nd}$	$\epsilon\text{Nd}_{(\text{CHUR0})}$	Nd (ppm)	$^{144}\text{Nd}/^{143}\text{Nd}$ (% Err.)	$\epsilon\text{Nd}$ (% Err.)	Nd (ppm) (% Error)
1	DH-1-24	0.48	0.511926	-13.88	17.33	0.0008	0.54	0.0031
2	DH-2-26	1.72	0.511934	-13.74	16.95	0.0008	0.60	0.0021
3	DH-3-37	2.94	0.511990	-12.64	14.87	0.0007	0.57	0.0025
4	DH-4-26	3.93	0.511974	-12.96	14.73	0.0010	0.79	0.0035
5	DH-4-44	4.29	0.511969	-13.04	15.45	0.0010	0.77	0.0032
6	DH-5-22	5.02	0.511991	-12.63	15.02	0.0011	0.90	0.0031
7	DH-5-48	5.54	0.511987	-12.70	14.75	0.0019	1.52	0.0044
8	DH-6-35	7.10	0.511924	-13.93	16.39	0.0008	0.57	0.0023
9	DH-7-62	11.18	0.511941	-13.60	17.16	0.0007	0.51	0.0022
10	DH-8-62	14.48	0.511965	-13.14	14.95	0.0007	0.51	0.0020
11	DH-9-38	16.96	0.511987	-12.70	15.35	0.0008	0.64	0.0021
12	DH-10-21	18.61	0.511967	-13.08	15.14	0.0009	0.67	0.0026
13	DH-11-15	20.52	0.511958	-13.26	16.39	0.0006	0.47	0.0022
14	DH-11-49	21.2	0.511877	-14.84	17.20	0.0007	0.50	0.0018
15	DH-12-64	23.34	0.511927	-13.87	15.53	0.0009	0.64	0.0027
16	DH-13-24	25.38	0.511926	-13.89	15.07	0.0009	0.66	0.0025
17	DH-14-29	26.64	0.511920	-14.00	16.57	0.0008	0.56	0.0018
18	DH-14-119	28.44	0.511943	-13.57	16.18	0.0010	0.71	0.0029
19	DH-15-29	29.93	0.511935	-13.71	15.25	0.0007	0.53	0.0025
20	DH-15-89	31.13	0.511935	-13.72	17.23	0.0014	1.02	0.0052
21	DH-17-72	36.67	0.511911	-14.18	18.99	0.0006	0.42	0.0019
22	DH-18-79	39.77	0.511922	-13.97	16.86	0.0010	0.70	0.0035
23	DH-19-74	42.91	0.511911	-14.19	15.43	0.0009	0.66	0.0025
24	DH-19-129	44.01	0.511903	-14.34	16.00	0.0013	0.90	0.0039
25	DH-20-79	46.15	0.511915	-14.10	17.22	0.0005	0.33	0.0014
26	DH-21-29	48.22	0.511919	-14.03	16.63	0.0004	0.31	0.0015

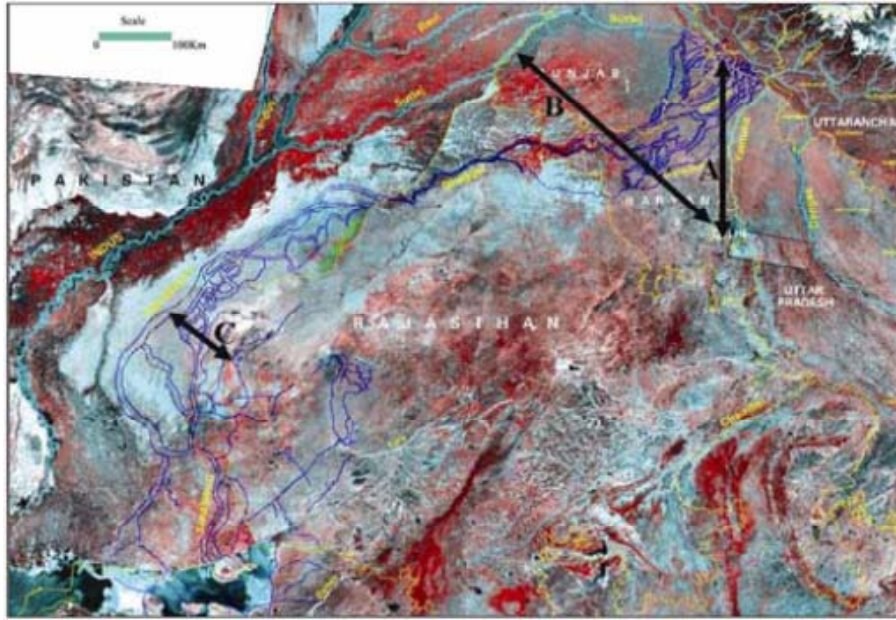
27	DH-22-49	51.57	0.511908	-14.23	17.33	0.0013	0.89	0.0034
28	DH-23-39	54.5	0.511933	-13.75	17.21	0.0004	0.32	0.0014
29	DH-24-51	58.45	0.511918	-14.05	17.41	0.0009	0.63	0.0023
30	BRD-1-19	0.38	0.511933	-13.75	15.96	0.0010	0.72	0.0024
31	BRD-3-48	3.21	0.511881	-14.76	19.22	0.0005	0.34	0.0017
32	BRD-4-19	3.98	0.511921	-13.98	16.28	0.0012	0.89	0.0036
33	BRD-4-86	5.32	0.511915	-14.11	16.11	0.0006	0.45	0.0022
34	BRD-5-26	6.47	0.511918	-14.05	15.15	0.0006	0.43	0.0017
35	BRD-5-134	8.63	0.511910	-14.20	16.37	0.0006	0.42	0.0020
36	BRD-6-76	10.81	0.511926	-13.89	15.88	0.0005	0.35	0.0018
37	BRD-7-106	14.5	0.511934	-13.74	15.34	0.0010	0.71	0.0030
38	BRD-8-29	15.98	0.511927	-13.88	15.39	0.0009	0.65	0.0029
39	BRD-8-109	17.58	0.511935	-13.72	7.94	0.0006	0.47	0.0017
40	BRD-9-49	19.38	0.511925	-13.91	16.46	0.0006	0.45	0.0024
41	BRD-10-139	24.57	0.511884	-14.70	17.22	0.0007	0.44	0.0019
42	BRD-11-76	26.88	0.511910	-14.21	17.36	0.0006	0.39	0.0014
43	BRD-12-19	29.16	0.511939	-13.63	15.52	0.0011	0.80	0.0042
44	BRD-12-134	32.86	0.511910	-14.20	15.63	0.0007	0.47	0.0026
45	BRD-13-26	32.96	0.511907	-14.26	15.35	0.0017	1.21	0.0055
46	BRD-13-136	35.16	0.511921	-13.99	16.57	0.0006	0.44	0.0014
47	BRD-14-16	36.38	0.511910	-14.19	15.96	0.0005	0.34	0.0018
48	BRD-14-66	37.38	0.511987	-12.71	9.48	0.0010	0.82	0.0027
49	BRD-16-19	42.92	0.511934	-13.72	16.13	0.0018	1.34	0.0058
50	BRD-16-56	43.66	0.511978	-12.87	11.33	0.0012	0.93	0.0025
51	BRD-17-16	47.18	0.511864	-15.11	13.95	0.0017	1.10	0.0051
52	LUNI	Channel	0.511922	-13.97	4.48	0.0029	2.10	0.0052
53	RUPEN	Channel	0.511876	-14.86	17.71	0.0005	0.34	0.0015
54	SARASWATI	Channel	0.511858	-15.22	5.60	0.0016	1.05	0.0031
55	BANAS	Channel	0.511865	-15.08	6.45	0.0065	4.30	0.0119

Figure 10.1 shows the possible sources of sediments with regard to the Kachchh basin. None of these rivers appear to be capable of filling up a large sedimentary basin like the Great Rann. However, it has been inferred that there was a large south flowing river system/s called the Saraswati river that originated in the Himalaya and flowed through the Thar desert and debouched into the Great Rann in post-LGM time (Oldham, 1928; Gleine and Evans, 1976; Valdia, 2002). The Saraswati-Ghaggar river system is identified from a series of palaeochannels mapped in the Thar desert and further north upto the foot hills of the Himalaya (Ghose et.al. 1979; Kar and Ghose, 1984). The evidence that these channels were active as recently as ~6- 2.9ka B.P. in the Thar desert has been revealed by OSL dating on fluvial sediments occurring these channels (Saini et.al. 2009).



**Figure 10.1** Map of Kachchh and adjoining regions showing multiple sediment sources.

In view of the strong possibility of the mixing of sediments from multiple hinterland sources, the Sr-Nd isotopic data generated on the core sediments were interpreted in the light of available isotopic signatures of all possible source regions. A comparison of the isotopic signatures of the possible sources are shown in Table 10.3.



**Figure 10.2** Satellite image showing the course of palaeo Saraswati River (Source: RRSSC, Jodhpur). A, Delhi–Kalka Ridge; B, Delhi–Sargodha Ridge; C, Jaisalmer–Mari Arch. (after Mitra and Bhadu, 2012).

**Table 10.3**  $^{87}\text{Sr}/^{86}\text{Sr}$  and  $\epsilon\text{Nd}$  isotopic composition of the potential end members for the rann sediment provenance.

Sr. No.	Site/Location	$^{87}\text{Sr}/^{86}\text{Sr}$	$\epsilon\text{Nd}$	Reference
1	Keti Bander, Indus delta	0.710 to 0.727	-10.80 to -15.20	Clift et.al. 2010
2	Ghaghar River	0.737 to 0.750	-15.30 to -16.60	Saini et.al. 2010
3	Thar Desert alluvium	0.729 to 0.734	-12.60 to 15.80	Saini et.al. 2011
4	Gularchy, Indus plains	0.719 to 0.725	13.20 to 14.20	Clift et.al. 2010
5	Kachchh volcanics	0.703 to 0.709	-3.46 to 6.39	Sen et.al. 2009
6	Luni R. (Aravallis)	0.7301	-13.96	Present Study
7	Rupen R. (Aravallis)	0.7311	-14.80	Present Study
8	Saraswati R. (Aravallis)	0.7346	-15.22	Present Study

Geographically, the Thar desert and Aravalli ranges in the north and east and Kachchh mainland in the south are the nearest sediment sources which can contribute to the Great Rann sediments. However, the Sr isotope values of rann sediments show considerable variations in radiogenic character from bottom to top. Generally,  $^{87}\text{Sr}/^{86}\text{Sr}$  ratio values are observed as less radiogenic for mafic rocks like basalts, Ophiolites ( $\sim 0.70$

- 0.71) and high radiogenic for older granitic (felsic) rocks those ranges from 0.73 and more (Singh et.al. 2008, Tripathy et.al. 2013).

It is evident that the rann sediments from both the cores contain high radiogenic Sr than the average Arabian Sea sediments (Fig. 10.3). Also, the typical Indus derived sediments in the lower reaches are less radiogenic in Sr as compared with rann (Fig. 10.3) indicating the high radiogenic character of the provenance regime. When compared with the surrounding lithologies, the present results do not indicate the proximal source like Deccan volcanic ( $^{86}\text{Sr}/^{87}\text{Sr} \sim 0.704$ , Sen et.al. 2009), Mesozoic and Tertiary lithologies in the Kachchh basin as they comprise low Sr radiogenic character. In fact the rann sediments are more inclined towards the older high radiogenic granitic terrains (Singh et.al. 2008). Such high Sr values are known from Lesser and Higher Himalayan terrains, Karakoram and in Siwaliks (Singh et.al. 2008, Clift et.al. 2002 and references therein).

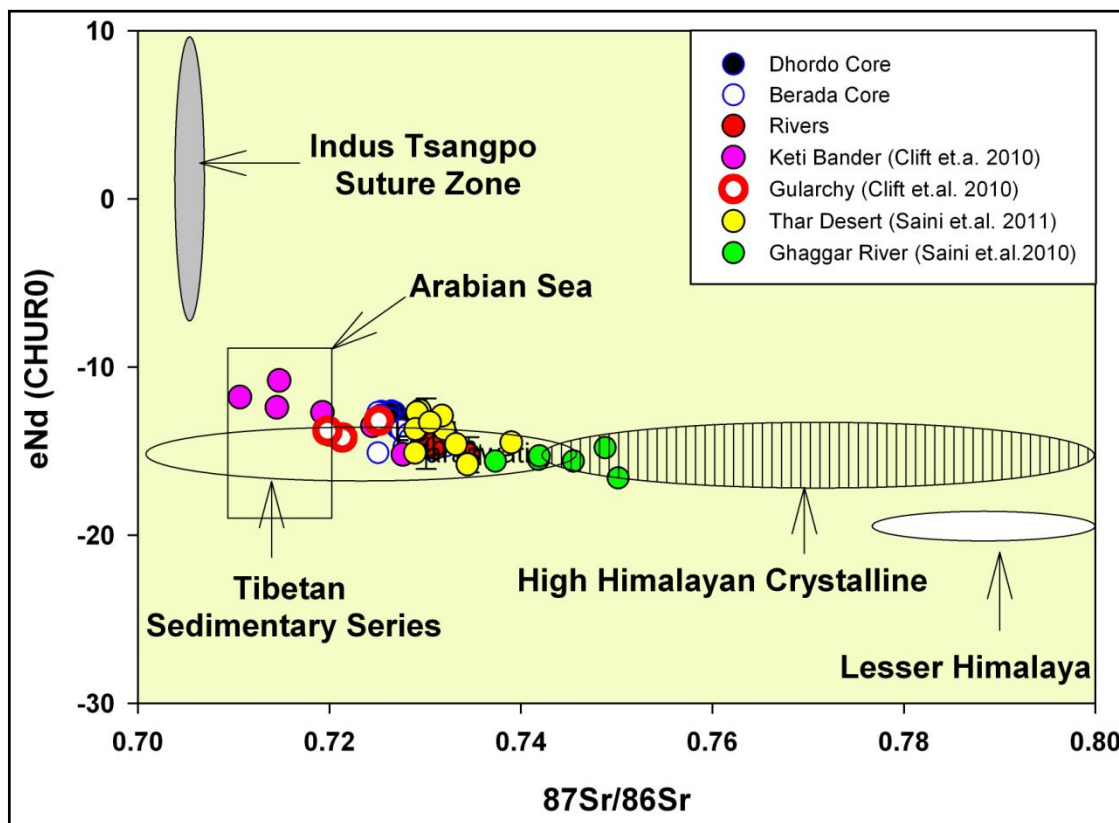


**Figure 10.3** Scatter plot showing the distribution of  $^{87}\text{Sr}/^{86}\text{Sr}$ ,  $\epsilon\text{Nd}$  isotopic composition of the Arabian Sea (Clift et.al. 2010; Kessarkar et.al. 2003), Indus-Tsangpo suture zone, Tibetan Sedimentary Series, High Himalayan Crystallines and Lesser Himalaya (Tripathy et.al. 2013 and references therein). Note that the Dhordo and Berada core samples show high radiogenic Sr values than the Arabian Sea and less radiogenic Nd.

The other possible source may be from the Aravallies as the modern channel sands analysed in the present study from Aravalli draining rivers which yielded high values. The Rupen and Saraswati rivers shows high  $^{86}\text{Sr}/^{87}\text{Sr}$  values  $0.73114 \pm 0.0008$  and  $0.73456 \pm 0.0012$  and less  $\epsilon\text{Nd}$  values  $-14.86 \pm 0.34$  and  $-15.22 \pm 1.05$  respectively. On the other hand, River Luni covers large range of  $\epsilon\text{Nd}$  i.e.  $-13.97 \pm 2.1$  and  $^{86}\text{Sr}/^{87}\text{Sr}$   $0.73010 \pm 0.0008$  that covers few samples of central basin (Figure 10.4; Table 10.3). The samples of the rivers studied here yield more or less close to rann sediment values with a narrow range for Sr content but variable  $\epsilon\text{Nd}$  values (Figure 10.4).

Considering these values one would conclude the primary source from the Aravallies but there are several factors to keep in mind before interpretations. If the dominating source is from the Aravallis then it should also reflect on the grain size, mineralogy of the sediments specifically during its short transport which is not clearly evident in rann. Instead, the rann sediments are characteristically fine grained nature i.e. silty-clay to clayey silts (Maurya et.al. 2013), dominated by white mica which is similar with the Indus derived sediments in offshore (Nair et.al. 1982, Kessarkar et.al. 2003). The Aravalli range, due to its proximity could be a possible source (with high  $^{86}\text{Sr}/^{87}\text{Sr}$  and lower  $\epsilon\text{Nd}$ ), however considering its lower relief, this proposition seems unlikely.

The Thar Desert occurring in the north is a complex terrain that may have played role in rann sedimentation that also is to be determined. The end member mixing plot (Figure 10.4) shows large scale variability in Sr-Nd isotopic composition of Thar sediments (Tripathy et.al. 2004, Saini et.al. 2010; 2011, Tripathy et. al. 2013 and references therein) that covers most of the rann sample values. Isotopically, such a large spread of the Sr-Nd isotopic composition appears similar with the rann sediments.

Again, in this case, understanding the sediment transport pathways and their dispersal mechanisms becomes important to understand the process of sedimentation in the basin. Looking into the possibilities, presently there are no rivers originating in the Thar that flow into the Great Rann. Neither there are any evidence of flood waters of the Indus and from the north reaching at both the core sites that may contribute sediments to the rann. This is also corroborated by the mono-dominant finer grain size pattern in the core sediments. The possibility of the aeolian transport is also ruled out as it could not be the primary mechanism to fill such a huge basin with selective mud deposition that is in

contrast with the sandy nature of the typical Thar sediments. Based on this deductive approach, the present scenario needs a suitable mechanism to explain the rann sediment filling by high radiogenic Sr source. Looking into the possibility of a large scale fluvial system draining through the high Sr-radiogenic lithologies in the hinterland and that could also supply high amount of fine grained sediments for the rann basin filling appears the most suitable mechanism.

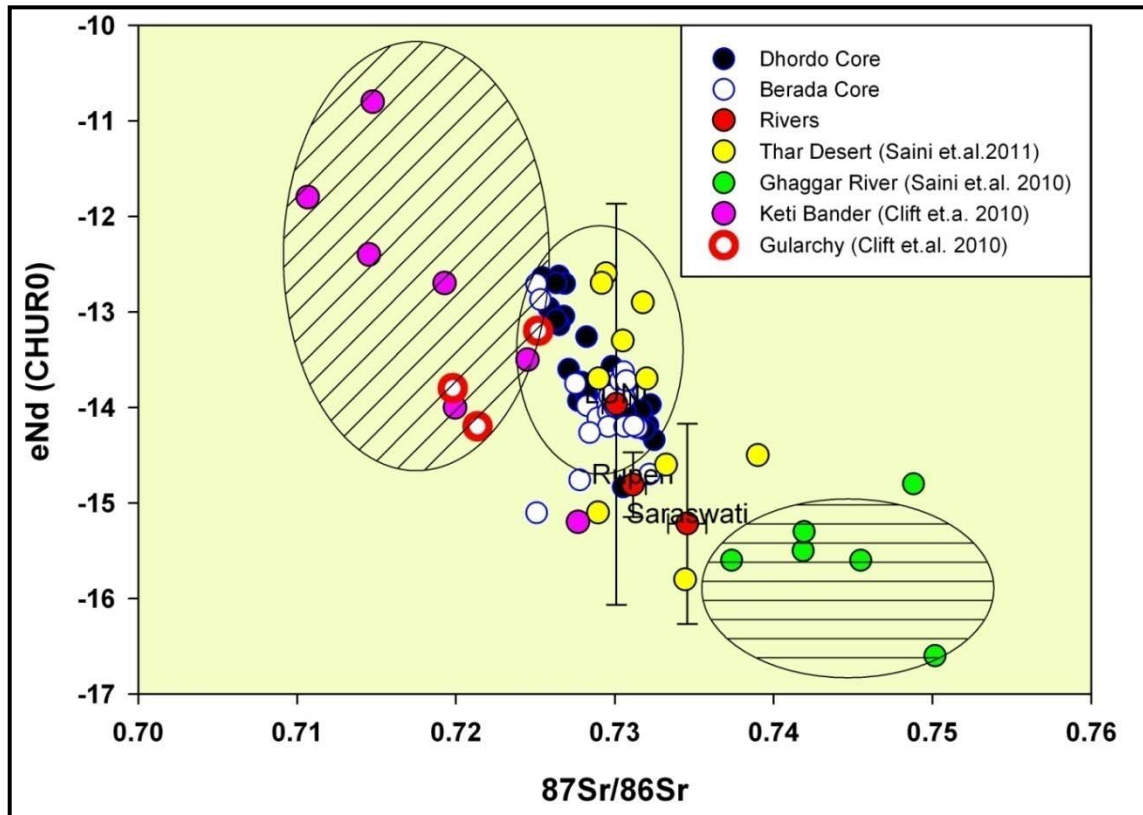


**Figure 10.4** Scatter plot showing the Sr-Nd isotopic composition of the Rann sediments from Dhordo and Berada Cores with various potential end members. Note that the Thar Desert values are from 1.8-9.1ka B.P. old sediments; Ghaggar River 3.4ka B.P.; 0 to 28ka B.P. and Gularchy 3-11ka B.P.

Such sub-Himalayan born large scale river/river system that flowed into rann is generally agreed to have existed during the recent past (Clift et.al. 2012, Glennie and Evans, 1976, Ghose et.al. 1969, Saini et.al. 2009). Several previous workers have contended that the river Indus and/or its distributary have contributed the sediments to the Great Rann of Kachchh in large proportion. In relation to this hypothesis, there may be two possibilities of large scale fluvial transport, either by the major tributaries of Indus or an independent river system with a potential to carry and supply huge sediments to the

basin i.e. Ghaggar/Saraswati. Isotopically, River Indus is one of the well studied river basin right from its point of origin to its flood plains, delta and also in offshore (Clift et.al., 2002, Clift et.al. 2010; Limmer et.al. 2012 and references therein). If River Indus predominantly provided sediments to rann, one would expect a good match in Sr-Nd isotopic composition of rann sediments with the river Indus, or similar values with another ancient large scale river system that existed in the region i.e. Ghaggar/Saraswati. Instead, the rann sediments are slightly different in the Sr-Nd composition with both these sources indicating mixing of more than one source in the hinterland before debouching into the Great Rann of Kachchh basin.

River Indus shows characteristically lower Sr/Sr values (less radiogenic Sr) as compared with the rann, whereas, the Ghaggar sediments comprises higher radiogenic Sr (Fig. 10.4). Also, varying Nd radiogenic character in bulk sediments is observed from upper to lower reaches of the Indus river system on account of the mixing of sediments from various lithologies (Clift et.al. 2002). The Sr-Nd isotopic character at the lower reaches of the Indus River differs with the rann values even after sediment mixing in uplands which negate the role of Indus predominant source for the rann sediments. Temporal records of Dhordo and Berada cores also shows opposite trends in  $^{86}\text{Sr}/^{87}\text{Sr}$  / $\epsilon\text{Nd}$  reduction/increase that clearly indicates that the sediments is unlikely to be attributed to increased input from the Indus distributary and/or alongshore transport of sediments into the rann (Fig. 10.5). When compared with the  $\epsilon\text{Nd}$  record of Keti Bunder for ~14ka till recent with the Dhordo and Berada cores, it is found that the Indus delta contains high radiogenic Nd source whereas the rann basin cores in contrast with Indus show low radiogenic Nd. Similarly, from terminal Pleistocene times to Early Holocene times the Indus delta shows high Nd values that remain almost stable till recent times. In contrast to these, the Dhordo and Berada cores show lowest radiogenic Nd at the bottom part above which the Nd radiogenic character increases upward.

The Sr-Nd isotopic studies in the fluvial sediments of Ghaggar-Hakra river also falls comparable with the Thar values for  $^{87}\text{Sr}/^{86}\text{Sr}$  0.73736 to 0.735016 and 0.72894 to 0.73444 and  $\epsilon\text{Nd}$  values ranges from -14.8 to -16.6 and -12.7 to -15.9 respectively (Saini and Mujtaba 2010, Tripathy et.al. 2004) but Ghaggar shows slightly high radiogenic Sr content (Fig. 10.4). This means the rann Sr values are less radiogenic than the Ghaggar-

Hakra river sediments that studied by Saini and Mujtaba, 2010, Tripathi et.al. 2004; 2013). Such decrease from the hinterland to the depositional basin is also observed in Indus system on account of mixing of various lithologies (Alizai et.al. 2011, Clift et.al. 2002). Hence the consistently high radiogenic Sr values in rann basin throughout the post Last Glacial Maximum approaches closer with the Ghaggar/Saraswati river sediments and to those of Thar Desert. U-Pb dating on Zircon grains by Clift et.al. (2012) also suggested that, the northern Thar region must have been an area with several major confluences and a large river with a combined flow arguably sufficient to reach as far as the Arabian Sea.

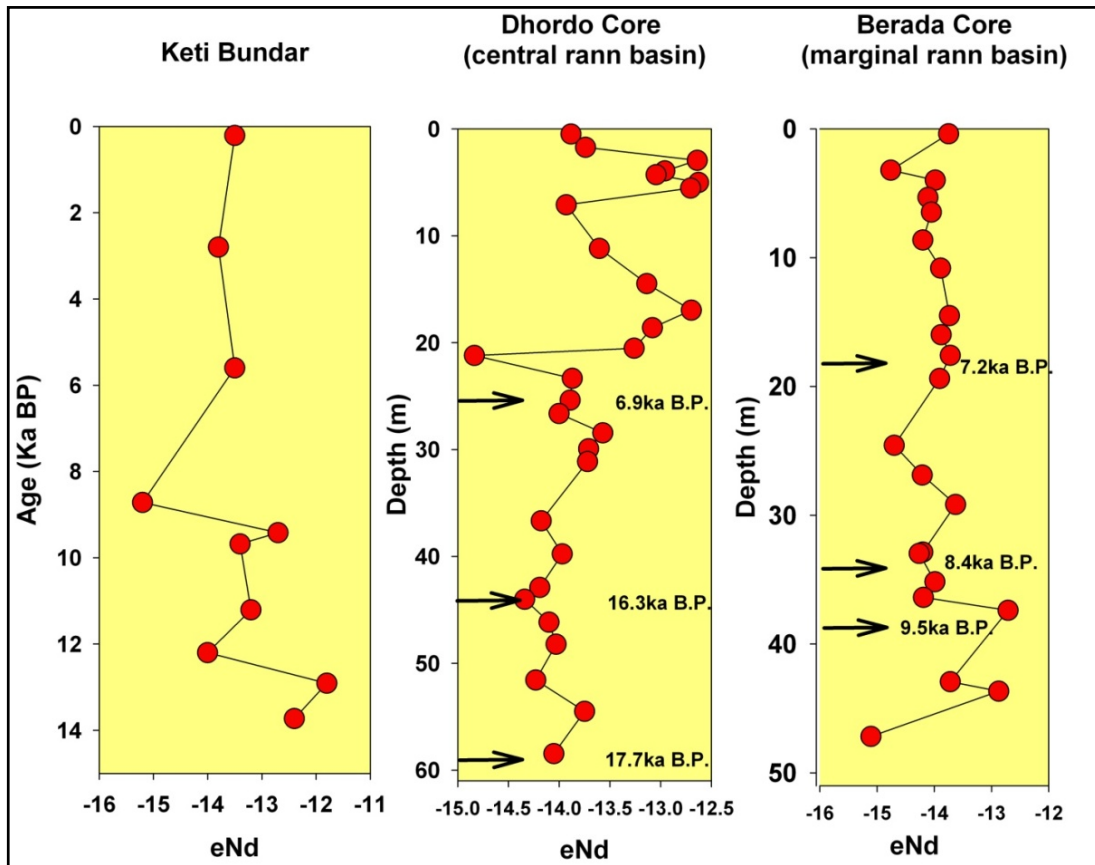


**Figure 10.5** Temporal scale variations in eNd values of Ketibundar (Indus delta), Dhordo Core (central rann basin) and Berada Core (marginal rann basin). Note that the Indus delta at its bottom to top varies with high to low radiogenic Nd (with stable values during most of the Holocene) whereas the rann samples as both locations shows opposite trend i.e. low radiogenic Nd at the bottom that changes into high radiogenic Nd upwards.

Integrating the data of the two cores with the available data from surrounding areas, it appears that a mighty river system i.e. Ghaggar/Saraswati in the north of the rann basin provided maximum amount of sediments to the rann basin since the post glacial

times till recent past. The present study provides concrete evidence for the existence of the Ghaggar/Saraswati drainage systems in the past as inferred by several previous (Oldham, 1893, Yashpal et.al. 1980, Kar and Ghosh 1984, Radhakrishna 1999, Kochar 2000; Valdia 2002, Ghose et.al. 1939, Kar and Ghose 1984, Clift et.al. 2012). Also, around 2/3<sup>rd</sup> of Harappan settlements (~1500 sites) that occurs in along the dried up palaeo-courses of the Saraswati river (Misra 1993).

### **TEMPORAL VARIATIONS IN DHORDO CORE**

This 60m long core is located in the central part of the Great Rann basin. Presence of marine microfossils (foraminifera) in the central Dhordo core (~61m depth) indicates the prevailing shallow marine environments during the deposition of these sediments. The down core variations in the Sr and Nd isotopic concentration and composition show interesting variations with a considerably large range. The  $^{87}\text{Sr}/^{86}\text{Sr}$  values ranges within 0.72545 to 0.73249 whereas  $\epsilon\text{Nd}$  varies from -14.84 to -12.63 indicating significant shifts in the provenance of the sediments. The major shifts occur near ~21m depth from the surface. Similar changes are also noted in clay mineralogy of these sediments. The grain size and other proxies also correlate with the large shift in the  $^{87}\text{Sr}/^{86}\text{Sr}$  proxy values suggesting a significant change in the environmental conditions of the basin. Interestingly, the isotopic concentration largely ranges in a relatively narrow band in the Lower zone of the core. The broad potential end member distribution for these sediments lies in Indus-Himalayas-Thar-Ghaggar-Aravalli-Kachchh Mainland Hills (Biswas 1993, Oldham 1928, Gleinee and Evans 1976 and others).

#### **Late Pleistocene sedimentation (~18 to ~16ka B.P.)**

In this zone, during the Late Pleistocene times, the  $^{87}\text{Sr}/^{86}\text{Sr}$  ratio varies from 0.73069 to 0.73249 and  $\epsilon\text{Nd}$  ranges from -14.34 to -13.75. From bottom to top of this core, the overall Sr ratio values marks positive shift indicating an increase in the Sr radiogenicity. However the maximum  $^{87}\text{Sr}/^{86}\text{Sr}$  value is recorded at ~44m depth (Fig. 10.6). Overall high values of  $^{87}\text{Sr}/^{86}\text{Sr}$  ratio essentially indicate the high radiogenic source for the rann sediments in the central part of the basin. Interestingly, during this time, the sediment supply to the rann basin was maximum with ~11mm/year sedimentation rate. In Dhordo core this high sediment input is marked by the occurrence of increase in silt

content and presence of laminated sediments. The  $^{87}\text{Sr}/^{86}\text{Sr}$  ratio in this zone indicates the relative less mixing of low radiogenic Sr flux. The  $^{87}\text{Sr}/^{86}\text{Sr}$  remains more radiogenic than the Luni river and less than Ghaggar river values and the  $\epsilon\text{Nd}$  values are closer to the Aravalli rivers (Fig. 10.4). This could be on account of the combined higher sediment input from the Himalayas and Aravallis during this time (Fig. 10.4; Fig. 10.6).

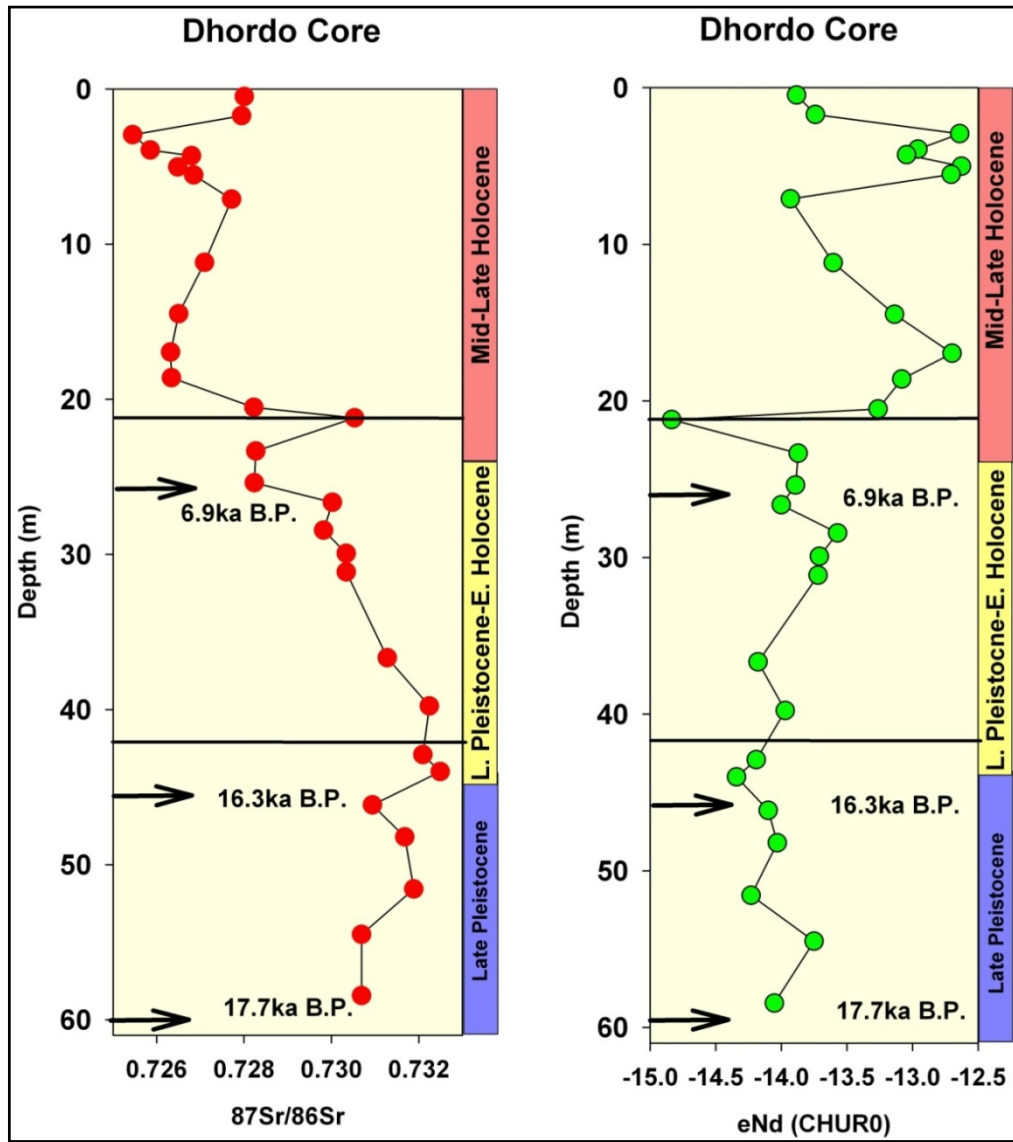


**Figure 10.6** Temporal variations in  $^{87}\text{Sr}/^{86}\text{Sr}$  and  $\epsilon\text{Nd}$  in Dhordo Core.

The clay mineralogy data shows cyclic changes in the humidity suggesting the punctuated spells of strengthening monsoonal conditions. However, the Himalayan terrain comprised greater snow cover during this time span that resulted in less erosion (Owen et al. 2002, Tripathi et al. 2011). Therefore, the sediment supply from the Himalayas at

this time may have been relatively less. However, non-glaciated sub-Himalayan terrain lithologies may have comprised the main bulk of sediment contribution from the north. On the other hand, the Aravallis, that also contains the high Sr (Fig. 10.4) also appears to have contributed significantly. The decreased chlorite content and increased kaolinite in the clay fraction evidenced in the clay mineralogy results support this contention. Furthermore, the dominant fine grained sediments comprises high amount of mica-illites and chlorites. The dominant illite and chlorite in the fine grained fraction revealed by X-Ray Diffraction studies indicates Himalayan input in the rann during the Late Pleistocene times. Therefore, it interpreted that during the Late Pleistocene, the Great Rann basin was filled with sediments from two sources – one from the non-glaciated lower Himalayas through the Ghaggar/Saraswati drainage system and Aravallis from the eastern side. The high sedimentation rate is attributed to the combined sediment input to the basin from two source regions.

#### **End Late Pleistocene and Early Holocene (~16ka to ~6ka)**

This unit covers a large span of time that witnessed significant climatic shifts from poor monsoonal conditions through the Terminal Pleistocene times to humid conditions with high monsoon intensity during the Early Holocene. The sedimentation model suggests many fold decrease in sedimentation rate (~2.04mm/year) at the central part of the basin. The timing of abrupt change in rate of sedimentation could not be precisely constrained due to limited chronologic data. The Sr-Nd isotopic composition shows significant changes during 16.3 to 7.1ka B.P. (Fig. 10.6). The  $^{87}\text{Sr}/^{86}\text{Sr}$  ranges from 0.73224- 0.72824 and  $\epsilon\text{Nd}$  show -13.57 to -14.84 values. The upward core values of  $^{87}\text{Sr}/^{86}\text{Sr}$  ratio shows a steep negative gradient indicating rapid decrease in radiogenic Sr in the sediments. These values are more radiogenic than the western Indus river sediments but less than the Ghaggar river. However, the Aravalli drainages show the comparable values (Fig. 10.4). The  $\epsilon\text{Nd}$  values on the other hand shows affinity to the values of Keti Bunder core in the Indus delta (Clift et. al., 2010) as compared with the largely variable Aravalli rivers. The high radiogenic Sr content at bottom of this unit may be derived from the Aravalli source as indicated above in the text, but the negative shift in the  $^{87}\text{Sr}/^{86}\text{Sr}$  ratio and the well constrained  $\epsilon\text{Nd}$  values matching with the Keti bander site points towards the influx from the mixed source in the confluence located to the north of the

rann. It is clearly evident that there is no single source dominates for the rann sediments. The river Ghaggar/Saraswati and river Luni (Aravalli) both contain more radiogenic Sr as compared with the upward decreasing values in this unit. To lose the radiogenicity there must be a mixing from less radiogenic Sr content which is documented from the lower reaches of Indus to into the off Arabian sea (Limmer et.al. 2012). This suggests the increasing influence due to mixing of less radiogenic Sr source towards the Mid-Holocene times. Another possibility is that, the decrease in Sr radiogenic component on account of the relative decrease from the source regions itself. This was the timing of the weakening strength of the river Ghaggar/Saraswati in hinterland ~6.5ka B.P. as documented by earlier studies (Tripathy et.al. 2013). Therefore, the observed strong negative shift in the  $^{87}\text{Sr}/^{86}\text{Sr}$  ratio may be on account of the decreased contribution from the Ghaggar/Saraswati river into the rann basin during the Early Holocene times. Consistent decrease/increase in  $^{87}\text{Sr}/^{86}\text{Sr}$ / $\epsilon\text{Nd}$  isotopes of sediments during Early to Mid Holocene times indicates gradual decline in sediment supply from the Ghaggar/Saraswati.

#### **Mid-Late Holocene**

During this time, the Sr radiogenic character further reduces as clearly seen in the graph between 19m depth towards top. These variations suggests the dilution effect on the high radiogenic Sr. That may happen either due to the abandonment of the large river system (less high radiogenic input to the basin) or increase in the Indus or Arabian Sea (contains low radiogenic Sr) influence in the rann basin. The upper part of this zone showing the wide scale fluctuations that may be on account of the regressive processes and/or sediment redistribution during the recent past.

#### **TEMPORAL VARIATIONS IN BERADA CORE**

In this core raised from the Banni plain forming the southern margin of the Great Rann basin which as submerged tentatively at the onset of the Early Holocene. The Sr-Nd isotopic variations are restricted in a narrow range except the bottom section of this core. The  $^{87}\text{Sr}/^{86}\text{Sr}$  varies from highest 0.72508 to low value 0.73219; and  $\epsilon\text{Nd}$  shows variations from -15.11 to -12.71 respectively. The lowest  $^{87}\text{Sr}/^{86}\text{Sr}$  values in Berada core are observed near the bottom core section at ~37m and 42 - 44m (Fig. 10.4). Environmentally, during this time the sediments were deposited after a fluvial phase that was terminated by the marine transgression during the Early Holocene. From ~37m towards the core top the

$^{87}\text{Sr}/^{86}\text{Sr}$  and  $\epsilon\text{Nd}$  values remains in a narrow range though all are high radiogenic as compared with the lower values. High Sr values are seen between 33-27m depths above which a significant decrease in the radiogenic Sr is observed.

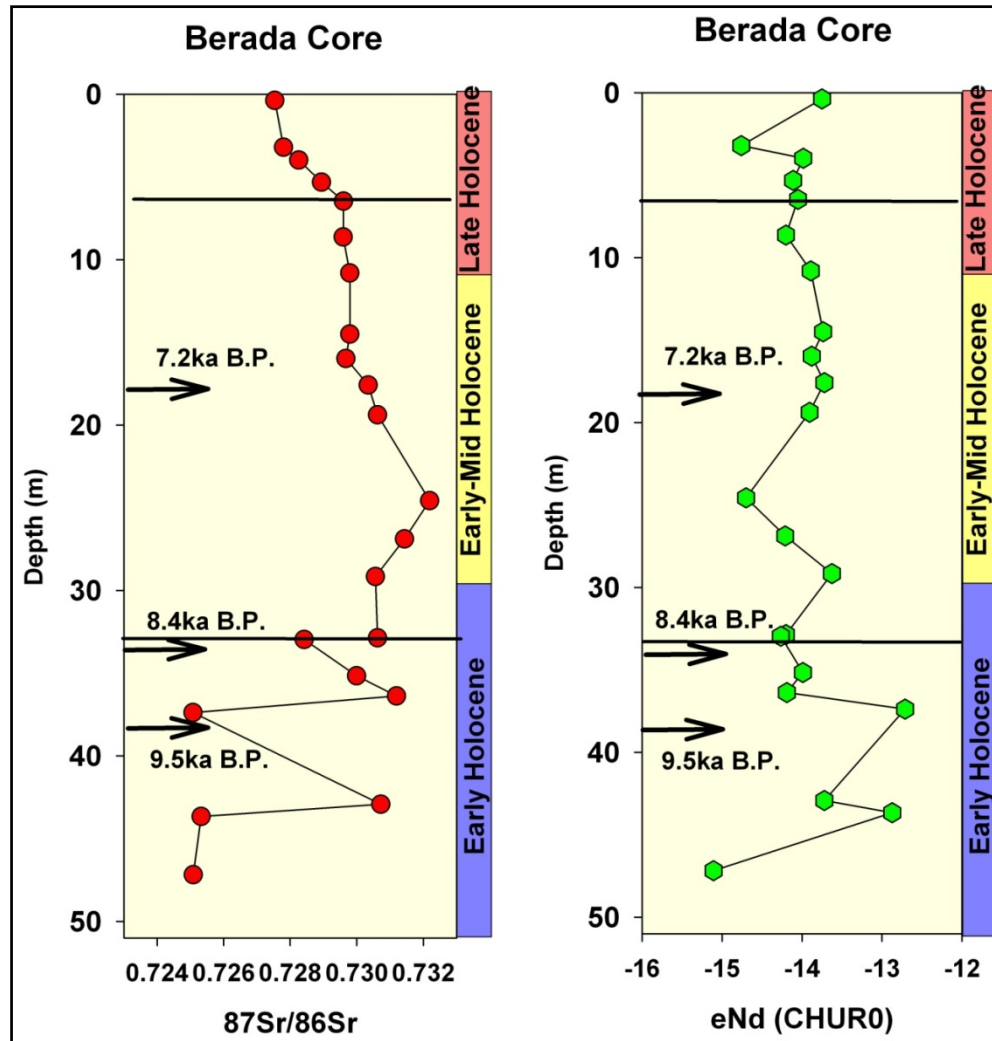


**Figure 10.7** Temporal variations in  $^{87}\text{Sr}/^{86}\text{Sr}$  and  $\epsilon\text{Nd}$  in Berada Core.

### Early Holocene

Isotopically, this marginal core shows the comparable Sr-Nd composition with that of the Dhordo core in the central part of the basin. The bottom most parts of Berada core show intercalation of the marine and fluvial sediments between ~40 to 51m depths. The lowest  $^{87}\text{Sr}/^{86}\text{Sr}$  ratio values ~0.725 were recorded in the fluvio-marine sediments, whereas, comparatively high values in  $^{87}\text{Sr}/^{86}\text{Sr}$  ratio ~0.731 are noted in top of the unit (Fig. 10.7). Such fluctuations are also noted in the clay mineralogy of Berada core. The

variations in clay mineralogy and isotopic composition mark the initiation of marine sedimentation in Banni Plains. Relatively high  $^{87}\text{Sr}/^{86}\text{Sr}$  values occur after  $\sim 9.3\text{ka}$  i.e. Early Holocene time (Fig. 10.7). As discussed earlier, the high radiogenic Sr influx can be supplied through either the Ghaggar/Saraswati River or rivers draining the Aravallis. The Dhordo core in the central rann however suggests the existence of the river Ghaggar during the Early Holocene time and also contribution from Aravallis. Therefore, based on the low  $^{87}\text{Sr}/^{86}\text{Sr}$  and  $\epsilon\text{Nd}$  values it is concluded that the Ghaggar/Saraswati or Aravalli sediments could not reach up to the core site was not submerged under shallow sea prior to  $\sim 9.3\text{ka}$  B.P. It is also concluded that the sediments brought from the hinterland sources from the northern and eastern sides were distributed all over the Great Rann basin.

### **Mid Holocene sedimentation**

The overall  $^{87}\text{Sr}/^{86}\text{Sr}$  increase from the lower values during the marine inundation in the Banni Plains continues to increase during the Early to Mid-Holocene times from  $\sim 32\text{ m}$  to  $26\text{ m}$  ( $^{87}\text{Sr}/^{86}\text{Sr}$  0.73063 to 0.73220) up to  $\sim 7.5\text{ka}$  at  $\sim 26\text{m}$  depth. Whereas,  $\epsilon\text{Nd}$  values show  $-13.65$  to  $-14.70$  corresponding to the Aravalli and lower Indus sediments (Fig. 10.7). The deposition in the central rann roughly during this time span also shows higher radiogenic Sr. In Berada core this may be on account of the mixed Aravalli-Ghaggar/Saraswati sources that were major contributors to the basin. However, a decrease in overall  $^{87}\text{Sr}/^{86}\text{Sr}$  values just before the Mid-Holocene times is noted in this zone ( $20$  to  $8\text{m}$  depth) suggesting relatively less radiogenic nature of the sediments (Fig. 10.7). In this zone, the consistently decreasing but high radiogenic  $^{87}\text{Sr}/^{86}\text{Sr}$  values  $\sim 0.730$  are also observed. This may be due to the gradual drying of the river Ghaggar/Saraswati resulting in decreased radiogenic Sr supply as is seen in the central rann core. However, still higher radiogenic Sr in the upper part of the unit is attributed to the continued supply from the Aravalli sediments and mixing of the Indus born input may have resulted in the observed Sr-Nd isotopic composition. Therefore, other archeological, geochemical evidences in Thar and surrounding regions are also in accordance with the obtained results from Berada core that suggest that the dessication of the Himalayan borne river system (Ghaggar/Saraswati) started at  $\sim 6.5\text{ka}$  B.P. (Saini et.al. 2009; Tripathy et.al. 2004; 2013).

## **Late Holocene**

The Late Holocene sedimentation pattern in the rann basin marks changes in the mineralogy, microfossil content and sediment nature both in the central and marginal part of the basin. This is due to the general regressive and shallowing environment throughout basin that led large scale reworking, re-distribution of the sediments (specifically of the fine grain sediments). The top few meters of this core records the continuous decrease in the  $^{87}\text{Sr}/^{86}\text{Sr}$  values towards top indicating the sediment reworking and increasing influence of the Indus derived sediments by the distributaries debouching in the western part. The shallowing of the basin and marked decrease in the fluvial input possibly increased the strength of the longshore currents from the west into the Great Rann basin. The  $^{87}\text{Sr}/^{86}\text{Sr}$  ratio remains high radiogenic than the Indus offshore values but  $\epsilon\text{Nd}$  lies within the range of Keti Bander values indicating increased interference of Indus sediments with the rann sediments as seen both in the central as well as the marginal parts of the basin.

Based on the present Sr-Nd studies on Dhordo and Berada Cores it is clearly demonstrated that the predominant source for the rann sedimentation lies in the Himalayan rocks. The significant contribution from the proximal sources like Deccan trap and other Cenozoic, Mesozoic rocks appear is ruled out however sediment input from the Aravallis is suggested. From the potential end members and suitable transport mechanism strongly suggests the existence of a large river system that draining from the Himalayas into the Great Rann basin. Temporal variations in Sr-Nd isotope compositions with available age control show stable signatures in Late Pleistocene. However, concomitant changes in  $^{87}\text{Sr}/^{86}\text{Sr}$  and  $\epsilon\text{Nd}$  are observed during Late Pleistocene/Early Holocene which is also seen in Berada core during Early Holocene. These records are in contrast with those observed in the Indus delta. The decreasing  $^{87}\text{Sr}/^{86}\text{Sr}$  and increasing  $\epsilon\text{Nd}$  patterns since Late Pleistocene/Early Holocene hints towards decreasing sediment supply from the Higher/Lesser Himalaya via the Ghaggar/Saraswati river. Variations in  $^{87}\text{Sr}/^{86}\text{Sr}/\epsilon\text{Nd}$  isotopes of sediments is unlikely due to increased input from the Indus distributary and/or alongshore sediment transport as these variations are opposite in the Indus. Consistent decrease/increase in  $^{87}\text{Sr}/^{86}\text{Sr}/\epsilon\text{Nd}$  isotopes of sediments during Early to Mid Holocene times indicates gradual decline in sediment supply from the Ghaggar/Saraswati.

**CONCLUDING DISCUSSION**

Kachchh is a pericratonic palaeo-rift graben located on the western continental margin of the Indian plate, which is seismically active suggesting active nature of the various faults. The voluminous literature that exists on the area mainly deals with the pre-Quaternary tectonic and sedimentary evolution of Kachchh. The Quaternary stratigraphy and neotectonic history of Kachchh is not fully understood and remains incomplete. The Rann of Kachchh is a crucial Quaternary terrain of western India, which has witnessed some of the best known earthquakes in the Indian subcontinent. However, very little information exists on the sedimentologic, stratigraphic and neotectonic aspects of the Rann sediments. Earlier studies carried out on a very limited scale indicate that the Ranns comprise Holocene marine sediments which possibly merge downward into fluvio-marine and fluvial Pleistocene sediments and have witnessed continuous sedimentation until very recent times. The evolution of the Great Rann of Kachchh has been linked to tectonic activity in recent times (Roy and Merh, 1981). The basin was filled up by sediments supplied from the Indus drainage basin while the surface has been smoothed by the frequent earthquakes (Platt, 1962). However, no information as yet exists on the sediments comprising the Ranns of Kachchh and its Quaternary evolutionary history.

Understanding the geological evolution of the Ranns of Kachchh essentially requires a chronologically well constrained subsurface stratigraphy and delineation of buried structural features within the sediments comprising the Ranns of Kachchh. The present study is an attempt at reconstruction of geological evolution of the Rann basin through a comprehensive approach involving delineation of subsurface stratigraphy and palaeoenvironmental conditions existing in the Ranns during Quaternary.

**GEOMORPHIC DIVISIONS**

The Great Rann is a tectonically formed basin that is bounded by the Kachchh Mainland Fault (KMF) in the south and the Nagar Parkar Fault (NPF) along the Indo-Pak border in the north (Biswas, 1987). The eastern margin is marked by the West Cambay Basin Margin Fault (WCBMF). Towards the west the basin opens up to the Arabian Sea and the Indus delta region. The Kachchh Mainland Fault (KMF) forms the

southern basin bounding fault of the Great Rann basin. The KMF is marked by E-W trending north facing line of scarps that separate the Northern Hill Range to the south and the Banni plain in the downthrown northern block. A 2 - 3m wide zone of deeply incised Quaternary colluvio-fluvial and fluvial deposits separate the Banni plain from the deformed Mesozoic rocks of the Northern Hill Range. Various rivers draining the mainland disappear into the Banni plain. Presumably, the Quaternary tectonic activity along the KMF and the NPF resulted in the subsidence of the Great Rann basin which facilitated the incursion of the sea and deposition of a huge thickness of marine sediments in the Great Rann basin. The basin formed a major sink for sediments that are believed to have come from variety of source regions viz. Aravalli rocks, Mesozoic and Tertiary rocks within the Kachchh basin and Himalayan rocks.

The major factor responsible for the unique present day environmental conditions of the rann surface is its periodic submergence by sea water and monsoon precipitation. The flat rann surface and the negligible gradient allows extensive inundation by sea water from the Arabian sea in the west and by river waters from the north east and south during the monsoon season (Roy and Merh, 1981). The inundation periods are separated by relative long periods of dry and hot saline wasteland conditions during the summer season. Overall, the alternate wet and dry condition in the Great Rann of Kachchh has resulted in a unique and hostile terrain whose environmental condition fluctuates between extremes.

Based on the present day submergence pattern and surficial characteristics, the Great Rann of Kachchh has been geomorphologically divisible into four units. Owing to very small variation in elevation and imperceptible gradient, the boundaries between the various divisions are gradational. The geomorphic divisions of the Great Rann as delineated in the present study are -the Banni plain, the Supra tidal salt flat, the Inland saline flat and the Bet zone.

The Banni plain is a vast flat terrain, highly vegetated with shrubs and grasses, and extending from the mainland Kachchh in the south and the Pachham island in the north (Fig. 2.1, 2.3a). It is a distinct geomorphic surface of the Great Rann that occurs at the highest elevation and is consequently completely free of marine influence (Fig. 2.2). The sediments are however, inherently saline in nature. It also forms the only part of the Great Rann that is inhabited. The surface morphology is shaped by the annual submergence by thin sheet monsoon rains and aeolian activity. The surface elevation varies from 4-10 amsl with the scattered villages occurring on isolated high grounds

while the rest of the part suffers annual submergence by rain water. Small depressions remain filled with water for longer periods of time and on drying up are covered by thin layer of salt. The entire terrain of the Banni plain is regarded as a vast raised mudflat (Kar, 1995) that coincides with the subsurface Median High. The southern part of the Banni plain is at a relatively lower level. The western half of the Banni plain slopes towards west. The highest elevations occur in N-S alignment passing through Bhirandiyala in the northern part of the Banni plain. This geomorphic high overlies a E-W subsurface structural high documented by Biswas (1987).

The supra tidal salt flat is a vast but linear and narrow E-W trending low lying zone with several centimeters thick salt crust between the Banni plain in the south and the Bet zone to the north. This zone occurs at the lowest elevation (~2m) in the west and gradually rises to ~4 m towards east. Being at the lowest elevation, this zone forms the main pathway through which the saline waters of the Arabian sea in the west enter and spread out submerging about two-thirds of the rann surface to varying degrees depending upon the volume/magnitude of the ingressions resulting in a thick salt crust. The very low gradients in the supra tidal salt flat allow storm-driven marine flooding to reach inland typically up to the region around Khadir island which is ~70 kms from the limit of normal high tide level in the west. This flooding gives rise to shallow sheet of sea water, which persists for at least few weeks until the water evaporates. Evaporation to dryness results in several centimeters thick, residual salt crusts, which characterize the surface of the supra tidal salt flats.

The inland saline flat comprises the easternmost part of the Great Rann that is not influenced by marine submergence, but is inundated by monsoon precipitation and by the rivers from the east and north. The elevation rises towards the margins of the zone, giving it a shallow bowl like morphology and comprise inherently saline rann sediments (Roy and Merh, 1981). The fringes of this zone are free of salt crust. However, the central deeper part of this zone may show very thin millimetre scale salt crust. This is formed by concentration of flooding waters in salt content due to evaporation.

The Bet zone comprises the flat rann surface in the northwestern part of the Great Rann shows several bets occurring few metres above the rann surface. The Bet zone is delimited by the Kuar and Bedia bets in the east and the supra tidal salt flat in the south. To the north lie the sand ridges of Sind (Pakistan). Towards the west, the Bet zone imperceptibly merges with the Indus delta. The southern boundary of the Bet

zone is marked by the Allahbund fault scarp. This zone comprises several bets (islands) of varying sizes with the rann surface occupying the inter-bet depressions. The region to the west and SW of Vigukot is prone to flooding frequently by river floods by few perennial rivers coming from the north and relatively less frequently by sea water influx from the south. In addition numerous small shallow (~0.5m deep) channels of uncertain affinity are also present. Overall, the role of rivers is evidently more pronounced in the western most part than the rest of the Bet zone. Contrary to the rest of the Great Rann, the Bet zone shows wide variation in elevation due to the presence of bets and is dotted by several seasonal short distance channels, pools i.e. local depressions and elevated surfaces.

Various coastal geomorphic features are seen at the toe of the northern escarpments of Bela and Khadir islands which are attributed to the paleo-sea which occupied the rann until ~ 500 yr BP. Erosional rocky platforms occur discontinuously at an elevation of 2-4 m above the rann surface all along the base of the Bela and Khadir escarpments. Two levels of notches designated as upper and lower notches are also observed at a height of 4m and 2m respectively. Notches are generally formed in the sheltered site away from the wave action (Rust & Kershaw, 2000). The preservation of two levels of notches can be account of rapid uplift (Cooper et al., 2005). Sea caves have also been noticed all along the base of the escarpments.

## **PALAEOENVIRONMENTS**

### **Raised Rann sediments**

The raised rann sediments that are found attached to the fringes of the rocky islands of Khadir, Bhanjada and Kuar bet in the central part of the Great rann basin (Fig. 5.1). The two samples from Khadir island section at 0.20 m and 1.80 m depths dated by OSL method yielded ages of  $543 \pm 67$  B.P. and  $1864 \pm 147$  B.P. respectively (Table 1). Samples from Bhanjada island section at 0.20 m and 4.75 m depths yielded ages of  $1862 \pm 159$  years B.P. and  $11181 \pm 1427$  years B.P. respectively. The OSL dates suggest uninterrupted sedimentation around the margins of the rocky islands in the Great Rann through Holocene up to ~500 yrs B.P. The OSL dates obtained are in conformity with historical accounts that describe ships reaching up to a port called Verawow in Nagar Parker hills located at the northern margin of the Great Rann, which was abandoned about ~500 years as the sea dried out (Frere 1870). The overall foraminiferal assemblage and vertical variations in the abundance suggests hyper-

saline to brackish conditions in the vicinity of the islands in the Great Rann. The variation in abundance of the foraminifera vertically through the sediment successions is significant (Figure 5). The graphs of abundance pattern in all the sections allow us to mark the different zones based on fluctuations in the absolute abundance of foraminiferal tests. The wide variations in abundance patterns of the foraminifera are attributed to changes in the salinity conditions due to periods of enhanced fresh water influx from the adjacent landmass. The largely homogeneous nature and absence of discordant sedimentary depositional feature or any abrupt termination or change in the nature of the sediments and the foraminiferal assemblage suggests that the conditions remained uniform with short term fluctuations from brackish to hypersaline. These conditions persisted along the island margins for a long period of time during the Holocene. The geomorphic setting, homogenous sediment nature and vertical distribution and abundance patterns of foraminifera suggests existence of fluctuating conditions from brackish to hypersaline along the island margins during the deposition of the sediments.

#### **Subsurface sediment cores**

To understand the geological evolution of the Great Rann and to delineate the palaeoenvironmental changes, two shallow continuous sediment cores were raised. Two continuous cores, one from the central part of the Great Rann basin (~60m depth) and the other from the marginal part of the basin in Banni plain (~51m) were raised. One core of ~60 m depth was raised from the southern fringe of the salt encrusted surface occurring to the north of Dhordo. This site falls in the central part of the Great Rann basin which is frequently inundated by marine waters coming from the east. The second core of ~51 m depth was raised from the Banni plain and is closer to the rocky mainland Kachchh in the south. This site located to the NE of Berada falls in the Banni plain that forms the southern marginal part of the Great Rann basin and is free of present day marine influence. The split sections of cores were visually examined for their physical and sedimentary characteristics. One half of both the cores was sampled at 2 cm interval while the other half has been preserved in sub-zero temperatures.

Grain size distribution of both the cores was investigated to characterize the reconstruction of lithostratigraphy and depositional environments. There are no significant changes in lithology and sediment texture is observed that any part of the core contains significant amounts of reworked material; therefore a continuous sedimentary sequence is believed to be found. Based on textural characteristics, the

Dhordo core is subdivided into 16 lithounits while the Berada core is subdivided into 13 lithounits. The sediment consists of silty clay to clayey silt with minor amount of sand in both the cores. No sand dominated lithologies are observed in the Dhordo core, whereas sand content is anomalously increased in the bottom part of the Berada core (95%). Berada core sand comprises highly angular and yellow unsorted grains where quartz followed by feldspar is also seen. The sediments of both the core show considerable colour variation from light brown-greyish green-greenish gray-bluish gray to dark gray colour. These silty clay and clayey silt are characterized by a total lack of structures, as noted in split section and X-radiograph analysis of Berada core. But very faint laminations are observed in Dhordo core, and thicknesses are generally of the order of few millimetres are also confirmed by X-ray radiographs. Complete and broken gastropod and bivalve shells and organic rich layer are also found to the core sediments.

The Dhordo and Berada cores shows continuous sedimentation with minor variations in depositional environment for a long period of time. Bottom parts of the Berada core indicates extension of fluvial deposits from the rocky mainland Kachchh to the south and marks the fluvial sedimentation before the transgression of the sea. Presence of lamination in Dhordo core may suggest turbulence free condition where shifting in energy condition is also prevailed. The broken shells also suggests some turbulent condition and may indicate some high energy event. Top part of both the core may indicate definite transitional phase from fully marine to present day condition existing in the Great Rann. Changes of colour in dominantly similar lithologies may also be attributed to variations in organic matter content.

The lithological similarity of the Dhordo and Berada cores is very striking even though they are located more than 50 km apart. Both cores are dominantly composed of fine grained lithology ranging from clayey silts to silty clays. The persistence of the fine grained lithology in both the cores is amazing. Physical examination of the split cores and detailed textural analysis carried out on the samples indicate subtle variations in the lithological composition which have allowed reconstruction of vertical variations in each core and also in establishing the distinctive characteristics of the two cores. The Dhordo core reveals the subsurface lithological characteristics of the Rann sediments upto ~60m depth. The sediment cores comprise dominantly clayey silts followed by silty clays. In fact, about 46 m (~75%) of the total length of the core consists of clayey silts while silty clays form the rest of the core. No sand dominated

lithologies are encountered in this core. The core also suggests that the thickness of the marine sediments is more than 60m in the central part of the Rann basin.

The Berada core also dominantly consists of clayey silts and silty clays. However, fluvial sands are encountered in the bottom part of the core which are obviously the extension of fluvial deposits from the mainland in the south. The sands are coarse grained and comprise about 6m of the total length of the core, However they form two lithounits (Unit 1 and 3) separated by a marine silty clay unit. The sands represent fluvial sedimentation before the onset of the marine transgression that finally flooded the Rann basin. The overlying finer lithologies comprising clayey silt and silty clays indicate uninterrupted marine sedimentation under shallow marine conditions. The clayey silt comprise about 39m (~76%) of the total length of the Berada core while silty clay forms only about 6 m of the total length of the core. This indicates an overwhelming domination of clayey silts in the sedimentary basinfill of the Rann. The overall lithological composition of the cores appear to be in conformity with the geomorphological setting of the Rann that suggests that it was an embayed shallow gulf in the past. The dominantly fine grained lithology of the cores suggest that the basin was filled up by sediments that underwent long distance transport from the distant source regions.

### **Foraminiferal studies**

The variation in foraminiferal assemblage were documented down the core by analysing core samples representing the individual lithounits and intervals marking marking lithological change. The foraminiferal studies on the two cores Dhordo and Berada yield a diverse assemblage of the foraminifera in the Great Rann of Kachchh basin. The foraminiferal assemblage comprises a total of 30 genera of benthic and planktic species. The downcore variation of these foraminiferal assemblage is interpreted in conjunction with the sedimentological characteristics. Micropalaeontological analysis of the two cores suggest continuous shallow marine sedimentation for long time in central as well as marginal areas of the Great Rann basin. The available chronological data suggests that the Dhordo core dates back ~18 ka BP while the interpreted marine section of the Berada core dates back to ~10ka BP. The occurrence of the typical marine microfossils i.e. foraminifera present throughout the studied samples which indicates the marine origin of these sediments.

The recovered foraminifera throughout the two cores show considerable variations in the abundance with depth. Based on the abundance patterns, Dhordo the

core is divided into four zones. The bottom most zone of the Dhordo core dominates by *Ammonia* genus which contributes more than 70% of the total assemblage. The bottom upward foraminiferal distribution shows that *A. beccarii* and *A. tepida* together dominate the assemblage. Based on the vertical variations this zone is characterized the two characteristic assemblages- 1) *Ammonia-Quniquiloculina-Troloculina-Brizalina* for the lower part between 60-48 m depth and 2) *Ammonia-Quniquiloculina-Bolovina* assemblage between 48 - 31m depth. The lower zone foraminiferal assemblage of *Ammonia-Quinquiloculina-Brizalina* is indicative of the initial phase of the marine incursion into the basin forming brakish to shallow marine conditions whereas the upper part assemblage of *Ammonia-Quniquiloculina-Bolovina* assemblage suggests the prevalence of the shallow water marine conditions.

The overlying zone is characterized by the large scale changes in the overall assemblage. The appearance of the broken and reworked specimens in significant amount suggests the high energy conditions and reworking (~25% of the total assemblage). Interestingly, the species diversity and overall abundance of foraminifera is maximum in this zone. This zone is characterized by *Ammonia-Globorotaloides-Nonionoides* assemblage. The high diversity in this zone may on account of the foraminiferal transport through the Arabian Sea and the broken and reworked foraminifera suggest redistribution of the sediments. This also may be on account of the increase in strength of fluvial systems due to strong monsoonal conditions.

In the third zone, the *Ammonia beccarii* reduces further whereas *A. tepida* is absent throughout. The planktonic component in this zone is found to be dominant. The overall species diversity reduces in this zone from bottom to top. In the fourth topmost part of the Dhordo Core, the *Ammonia* species dominates again contributing more than 80% of the total assemblage. This unit is mostly dominated by the *Ammonia-Nonian-Elphidium* species. The similar assemblage is also observed during the surface sediment studies along the Bet Zone. The top most zone indicates the typical shallow marine conditions existed during the deposition as also indicated by the lowest abundance and diversity of the foraminifera in these sediments.

On the basis of the abundance patterns, the Berada core is divided in three zones that suggest variations in the environmental conditions. The marine transgression in Berada core is indicated during the Early Holocene times (~10ka BP). The fresh foraminifera recovered are found to primarily belong to the *Ammonia* and *Elphidium* genera. In the second zone, the species diversity also ranges between 10 -

15 throughout this unit indicating the favourable environmental conditions for the survival of foraminifera. The lower most part of this zone is characterized by the predominant *A. beccarii* followed by *Elphidium* and *Qunquiloculina* genus. The reworked or older foraminifera are completely absent.

The topmost third zone of this core yields more or less similar fauna assemblage to that of the lower zone but characteristically differs in the abundance pattern. The genus *Ammonia* dominates in this unit also by contributing more than 60-85% of the total assemblage. The presence of *A. parkinsoniana* is also observed throughout this unit. The drastically increased abundance of the *Qunquiloculina* species along with the *Elpidium-Nonian* indicates the brackish to marine conditions whereas the increased abundance of *Nonionella sp* indicates the increased fresh water influx into the basin. The largely fluctuating species diversity in this zone may be on account of the rapidly changing environmental conditions that led to the domination of only the tolerant taxa.

#### **Major and Trace element studies**

The relative abundance of many major and trace elements and their ratios are identified to vary with the erosional processes, sediment transport, grain size, productivity and bottom water conditions. Detailed geochemical studies on the core samples was carried out to understand the nature of the sediments deposited in the basin. The major elements Al, Ca, Fe, Mg, and K show significant variations in the Dhordo core from bottom upwards. In Dhordo core Al is correlated with the Fe (0.74), K (0.58), Mg (0.56) whereas poor correlation of Al with Ca is seen (0.31). Similarly, positive correlation of Mg/Al versus K/Al (0.65) and Fe/Al versus K/Al (0.64) is observed. Based on distribution of major elements, the Dhordo core is divisible into three zones indicating the change in environment and nature of detrital flux into the central rann basin.

In case of trace elements, the downcore variations of Cu, Mn, Co and Ni in the Dhordo core vary from 12.14-19.70, 107-96-155.27, 6.73-11.15 and 4.86-30.38 respectively. The Cr-Ni and Cr-Mn shows high correlation coefficients (0.90, 0.67) in throughout the core, however, Cr-Cu shows relatively poor correlation (0.36). Cr/Al, Co/Al ratio remains in a narrow range whereas minor variations seen in Mn/Al and Ni/Al show minor positive shift after ~45m depth. Ni/Co ratio also indicates the prevailing oxic conditions prevailing during the deposition of these sediments (Jones and Manning, 1997). These results are in conformity with the shallow marine settings

of the Great Rann of Kachchh basin. The nutrient conditions are reconstructed using Cu, Zn, Cd, Co, Pb and Ba elements that are normalized with the aluminum concentration in the sediments. The down core variations in concentration of these elements provide the relative changes in the nutrient conditions from the nutrient-rich to nutrient-depleted conditions.

Based on the variations in major elements, the Berada core is divided into four zones. The bottom unit marking the beginning of marine sedimentation in the marginal part basin is characterized by the high values of Al and positive slopes of Fe/Al, Mg/Al and K/Al. Increase in these elements provides strong evidence for high terrestrial input into the basin. The bottom of this zone marks the beginning of marine sedimentation in the marginal part basin at ~9.3ka B.P. The second zone is characterized by the high values of Al and positive slopes of Fe/Al, Mg/Al and K/Al. Increase in these elements provides strong evidence for high terrestrial input into the basin. The third zone again shows positive slope in the Al content in the sediments whereas the Ca/Al proportion remains almost restricted in a narrow range with minor positive slope. The topmost zone of the Berada core shows interesting changes in the elemental composition in Al, Ca, Mg, Fe and K. This part marks the marine regressive phases during the recent times. The bottom upward variations in Al, Fe/Al, Mg/Al and K/Al show correlatable changes in the form of high values in the bottom samples whereas the in the top samples the concentrations of these elements is found to be relatively depleted. The variations in the trace elements and their proportion in the Berada core suggest the oxic conditions throughout.

### **C/N Ratios**

The C/N ratio is a useful indicator for studying land and marine interaction on temporal scales. Basically it reflects the ratio of aquatic organic matter compared to the terrestrial organic matter (Meyers and Lallier-Vergas, 1999). The inorganic carbon content and C/N ratios determined for both the cores show broad correlatability with the palaeoenvironmental records from the Arabian sea. The post-LGM period witnessed a relatively weaker monsoonal strength with abrupt short periods of wetter phases as recorded in the northern Arabian Sea and other archives in western India. The Dhordo core data shows relatively strengthened monsoonal system since 15ka upto 13.5ka, this increase in monsoonal strength was accompanied by an increase in continental flux of carbon. A short dry period was also noticed which also coincided with increase of carbon flux predominantly due to marine processes. Similar to Berada

core a strengthened monsoonal strength reflected by increased  $\text{CaCO}_3$  concentration is observed up to 8ka, which was punctuated by a short spell of weak monsoon and again followed by strengthened monsoon till 6.6ka. This was then followed by relative drop in monsoonal strength but surprisingly the continent derived carbon flux increased. The period between approximately 6ka to 2ka witnessed an increase in monsoonal strength with significant contribution by both marine and continental forms of carbon flux. The period since 2ka saw a fluctuating monsoonal variability accompanied by increase in marine processes followed by continental flux of carbon.

The data from Berada core gives a record from ~10ka BP onwards. The early Holocene period from 8 - 10ka BP is recognised as a humid interval when monsoon intensity was at its maximum in the western and north western Arabian sea (Overpeck et al 1996, Sirocko et.al., 2000). This is also observed in the data in terms of increase in  $\text{CaCO}_3$  percentage. Simultaneously the C/N data also showed increasing continental flux (values > 10). But during the period of approximately 10 - 9ka, marine activities are dominant and it is also confirmed by the increased  $\text{CaCO}_3$  percentage. It is suggested that strong monsoonal strength prevailed at that time as input from continental areas is more.

Between 8.6ka to 6.8ka two zones of marine input and one zone of continental input flux are observed where marine processes are dominant. Therefore monsoonal strength enhanced for a short period followed by two phases of weakening monsoon period. During this time river input is less as compared to marine processes. Concentration of  $\text{CaCO}_3$  does not show any significant fluctuations. Gupta et al. (2003) also reported weakening spell of Indian summer monsoon during 8400 to 8000 yr BP from the Arabian Sea. The climate saw a gradual weakening from 6.8ka up to 6m depth where C/N values are gradually decreasing i.e. input from continent is less and from 6 m to 0 m depth continent input is gradually increasing. At the same time the C/N ratio also showed relative increasing continental contribution. Further ahead the monsoonal strength increased slightly and following which it witnessed a short weakening of monsoonal strength for a short period, since which it is stable and at same time C/N ratio continues to show relatively more continental contribution of carbon. Similarly  $\text{CaCO}_3$  also shows continental input from hinterland which is high as compared to marine input.

### Clay mineralogical studies

As the clay is a significant contributor in bulk grain size of the core sediments throughout, it necessitates characterization of bulk clay mineralogy to understand the source for the clay minerals in hinterland. In the present study, the clay mineralogy of the core sediments was used to assess the spatial and temporal changes in palaeoenvironmental conditions and provenance of the subsurface rann sediments. The major clay minerals present in all the sediment samples are: Smectite, Illite, Kaolinite and Chlorite. The down core distribution of these clay minerals clearly indicates the dominance of the Illite and Chlorite over Smectite and Kaolinite. In Dhordo core Illite shows the narrowest range of variations followed by Chlorite whereas Smectite shows wide range of variations. Berada core comprises relatively less Illite, increased Chlorite and Kaolinite as compared to Dhordo core record.

In Dhordo core, the bottommost zone, the Sm/Ka Vs Illite crystallinity and Ka/(Ill+Ch) Vs Illite crystallinity plots points towards the warm wet climate with moderate to high leaching (Fig. 8.4a and 5a). The higher degree of crystallinity in these graphs (Fig. 8.1b, 8.4a and 8.5a) shows low hydrolyzation during the deposition of these minerals that may points toward the rapid deposition of the sediments. In the second zone, the variations in the ratios are in conformity with the other paleoclimatic studies stating that the strengthening monsoonal condition during Late-Pleistocene-Early Holocene times as a rapid response to the post glacial climate change (Campo *et.al.* 1982; Sirocko *et.al.* 1993; Overpeck *et.al.* 1996; van; Thmaban *et.al.* 2001, 2002). The overall clay mineral record shows the strengthened monsoonal condition during the Early Holocene towards Mid Holocene times by its maxima prior to 6.9ka B.P. as evidenced by the largest positive shifts in the values at ~24-28m depth. In the third zone, the low constant values in Sm/(Ill+Ch) ratio, and Ka/(Ill+Ch) shows low values (except one sample ~14.4m) indicating relatively less chemical weathering and weathering (Fig. 8.1b). The chemical weathering can be correlated with the precipitation in the region on temporal scales (Chamley, 1989). Therefore, these results are suggestive of the overall weakening monsoonal conditions with decreased humidity in the region (Thamban *et.al.* 2002).

In Berada core, the clay mineral ratio for climate proxies (Ka/Ch; Ka/Ill) show relatively humid phase in the bottom of the marine section whereas upper part of the zone shows lowered values indicating falling humidity and increased dry arid climate as also evident by increase in Smectite proportion. Leaching and chemical weathering

proxies are also in conformity with these signatures suggesting phase of strengthening monsoonal pattern after ~8.4ka BP. In the following zone, the chemical weathering proxy (Sm/(Ill+Ch) and leaching proxy (Ka/(Ill+Ch) together indicating the high chemical weathering and reduced leaching (Fig 8.4b and 8.5b) are indicative of dry seasonal climatic conditions (Alizai *et.al.* 2012). Also, the climate proxies (Ka/Ch, Ka/Ill and Ka/Sm) together indicate dry seasonal climatic conditions prevailing during the deposition of these sediments (Chamley 1989; Thamban *et.al.* 2002). The recorded loss of the humid climate to seasonal dry period appears after 7ka B.P. The topmost zone of the Berada core is characterised by significant changes in the clay mineral records. Remarkable changes include the upward increase in Illite, and Kaolinite content whereas Smectite and Kaolinite shows decreased values to its lowest throughout the core. On account of marine regression there might be significant changes in the sediment distribution, re-distribution in this region. Therefore, the sediments in the upper parts of the cores may not reflect the true palaeoclimatic signatures.

### **Provenance studies**

#### ***Clay mineralogy***

The dominance of the Illites in Great Rann sediments can be related with the Himalayan source but another Illite source is alluvial plains in Rajasthan i.e. Aravallis (Pandharinath *et.al.* 1999; Sharma *et.al.* 2010). The Illite chemistry varies from Fe-Mg rich to Al rich Illites with increasing leaching effects (Chamley *et.al.* 1989). This leaching effects and crystal widening is expected more in the alluvial plains of Rajasthan (Aravalli source) as the weathering processes are more prone to change degree of crystallinity and chemistry (Thiry, 2000). The Illite chemistry record at both core sites shows low values indicating Fe-Mg rich Illites that means fresh Illite deposition (Fig. 8.1a and 8.2a). This is also in conformity with the overall low values of Indus Illites where the degree of hydrolization is relatively less as indicated by Fe-Mg rich Illites (Alizai *et.al.* 2012; Limmer *et.al.* 2012). Another point is the rann sediments are rich in Illite and Chlorites and less in Smectites and more Kaolinite as compared with the Indus sediments. Therefore, the Illites in Great Rann sediments are more likely to have been derived from the Himalayas. The dominant Chlorite and Illites in the rann sediments strongly points towards the distal Himalayan source for rann sediments as compared with the local/proximal Kachchh Mainland Hills and/or Aravallies. Overall, mostly the provenance of the Great Rann basin can be inferred that

the major contribution comes from the Himalayan derived sediments which strongly masks the peninsular, local and proximal sources (Smectite and Kaolinite) such as the Aravalli, and Mainland Kachchh.

### ***Sr-Nd Isotopic studies***

By virtue of its location, the Great Rann basin is primarily expected to be filled by sediments from multiple sources. The Sr-Nd isotopic studies were carried out on the core samples for tracking the sources of the Great Rann sediments. Geographically, the Thar desert and Aravalli ranges in the north and east and Kachchh mainland in the south are the nearest sediment sources which can contribute to the Great Rann sediments. However, the Sr isotope values of rann sediments show considerable variations in radiogenic character from bottom to top. When compared with the surrounding lithologies, the present results do not indicate the proximal source like Deccan volcanic ( $^{86}\text{Sr}/^{87}\text{Sr} \sim 0.704$ ; Sen et.al. 2009), Mesozoic and Tertiary lithologies in the Kachchh basin as they comprise low Sr radiogenic character. In fact the rann sediments are more inclined towards the older high radiogenic granitic terrains (Singh et.al. 2008). Such high Sr values are known from Lesser and Higher Himalayan terrains, Karakoram and in Siwaliks (Singh et.al. 2008; Clift et.al. 2002). If River Indus predominantly provided sediments to rann, one would expect a good match in Sr-Nd isotopic composition of rann sediments with the river Indus, or similar values with another ancient large scale river system that existed in the region i.e. Ghaggar/Saraswati. Instead, the rann sediments are slightly different in the Sr-Nd composition with both these sources indicating mixing of more than one source in the hinterland before debouching into the Great Rann of Kachchh basin. Integrating the data of the two cores with the available data from surrounding areas, it appears that a mighty river system i.e. Ghaggar/Saraswati in the north of the rann basin provided maximum amount of sediments to the rann basin since the post glacial times till recent past. The present study provides concrete evidence for the existence of the Ghaggar/Saraswati drainage systems in the past as inferred by several previous (Oldham, 1893; Yashpal et.al. 1980 and Kar and Ghosh, 1984; Radhakrishna, 1999; Kochar, 2000; Valdia 2002; Ghose et.al. 1939; Kar and Ghose, 1984; Clift et.al. 2012).

### **EMERGENCE PATTERN OF THE GREAT RANN**

Based on the AMS dates of obtained from Dhordo core at a depth of 60.13m, it is inferred that the central part of the Great Rann basin corresponding to the present

day Supratidal salt flat, was submerged by a shallow sea by ~18ka. However, the submergence of the entire basin appears to have taken place gradually. The AMS date obtained from the Berada core at 38.88 m depth suggests that marginal parts including the present day Banni plain were submerged by ~10ka BP. Since then, continuous marine sedimentation took place through the Holocene in the entire basin under shallow marine conditions.

The top parts of the cores (1 - 3m) appear to indicate a definite transition phase which turned the Rann from a fully marine basin to the present subaerially exposed land with peculiar geomorphological characteristics. It is inferred that the emergence of the rann surface may have occurred gradually in the recent past which led to the formation of the distinct morphologic units viz. the Banni plain, the Bet zone and the Linear Trench zone. The Banni plain astrides the subsurface Median high and is separated from the rest of the Rann basin by the Banni Fault to the north (Biswas, 1974). Similarly, the Bet zone is delimited by the Allahbund Fault to its south (Roy and Merh, 1981). The close association of these units with faults suggest differential tectonic activity along subsurface faults within the Great Rann basin may have played a major role in the emergence of various morphologic units at different times. Based on elevation and present day submergence characteristics, the Banni plain appears to be the first to emerge followed by the Bet zone and the Supratidal salt flat which still gets submerged by marine waters regularly.

### CONCLUSIONS

The present study has led to the following conclusions.

1. Based on the present day submergence pattern and surficial characteristics, the Great Rann of Kachchh has been geomorphologically divided into four units. Owing to very small variation in elevation and imperceptible gradient, the boundaries between the various divisions are gradational. The geomorphic divisions of the Great Rann as delineated in the present study are -the Banni plain, the Supra tidal salt flat, the Inland saline flat and the Bet zone.
2. The major geomorphic components of the rocky island belt are the north facing escarpment forming the northern margins of the islands, south sloping tectonically controlled backslopes, raised intertidal flats, notches and other marine erosional features attributed to the palaeo-sea that occupied the rann surface. Raised marine terraces exposing 5-6 m of raised rann sediments deposited in inter tidal conditions are documented from the western margin of Khadir island, eastern margin of Bhanjada island and southern margin of the Kuar bet island. The overall foraminiferal assemblage and vertical variations in the abundance suggests hypersaline to brackish conditions in the vicinity of the islands in the Great Rann. These conditions persisted along the island margins for a long period of time during the Holocene.
3. The chronological data indicates that active marine sedimentation along the margins of the rocky islands continued up to ~500 yrs B.P. The OSL dates obtained are in conformity with historical accounts that describe ships reaching up to a port called Verawow in Nagar Parker hills located at the northern margin of the Great Rann, which was abandoned about ~500 years as the sea dried out.
4. The formation of the terraces along the island belt is attributed to tectonic uplift during late Holocene. Tectonic tilting of the islands during this period is testified by the southward decrease in the elevation of terraces. The raised intertidal flats exhibit terraced surfaces that are tilted southwards and comprise mainly laminated clayey silts with thin layers of fine sand. In addition, erosional features like two levels of

notches, platforms and sea caves are observed along the base of the northern escarpments. The presence of raised marine depositional and erosional features at the base of the escarpments point to mid-late Holocene uplift of the islands in a tilted manner due to tectonic activity along the IBF during the last ~500 yrs BP.

5. To facilitate the study of subsurface sediments of the Great Rann, two continuous cores were raised. One core (~60 m depth) was raised from the southern fringe of the salt encrusted surface to the north of Dhordo in the central part of the Great Rann basin while the second core (~51 m depth) was obtained from northeast of Berada in the southern Banni plain and falls in the southern marginal part of the basin. Core drilling could not be undertaken in the Little Rann basin as it is a notified sanctuary area.
6. Based on textural characteristics, the Dhordo core is subdivided into 16 lithounits while the Berada core is subdivided into 13 lithounits. Both cores are dominantly composed of fine grained lithology ranging from clayey silts to silty clays. The persistence of the fine grained lithology in both the cores is striking. No fluvial sediments are encountered in the Dhordo core, however, fluvial sands are encountered in the bottom part of the Berada core which are obviously the extension of fluvial deposits from the mainland in the south and mark fluvial sedimentation before the transgression of the sea into the Great Rann basin. Overall, both cores together, suggest continuous sedimentation in shallow marine conditions for a long period of time, with minor variations in depositional conditions.
7. Based on the C14 dating on selected samples, foraminiferal abundance and grain size variations in both the cores it is inferred that the Great Rann basin preserves a continuous marine record since the last ~18 ka BP. The present study indicates that the Great Rann basin was a gulf like extension of the Arabian Sea and remained a sheltered basin throughout its geological evolution. Micropalaeontological analysis of the two cores suggest continuous shallow marine sedimentation for long time in central as well as marginal areas of the Great Rann basin. The occurrence of foraminifera throughout the cores confirms the marine origin of these sediments. The recovered foraminifera throughout the two cores show considerable variations in the abundance and test morphology with depth. The abundance pattern and diversity of total foraminifera is a reflection of the regional scale palaeoenvironmental changes.

8. The presents study provides conclusive evidence in respect of the uninterrupted marine sedimentation in the tectonically formed basins of the Ranns of Kachchh since ~18 ka BP. Based on the AMS date of ~18 Ka BP obtained from Dhordo core at a depth of 60.13 m and ~10 ka BP obtained from the basal part of the marine sequence in Berada core at 38.88 m depth, it is inferred that the central part of the Great Rann basin was submerged by a shallow sea by ~18 ka while the marginal parts including the Banni plain were completely submerged by ~10 ka BP. Overall, both cores together, suggest continuous sedimentation in shallow marine conditions for a long period of time, with minor variations in depositional conditions.
9. Foraminiferal studies on the Berada and Dhordo cores revealed the significant palaeoenvironmental changes throughtout the past ~18 ka BP. In the Dhordo core, the marine incursion is marked by the presence of Ammonia-Quinquelocula-Triloculina-Brizalina assemblage in bottom most unit 60-48m depth. During this time brackish-marine conditions with the typical shallow, coastal assemblage is inferred. The upper zone ~16ka BP (48-31m) suggest the increased marine dominance in the regions that is evidenced by the abrupt increase in the abundance of foraminifera. In Berada core the fist marine excursion is denoted by the Ammonia-Elphidium-Nonian assemblage around ~10 ka BP. The covariant changes are also observed during the Mid-Holocene times with phases of reworking.
10. The clay mineralogical results revealed the dominance of the Illite and Chlorite mica in the rann sediments (<76-70%), that indicated the first approximation of the Himalayan origin of the rann sediments. The clay minerals also indicate pchanges in palaeoenvironmental conditions that are consistent with similar changes in the region.
11. The Sr-Nd isotopic studies on the rann sediments yield high radiogenic Sr at the bottom of Dhordo core suggest the high radiogenic supply into the rann. Most of the  $^{87}\text{Sr}/^{86}\text{Sr}$  values ranges more than or equal to 0.73 strongly points towards the granitic, higher Himalayan source. The end member mixing plot suggests the higher input through the river Ghaggar/Saraswati into the Great Rann since ~18 ka till ~7 ka BP. The temporal scale isotopic records suggests gradual decline of the large river system during the Mid-Holocene times as the high  $^{87}\text{Sr}/^{86}\text{Sr}$  ratio values decrease. This is due to the dilution effect by removal of the high radiogenic Sr and/or mixing

of the less radiogenic due the decline of the large river system or may related either with the influence of Arabian Sea or the Indus delta.

12. The top parts of the cores (~5 m) appear to indicate a definite transition phase which turned the Rann from a fully marine basin to the present subaerially exposed land with peculiar characteristics. The emergence of the rann surface occurred gradually in the recent past which led to the formation of the distinct morphologic units.
13. The close association of these units with faults suggest differential tectonic activity along subsurface faults within the Great Rann basin may have played a major role in the emergence of various morphologic units at different times. Based on elevation and present day submergence characteristics, the Banni plain appears to be the first to emerge (at ~2000 yrs BP) followed by the Bet zone and the extensive Supra tidal salt flat (at ~500 yrs BP) which still gets submerged by marine waters regularly.

## REFERENCES

- Abuhejleh, A.N. and Znidarcic, D. (1995) Desiccation theory for soft cohesive soils. *J. Geotech. Eng.*, ASCE, 121, 493-502.
- Adatte, T., Keller, G., and Stinnesbeck, W. (2002). Late Cretaceous to early Paleocene climate and sea-level fluctuations: the Tunisian record. *Palaeogeography, Palaeoclimatology, Palaeoecology*, 178(3), 165-196.
- Agnihotri (2001) PhD Thesis: Chemical and Isotopic studies of sediments from the Arabian Sea and Bay of Bengal, Mohanlal Sukhadia University, Udaipur. 145pp.
- Agrawal, S. K. (1957). Kutch Mesozoic: A study of the Jurassic of Kutch with special reference to the Jhura Dome. *J. Paleontol. Soc. India*, 119-130.
- Almogi-Labin, A., Perelis-Grossovicz, L., and Raab, M. (1992). Living Ammonia from a hypersaline inland pool, Dead Sea area, Israel. *The Journal of Foraminiferal Research*, 22(3), 257-266.
- Alizai, A., Hillier, S., Clift, P. D., Giosan, L., Hurst, A., Van Laningham, S., and Macklin, M. (2012). Clay mineral variations in Holocene terrestrial sediments from the Indus Basin. *Quat. Res.*, 77(3), 368-381.
- Alve, E., and Murray, J. W. (1999). Marginal marine environments of the Skagerrak and Kattegat: a baseline study of living (stained) benthic foraminiferal ecology. *Palaeogeography, Palaeoclimatology, Palaeoecology*, 146(1), 171-193.
- Amin, B. S., Likhite, S. D., Radhakrishnamurty, C., & Somayajulu, B. L. K. (1972, March). Susceptibility stratigraphy and paleomagnetism of some deep Pacific Ocean cores. In *Deep Sea Research and Oceanographic Abstracts* (Vol. 19, No. 3, pp. 249-252). Elsevier.
- Backman J., Moran K., McInroy D.B., Mayer L.A. and the Expedition 302 Scientists (2006). Sites M0001–M0004. *Proceedings of the Ocean Drilling Program*. Scientific Results 302.
- Balgopal, A. T., and Srivastava, V. K. (1973). Petrography and classification of the arenites of the Chari Series in the Jurassic rocks of Central Kutch, Gujarat (India). *Sedimentary Geology*, 10(3), 215-224.
- Baskaran, M., Marathe, A. R., Rajaguru, S. N., and Somayajulu, B. L. K. (1986). Geochronology of palaeolithic cultures in the Hiran Valley, Saurashtra, India. *Journal of Archaeological Science*, 13(6), 505-514.

- Bhushan, R., Somayajulu, B. L. K. (2001) Concentrations of the burial fluxes of organic and inorganic carbon on the eastern margins of the Arabian Sea. *Mar. Geol.* 178, 95-113.
- Bilham, R. (1998). Slip parameters for the Rann of Kachchh, India, 16 June 1819, earthquake, quantified from contemporary accounts. *Geological Society, London, Special Publications*, 146(1), 295-319.
- Biscay, P. E. (1965). Mineralogy and sedimentation of recent deep-sea clay in the Atlantic Ocean and adjacent seas and oceans. *Geological Society of America Bulletin*, 76(7), 803-832.
- Biswas, S. K., (1971). The miliolite rocks of Kutch and Kathiawar. *Sedimentary Geology*, 5, 147-164.
- Biswas, S. K., and Deshpande, S. V. (1973). A note on the mode of eruption of the Deccan Trap lavas with special reference to Kutch. *J. Geol. Soc. India*, 14(2), 134-141.
- Biswas, S.K. (1974). Landscape of Kutch - A morphotectonic analysis. *Indian Journal of Earth Science*, v. 1(2), pp. 177-190.
- Biswas, S.K. (1977). Mesozoic Rock Stratigraphy of Kutch. *Quarterly Journal of the Geological, Mining and Metallurgical Society of India*. 49:52 1-52.
- Biswas, S. K. (1981). Basin framework, Palaeo-environment and depositional history of the Mesozoic sediments of Kutch basin, Western India. *Quarterly Journal of Geology Mining Metallurgy Society of India*, 53, 56-85.
- Biswas, S. K. (1982). Rift basins in western margin of India and their hydrocarbon prospects with special reference to Kutch basin. *AAPG Bulletin*, 66(10), 1497-1513.
- Biswas, S.K. (1987). Regional tectonic framework, structure and evolution of western marginal basins of India. *Tectonophysics*, 135, 307-327.
- Biswas, S. K. (1992). Tertiary stratigraphy of Kutch. *Journal of Palentological. Soc. of India* 37: 1-29
- Biswas, S. K. (1993). Geology of Kutch, K.D. Malaviya Institute of Petroleum Exploration, Dehradun, 450 pp.
- Biswas, S. K., and Khattri, K. N. (2002). A geological study of earthquakes in Kachchh, Gujarat, India. *Jour. Geol. Soc. India*, 60, 131-142.
- Boltovskoy, E. and Wright, R. (1976). Recent Foraminifera, B. V. Publishers-The Hague.

- Bordovskiy, O. K. (1965). Sources of organic matter in marine basins. *Marine Geology*, 3(1), 5-31.
- Boulay, S., Colin, C., Trentessaux, A., Frank, N., Liu, Z., Yim, W.W.S. (2004). Variations of terrigenous sediment supply associated with the East-Asian monsoon intensity — implications for sedimentary sources and South China Sea currents. *Abstracts of 8<sup>th</sup> International Conference on Paleoceanography*, 5–10 September 2004, Biarritz, France, pp. 136–137
- Bradshaw, J., (1961). Contribution from the Cushman Foundation for Foraminiferal Research, 12(3), 87-106.
- Brooks, A. L. (1967). Standing crop, vertical distribution, and morphometrics of *Ammonia beccarii* (Linne). *Limnology and Oceanography*, 667-684.
- Butler, G. P. (1969). Modern evaporite deposition and geochemistry of coexisting brines, the sabkha, Trucial Coast, Arabian Gulf. *Journal of Sedimentary Research*, 39(1).
- Burnes, A. (1835). A memoir on the Eastern Branch of River Indus giving an account of alteration produced by it by an earthquake in 1819, also a theory of the Runn, and some conjectures on the root of Alexander the great, drawn up in the year 1827-28. *Roy. Asiatic Soc.* 3: 550-558.
- Calvert, S. E., and Pedersen, T. F. (1993). Geochemistry of recent oxic and anoxic marine sediments: implications for the geological record. *Marine geology*, 113(1), 67-88.
- Cann, J. H. and De Deckker, P. D. (1981). Fossil Quaternary and living foraminifera from athalassic (non-marine) saline lakes, Southern Australia. *Journal of Paleontology*, 55: 660–670.
- Cann, J.H., Belperio, A.P., Murray-Wallace, C.V. (2000a). Late Quaternary paleosealevels and paleoenvironments inferred from foraminifera, northern Spencer Gulf, South Australia. *J. Foraminiferal Res.* 30, 29– 53.
- Cann, J.H., Bourman, R.P., Barnett, E.J. (2000b). Holocene foraminifera as indicators of relative estuarine-lagoonal and oceanic influences in estuarine sediments of the River Murray, South Australia. *Quat. Res.* 53, 378– 391.
- Cearreta, A. (1988). Population dynamics of benthic foraminifera in the Santona estuary, Spain. *Revue de Paléobiologie*, 2, 721-724.
- Cearreta, A. (1989). Foraminiferal assemblages in the ria of San Vicente de la Barquera (Cantabria, Spain). *Revista Española de Micropaleontología*, 21, 67-80.

Carboni M. G. and Di Bella L. (1996). Morphological variation in the genus *Ammonia* Brunnich in the Plio-Pleistocene of the Sabina (Latium). In Cherchi A. (ed.) "Autecology" *Bull. Soc. Pal. Special* 3, 63-76.

Chakrabarti, A., Somayajulu, B. L. K., Baskaran, M., Kumar, B., (1993). Quaternary miliolites of Kutch and Saurashtra, western India: Depositional environments in the light of physical sedimentary structures, biogenic structures and geochronological setting of the rocks. *Senckenbergiana Maritima*. 23, 7-28.

Chamley, H., (1989). *Clay Sedimentology*. Springer-Verlag, Berlin, 623.

Chowksey, V., Maurya, D. M., Khonde, N. and Chamyal, L. S (2010). Tectonic geomorphology and evidence for active tilting of the Bela, Khadir and Bhanjada islands in the seismically active Kachchh palaeorift graben, Western India. *Zeitschrift für Geomorphologie*, 54(4), 467-490.

Chowksey, V., Maurya, D. M., Joshi, P., Khonde, N., Das, A., and Chamyal, L. S. (2011). Lithostratigraphic development and neotectonic significance of the Quaternary sediments along the Kachchh Mainland Fault (KMF) zone, western India. *Journal of earth system science*, 120(6), 979-999.

Chauhan, O.S. (1994). Influence of macrotidal environment on shelf sedimentation, Gulf of Kachchh, India. *Continental Shelf Research*, 14, 1477-1493.

Chauhan, O. S., Sukhija, B. S., Gujar, A. R., Nagabhushanam, P. and Paropkari, A. L. (2000). Late Quaternary variations in clay minerals along SW continental margin of India: evidence of climatic variations. *Geo marine letters*, 20, 118-122.

Chauhan, O.S., Jayakumar, S., Menezes, A.A., Rajawat, A.S., and Nayak, S.R. (2006). Anomalous inland influx of River Indus, Gulf of Kachchh, India. *Marine Geology*, 229, 91-100.

Chung, W and Gao, H. (1995). Source parameters of the Anjar earthquake of July 21, 1956, India, and its seismotectonic implications for the Kutch rift basin. *Tectonophysics*, 242: 281-292.

Clift, P. D., N. Shimizu, G. D. Layne, J. S. Blusztajn, C. Gaedicke, H-U. Schlüter, M. K. Clark, and S. Amjad (2001). Development of the Indus Fan and its significance for the erosional history of the Western Himalaya and Karakoram. *Geological Society of America Bulletin*, 113(8), 1039-1051.

Clift, P., Lee, J. I., Clark, M. K., and Blusztajn, J. (2002). Erosional response of South China to arc rifting and monsoonal strengthening; a record from the South China Sea. *Marine Geology*, 184(3), 207-226.

Clift P.D., Goisan. L., Blusztajn. J., Champbell. I. H., Allen. C., Pringle. M., Tabrez. A. R., Danish. M., Rabbani. M. M., Alizai. A., Carter. A. and Luckge. A. (2008). Holocene erosion of the Lesser Himalaya triggered by intensified summer monsoon. *Geology*, 36, 79-82.

Colin, C., Frank, N., Copard, K., and Douville, E. (2010). Neodymium isotopic composition of deep-sea corals from the NE Atlantic: implications for past hydrological changes during the Holocene. *Quaternary Science Reviews*, 29(19), 2509-2517.

Cooper, F.J., Roberts, G.P., and Underwood, C.J. (2007). A comparison of  $10^3$ - $10^5$  year uplift rates on the South Alkyonides Fault, central Greece: Holocene climate stability and the formation of coastal notches. *Geophysical Research Letters*, 33, 1-6.

Dean, W. E., and Gorham, E. (1998). Magnitude and significance of carbon burial in lakes, reservoirs, and peatlands. *Geology*, 26(6), 535-538.

Debenay J B, (2000). Distribution trends of foraminiferal assemblages in peralic environments-A base for using foraminifera as bioindicators, *Topics in Geobiology*, v-15 Ed. Ronald and Martin, Kluwer academic

Degens E.T. and Ittekkot, V. (1984). A new look at clay-organic interactions. *Mitt. Geol. Palaontol. Inst. Univ. Humburg Festband Georg Knetsh*, 56, 229-248.

Dellwig, L. (1955). Origin of the Salina Salt of Michigan. *J. Sedim. Petrol.*, 25, 83±100.

Deo, Sushama G., Savita Ghatе, and S. N. Rajaguru. (2011). Holocene environmental changes and cultural patterns in the coastal western India: A geoarcheological perspective. *Quaternary International*, 229, 132-139.

Dill H. (1986). Metallogenesis of early Palaeozoic graptolites shales from the Graefenthal Horts (Northern Bavaria-Federal Republic of Germany), *Econ. Geol.*, 81, 889-903

Dymond, J., Suess, E., and Lyle, M. (1992). Barium in deep-sea sediment: A geochemical proxy for paleoproductivity. *Paleoceanography*, 7(2), 163-181.

Enzel. Y., Ely. L.L., Mishra. S., Ramesh. R., Amit. R., Lazar. B., Rajaguru. S. N., Baker. V. R., and Sandler. A. (1999). High-resolution Holocene environmental changes in the Thar desert, northwestern India. *Science*, 284, 125-128.

Esquevin, J. (1969). Influence de la composition chimique des illites sur cristallinite. *Bull. Cent. Rech. Pau SNPA*, 3(1), 147-153.

Fleitmann, D., Burns, S. J., Mudelsee, M., Neff, U., Kramers, J., Mangini, A., & Matter, A. (2003). Holocene forcing of the Indian monsoon recorded in a stalagmite from southern Oman. *Science*, 300, 1737–1739.

Flemming, B. W. (2000). A revised textural classification of gravel-free muddy sediments on the basis of ternary diagrams. *Continental Shelf Research*, 20(10), 1125-1137.

Folk, R. L., (1974). Petrology of sedimentary rocks. Hemphill Publishing Co. Texas pp. 184.

France-Lanord, C., Derry, L., and Michard, A. (1993). Evolution of the Himalaya since Miocene time: isotopic and sedimentological evidence from the Bengal Fan. *Geological Society, London, Special Publications*, 74(1), 603-621.

Frere, H. B. E. (1870). Notes on the Runn of Cutch and neighbouring region. *Journal of the Royal Geographical Society of London*, 181-207.

Fürsich, F. T., Singh, I. B., Joachimski, M., Krumm, S., Schlirf, M., & Schlirf, S. (2005). Paleoclimatic reconstructions of the Middle Jurassic of Kachchh (Western India): An integrated approach based on paleoecological, oxygen isotopic and clay mineralogical data. *Paleogeography, Paleoclimatology, Paleoecology*, 217, 289-309

Gaur A.S. and Vora K. H., (1999). Ancient shorelines of Gujarat, India, during the Indus civilization (Late-Mid-Holocene): A study based on archeological evidences. *Current Science*, 77, 180-185.

Geddes A., (1960). The alluvial morphology of the Indo-Gangetic Plain. *Trans. Inst. Brit. Geog.*, 252-264.

Gennari, Giordana, Thomas Rosenberg, Silvia Spezzaferri, Jean-Pierre Berger, Dominik Fleitmann, Frank Preusser, Mahmoud Al-Shanti, and Albert Matter. (2011). Faunal evidence of a Holocene pluvial phase in southern Arabia with remarks on the morphological variability of *Helenina anderseni*. *Journal of Foraminiferal Research*, 41 (3), 248-259.

Ghosh, A., Saha, S., Saraswati, P. K., Banerjee, S., Burley, S., & Gundu Rao, T. K. (2008). *Gallitellia*-a proxy for palaeomonsoonal upwelling on the western coast of India? *Current Science*, 95, 1608-1611.

Ghose, B., Kar, A., and Husain, Z. (1979). The lost courses of the Saraswati River in the Great Indian Desert: New evidence from landsat imagery. *Geographical Journal*, 446-451.

Gibbs R.J. (1977). Clay mineral segregation in the marine environment. *Journal of sedimentary petrology*, 747, 237-243.

Gingele, G.X., (1996). Holocene climatic optimum in Southwest Africa-evidence from the marine clay mineral record. *Paleogeography, Paleoclimatology, Paleoecology*, 122, 77-87.

Giosan, L., Clift, P. D., Blusztajn, J., Tabrez, A., Constantinescu, S., & Filip, F. (2006). On the control of climate- and human-modulated fluvial sediment delivery on river delta

development: The Indus: Eos (*Transactions, American Geophysical Union*), 87, 52, OS14A–04.

Glennie, K. W. and G. Evans (1976). A reconnaissance of the recent sediments of the Ranns of Kutch, India. *Sedimentology*, 1976, 23, 625-64.

Goodall, T.M. and Al-Belushi, J.D. (1997). A glossary of Arabic desert terminology used in southeastern Arabia. In: *Quaternary Deserts and Climatic Change* (Eds A.S. Alsharhan, K.W. Glennie and G.L. Whittle), pp. 611±619. A.A. Balkema, Rotterdam.

Goodall, T. M., North, C. P., and Glennie, K. W. (2000). Surface and subsurface sedimentary structures produced by salt crusts. *Sedimentology*, 47(1), 99-118.

Gopala Rao, D. (1988). A shallow seismic reflection study of the Gulf of Kutch, northwest India — Observations on its structural evolution. *Marine Geology*, 82, 277-283.

Griffin, J. J., Windom, H., & Goldberg, E. D. (1968). The distribution of clay minerals in the world ocean. *Elsevier*, Amsterdam.

Grim R.E. (1968). Clay mineralogy. *McGraw Hill*, New York, 596.

Gupta S. K. (1975). Silting of the Rann of the Kutch during the Holocene. *Ind. Jour. of Earth Sci.* 2, 163-175.

Gupta, B. K. S. (Ed.). (2002). Modern foraminifera. *Springer*.

Handford, C.R. (1991). Marginal marine halite: sabkhas and salinas. In: *Evaporites, Petroleum and Mineral Resources* (Ed. J.L. Melvin), pp. 1±66. Developments in Sedimentology, 50, Elsevier, Amsterdam.

Hashimi, N.H., Nigam, R., Nair, R.R. and Rajgopalan, G. (1995). Holocene sea level fluctuations on western Indian continental margin: An update. *Jour. Geol. Soc. of India*, 46, 157-162.

Hayward, B. W. (1993). Estuarine foraminifera, Helena Bay, Northland, New Zealand. *Tane*, 34, 79-88.

Hayward, B.W. and Hollis, C. J. (1994). Brackish foraminifera in New Zealand: a taxonomic and ecological review, *Micropaleontology*, 42, 395-413.

Hedges, J. I., Clark, W. A., Quay, P. D., Richey, J. E., Devol, A. H., and Santos, U. D. M. (1986). Compositions and fluxes of particulate organic material in the Amazon River. *Limnology and Oceanography*, 31(4), 717-738.

Herzschuh, U., (2006). Palaeo-moisture evolution in monsoonal Central Asia during the last 50,000 years. *Quaternary Science Reviews*, 25, 163–178.

Horton, B. P., & Murray, J. W. (2007). The roles of elevation and salinity as primary controls on living foraminiferal distributions: Cowpen Marsh, Tees Estuary, UK. *Marine Micropaleontology*, 63(3), 169-186.

I. A. R. (Indian Archaeology: A review), *Bull. Archeol. Sur. India*, (1994-99), Archaeological Survey of India, New Delhi.

Jain, M. and Tandon, S.K., (2003). Quaternary alluvial stratigraphy and paleoclimatic reconstruction at the Thar margin. *Current science*, 84, 1048-1055.

Jones, B., Manning, D.A.C., (1994). Comparison of geochemical indices used for the interpretation of palaeoredox conditions in ancient mudstones. *Chem. Geol.* 111, 111 –129.

Kar, A., and Ghose, B. I. M. A. L. (1983). Geomorphological research on Indian desert. *A Survey of Research in Physical Geography*, 61-74.

Kar, A. (1995). Geomorphology of arid western India. *Memoirs-Geological Society of India*, 168-190.

Kendall, A.C. (1984). Continental and supratidal (sabkha) evaporites. In: *Facies Models*, 2nd ed (Ed. R.G. Walker), pp. 145±157. *Geoscience Canada Reprint Series 1*. Geological Association of Canada, Toronto, Canada.

Kessarkar, P. M., Rao, V. P., Ahmad, S. M., & Babu, G. A. (2003). Clay minerals and Sr-Nd isotopes of the sediments along the western margin of India and their implication for the sediment provenance. *Marine Geology*, 202, 55-69.

Konrad, J.M. and Ayad, R. (1997). Desiccation of a sensitive clay: Field experimental observations. *Can. Geotech. J.*, 34, 929-942.

Koshal, V. N. (1984). Differentiation of Rhaetic sediments in subsurface of Kutch based on palynofossils. *Petroleum Asia Jour.*, 3, 102-105.

Khonde, N., Maurya, D. M., Sing, A. D., Chowksey, V. and Chamyal, L. S. (2011). Environmental significance of raised rann sediments along the margins of Khadir, Bhanjada and Kuar bet islands in Great Rann of Kachchh, Western India. *Current Science*, 101, 11, 1429-1434.

Khonde N, Maurya D M, Singh A D, Das Archana and Chamyal L. S. (In Press) Sediment Characteristics and Foraminiferal Distribution in the Bet Zone of the Great Rann of Kachchh, Western India, *Spec. Pub. Geo. Soc. India*. 1-18.

Kolla V., Kostecki, J.E., Robinson, F., and Biscaye, P.E., (1981). Distribution and origin of clay minerals and quartz in surface sediments of the Arabian Sea. *Journal of Sedimentary Petrology*, 51, 563-569.

Konta J., (1985). Mineralogy and chemical maturity of suspended matter in major rivers sampled under SCOPE/UNEP project. *Mitt. Geology. paleontol. Inst. Univ. Hamburg*, 58, 557-568.

Lachenbruch, A.H. (1962). Mechanics of thermal contraction cracks and ice-wedge polygons in permafrost. *Geol. Soc. Am. Spec. Paper*, 70, New York.

Lamb, A. L., Wilson, G. P., and Leng, M. J. (2006). A review of coastal palaeoclimate and relative sea-level reconstructions using  $\delta^{13}\text{C}$  and C/N ratios in organic material. *Earth Science Reviews*, 75(1), 29-57.

Laprida, C., Chandler, D. E. C., Mercau, J. R., López, R. A., and Marcomini, S. (2011). Modern foraminifera from coastal settings in northern Argentina: implications for the paleoenvironmental interpretation of Mid Holocene littoral deposits. *Revista Mexicana de Ciencias Geológicas*, 28(1), 45-64

Lim, D.I., Jung, H.S., Choi, J.Y., Yang, S., and Ahn, K.S. (2006) Geochemical compositions of river and shelf sediments in the Yellow Sea: grain size normalization and sediment provenance. *Continental Shelf Research*, 26, 15–24.

Limmer, David R., Philipp Böning, Liviu Giosan, Camilo Ponton, Cornelia M. Köhler, Matthew J. Cooper, Ali R. Tabrez, and Peter D. Clift. (2012). Geochemical record of Holocene to Recent sedimentation on the Western Indus continental shelf, Arabian Sea. *Geochemistry, Geophysics, Geosystems*, 13(1).

Loeblich, A. R. and Tappan, H. N. (1988). Foraminiferal Genera and their Classification, *Van Nostrand Reinhold*, New York, 1728.

Lowenstein, T.K. and Hardie, L.A. (1985). Criteria for the recognition of salt-pan evaporites. *Sedimentology*, 32, 627-644.

Mackenzie, A. S., Quirke, J. M. E., and Maxwell, J. R. (1980). Molecular parameters of maturation in the Toarcian shales, Paris Basin, France—II Evolution of metalloporphyrins. *Physics and Chemistry of the Earth*, 12, 239-248.

Maldonado A., and Stanley D.J. (1981). Clay mineral distribution as influenced by depositional processes in the southeastern Levantine Sea. *Sedimentology*, 28, 21-32.

Malik, J.N., Merh, S.S., Sridhar, V. (1999). Palaeo-delta complex of Vedic Sarasvati and other ancient rivers of northwestern India. *Geological Society of India Memoirs*, 42, 163–174.

- Martin, R. E. (Ed.). (2000). Environmental micropaleontology: the application of microfossils to environmental geology (Vol. 15). *Springer*.
- Maurya, D.M., Thakkar, M.G., and Chamyal, L.S. (2003) Implications of transverse fault system on tectonic evolution of Mainland Kachchh, western India. *Current Science*, 85, 661-667.
- Maurya, D. M., Goyal, B., Patidar, A. K., Mulchandani, N., Thakkar M. G. and Chamyal, L. S. (2006). Ground penetrating radar imaging of two large sand blow craters related to the 2001 Bhuj earthquake, Kachchh, Western India. *Jour. Applied Geophysics*, 60, 142-152.
- Maurya, D. M., M. G. Thakkar, A. K. Patidar, S. Bhandari, B. Goyal and L. S. Chamyal (2008). Late Quaternary geomorphic evolution of the coastal zone of Kachchh, Western India. *J. of Coastal Research*, 24, 746-758.
- Maurya, D. M., Thakkar, M. G., Khonde, N., and Chamyal, L. S (2009). Geomorphology of Little Rann of Kachchh, Western India: Implication for basin architecture and Holocene paleo-oceanographic conditions. *Zeitschrift fur Geomorphologie*, 53, 69-80.
- Maurya, D. M., Khonde, N., Das, A., Chowksey, V., and Chamyal, L. S. (2013). Subsurface sediment characteristics of the Great Rann of Kachchh, western India based on preliminary evaluation of textural analysis of two continuous sediment cores. *Current Science*, 104(3), 1.
- McDaniel, D. K., Hemming, S. R., McLennan, S. M., and Hanson, G. N. (1994). Resetting of neodymium isotopes and redistribution of REEs during sedimentary processes: the Early Proterozoic Chelmsford Formation, Sudbury Basin, Ontario, Canada. *Geochimica et Cosmochimica Acta*, 58(2), 931-941.
- McHugh, Cecilia MG, Damayanti Gurung, Liviu Giosan, William BF Ryan, Yossi Mart, Ummuhan Sancar, Lloyd Burckle, and M. Namik Çagata (2008). The last reconnection of the Marmara Sea (Turkey) to the World Ocean: A paleoceanographic and paleoclimatic perspective. *Marine geology*, 255(1), 64-82.
- Meyers, P. A. (1994). Preservation of elemental and isotopic source identification of sedimentary organic matter. *Chemical Geology*, 114(3), 289-302.
- Meyers, G. (1996). Variation of Indonesian throughflow and the El Niño-Southern Oscillation. *Journal of Geophysical Research: Oceans (1978–2012)*, 101(C5), 12255-12263.
- Meyers, P. A., and Lallier-Vergès, E. (1999). Lacustrine sedimentary organic matter records of Late Quaternary paleoclimates. *Journal of Paleolimnology*, 21(3), 345-372.
- Merh, S. S. (1995). Geology of Gujarat. *Geological Society of India*.

- Merh, S. S. (2005). The Great Rann of Kachchh: Perceptions of a field Geologists. *Jour. Geol. Soc. India*, 65, 9-25.
- Misra, Virendra Nath (1993). "Indus civilization and the Rigvedic Saraswati." *South Asian Archaeology*, 2, 511-525.
- Mitra, D. S., and Bhadu, B. (2012). Possible contribution of River Saraswati in groundwater aquifer system in western Rajasthan, India. *Current Science*, 102(5), 685-689.
- Moodley, L., and Hess, C. (1992). Tolerance of infaunal benthic foraminifera for low and high oxygen concentrations. *The Biological Bulletin*, 183(1), 94-98.
- Moore, D. M., and Reynolds Jr, R. C. (1989). X-ray diffraction and the identification and analysis of clay minerals. *Oxford University Press* (OUP).
- Morgan-Jones, M. (1977). Mineralogy of the non-carbonate material from the Chalk of Berkshire and Oxfordshire, England. *Clay Minerals*, 12(4), 331-344.
- Müller, P. J., and Suess, E. (1979). Productivity, sedimentation rate, and sedimentary organic matter in the oceans—I. Organic carbon preservation. *Deep Sea Research Part A. Oceanographic Research Papers*, 26(12), 1347-1362.
- Murray, J. W. (1991). Ecology and palaeoecology of benthic foraminifera (397). *Harlow: Longman Scientific & Technical*.
- Murray, J. W. (2001). The niche of benthic foraminifera, critical thresholds and proxies. *Marine Micropaleontology*, 41(1), 1-7.
- Murray, J. W. (2006) Ecology and Applications of Benthic Foraminifera, *Cambridge University Press*, 426.
- Naidu P.D. and Malmgren B.A., (1996). A high-resolution record of the late Quaternary upwelling along the Oman margin, Arabian Sea, bases on planktic foraminifera. *Palaeoceanography*, 11, 129-140.
- Nair, R. R., and Hashimi, N. H. (1982). Distribution and dispersal of clay minerals on the western continental shelf of India. *Marine Geology*, 50(1), M1-M9.
- Neal, J.T., Langer, A.M. and Kerr, P.F. (1968). Giant desiccation polygons of Great Basin playas. *Bull. Geol. Soc. Am.*, 79, 69-90.
- Nigam R. and Khare N. (1999). Spatial and temporal distribution of foraminifera in sediments off the central west coast of India and Use of their test morphologies for the reconstruction of palaeomonsoonal precipitation. *Micropaleontology*, 45, 3, 285-303.

- Nigam R. & Chaturvedi S. K. (2000). Foraminiferal study from Kharo creek, Kachchh (Gujarat), North West coast of India. *Ind. jour. Mar. Sci.* 29, 133-138.
- Nisha N. R. (2002). Ph. D. Thesis (Unpublished) Foraminiferal and Pteropod records in the late quaternary sequence off Northern Kerala and their oceanographic and climatic significance.
- Nisha, N. R., and Singh, A. D. (2012). Benthic foraminiferal biofacies on the shelf and upper continental slope off North Kerala (Southwest India). *Journal of the Geological Society of India*, 80(6), 783-801.
- Oldham R. D., (1926). The Cutch (Kachh) earthquake of 16th June 1819 with a revision of the great earthquake of 12th June 1897. *Mem. Geol. Soc. of India*, 46, 1-77.
- Overpeck, J., Anderson, D., Trumbore, S., & Prell, W. (1996). The southwest Indian monsoon over the last 18000 years, *Climate dynamics*, 12, 213-225.
- Owen, L. A., Finkel, R. C., and Caffee, M. W. (2002). A note on the extent of glaciation throughout the Himalaya during the global Last Glacial Maximum. *Quaternary Science Reviews*, 21(1), 147-157.
- Pandarinath, K., Prasad, S., Deshpande, R. D., & Gupta, S. K. (1999). Late Quaternary sediments from Nal Sarovar, Gujarat, India: Distribution and provenance. *Indian Acad. Sci. (Earth Planet sci.)*, 108, 107-116.
- Pandharinath K. (2009). Clay minerals in SW Indian continental shelf sediment cores as indicators of provenance and palaeomonsoonal conditions: a statistical approach, *International Geology Review*, 51, 2, 145-165.
- Patterson, R. T., Roland Gehrels, W., Belknap, D. F., & Dalby, A. P. (2004). The distribution of salt marsh foraminifera at Little Dipper Harbour New Brunswick, Canada: implications for development of widely applicable transfer functions in sea-level research. *Quaternary International*, 120(1), 185-194.
- Phleger, F. B. (1970). Foraminiferal populations and marine marsh processes. *Limnology and Oceanography*, 522-534.
- Phipps, M. D., Kaminski, M. A., and Aksu, A. E. (2010). Calcareous benthic foraminiferal biofacies along a depth transect on the southwestern Marmara shelf (Turkey). *Micropaleontology*, 56(3), 377.
- Piper DZ and Perkins RB (2004). A modern vs Permian black shale—the hydrography, primary productivity, and water-column chemistry of deposition. *Chem. Geol.*, 206, 177-197.

- Pirazzoli, P. A. (1986). Marine notches. *Sea-Level Research: A Manual for the Collection and Evaluation of Data. GeoBooks*, Norwich, 361-400.
- Prasad S. and Enzel Y. (2006). Holocene paleoclimates of India. *Quaternary Research*, 66, 442-453.
- Prell W. L. (1984). Variation of the monsoonal upwelling: A response to changing solar radiation. In: Hansen, J.E., Takahashi, T. (Eds.), *Climate Processes and Climate Sensitivity. Geophysical Monograph, American Geophysical Union*, Washington, DC. 48-57.
- Rahaman, W., Singh, S. K., Sinha, R., and Tandon, S. K. (2009). Climate control on erosion distribution over the Himalaya during the past~ 100 ka. *Geology*, 37(6), 559-562.
- Rajagopalan, G., Sukumar, R., Ramesh, R., & Pant, R. K. (1997). Late Quaternary vegetational and climatic changes from the tropical peats in the southern India- an extended record up to 40 000 years B.P. *Current Science*, 73, 60-63.
- Raj Nath (1942). The Jurassic rocks of Kutch. Their bearing on some problems of Indian geology. *Presidential Address, Geol. and Geog. Sec. Ind. Sci. Congress*.
- Rajendran, C. P., Rajendran, K., and John, B. (1998). Surface deformation related to the 1819 Kachchh earthquake: Evidence for recurrent activity. *Current Science*, 75(6), 623-626.
- Rajendran, C. P. and Rajendran, K. (2001). Characteristics of Deformation and Past Seismicity Associated with the 1819 Kutch Earthquake, Northwestern India. *Bull. Seismol. Soc. America*, 91, 407-426.
- Rajshekhhar C., Praveen Gawali, Mudgal T. R., Reddy P. P., and Basavaiah N. (2004). Micropaleontology and mineral magnetic evidences of the Holocene mudflats of Navlakhi, Gulf of Kachchh. *Jour. Ind. Geophys. Union*, 8, 71-77.
- Rao, V.P. (1991). Clay mineral distribution in the continental shelf and slope off Saurashtra, west coast of India. *Indian Journal of Marine science*, 20, 1-6.
- Rao V.P., and Rao, B.R., (1994). Provenance and distribution of clay minerals sediments in sediments of the western continental shelf and slope of India. *Continental Shelf Research*, 15 (14), 1757-1771.
- Reichert, P., and Omlin, M. (1997). On the usefulness of overparameterized ecological models. *Ecological Modelling*, 95(2), 289-299.
- Roy and Merh S S (1981). The Great Rann of Kutch-An intriguing Quaternary terrain. *Recent Researches in Geology* (Hindustan Pub. Corporation), 9, 100-108.

Rust, D. and Kershaw, S (2000). Holocene tectonic uplift pattern in northeastern Sicily: Evidence from marine notches in coastal outcrops. *Marine Geology*, 167, 105-126.

Saini, H., & Mujtaba, S. (2010). Luminescence dating of the sediments from a buried channel loop in Fatehabad area, Haryana: insight into Vedic Saraswati River and its environment. *Geochronometrica*, 37, 29-35.

Scott, D. B., Mudie, P. J. and Bradshaw, J. S., (1976). *Jour. Foraminiferal Research*, 6, 59-75.

Sen Gupta BK, (1999). Modern Foaminifera, Dordrecht: Kluwer.

Gupta, B. S., & Platon, E. (2006). Tracking past sedimentary records of oxygen depletion in coastal waters: Use of the Ammonia-Elphidium foraminiferal index. *Journal of Coastal Research*, 1351-1355.

Sen, G., Bizimis, M., Das, R., Paul, D. K., Ray, A., and Biswas, S. (2009). Deccan plume, lithosphere rifting, and volcanism in Kutch, India. *Earth and Planetary Science Letters*, 277(1), 101-111.

Sharma, R. P., Rathore, M. S., Singh, R. S., & Qureshi, F. M. (2010). Mineralogical Framework of Alluvial Soils Developed on the Aravalli Sediments. *Journal of the Indian Society of Soil Science*, 58, 1, 70-75.

Sharma, A., Sensarma, S., Kumar, K., Khanna, P. P., and Saini, N. K. (2012). Mineralogy and geochemistry of the Mahi River sediments in tectonically active western India: Implications for Deccan large igneous province source, weathering and mobility of elements in a semi-arid climate. *Geochimica et Cosmochimica Acta*.

Shaw, P. and Thomas, D.S.G. (1997). Pans, playas and salt lakes. In: *Arid Zone Geomorphology: Process, Form and Change in Drylands*, 2nd edn (Ed. D.S.G. Thomas), pp. 293-317. Wiley, Chichester.

Shetye, S. R. (1999). Tides in the Gulf of Kutch, India. *Cont. Shelf Res.* 19, 1771-1782.

Singer, A., (1984). The paleoclimatic interpretation of clay minerals in sediments- a review. *Earth science review*, 21, 251-293.

Singh S.K., Rai S.K., and Krishnaswami S. (2008). Sr and Nd isotopes in river sediments from the Ganga Basin: Sediment provenance and hot-spots of physical erosion. *Journal of Geophysical Research*, 113.

Singh B.P. (ed) (1996). Indian archeology 1991-92-A review, *Archeological Survery of India.*, 324.

- Singh, B. P., Hatton, B. J., Singh, B., Cowie, A. L., and Kathuria, A. (2010). Influence of biochars on nitrous oxide emission and nitrogen leaching from two contrasting soils. *Journal of Environmental Quality*, 39(4), 1224-1235.
- Sirocko F. and Lange H. (1991). Clay accumulation rates in the Arabian Sea during the Late Quaternary. *Marine Geology*, 97, 105-119.
- Sirocko, F., Sarnthein, M., Erlenkeuser, H., Lange, H., Arnold, M., and Duplessy, J. C. (1993). Century-scale events in monsoonal climate over the past 24,000 years. *Nature*, 364, 322-324.
- Sirocko, F., Garbe-Schönberg, D., and Devey, C. (2000). Processes controlling trace element geochemistry of Arabian Sea sediments during the last 25,000 years. *Global and Planetary Change*, 26(1), 217-303.
- Snow, R. S. and Slingerland, R. L. (1990). Stream Profile Adjustment to Crustal Warping: Nonlinear Results from a Simple Model. *The Journal of Geology*, 98, 699-708.
- Sohoni, P. S., and Malik, J. N. (1998). Remnants of large magnitude earthquakes: evidences from the Great Rann sediments, Kachchh, western India. *Current science*, 74(11), 985-989.
- Somayajulu, B.L.K., (1993). Age and mineralogy of the miliolites of Saurashtra and Kachchh, Gujarat. *Current Science*, 64, 926-928.
- Srivastava, P. K. (1971). Recent sediments of the Rann of Kutch. *Jour. Geol. Soc. of India*, 29, 392-395.
- Stuiver, Minze, Paula J. Reimer, Edouard Bard, J. Warren Beck, George S. Burr, Konrad A. Hughen, Bernd Kromer, Gerry McCormac, Johannes Van Der Plicht, and Marco Spurk. (2006). INTCAL98 radiocarbon age calibration, 24 000-0, cal B.P., *Radiocarbon*, 40, 1041-1083.
- Swallow, J. E. (2000). Intra-annual variability and patchiness in living assemblages of salt-marsh foraminifera from Mill Rythe Creek, Chichester Harbour, England. *Journal of Micropalaeontology*, 19(1), 9-22.
- Thakkar, M. G., Maurya, D. M., Raj. R. and Chamyal, L.S., (1999). Quaternary tectonic history and terrain evolution of the area around Bhuj, Mainland Kachchh, Western India. *Jour. Geol. Soc. of India*, 53, 601-610.
- Thakkar, M. G., Goyal, B., Maurya, D. M., and Chamyal, L. S. (2012). Internal geometry of reactivated and non-activated sandblow craters related to 2001 Bhuj earthquake, India: A modern analogue for interpreting paleosandblow craters. *Journal of the Geological Society of India*, 79(4), 367-375.

- Thamban, M., Purnachandra Rao, V., & Schneider, R. R. (2002). Reconstruction of late Quaternary monsoon oscillations based on clay mineral proxies using sediment cores from the western margin of India. *Marine Geology*, 186, 527-539.
- Thamban, M., Rao, V.P., (2005). Clay minerals as paleomonsoon proxies: Evaluation and relevance to the late Quaternary records from SE Arabian Sea. *Antarctic Geosciences, ocean-atmosphere interaction and paleoclimatology*, 198-215.
- Tribovillard, N., Algeo, T. J., Lyons, T., and Riboulleau, A. (2006). Trace metals as paleoredox and paleoproductivity proxies: An update. *Chemical Geology*, 232(1), 12-32.
- Thiry M., (2000). Paleoclimatic interpretation of clay minerals in marine deposits: an outlook from the continental origin. *Earth Science Review*, 49, 201-221.
- Tripathi, J. K., Bock, B., Rajamani, V., and Eisenhauer, A. (2004). Is River Ghaggar, Saraswati? Geochemical constraints. *Current Science*, 87(8), 1141-1145.
- Tripathi, J. K., Bock, B., and Rajamani, V. (2013). Nd and Sr isotope characteristics of Quaternary Indo-Gangetic plains sediments: Source distinctiveness in different geographic regions and its geological significance. *Chemical Geology*.
- Tuttle, M.P., Hengesh, J., Tucker, K.B., Lettis, W., Deaton, S.L., and Frost, J.D. (2002). Observations and comparisons of liquefaction features and related effects induced by the Bhuj earthquake. *Earthquake Spectra*, 18, 79–100.
- Tucker, R.M. (1981). Giant polygons in the Triassic salt of Cheshire, England: a thermal contraction model for their origin. *J. Sedim. Petrol.*, 51, 779-786.
- Tyagi, A. K., Shukla, A. D., Bhushan, R., Thakker, P. S., Thakkar, M. G., and Juyal, N. (2012). Mid-Holocene sedimentation and landscape evolution in the western Great Rann of Kachchh, India. *Geomorphology*, 151-152, 89-98.
- Unnikrishnan, A. S., and Luick, J. L. (2003). A finite element simulation of tidal circulation in the Gulf of Kutch, India. *Estuarine, Coastal and Shelf Science*, 56(1), 131-138.
- Valdiya, K. S. (2002). Saraswati: The River that Disappeared. *Universities Press*. 3
- Van Campo, E., Duplessy, J. C., and Rossignol-Strick, M. (1982). Climatic conditions deduced from a 150kyr oxygen isotope–pollen record from the Arabian Sea. *Nature*, 296(5852), 56-59.
- Van Campo, E. (1986). Monsoon fluctuations in two 20,000-yr BP oxygen-isotope/pollen records off southwest India. *Quaternary Research*, 26(3), 376-388.

Vanderaverroet, P., Averbuch, O., Deconinck, J. F., & Chamley, H. (1990). A record of glacial/interglacial alternations in Pleistocene sediments off New Jersey expressed by clay mineral, grain size and magnetic susceptibility data. *Marine Geology*, 159, 79-92.

von Rad, U., Schulz, H., Riech, V., den Dulk, M., Berner, U., and Sirocko, F. (1999). Multiple monsoon-controlled breakdown of oxygen-minimum conditions during the past 30,000 years documented in laminated sediments off Pakistan. *Palaeogeography, Palaeoclimatology, Palaeoecology*, 152(1), 129-161.

Waagen, W. (1877). Jurassic fauna of Kutch, Cephalopoda. *Paleo. Ind., Calcutta*, 9(1), 1-247.

Warren, J. K. (2006). *Evaporites: sediments, resources and hydrocarbons* (Vol. 1035). Berlin: Springer.

Wadiya D. N., (1975) *Geology of India* (revised version), *Mc Graw Hill*.

Wan, S., Li, A., Clift, P.D., and Stuut, J.B.W. (2007). Development of the East Asian monsoon: mineralogical and sedimentologic records in the northern South China Sea since 20 Ma. *Palaeogeography, Palaeoclimatology, Palaeoecology*, 254, 561–582.

Walton, W.R. and Sloan B.J., (1990). The Genus *Ammonia* Brunnich, 1772: its geographic distribution and morphologic variability. *Journal of Foraminiferal Research*, 20 (2), 128-156.

Wood, W.W. and Sanford, W.E. (1995). Eolian transport, saline lake basins, and groundwater solutes. *Water Resources Res.*, 31, 3121±3129.

Wünnemann, B., Demske, D., Tarasov, P., Kotlia, B. S., Reinhardt, C., Bloemendal, J., Diekmann B., Hartmann K., Krois J., Riedel F. and Arya N. (2010). Hydrological evolution during the last 15 kyr in the Tso Kar lake basin (Ladakh, India), derived from geomorphological, sedimentological and palunological records. *Quaternary Science Reviews*, 29, 1138-1155.

Wynne, A. B., and Fedden, F. (1872). *Memoir on the Geology of Kutch: To Accompany the Map Compiled by AB Wynne and F. Fedden, During the Seasons of 1867-68 and 1868-69. Geological survey of India.*

Zaninetti, L., (1982). Les foraminifères des marais salants de Salins de Giraud (Sud de la France): Milieu de Vie et transport dans le salin, comparaison avec les microfaunes marines. *Ge'ol. Me'diterr.* 9 (4), 447–470. eir oceanographic and climatic significance.

## LIST OF PUBLICATIONS BY THE CANDIDATE

1. Geomorphology of the Little Rann of Kachchh, W. India: Implication for basin architecture and Holocene palaeo-oceanographic conditions., D. M. Maurya, M. G. Thakkar, **N. Khonde** and L. S. Chamyal; *Zeitschrift für Geomorphologie*, **2009**, V-53,1, 69-80.
2. Tectonic geomorphology and evidence for active tilting of the Bela, Khadir and Bhanjada islands in the seismically active Kachchh palaeorift graben, Western India., V. Chowksey, D. M. Maurya, **N. Khonde** and L. S. Chamyal; *Zeitschrift für Geomorphologie*, **2010**, V-54, 4, 467-490.
3. Tectonic geomorphology of Chang river basin in the SE Wagad, Kachchh, Western India., **N. Khonde**, D. M. Maurya, V. Chowksey, M. G. Thakkar and L. S. Chamyal; Geological Processes and Climate Change, Edi. D. S. Singh/Chap.1, pp.1-12, **2011**.
4. Lithostratigraphic development and neotectonic significance of the Quaternary sediments along the Kachchh Mainland Fault (KMF) zone, western India., V. Chowksey, D. M. Maurya, P. Joshi, **N. Khonde**, A. Das and L. S. Chamyal; *Jour. Ear. Sys. Sci.*, **2011**, V-120, 6, 979-999.
5. Environmental significance of raised rann sediments along the margins of Khadir, Bhanjada and Kuar Bet islands in Great Rann of Kachchh, Western India., **N. Khonde**, D. M. Maurya, A. D. Singh, V. Chowksey and L. S. Chamyal; *Current Science*, **2011**, 101, 11, 1429-1434.
6. Subsurface sediment characteristics of Great Rann of Kachchh, western India based on preliminary evaluation of textural analysis of two continuous sediment cores., D. M. Maurya, **N. Khonde**, Archana Das, V. Chowksey and L. S. Chamyal, *Current Science*, **2013**, 104, 8, 1071-1077.
7. Sediment Characteristics and Foraminiferal Distribution in the Bet Zone of the Great Rann of Kachchh, Western India., **N. Khonde**, D. M. Maurya, A. D. Singh and L. S. Chamyal; *Jour. Geol. Soc. Sp. Pub. (In Press)*.
8. Microbial activity and culturable bacterial diversity in sediments of the Great Rann of Kachchh, Western India., G. Subrahmanyam, **N. Khonde**, D. M. Maurya, L. S. Chamyal and G. Archana; *Pedosphere*, **2014**, V-24, 1, 45-55.